Dissertation
submitted to the
Combined Faculties for the Natural Sciences and for Mathematics
of the Ruperto-Carola University of Heidelberg, Germany
for the degree of
Doctor of Natural Sciences

presented by
Tobias Thomas Schmidt, M.Sc.
Born in Bad Soden am Taunus
Oral examination: 10.12.2018

Studies on DNA replication fidelity in *Saccharomyces cerevisiae*

Referees: Prof. Dr. Sylvia Erhardt

Dr. Hans Hombauer

SUMMARY

High DNA replication fidelity is achieved by the interplay of DNA polymerase nucleotide selectivity and proofreading activity and the DNA mismatch repair (MMR) system. Moreover, the overall concentration and the balance between the different dNTPs influence DNA polymerase fidelity. Consequently, deregulations in any of these four processes are frequently associated to increased mutagenesis and cancer susceptibility. This work addresses first, whether additional previously unrecognized genes support DNA replication fidelity and second, how altered dNTP pools impact on DNA replication fidelity in *Saccharomyces cerevisiae*.

To identify previously unrecognized genes that prevent the accumulation of mutations, the budding yeast non-essential gene deletion collection was screened for increased mutagenesis in the presence of either the WT or low-fidelity DNA polymerase active-site mutants used as “sensitized mutator backgrounds”. This screen identified that loss of the folylpolyglutamate synthetase Met7 caused an increased mutator phenotype as well as increased gross chromosomal rearrangements (GCRs). GCRs were driven in large by dUTP accumulation and processing of uracil misincorporated into genomic DNA. Further characterization revealed that the accumulation of uracil alone is not sufficient to cause GCRs in budding yeast suggesting that GCRs in the absence of Met7 are the combined result of uracil accumulation and a DNA double-strand break repair defect.

The genome-wide screen also revealed a group of genes that become critically important if DNA replication fidelity is compromised. Loss of either the CTP synthetase Ura7 or glutamine deficiency due to the absence of the transcription factor Gln3, resulted in reduced *de novo* CTP production. This alteration in the dNTP precursor pool caused a severe dNTP imbalance with a high mutagenic potential for which neither the ribonucleotide reductase (RNR) nor any mechanism downstream RNR could compensate. Thus, this study highlights the importance of the dNTP precursor metabolism on dNTP homeostasis and DNA replication fidelity and suggests that low CTP/dCTP pools are the Achilles’ heel of dNTP pool regulation.

To investigate the effect of different dNTP pool alterations on DNA replication fidelity a *RNR1* random mutagenesis screen was performed. The screen revealed key residues in *RNR1*, the large subunit of RNR, with crucial functions for dNTP homeostasis. The identified *rnr1* alleles caused highly mutagenic dNTP alterations with different dependencies on DNA proofreading and MMR. dNTP imbalances characterized by one limiting dNTP facilitated not only base pair substitutions, but also frameshift mutations. In the subset of the identified dNTP alterations, the ones with low dATP and strongly elevated dGTP pools were most detrimental for DNA replication fidelity causing strong mutator phenotypes even in the presence of WT DNA polymerases and MMR.

Taken together, this study highlights the pivotal role of the cellular metabolism and dNTP pool homeostasis on DNA replication fidelity. The identified genes and conditions may play a role as mini-drivers during tumor evolution and potentially represent future drug targets or prognostic markers.

ZUSAMMENFASSUNG

Das Zusammenspiel von der Nukleotidselektivität und der DNA-Proofreading Funktion der DNA-Polymerasen mit der DNA Mismatch-Reparatur ermöglicht die extreme hohe Genauigkeit der DNA-Replikation. Des Weiteren beeinflussen die Konzentration und das Verhältnis der dNTPs, den Bausteinen der DNA-Replikation, die Genauigkeit der DNA-Polymerasen. Dementsprechend kann die Deregulation der vier Mechanismen zu erhöhter Anzahl von Mutationen und Krebsprädisposition führen. Diese Arbeit beschäftigt sich daher mit den Fragen, ob erstens weitere, bis jetzt unbekannte Gene die Genauigkeit der DNA-Replikation erhöhen und zweitens, wie veränderte dNTP Konzentrationen die Genauigkeit der DNA-Replikation in *Saccharomyces cerevisiae* beeinflussen.

Um bis jetzt unbekannte Gene zu identifizieren, die die Anhäufung von Mutationen verhindern, wurde die nicht-essentielle Gendeletionskollektion der Bäckerhefe in der Gegenwart von entweder WT oder DNA-Polymerasemutanten, die durch Mutationen im katalytisch aktiven Zentrum mehr Replikationsfehler generieren und deswegen im Experiment als „sensitiver Hintergrund“ dienen, auf erhöhte Mutationen hin untersucht. Die Abwesenheit der Folylpolyglutamatsynthetase Met7 verursachte nicht nur Mutationen, sondern auch „gross chromosomal rearrangements“ (GCRs). Zum Großteil wurden diese durch die dUTP-Akkumulation und der Verarbeitung von genomischen Uracil ausgelöst. Weitere Untersuchungen zeigten, dass die dUTP-Anhäufung alleine nicht ausreichend für einen GCR-Phänotyp in Bäckerhefe ist, was darauf hindeutet, dass die GCRs in der Abwesenheit von Met7 durch eine Kombination aus Uracilakkumulation und einem Doppelstrangbruchreparaturdefekt ausgelöst werden. Untersuchungen im „sensitiven Mutationshintergrund“ identifizierte eine Gruppe von Genen, deren Funktion insbesondere dann wichtig ist, wenn die Genauigkeit der Replikation beeinträchtigt ist. In der Abwesenheit der CTP-Synthethase Ura7 oder in Situationen, in denen Glutamin limitierend ist, wie in der Abwesenheit des Transkriptionsfaktors Gln3, ist die *de novo* CTP-Synthese stark reduziert. Dieses NTP-Ungleichgewicht führt zu einem schwerwiegenden dNTP-Ungleichgewicht, das weder durch die Ribonukleotidreduktase (RNR) noch durch irgendeinem anderen RNR nachgeordneten Mechanismus ausgeglichen werden kann. Deshalb hebt diese Studie die Wichtigkeit des NTP-Gleichgewichts für das dNTP-Gleichgewicht und für die Genauigkeit der DNA-Replikation hervor und deutet an, dass niedrige CTP/dCTP-Konzentrationen die Achillesferse der dNTP-Gleichgewichtsregulation sein könnten.

Um den Effekt von verschiedenen dNTP-Konzentrationsveränderungen auf die Genauigkeit der DNA-Replikation zu untersuchen, wurden zufällig generierte *rnr1* Mutanten auf erhöhte Mutationsphänotypen getestet. So konnten Schlüsselaminosäuren in Rnr1, der großen Untereinheit von RNR, für das dNTP-Gleichgewicht identifiziert werden. Die gefundenen *rnr1* Allele verursachten stark mutagene dNTP-Konzentrationsveränderungen mit unterschiedlicher Abhängigkeit für DNA Polymerase Proofreading und DNA Mismatch-Reparatur. Die dNTP-Ungleichgewichte mit einem limitierenden dNTP verursachten nicht nur Basenpaarsubstitutionen, sondern auch Leserastermutationen. Unter den identifizierten dNTP-Konzentrationsveränderungen waren diese mit niedrigen dATP- und stark erhöhten dGTP-Konzentrationen am verheerendsten

für die Genauigkeit der DNA-Replikation und führten sogar in der Gegenwart von WT DNA Polymerasen und der DNA Mismatch-Reparatur zu starken Mutationsphänotypen.
Zusammenfassend zeigt diese Arbeit die herausragende Rolle des zellulären Metabolismus, insbesondere des dNTP-Gleichgewichts, für die Genauigkeit der DNA-Replikation. Die identifizierten Gene und Konditionen könnten eine Rolle als „Mini-Driver“ in der Krebsevolution spielen und könnten potentielle zukünftige Kandidaten für die Arzneimittelforschung darstellen oder als prognostischer Marker dienen.

PREFACE

This work includes the characterization of a group of mutants presented in section 4.2 and 4.3 that were identified in a genome-wide screen in *Saccharomyces cerevisiae* (section 4.1) carried out jointly by Tobias Thomas Schmidt, Dr. Gloria Reyes, Kerstin Gries, Cemille Ümran Ceylan and Dr. Hans Hombauer with technical support from Matthias Meurer and Prof. Dr. Michael Knop (DKFZ and University of Heidelberg). The majority of data shown in section 4.3 has been published in (Schmidt *et al.* 2017). The collection of ribonucleotide reductase 1 (Rnr1) mutants characterized in this work (section 4.4) is the follow-up of an *RNR1* random mutagenesis screen performed by Maike Groß and Kerstin Gries (section 4.4.1).
I played a major role in the preparation, execution, analysis and interpretation of the here presented data.

Contributions from colleagues and collaboration partners are the following:

- Kerstin Gries, DKFZ: initial genome-wide screen (section 4.1) and *RNR1* random mutagenesis screen (section 4.4.1), help with determination of mutation rates (Table 4.6, 4.7, 4.8, 4.14, 4.16, 4.19), mutation spectra analysis (Table 4.10, 4.12, 4.21, 4.23), patches shown in Fig. 4.13 and general technical assistance.
- Dr. Gloria Reyes, DKFZ: initial genome-wide screen (section 4.1), help with generation of yeast strains and technical/scientific support.
- Cemille Ümran Ceylan, DKFZ: initial genome-wide screen (section 4.1), generation of yeast strains and plasmids used in Fig. 4.8.
- Maike Groß, DKFZ: Performed the *RNR1* random mutagenesis screen that resulted in the identification of the mutants (section 4.4.1).
- Prof. Dr. Chabes and Dr. Sushma Sharma, Umeå University: NTP/dNTP concentration measurements and analysis (Table 4.3, 4.9, 4.17, 4.18, 4.20; Fig. 4.5A,B, 4.6A, 4.10, 4.16A, 4.17A).
- Prof. Dr. Brian Luke and Tina Wagner, IMB: telomere-specific Southern blot (Fig. 4.7D).

TABLE OF CONTENTS

LIST OF FIGURES

LIST OF SUPPLEMENTARY FIGURES

LIST OF TABLES

LIST OF ABBREVIATIONS

A-site	activity site
Arg	arginine
ARS	autonomous replicating sequence
AP	apurinic/apyrimidinic
APE	apurinic/apyrimidinic endonuclease
APS	ammonium persulfate
ATP	adenosine triphosphate
BER	base excision repair
bp	base pair
BSA	bovine serum albumin
Can^R	canavanine-resistant
CI	confidence interval
C-site	catalytic site
CTP	cytidine triphosphate
d	day(s)
dADP	deoxyadenosine diphosphate
dATP	deoxyadenosine triphosphate
dCMP	deoxycytidine monophosphate
dCDP	deoxycytidine diphosphate
dCTP	deoxycytidine triphosphate
DDR	DNA damage response
dGMP	deoxyguanosine monophosphate
dGDP	deoxyguanosine diphosphate
dGTP	deoxyguanosine triphosphate
DMSO	dimethyl sulfoxide
DNA	deoxyribonucleic acid
dNMP	deoxyribonucleoside 5’-monophosphate
dNTP	deoxynucleotide triphosphate
DSB	double-strand break
dTMP	deoxythymidine monophosphate
DTT	dithiothreitol
dTTP	deoxythymidine triphosphate
dUMP	deoxyuridine monophosphate
dUDP	deoxyuridine diphosphate
dUTP	deoxyuridine triphosphate
EDTA	ethylenediaminetetraacetic acid
E. coli	*Escherichia coli*
EtOH	ethanol
FACS	fluorescence-activated cell sorting
fMet-tRNA	formyl-methionyl-tRNA

5-FOA	5-fluoroorotic acid monohydrate
5-FOA^R	5-fluoroorotic acid monohydrate-resistant
FPGS	folylpolyglutamate synthetase
GCR	gross chromosomal rearrangement
GD	growth defects
GOI	gene of interest
GTP	guanosine triphosphate
HNPCC	hereditary nonpolyposis colorectal cancer
hph	hygromycin B
HRP	horseradish peroxidase
HU	hydroxyurea
IgG	immunoglobulin G
Indels	insertion and deletion mutations
kDa	kilodalton
Leu	leucine
Lys	lysine
M	molar
MLH	MutL-homolog
MMR	DNA mismatch repair
MSH	MutS-homolog
MSI	microsatellite instability
Nat	nourseothricin
NHEJ	non-homologous end joining
NMP	nucleoside 5'-monophosphate
nt	nucleotides
OD	optical density
o/n	over night
PBS	phosphate buffered saline
PCNA	proliferating cell nuclear antigen
PCR	polymerase chain reaction
pH	potential of hydrogen
PIP	PCNA-interacting protein
PMSF	phenylmethylsulfonyl fluoride
Pol	polymerase
PRR	post-replicative repair
RER	ribonucleotide excision repair
RNR	ribonucleotide reductase
RPA	replication protein A
rpm	rounds per minute
RT	room temperature
S. cerevisiae	*Saccharomyces cerevisiae*

SD	standard deviation
SD	synthetic dropout (media)
SDS	sodium dodecyl sulphate
SDS-PAGE	sodium dodecyl sulphate–polyacrylamide gel electrophoresis
SGA	synthetic genetic array
SL	synthetic lethality
S phase	synthesis phase
S-site	specificity site
TBE	tris/borate/EDTA (buffer)
TBS	tris-buffered saline (buffer)
TCA	trichloroacetic acid
THF	tetrahydrofolate
Thr	threonine
TLS	translesion synthesis
TOR	target of rapamycin
U	units
UDG	uracil-DNA glycosylase
Ura	uracil
UTP	uridine triphosphate
V	volt
Vol%	volume percent
v/v	volume/volume
WT	wild-type
w/v	weight/volume
YPD	yeast extract-peptone-dextrose
YPG	yeast extract-peptone-glycerol

1 INTRODUCTION

1 INTRODUCTION

1.1 Eukaryotic DNA replication fork

One fundamental principle of life is that all living organisms have to copy their genome prior mitotic cell division. For this, the genetic information encoded within the DNA is replicated during the synthesis phase (S phase) of the cell cycle in a semiconservative manner. By doing so, each parental DNA strand serves as template for DNA polymerases (Pol), which synthesize the daughter strand according to the Watson-Crick model (WATSON AND CRICK 1953). In eukaryotes, the genome is organized as linear chromosomes. Due to the size of the eukaryotic genomes (e.g. ~12 million base pairs for haploid *Saccharomyces cerevisiae* (*S. cerevisiae*) cells (GOFFEAU *et al.* 1996) and ~3 billion base pairs in haploid human cells (INTERNATIONAL HUMAN GENOME SEQUENCING *et al.* 2001; VENTER *et al.* 2001), DNA replication is initiated at multiple replication origins per chromosome (RAGHURAMAN *et al.* 2001; WYRICK *et al.* 2001). To assure that each DNA is replicated only once per cell cycle, origin licensing during G1 phase and origin firing during S phase are highly regulated by different protein complexes and cell cycle regulated kinases (BELL AND LABIB 2016). At an activated origin, the two head-to-head loaded CMG helicases (Cdc45[1] (SANCHEZ-PULIDO AND PONTING 2011; MAKAROVA *et al.* 2012), Mcm2-7 (DAVEY *et al.* 2003; BOCHMAN AND SCHWACHA 2008), and GINS (Sld5 and Psf1-3)(TAKAYAMA *et al.* 2003)) pass each other (DOUGLAS *et al.* 2018) and unwind the DNA double-strand forming two divergent DNA replication forks (BURGERS AND KUNKEL 2017). The resulting single-stranded DNA is coated and stabilized by the single-strand binding protein replication protein A (RPA (Rfa1-3))(BRILL AND STILLMAN 1991; ALANI *et al.* 1992; LONGHESE *et al.* 1994). As DNA polymerases can only replicate genetic information in a 5' to 3' orientation, DNA replication forks are asymmetric (LUJAN *et al.* 2016). The leading strand is synthesized continuously, whereas the lagging strand is replicated discontinuously in ~100-200 nucleotide (nt) long Okazaki fragments (OKAZAKI *et al.* 1968; SMITH AND WHITEHOUSE 2012). At each origin and Okazaki fragment DNA synthesis is initiated by the Pol α-primase complex (Pol1, Pol12, Pri1 and Pri2)(BELL AND LABIB 2016). Primase synthesizes a 7-10 nt long RNA primer, which is than further extended up to 20 deoxynucleotides by Pol α before the high-fidelity DNA polymerases Pol δ (Pol3, Pol31 and Pol32)(BYRNES *et al.* 1976; GERIK *et al.* 1998) and Pol ε (Pol2, Dpb2-4)(HAMATAKE *et al.* 1990; MORRISON *et al.* 1990; CHILKOVA *et al.* 2003) continue to replicate the majority of the genome (JOHANSSON AND DIXON 2013; BELL AND LABIB 2016; LUJAN *et al.* 2016). In addition to their polymerase domain, the B-type DNA polymerases Pol δ and Pol ε possess a 3' to 5' exonuclease function, required for proofreading of the newly synthesized DNA strand and consequently high DNA replication fidelity (BYRNES *et al.* 1976; MORRISON *et al.* 1991; MORRISON AND SUGINO 1994). Furthermore, Pol ε contributes to origin assembly (MURAMATSU *et al.* 2010) as well as to S-phase checkpoint activation (NAVAS *et al.* 1995). Pol δ not only proofreads Pol α replicated DNA (PAVLOV *et al.* 2006), but also the leading strand *in trans* (FLOOD *et al.* 2015). Moreover, Pol δ plays an additional role in DNA strand displacement repair, whereby a nicked strand is separated from the complementary strand by the advance of Pol δ creating a flap which is then further removed by the flap endonuclease Rad27 (PRINDLE AND LOEB 2012). The ring-shaped

[1] All gene nomenclature refers to *Saccharomyces cerevisiae* if not differentially stated.

homotrimeric sliding clamp proliferating cell nuclear antigen (PCNA)(Pol30 in budding yeast)(BAUER AND BURGERS 1990; KRISHNA *et al.* 1994) supports Pol δ and Pol ε processivity by binding them and anchoring them to DNA (CHILKOVA *et al.* 2007). Furthermore, PCNA acts as loading platform for various other proteins and allows coupling of different processes, including DNA repair and nucleosome assembly to DNA replication (MAILAND *et al.* 2013). PCNA is loaded on double-stranded DNA by the replication factor C (RFC) clamp loader complex (Rfc1-5)(BOWMAN *et al.* 2004).

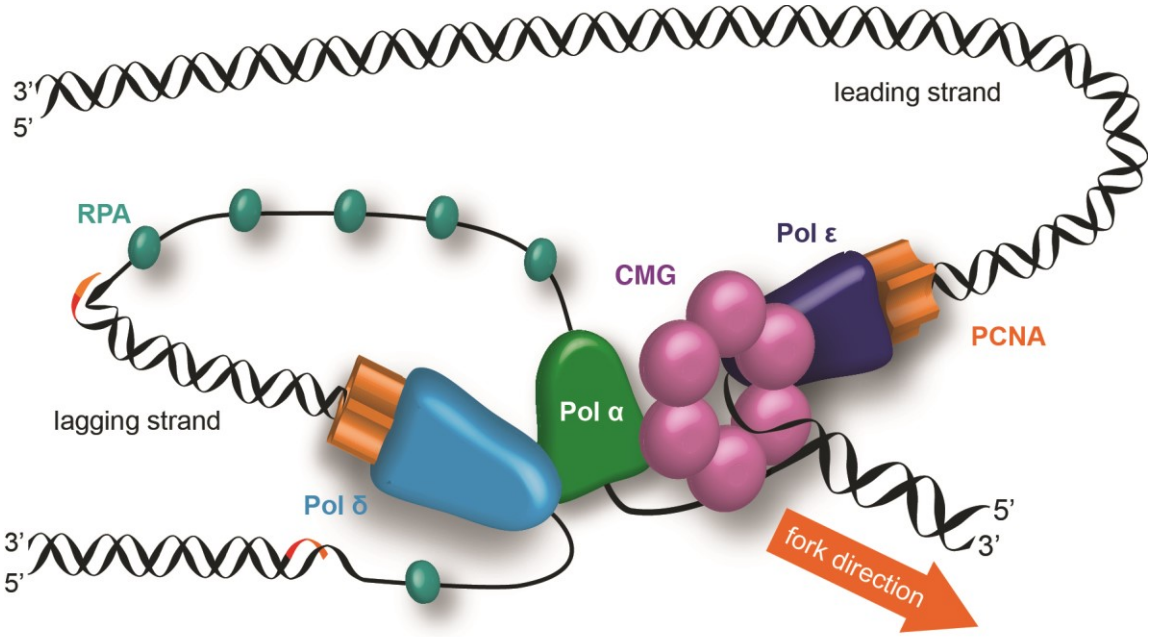

Fig. 1.1 The eukaryotic replication fork.
The CMG helicase unwinds the DNA double strand. Primase initiates replication at each origin and Okazaki fragment by synthesizing a short RNA primer (orange), which is further elongated by Pol α with up to 20 nt DNA (red). Pol ε replicates the leading strand in a continuous manner, whereas Pol δ synthesizes the lagging strand discontinuously as Okazaki fragments. The single-strand binding protein RPA binds and stabilizes single-stranded DNA. The sliding clamp PCNA supports DNA polymerase fidelity and serves as loading platform to couple various processes to the replication fork.

Whereas it is widely accepted that the minimal eukaryotic replisome consists of the CMG helicase, the Pol α-primase, the sliding clamp PCNA, the RFC clamp loader complex, the high-fidelity DNA polymerases Pol δ and Pol ε, as well as the single-strand binding protein RPA (ZHANG AND O'DONNELL 2016), the contribution of Pol δ and Pol ε to leading- and lagging-strand synthesis is still under debate. The most accepted model for DNA replication is the “division of labor” model (LUJAN *et al.* 2016), in which Pol ε (catalytic subunit Pol2) is the leading-strand polymerase (PURSELL *et al.* 2007) and Pol δ (catalytic subunit Pol3) synthesizes the lagging strand (NICK MCELHINNY *et al.* 2008) (Fig. 1.1). The Kunkel lab proposed this model based on the characterization of active-site mutant alleles of Pol ε (*pol2-M644G*) (PURSELL *et al.* 2007) and Pol δ (*pol3-L612M*) (NICK MCELHINNY *et al.* 2008) in budding yeast. These low-fidelity DNA polymerase alleles confer a weak mutator phenotype and a specific mutational signature. Mutational hotspot analysis of a reporter (*URA3*) placed in two orientations next to a well-characterized origin (autonomous replicating sequence (ARS) *ARS306*) (STINCHCOMB *et al.* 1979; POLOUMIENKO *et al.* 2001) allowed to link Pol δ

to lagging-strand and Pol ε to leading-strand replication. Several lines of evidences have further supported these initial findings and the "division of labor" model. First, low-fidelity DNA polymerase alleles, which incorporate ribonucleotides with a higher frequency, were introduced in *S. cerevisiae* (NICK MCELHINNY *et al.* 2010a) and *S. pombe* (MIYABE *et al.* 2011). Based on the genome-wide distribution of misincorporated ribonucleotides Pol δ and Pol ε were assigned to the lagging and leading strand, respectively (CLAUSEN *et al.* 2015; KOH *et al.* 2015; REIJNS *et al.* 2015) (DAIGAKU *et al.* 2015). Second, Pol δ was specifically linked to the lagging strand and Pol ε to the leading strand using eSPAN (enrichment and sequencing of protein-associated nascent strand DNA). For this, chromatin immunoprecipitation of Pol δ and Pol ε was followed by the enrichment for the BrdU marked and thus nascent single-stranded DNA. Subsequent DNA sequencing and mapping revealed strong enrichment for Pol δ at the lagging strand and Pol ε at the leading strand (YU *et al.* 2014). Third, biochemical reconstitution experiments of the eukaryotic replisome using a nucleotide-biased forked substrate also supported the "division of labor model" and indicated a role of the CMG helicase in dividing the labor (GEORGESCU *et al.* 2015). Despite the growing evidence for Pol ε as leading-strand DNA polymerase, one study questioned whether Pol ε functions as major leading-strand DNA polymerase (JOHNSON *et al.* 2015). This study proposed that Pol δ is the major DNA polymerase for both the leading and lagging strand. According to this model, Pol ε functions in DNA proofreading of the leading strand and in the activation of the S-phase checkpoint. Nonetheless, there is a general agreement that Pol α and Pol δ replicate the lagging strand. Due to the strong supportive data for the "division of labor" model, Pol ε will be assigned as leading strand DNA polymerase in this thesis. However, further studies are needed to clarify the contribution of Pol δ and Pol ε to leading-strand synthesis.

Besides the essential DNA polymerases Pol α, Pol δ and Pol ε (also referred to as replicative DNA polymerases), other specialized error-prone DNA polymerases, termed translesion synthesis (TLS) DNA polymerases, contribute to DNA replication under certain conditions (MCCULLOCH AND KUNKEL 2008; LANGE *et al.* 2011). These TLS polymerases are recruited to stalled replication forks to bypass sites of exogenous or spontaneous DNA damage and to complete DNA replication. Alternatively, the newly synthesized sister chromatid and template switching is used for error-free DNA damage bypass (BOITEUX AND JINKS-ROBERTSON 2013). The pathway choice for both branches of post-replicative repair (PRR) depends on the ubiquitination status of PCNA: TLS polymerases are recruited by PCNA mono-ubiquitination whereas template switching is induced upon PCNA poly-ubiquitination (HOEGE *et al.* 2002).

1.2 DNA replication fidelity

Eukaryotic cells have to replicate their genomes fast and with high accuracy to allow efficient cell proliferation and to pass high quality genetic information to their progeny. Remarkably, *S. cerevisiae* replisomes progress with approximately 50 nucleotides per second (RAGHURAMAN *et al.* 2001) and generate in diploid wild-type cells less than one mutation per ten billion replicated nucleotides (1.7×10^{-10} average genome-wide base mutation rate per base pair) (LYNCH *et al.* 2008; LANG *et al.* 2013; LUJAN *et al.* 2014). Human cells replicate their genome with similar fidelity (10^{-9} to 10^{-11}) (DRAKE *et al.* 1998; LOEB 2001). The high replication fidelity in eukaryotic cells is

achieved by the interplay of DNA polymerases' nucleotide selectivity and proofreading function and the post-replicative DNA mismatch repair (MMR) system (ARANA AND KUNKEL 2010; KUNKEL AND ERIE 2015). Furthermore, the levels and balance of the deoxynucleoside triphosphates (dNTPs) influence DNA polymerases' fidelity (Fig. 1.2) (KUNZ *et al.* 1994; PAI AND KEARSEY 2017). Accordingly, defects in any of these four processes have been linked to increased mutagenesis and cancer predisposition (PELTOMAKI 2003; BOLAND AND GOEL 2010; BRIGGS AND TOMLINSON 2013; MATHEWS 2015). Furthermore, 66% of all mutations found in cancers worldwide were proposed to originate from DNA replication errors (TOMASETTI *et al.* 2017). Replication errors are frequently base substitution mutations, which are either transitions (purine-purine and pyrimidine-pyrimidine mispairs) or transversions (purine-pyrimidine mispairs) (ARANA AND KUNKEL 2010). Their frequency depends on the nucleotide selectivity of the replicating DNA polymerase and the balance between the different dNTPs. Insertion and deletion (indels) frameshift mutations are another type of replication error. Frameshift mutations originate from DNA polymerase slippage events and occur most frequently at repetitive sequences like tandem repeats or mononucleotide runs, so called microsatellites (KROUTIL *et al.* 1996).

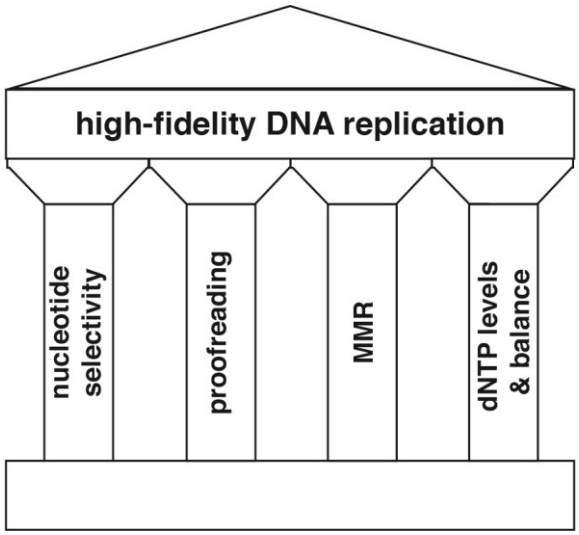

Fig. 1.2 The four pillars of high-fidelity DNA replication.
High-fidelity DNA replication depends on DNA polymerase proofreading activity and nucleotide selectivity, both influenced by the levels and balance of the dNTP pools. In addition, the DNA mismatch repair (MMR) pathway corrects replication errors, increasing about 100-1000x DNA replication fidelity. Consequently, mutations affecting DNA polymerase proofreading activity or nucleotide selectivity as well as mutations inactivating MMR function are known drivers of genome instability and human cancer.

Even though not necessarily a mutagenic, the most frequent DNA replication error is the misincorporation of ribonucleotides (WILLIAMS *et al.* 2016). During each round of DNA replication replicative DNA polymerases insert approximately one ribonucleotide per 1200 incorporated nucleotides in *S. cerevisiae* (NICK MCELHINNY *et al.* 2010b) and one ribonucleotide per 7600 in mice (REIJNS *et al.* 2012). Misincorporated ribonucleotides are normally efficiently removed from genomic DNA by ribonucleotide excision repair (RER)(WILLIAMS *et al.* 2016). However, in the absence of RER topoisomerase 1-dependent removal of ribonucleotides can lead to 2 to 5 bp deletion events in tandem repeats and genome instability (NICK MCELHINNY *et al.* 2010a; KIM *et al.* 2011).

1.3 DNA polymerase nucleotide selectivity and proofreading

Replication errors are counteracted by two intrinsic properties of eukaryotic DNA polymerases - high nucleotide selectivity and DNA proofreading. Among all factors that determine the high DNA replication fidelity in eukaryotes (one replication error per 10^9 - 10^{11} synthesized nucleotides

(DRAKE *et al.* 1998; LOEB 2001; LYNCH *et al.* 2008; LANG *et al.* 2013; LUJAN *et al.* 2014)), the largest contribution is set by the DNA polymerase nucleotide selectivity (Fig. 1.2) (KUNKEL 2009). Remarkably, *S. cerevisiae* DNA Pol α, δ and ε generate just one replication error per 10^4 to 10^5 synthesized nucleotides *in vitro* (KUNKEL *et al.* 1989; SHCHERBAKOVA *et al.* 2003; FORTUNE *et al.* 2005). This high stringency of the DNA polymerase active-site to discriminate against incorrect dNTPs and to prevent their incorporation is achieved by the concerted action of three processes: Hydrogen bonding of the template and incoming nucleotide (KOOL 2002), enthalpy-entropy compensation (PETRUSKA AND GOODMAN 1995) and the complementary architecture of the nucleotide binding pocket, which binds the four canonical Watson-Crick nucleotide pairs without steric clashes (ECHOLS AND GOODMAN 1991; GOODMAN 1997; MCCULLOCH AND KUNKEL 2008). Furthermore, the balance between the different dNTP pools influences nucleotide selectivity (PAI AND KEARSEY 2017).

Mutation studies of the highly conserved mofif A in the active-site of the bacteriophage T4 DNA polymerase revealed mutant polymerase alleles that possess a modest mutator phenotype, but are proofreading proficient and moreover result in sensitivity to the viral DNA polymerase inhibitor phosphonoacetic acid (REHA-KRANTZ AND NONAY 1994; STOCKI *et al.* 1995), Based on this pioneering work the homologous active-site mutations have been introduced in the budding yeast DNA polymerases Pol α (*pol1-L868M*), Pol δ (*pol3-L612M*) and Pol ε (*pol2-M644G*). These active-site mutations allow normal growth *in vivo* and, in case of Pol δ and ε, do not compromise the DNA proofreading function. However, the mutant alleles confer a mild mutator phenotype and a characteristic mutational signature (NIIMI *et al.* 2004; PAVLOV *et al.* 2006; VENKATESAN *et al.* 2006; PURSELL *et al.* 2007; NICK MCELHINNY *et al.* 2008). The *pol3-L612M* allele shows elevated T-A to C-G transitions and generates T-dGTP mismatches ≥28 fold more frequently than A-dCTP mismatches. Furthermore, G-C to A-T transitions and single A/T base deletions are also increased in *pol3-L612M* and driven by G-dTTP mismatches and T deletions, respectively (NICK MCELHINNY *et al.* 2007; NICK MCELHINNY *et al.* 2008). In contrast, the *pol2-M644G* mutational signature is characterized by T-A to A-T transversions and the allele generates T-dTTP mismatches ≥39 fold more frequently than A-dATP mismatches (PURSELL *et al.* 2007). These mutational biases for certain mismatches have been utilized in combination with reporter (PURSELL *et al.* 2007; NICK MCELHINNY *et al.* 2008) or genome-wide sequencing (LUJAN *et al.* 2014) to propose the “division of labor model” (LUJAN *et al.* 2016). Besides some similarities between the active-site DNA polymerase mutant alleles (*pol1-L868M*, *pol2-M644G* and *pol3-L612M*), one major difference is that only *pol2-M644G* requires an active S-phase checkpoint and elevated dNTP levels for survival (WILLIAMS *et al.* 2015; SCHMIDT *et al.* 2017).

Strikingly, previous reports have identified DNA polymerase active-site mutations have been identified in human cancer patients (BRIGGS AND TOMLINSON 2013; MERTZ *et al.* 2015). Moreover, the analysis of inherited biallelic MMR-deficient tumors revealed in some of them acquired somatic mutations in Pol δ and Pol ε resulting in ultra-hypermutated cancers (SHLIEN *et al.* 2015). Interestingly, one of the identified Pol δ driver mutations was *POLD1-L606M*, which is the exact homologous mutation to the budding yeast *pol3-L612M* allele. Furthermore, in mice the replacement of the homologous residue *L604G/K* in murine Pol δ is homozygous lethal and the

heterozygous mutation causes increased genome instability and tumorigenesis (VENKATESAN *et al.* 2007). Thus, evidence from biochemical to *in vivo* studies, and from phage T4 to humans, highlight the importance of nucleotide selectivity for high-fidelity DNA replication.

As mentioned earlier, high-fidelity DNA polymerases Pol δ and ε possess in addition to the 5' to 3' DNA polymerase domain a second domain with 3' to 5' exonuclease function (MORRISON *et al.* 1991; MORRISON AND SUGINO 1994). This domain allows proofreading of the last-incorporated nucleotide. Therefore, to suppress replication errors by DNA proofreading, the excision of the terminal misincorporated nucleotide has to occur before DNA polymerase further extends the misincorporated nucleotide. The balance between DNA synthesis and DNA proofreading heavily depends on the dNTP concentrations (Fig. 1.3) (ROBERTS *et al.* 1991; ROBERTS *et al.* 1993; REHA-KRANTZ 2010). The next-nucleotide effect describes the influence of the nucleotide that is going to be incorporated next on DNA proofreading efficiency of the last-incorporated nucleotide. High dNTP levels are mutagenic as they favor DNA synthesis over DNA proofreading. In contrast, low dNTP levels slow down DNA replication and increase DNA replication fidelity by giving more time for DNA proofreading and repair (REHA-KRANTZ 2010). Furthermore, *in vitro* studies suggest that DNA proofreading is inhibited by nucleoside 5'-monophosphate (NMPs) / deoxyribonucleoside 5'-monophosphate (dNMPs) (QUE *et al.* 1978; FERSHT AND KNILL-JONES 1983). As dNMPs are the products of the 3' to 5' exonuclease reaction, this may represent a product inhibition mechanism to prevent excessive excision of the newly synthesized strand.

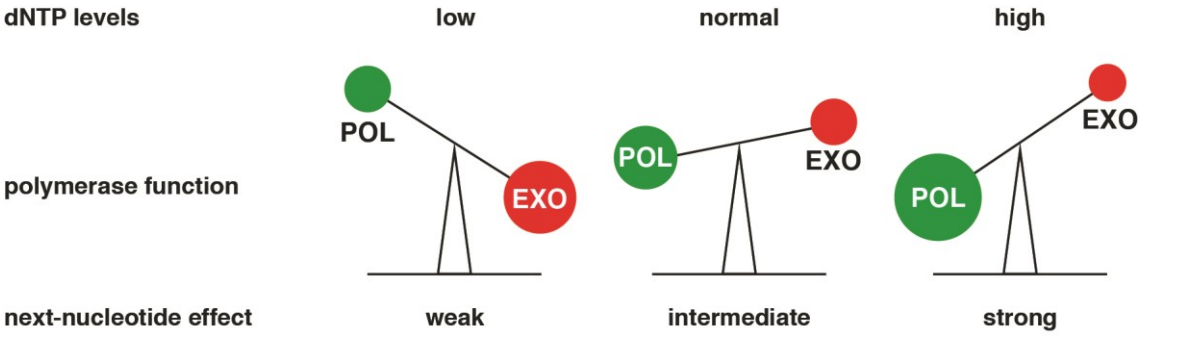

Fig. 1.3 The dNTP pool size influences DNA polymerase function.
dNTPs are the substrates for DNA polymerases polymerization domain (POL). However, the high-fidelity DNA polymerases Pol δ and Pol ε also possess a 3'-5' exonuclease domain (EXO), which allows proofreading of the last-incorporated nucleotide. The balance between synthesis and excision (proofreading) strongly depends on the dNTP levels, in particular the concentration of the nucleotide that has to be incorporated after the last-incorporated nucleotide (next-nucleotide effect). High dNTP concentrations promote DNA polymerase polymerization on the expense of proofreading, whereas low dNTP pools slow down replication and give more time for proofreading.

In *S. cerevisiae* the DNA polymerase exonuclease-deficient alleles *pol2-04* (MORRISON *et al.* 1991) and *pol3-01* (MORRISON *et al.* 1993) cause a mutator phenotype (MORRISON AND SUGINO 1994; TRAN *et al.* 1999). Interstingly, the mutator phenotype of *pol3-01* is approximately 10-fold stronger than *pol2-04* (MORRISON AND SUGINO 1994; TRAN *et al.* 1999). This difference may be explained by reports that Pol δ proofreads a higher proportion of the genome than Pol ε: Pol δ not only proofreads Pol δ-replicated DNA, but also DNA synthesized by Pol α (PAVLOV *et al.* 2006) as well as the leading strand *in trans* (FLOOD *et al.* 2015). Furthermore, Pol δ performs DNA repair

synthesis and consequent proofreading of repaired DNA sequences (PRINDLE AND LOEB 2012). Moreover, in haploid yeast both *pol2-04* and *pol3-01* cause synthetic lethality in the absence of MMR (TRAN *et al.* 1999; GREENE AND JINKS-ROBERTSON 2001; WILLIAMS *et al.* 2013). This type of lethal interactions occurs when the mutation rate is so high that at least one essential gene is inactivated per round of DNA replication and has been referred to as “error-induced extinction” phenotype (HERR *et al.* 2011). In line with a conserved function of DNA proofreading in mutation avoidance, DNA proofreading deficiency in mice causes increased tumorigenesis and shorter lifespan (GOLDSBY *et al.* 2001; GOLDSBY *et al.* 2002; ALBERTSON *et al.* 2009). Furthermore, sequencing of human cancer patient genomes revealed DNA proofreading-deficient polymerase as driver of cancer progression (BRIGGS AND TOMLINSON 2013; CHURCH *et al.* 2013; PALLES *et al.* 2013; SHLIEN *et al.* 2015). In summary, both Pol δ and Pol ε DNA proofreading function contribute to eukaryotic DNA replication fidelity.

1.4 DNA mismatch repair

Unrepaired replication errors become permanent mutations during the next round of DNA replication. To counteract the propagation of replication errors that escaped DNA polymerase proofreading, most living organisms possess a spell-checking mechanism named DNA mismatch repair (MMR). This post-replicative MMR system recognizes and repairs replication errors, increasing replication fidelity approximately 100-fold (LANG *et al.* 2013; LUJAN *et al.* 2014). Interestingly, the MMR correction efficiency *in vivo* is proportional to the frequency of generated DNA replication errors (KUNKEL AND ERIE 2015). Thus, MMR is most effective in the suppression of frequently generated frameshift mutations. Consequently, defects in MMR results not only in an overall increased mutator phenotype, but specifically in increased frameshift mutations. The seminal discovery that increased mutations rates caused by defects in human MMR genes are responsible for the predisposition to develop an early-onset form of colon cancer called hereditary nonpolyposis colorectal cancer (HNPCC) or Lynch syndrome (BOLAND AND GOEL 2010; BOLAND AND LYNCH 2013; KOLODNER 2016), further stresses the importance of MMR as genome stability mechanism. Of note, HNPCC is the most prevalent human hereditary cancer predisposition and HNPCC tumors as well as tumors, which have sporadically inactivated MMR, show a microsatellite instability (MSI) phenotype (PELTOMAKI 2003).

The MMR mechanism is best understood in *Escherichia coli* (*E. coli*) (IYER *et al.* 2006). In *E. coli*, the mismatch is recognized by the MutS homodimer (where “Mut” stands for mutator). This MutS recognition complex recruits a MutL homodimer to the site of the mismatch. Next, the MutL repair intermediate complex recruits MutH, a DNA methylation-sensitive endonuclease. Upon activation by MutL, MutH introduces a nick in the newly synthesized strand. In *E. coli*, hemi-methylation of d(GATC) sites is the strand discrimination signal (PUTNAM 2016). Directly after DNA replication the newly synthesized DNA strand is transiently unmethylated which allows the MutH endonuclease to discriminate the daughter from the parental strand and specifically introduce the nick in the daughter strand (LANGLE-ROUAULT *et al.* 1987; WELSH *et al.* 1987). The generated nick acts then as entry site for single-strand specific exonucleases that excise part of the newly synthesized strand. Repair is completed by DNA PolIII-dependent re-synthesis.

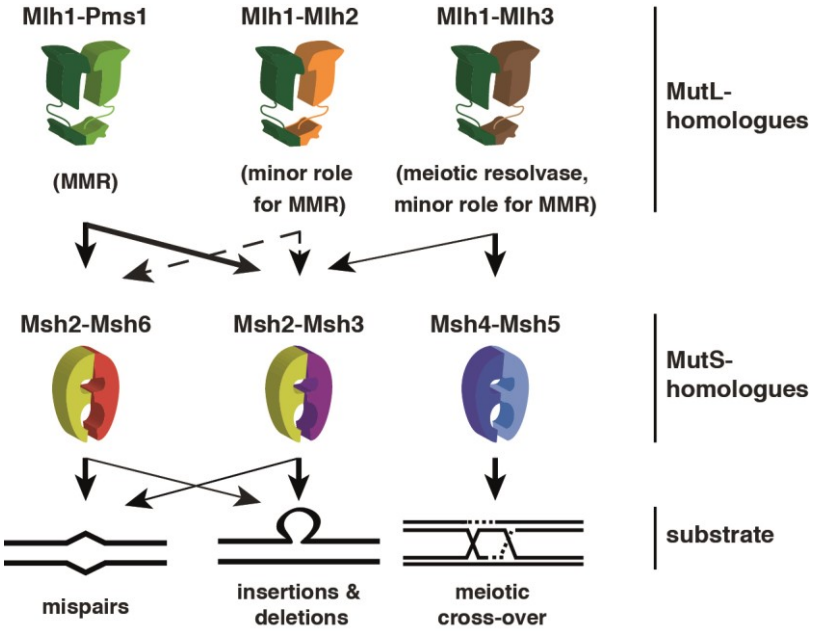

Fig. 1.4 The *S. cerevisiae* MSH and MLH complexes. Arrows represent the functional interaction and the potential role *in vivo*. Thick arrows indicate major roles in the process, whereas thin arrows represent minor contributions. Dashed arrows indicate functional relevance for the process only in certain genetic backgrounds. Figure is adapted from (REYES *et al.* 2015)

Key aspects of the MMR mechanism are conserved between bacteria and eukaryotes and as in bacteria MutS-homolog (MSH) and MutL-homolog (MLH) family members play critical roles in the eukaryotic repair process (Fig. 1.4) (IYER *et al.* 2006; REYES *et al.* 2015). In eukaryotes, several MSH proteins exist which are active as heterodimers. Mismatches in eukaryotes are recognized by Msh2-Msh6 and Msh2-Msh3, as well as by Msh2-Msh7 in plants (CULLIGAN AND HAYS 2000). Furthermore, an additional MSH complex called Msh4-Msh5 has been reported (ROSS-MACDONALD AND ROEDER 1994) (HOLLINGSWORTH *et al.* 1995). However, in contrast to the previously mentioned complexes it does not play a role in MMR but during meiotic cross-over (SANTUCCI-DARMANIN *et al.* 2002; SNOWDEN *et al.* 2004; KOLAS *et al.* 2005). In contrast to human cells, in which the Msh2-Msh6 complex is the major mismatch recognition complex, Msh2-Msh6 and Msh2-Msh3 play a more balanced role in *S. cerevisiae* (MARSISCHKY *et al.* 1996; SIA *et al.* 1997). However, the two yeast complexes differ in their substrate specificity. Yeast Msh2-Msh6 recognizes seven out of the eight possible base substitutions (C-C mispairs are poorly recognized), as well as one and two nucleotide indels (SRIVATSAN *et al.* 2014). In contrast, yeast Msh2-Msh3 functions preferentially on smaller and larger indels and to a lesser degree on base substitutions (ACHARYA *et al.* 1996; MARSISCHKY *et al.* 1996; HARRINGTON AND KOLODNER 2007; SRIVATSAN *et al.* 2014). Msh2-Msh3 and Msh2-Msh6 recruit heterodimeric MLH repair intermediate complexes to the mismatch site. Three repair intermediate complexes exist in eukaryotes – Mlh1-Pms1 (human Mlh1-Pms2), Mlh1-Mlh2 (human Mlh1-Pms1) and Mlh1-Mlh3. The Mlh1-Pms1 complex is essential for the MMR reaction (KUNKEL AND ERIE 2015; REYES *et al.* 2015), whereas Mlh1-Mlh2 (PROLLA *et al.* 1998; HARFE *et al.* 2000; CAMPBELL *et al.* 2014) and Mlh1-Mlh3 play only minor roles in MMR (FLORES-ROZAS AND KOLODNER 1998; CHEN *et al.* 2005). In contrast to *E. coli*, eukaryotes do not encode for a MutH endonuclease homolog. However, the Mlh1-Pms1 (KADYROV *et al.* 2006) and Mlh1-Mlh3 (NISHANT *et al.* 2008) complexes possess endonuclease activity that is stimulated by the interaction with PCNA (KADYROV *et al.* 2006; PLUCIENNIK *et al.* 2010).

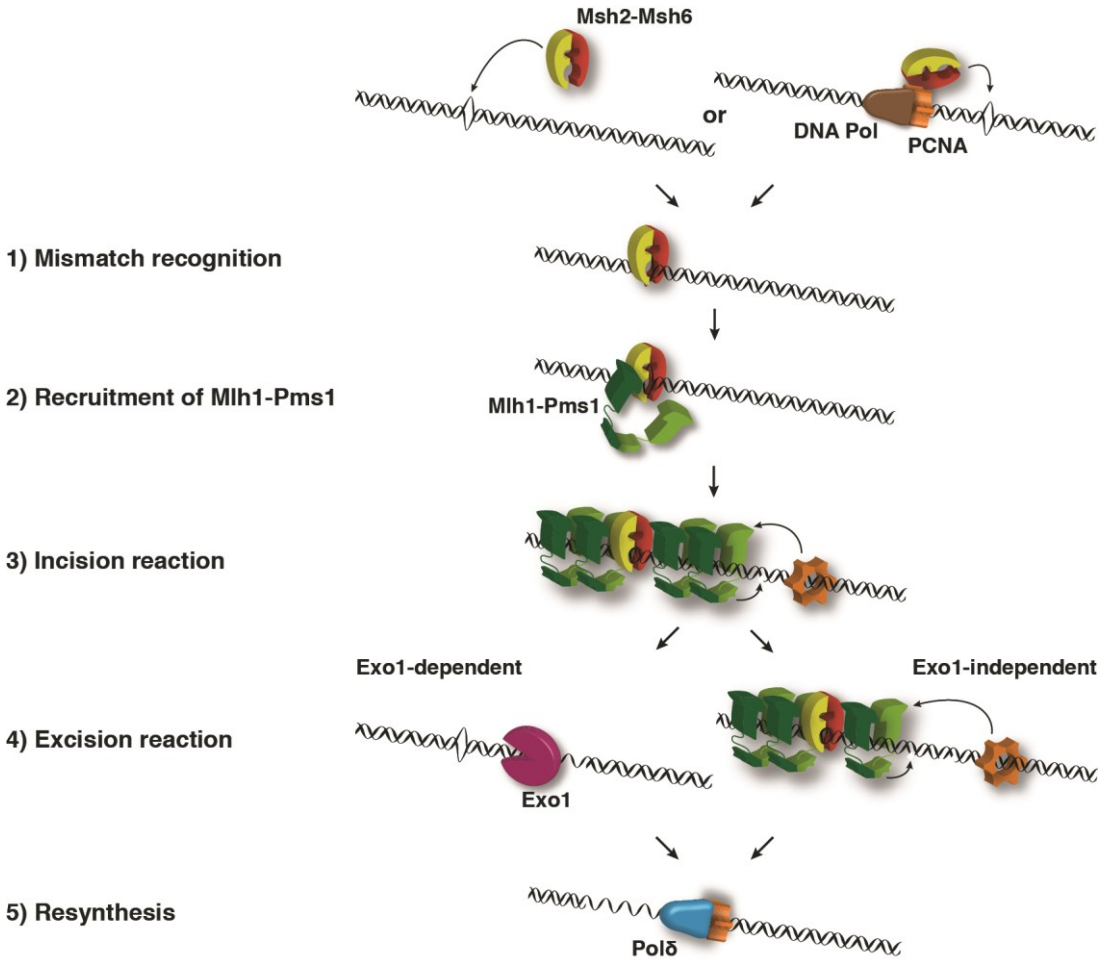

Fig. 1.5 Mechanistic model about the MMR reaction in *S. cerevisiae*.
(1) The Msh2-Msh6 heterodimer recognizes the mismatch either coupled or uncoupled to the DNA replication fork. (2) Msh2-Msh6 recruits Mlh1-Pms1 to the mismatch site and facilitates the catalytic loading of Mlh1-Pms1 complexes. (3) Upon activation by the sliding clamp PCNA, Mlh1-Pms1 endonuclease nicks the DNA. (4) The newly synthesized strand is excised either in an exonuclease 1 (Exo1)-dependent or in an Exo1-independent reaction. The latter, was proposed to involve multiple rounds of nicking catalyzed by Mlh1-Pms1. (5) Finally, Pol δ resynthesizes the DNA. For details see text.

Taken together, the current model of the eukaryotic MMR reaction (exemplified using the *S. cerevisiae* MMR protein names) can be outlined in five steps (Fig. 1.5)(KUNKEL AND ERIE 2015; REYES *et al.* 2015): (1) Mismatch recognition: Msh2-Msh3 or Msh2-Msh6 either coupled or uncoupled to the DNA replication fork recognizes the mismatch. Coupling of mismatch recognition complexes to DNA replication forks is achieved by tethering Msh2-Msh3 and Msh2-Msh6 to PCNA using PCNA-interacting protein (PIP) motifs present at the N-terminus of Msh3 and Msh6 (CLARK *et al.* 2000; FLORES-ROZAS *et al.* 2000; KLECZKOWSKA *et al.* 2001). (2) Mlh1-Pms1 recruitment: Mismatch recognition complexes recruit Mlh1-Pms1 to sites of damage and facilitate catalytic loading of these repair intermediate complexes on DNA (HOMBAUER *et al.* 2011a). (3) Incision reaction: PCNA stimulates the Mlh1-Pms1 endonuclease that nicks the newly synthesized strand. (4) Excision reaction: The exonuclease 1 (Exo1), a 5' to 3' exonuclease, uses the generated nick as entry site to excise the newly synthesized strand. As the absence of Exo1 causes only a mild mutator phenotype in *S. cerevisiae* (TISHKOFF *et al.* 1998; AMIN *et al.* 2001) and mouse (WEI *et al.* 2003; EDELMANN AND EDELMANN 2004) and no other exonuclease functioning in MMR has been

discovered so far (GOELLNER *et al.* 2015), it has been proposed that multiple rounds of Mlh1-Pms1-dependent nicking may substitute for the loss of Exo1 (GOELLNER *et al.* 2014). Therefore, the eukaryotic MMR excision can either be a fast Exo1-dependent or a slower Exo1-independent reaction. However, the exact mechanism still remains elusive.

(5) DNA re-synthesis: MMR reaction is completed by Pol δ-dependent re-synthesis of the daughter strand using the parental strand as template.

As MMR functions coupled to DNA replication, it has been suggested that strand discrimination is accomplished by making use of a transient DNA replication-associated signal, which allows repair in a short time frame (KLECZKOWSKA *et al.* 2001; HOMBAUER *et al.* 2011a; HOMBAUER *et al.* 2011b). In contrast to *E. coli*, eukaryotes as well as most of the bacteria that do not belong to the gammaproteobacterial, do not use the hemi-methylation status of d(GATC) sites as strand discrimination signal (GAO *et al.* 2009; PUTNAM 2016). Several not mutually exclusive strand discrimination signals have been proposed for eukaryotic MMR: transient nicks between Okazaki fragments on the lagging strand (HOLMES *et al.* 1990; THOMAS *et al.* 1991; FANG AND MODRICH 1993), transient nicks generated due to the removal of misincorporated ribonucleotides by RER (GHODGAONKAR *et al.* 2013; LUJAN *et al.* 2013) or loading of PCNA in a specific orientation (PLUCIENNIK *et al.* 2010). However, nicks due to Okazaki fragments do not explain the strand discrimination at the continuously synthesized leading strand. Furthermore, the absence of RER and ribonucleotide removal does not cause a strong MMR-defect. Moreover, PCNA has been shown to be less important for leading strand processivity (GEORGESCU *et al.* 2014) and therefore most likely does not serve as strand discrimination signal during leading strand replication. Hence, none of the proposed signals sufficiently explain eukaryotic strand discrimination (REYES *et al.* 2015) and further studies are required to unravel the strand discrimination signal in eukaryotes.

Besides the important role of MMR in DNA replication fidelity, MMR complexes also play non-canonical roles in various other processes, like the DNA damage response (LI *et al.* 2016), somatic hypermutation of immunoglobulins (ZANOTTI AND GEARHART 2016), triplet-repeat expansion (CROUSE 2016), meiotic crossing overs (MANHART AND ALANI 2016) and homeologous recombination (THAM *et al.* 2016).

In summary, MMR proteins prevent the accumulation of mutations and counteract the development of cancer.

1.5 dNTP pool homeostasis

dNTPs are the building blocks for genome replication in living organisms. In most organisms, in which dNTP pools have been determined, the concentration of different dNTPs is not equimolar but rather exist in a natural imbalance that is apparently beneficial for DNA replication fidelity. dTTP is the most abundant dNTP pool followed by dATP and dCTP. dGTP is always the least abundant, contributing just 5-10% to the total dNTP pool (MATHEWS AND JI 1992; MARTOMO AND MATHEWS 2002; CHABES *et al.* 2003). Interestingly, mitochondrial dNTP pools, which represent a physically and metabolically distinct compartment, are dominated by dGTP (SONG *et al.* 2005; NIKKANEN *et al.* 2016). This difference between nuclear and mitochondrial dNTP pools has been suggested to be an adaptation to the oxidative environment present in the mitochondria, which may potentially favor

oxidation of dGTP to mutagenic 8-oxo-dGTP (MATHEWS 2006). Remarkably, the underrepresentation of dGTP found in nuclear dNTP pools does not strongly affect replication fidelity in comparison to equimolar dNTP concentrations used in *in vitro* DNA replication reactions (MARTOMO AND MATHEWS 2002). Furthermore, the telomere length seems to be positively correlated with the dGTP concentration in *S. cerevisiae* (GUPTA *et al.* 2013; MAICHER *et al.* 2017).

In eukaryotes, dNTP concentrations peak during S phase (CHABES *et al.* 2003; HÅKANSSON *et al.* 2006a; HÅKANSSON *et al.* 2006b). However, even during S phase dNTP levels are not sufficient to allow DNA replication of the whole genome (REICHARD 1988). Thus, to complete genome replication dNTPs have to be constantly generated during S phase. In agreement with dNTP pools being a limiting factor for the speed of DNA replication, elevated dNTP pools increase replication fork progression and shorten S-phase length in *S. cerevisiae* (POLI *et al.* 2012; DOVRAT *et al.* 2018). Even though it is still not fully understood why it could be advantageous for eukaryotic cells to prolong their S phase by limiting the dNTP pools, there might be several arguments to do so: First, elevated dNTP pools cause increased mutagenesis *in vitro* (ROBERTS *et al.* 1991; ROBERTS *et al.* 1993) and *in vivo* (CHABES *et al.* 2003). Thus, lower dNTP levels might increase DNA replication fidelity presumably by diminishing the next-nucleotide effect and therefore promoting DNA polymerase proofreading. Second, as TLS polymerases require high dNTP concentrations, low dNTP pools may restrict the contribution of error-prone TLS polymerases to overall DNA synthesis to those situations in which they are absolutely required (PRAKASH AND PRAKASH 2002; LANGE *et al.* 2011). Third, high activity of the ribonucleotide reductase (RNR) complex, the rate limiting enzyme in the *de novo* synthesis of dNTPs (NORDLUND AND REICHARD 2006), may cause accumulation and incorporation of potentially mutagenic dUTP in situations in which dTTP synthesis is impaired (HU *et al.* 2012; CHEN *et al.* 2016). Fourth, increased dNTP pools in G1 result in a delayed S-phase entry in budding yeast (CHABES AND STILLMAN 2007) and mammalian cells (FRANZOLIN *et al.* 2013). However, the mechanism is not understood. Finally, a longer S phase may give sufficient time to not only replicate the genetic, but also the epigenetic information with high accuracy (PAI AND KEARSEY 2017).

However, also dNTP deficiency can lead to impaired chromatin replication (JASENCAKOVA AND GROTH 2010; PAPADOPOULOU *et al.* 2015) and prevent high-fidelity DNA replication (BESTER *et al.* 2011). So, low dNTP pools can result in increased misincorporation of ribonucleotides (WANROOIJ *et al.* 2017), stalled replication forks and underreplicated regions which can lead to anaphase bridges and chromosome loss (MAGDALOU *et al.* 2014). Thus, dNTP levels are a critical parameter for high-fidelity DNA replication that balances replication fork progression and DNA proofreading.

In addition to dNTP levels also the balance between the different dNTP pools is of outmost importance for high-fidelity DNA replication. In *in vitro* DNA replication reactions, imbalanced dNTP pools not only result in increased base pair substitutions (ROBERTS AND KUNKEL 1988; MARTOMO AND MATHEWS 2002) but also promote the generation of frameshift mutations (BEBENEK *et al.* 1992). Furthermore, dNTP pool imbalances *in vivo* lead to increased mutagenesis and characteristic changes in the mutation spectra in *E. coli* (LU *et al.* 1995; MILLER *et al.* 2002; TSE *et al.* 2016), *S. cerevisiae* (KUMAR *et al.* 2010; KUMAR *et al.* 2011; WATT *et al.* 2016) and mammalian cells (WEINBERG *et al.* 1981; TRUDEL *et al.* 1984; WEINBERG *et al.* 1985; MATTANO *et al.* 1990; RENTOFT *et*

al. 2016). Thus, the relative ratio between different dNTPs influences DNA polymerases' nucleotide selectivity and impacts on DNA replication fidelity. However, why certain dNTP imbalances are more mutagenic than others, is still not fully understood.

1.6 *de novo* dNTP biosynthesis

Given the importance of dNTP pool homeostasis for DNA replication fidelity, dNTP biosynthesis is highly regulated (Fig. 1.6)(GUARINO *et al.* 2014). In *S. cerevisiae* dNTP pools are maintained exclusively by *de novo* dNTP biosynthesis in the cytoplasm, whereas in mammalian cells dNTP salvage pathways also contribute to the total dNTP pools (MATHEWS 2015; PAI AND KEARSEY 2017). The master regulator of the *de novo* dNTP biosynthesis and dNTP pools is the RNR complex, which catalyzes the reduction of ribonucleoside diphosphates (NDPs) to their corresponding deoxyribonucleoside diphosphates (dNDPs) (NORDLUND AND REICHARD 2006; GUARINO *et al.* 2014). Next, NDP kinase (Ynk1) phosphorylates dNDPs to the corresponding dNTPs (JONG AND MA 1991; TSUNEHIRO *et al.* 1993). Whereas dATP, dGTP and dCTP are direct substrates for high-fidelity DNA synthesis, dUTP has to be further converted to dTTP. For this, dUTPase (Dut1) dephosphorylates dUTP to dUMP (GADSDEN *et al.* 1993). Next, thymidylate synthase (Cdc21) catalyzes the reductive methylation of dUMP to dTMP (TAYLOR *et al.* 1982). dTMP is than subsequently phosphorylated to dTTP by thymidylate kinase (Cdc8) (KUO AND CAMPBELL 1983; JONG *et al.* 1984) and NDP kinase. Furthermore, dCMP deaminase (Dcd1) balances dCTP and dTTP pools downstream of RNR by converting dCMP to dUMP (MCINTOSH AND HAYNES 1984). Consequently, dCTP pools are increased and dTTP pools decreased in the absence of Dcd1 (KOHALMI *et al.* 1991; SANCHEZ *et al.* 2012)

1.7 The ribonucleotide reductase

The RNR complex is essential for the *de novo* dNTP biosynthesis in all living organisms. In eukaryotes, the minimal RNR complex ($\alpha_2\beta_2$) is composed of a dimer of two large α subunits (Rnr1-Rnr1 in *S. cerevisiae* and Rrm1-Rrm1 in human) and a dimer of two small β subunits (Rnr2-Rnr4 in *S. cerevisiae* and Rrm2-Rrm2 in human) (NORDLUND AND REICHARD 2006; GUARINO *et al.* 2014). Moreover, *S. cerevisiae* encodes also for an alternative large subunit *RNR3*, which is only weakly expressed under normal growth conditions, but is strongly induced upon DNA replication stress or DNA damage (ELLEDGE AND DAVIS 1990). In contrast to *S. cerevisiae*, the expression of an alternative small subunit p53R2 is induced by p53 upon DNA damage in mammals (TANAKA *et al.* 2000; GUITTET *et al.* 2001).

While the small RNR subunits stabilize the diferric-tyrosyl radical cofactor which is required to initiate the radical driven reduction of NDPs at the catalytic site (C-site), each large subunit contains one C-site as well as two allosteric sites - the activity site (A-site) and the specificity site (S-site) (Fig. 1.7A) (NORDLUND AND REICHARD 2006). The A-site, which is located at the N-terminus of Rnr1, regulates the overall activity of RNR by binding ATP or dATP. ATP binding to the A-site stimulates RNR activity, whereas dATP acts as negative feedback inhibitor by inducing the formation of inactive $\alpha_6\beta_2$ oligomers in yeast and human RNR (Fig. 1.7C) (FAIRMAN *et al.* 2011).

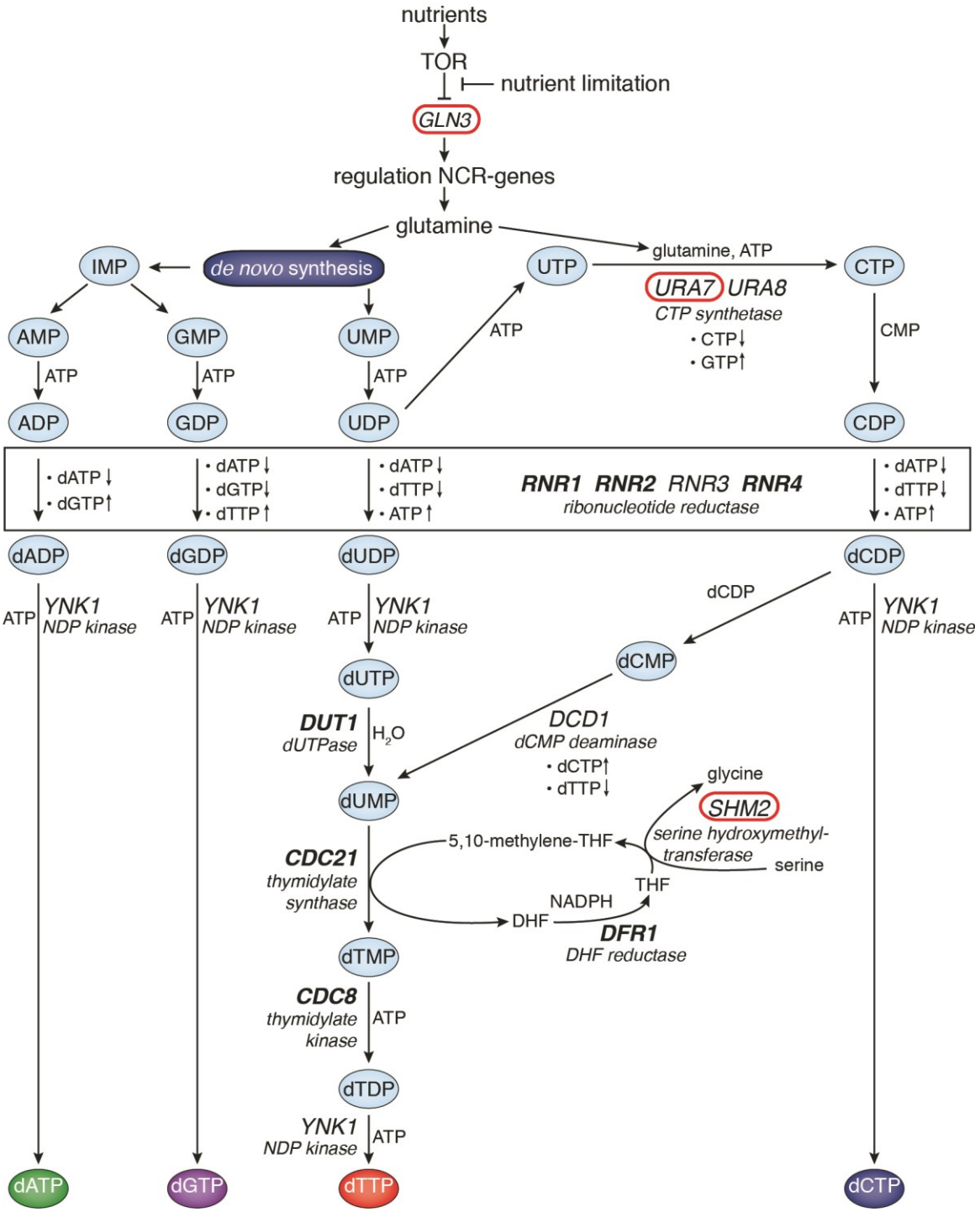

Fig. 1.6 The *de novo* dNTP biosynthesis pathway in *S. cerevisiae*.
Metabolic genes identified in the genome-wide screen are encircled in red. Figure was adapted from (MATHEWS 2015) and (SCHMIDT *et al.* 2017).

Consequently, the expression of a *rnr1* allele (*rnr1-D57N*) in *S. cerevisiae* that lacks dATP feedback inhibition results in an overall increase in dNTP levels, a mild mutator phenotype and an increased resistance to exogenous DNA damage (CHABES *et al.* 2003). The S-site regulates the balance between the different dNTP pools by sensing three out of the four dNTPs and priming the C-site for binding to specific NDP substrates. So, binding of dATP or ATP to the S-site promotes the reduction of CDP and UDP at the C-site, whereas dTTP and dGTP binding to the S-site facilitates the reduction of GDP and ADP, respectively (Fig. 1.7B). Two conserved flexible loops

play important functions in the S-site allosteric regulation of RNR: loop 1 interacts with the bound dNTP effector at the S-site and loop 2 interconnects the S-site of one subunit with the C-site of the other subunit (XU *et al.* 2006a). Based on the RNR crystal structure, loop 2 has been proposed to be critical for dNTP homeostasis (XU *et al.* 2006a). In line with this, expression of *rnr1* alleles in *S. cerevisiae* carrying point mutations in the loop 2 cause severe dNTP imbalances, increased mutator phenotypes and in some cases growth defects and S-phase checkpoint activation (KUMAR *et al.* 2010; KUMAR *et al.* 2011).

In addition to the intrinsic allosteric regulation of RNR, its activity and dNTP pools are controlled on three other levels in *S. cerevisiae* (Fig. 1.7D): First, RNR gene expression peaks during S phase (ELLEDGE AND DAVIS 1990; ELLEDGE *et al.* 1993; TSAPONINA *et al.* 2011) and is otherwise transcriptionally repressed by Crt1 (HUANG *et al.* 1998). Second, the small unstructured protein Sml1 acts as an RNR inhibitor by directly binding to Rnr1 at equimolar concentrations (CHABES *et al.* 1999; ZHAO *et al.* 2000). Third, outside S phase Dif1 shuttles Rnr2-Rnr4 into the nucleus (LEE *et al.* 2008) where Wtm1 acts as a nuclear anchor for the heterodimer (LEE AND ELLEDGE 2006; ZHANG *et al.* 2006). In this way, the large and small subunits of RNR are spatially separated in the cytoplasm and nucleus, respectively, and cannot form an active cytoplasmic complex.

Recently, another small unstructured protein Hug1 has been implicated to negatively regulate RNR in *S. cerevisiae*. Hug1 binds to Rnr2 and promotes the dissociation of the RNR tetramer. This way, Hug1 suppresses RNR activity and may prevent excessive dNTP pool expansion after completed DNA replication or repair (AINSWORTH *et al.* 2013; MEURISSE *et al.* 2014).

In mammalian cells, dNTP pools are even more strictly regulated and actively downregulated outside S phase by the dNTP triphosphohydrolase sterile alpha motif and histidine-aspartate domain-containing protein 1 (SAMHD1) (POWELL *et al.* 2011; FRANZOLIN *et al.* 2013). Elevated dNTP levels outside S phase in mammalian cells promote viral DNA replication (GOLDSTONE *et al.* 2011; LAGUETTE *et al.* 2011) and genome instability (GUARINO *et al.* 2014; KOHNKEN *et al.* 2015). Accordingly, mutations in SAMHD1 as well as reduced SAMHD1 expression levels have been reported in several cancers (KOHNKEN *et al.* 2015; RENTOFT *et al.* 2016).

dNTP pools are upregulated upon DNA damage or DNA replication stress as part of the DNA damage response (DDR) (CICCIA AND ELLEDGE 2010; PARDO *et al.* 2017) in bacteria (GON *et al.* 2011), yeast (CHABES *et al.* 2003) and to a lesser extend in mammalian cells (HÅKANSSON *et al.* 2006b; ZHANG *et al.* 2011). In *S. cerevisiae*, Mec1 phosphorylates the mediators Rad9 or Mrc1, which phosphorylate the effector kinase Rad53 on multiple sites. One function of Rad53 is the activation the Dun1 kinase that phosphorylates the inhibitors of RNR (Sml1, Crt1 and Dif1) and mark them for degradation (PARDO *et al.* 2017). Consequently, RNR expression levels, in particular Rnr2, Rnr3 and Rnr4, and RNR activity raise leading to increased dNTP pools. Elevated dNTP pools facilitate DNA fork re-start and DNA synthesis by TLS polymerases to bypass replication obstacles. Moreover, elevated dNTP pools supply DNA repair processes with sufficient dNTPs in particular outside S phase (PAI AND KEARSEY 2017). In conclusion, RNR plays a key role for dNTP pool homeostasis and its regulation allows fine tuning of dNTP biosynthesis during normal DNA replication as well as under DNA damage conditions. Hence, inhibitors of RNR, like hydroxyurea

(HU) or gemcitabine, are potent chemotherapeutics (XU *et al.* 2006b; WANG *et al.* 2007; WANG *et al.* 2009; AYE *et al.* 2014).

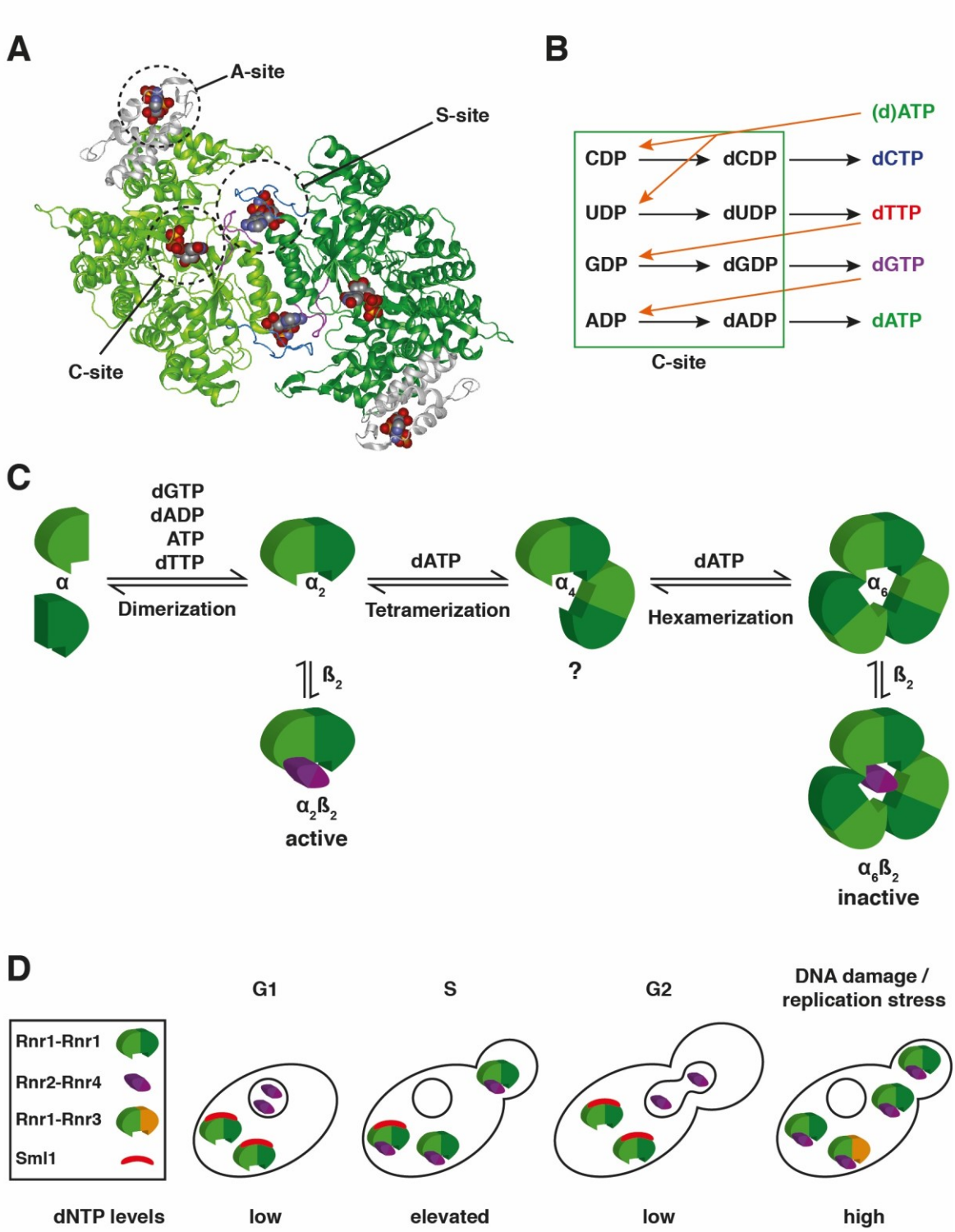

Fig. 1.7 Regulation of ribonucleotide reductase in *S. cerevisiae*.
(A) Model of the Rnr1-Rnr1 homodimer based on the crystal structure (PDB: 2cvv and 3hne). The catalytic site (C-site) and the two allosteric sites, the activity site (A-site) and the specificity site (S-site), are labeled in one subunit. Loop 1 and the loop 2 are colored in blue and violet, respectively. (B) Schematic representation of the regulation of the C-site by the S-site. Depending on which dNTP (right) binds to the S-site, the C-site is primed for a specific NDP substrate (indicated by the orange arrows). (C) Model for the regulation of RNR overall activity by the A-site. Upon nucleotide binding to the S-site two large subunits (α) (green) form a dimer. Together with a small subunit (β) dimer (violet) the minimal active RNR ($\alpha_2\beta_2$) is assembled. dATP binding to

the A-site induces catalytic inactive RNR hexamers. In the process of hexamerization a short-lived tetrameric intermediate (marked with ?) has been postulated. Figure panel was modified from (FAIRMAN *et al.* 2011). (D) *S. cerevisiae* RNR activity throughout the cell cycle and upon DNA damage and replication stress. In G1 and G2 phase, the RNR dimers are spatially separated and Sml1 inhibits Rnr1-Rnr1 dimers. Consequently, dNTP levels are low. During S phase Sml1 levels are reduced, functional cytoplasmic RNR complexes are formed and dNTP pools are elevated. Upon damage or replication stress, the DNA damage checkpoint induces the expression of RNR subunits and the degradation of negative regulators of RNR, which results in high dNTP pools.

1.8 Folate one-carbon metabolism

The one-carbon metabolism is central for various biosynthetic processes including the biosynthesis of dTMP, purines, amino acids, vitamins, and formyl-methionyl-tRNA (fMet-tRNA), which is required for the initiation of bacterial, chloroplast and mitochondrial protein biosynthesis (APPLING 1991; DUCKER AND RABINOWITZ 2017).

All of these processes have in common that the interconvertible folate cofactors serve as one-carbon donors (STOVER AND FIELD 2011). Consequently, due to the fundamental role of folates in promoting cell proliferation and growth, antifolate drugs have been developed and are widely used as chemotherapeutics, in the treatment of chronic autoimmune diseases and as drugs against bacterial or parasite infections (VAN TRIEST *et al.* 2000; NZILA 2006; CHATTOPADHYAY *et al.* 2007; VISENTIN *et al.* 2012; MURIMA *et al.* 2014).

Folate cofactors differ in the oxidation state and position of the one-carbon unit that is either bound to N^5, N^{10} or both of tetrahydrofolate (THF) (Fig. 1.8A) (STOVER AND FIELD 2011). In eukaryotic cells, the folate one-carbon metabolism is highly compartmentalized (Fig. 1.8B)(APPLING 1991; STOVER AND FIELD 2011). In the mitochondria, the one-carbon metabolism is required for glycine biosynthesis, formylation of the initiator tRNA and the production of formate for the cytoplasmic one-carbon metabolism. In the cytoplasm, one-carbon metabolism facilitates the *de novo* synthesis of purines and thymidylate as well as the remethylation of homocysteine to methionine (FOX AND STOVER 2008). Moreover, serine and glycine can be interconverted in the mitochondria and cytoplasm by compartment-specific isoforms of serine hydroxymethyl transferase (mitochondrial Shm1 and cytoplasmic Shm2)(MCNEIL *et al.* 1994). Furthermore, in both compartments the folylpolyglutamate synthetase (FPGS) (Met7) catalyzes the addition of glutamate chains at the γ-carboxyl residue of folate cofactors under the consumption of ATP (DESOUZA *et al.* 2000). Folate polyglutamylation is critical for the cellular one-carbon metabolism because it increases intracellular retention of folates and enhances the affinity of folates to folate-metabolizing enzymes (SCHIRCH AND STRONG 1989). As FPGS not only modifies folates, but also classical antifolates, increasing as well their cellular retention and toxicity, inactivation of FPGS has been identified as a common resistance mechanism of cancer cells upon antifolate treatment (GONEN AND ASSARAF 2012; VISENTIN *et al.* 2012).

In contrast to most of the bacteria, yeast and plants, which can synthesize folates *de novo*, animals depend on dietary folate intake (DUCKER AND RABINOWITZ 2017). Therefore, insufficient folate intake or defects in one-carbon metabolizing enzymes results in folate deficiency leading to anemia in adult humans and to neural tube and congenital heart defects in the developing embryo (BAILEY AND BERRY 2005; BEAUDIN AND STOVER 2009). Thus, the folate one-carbon metabolism is crucial for cellular proliferation and an attractive drug target for anti-proliferative therapies.

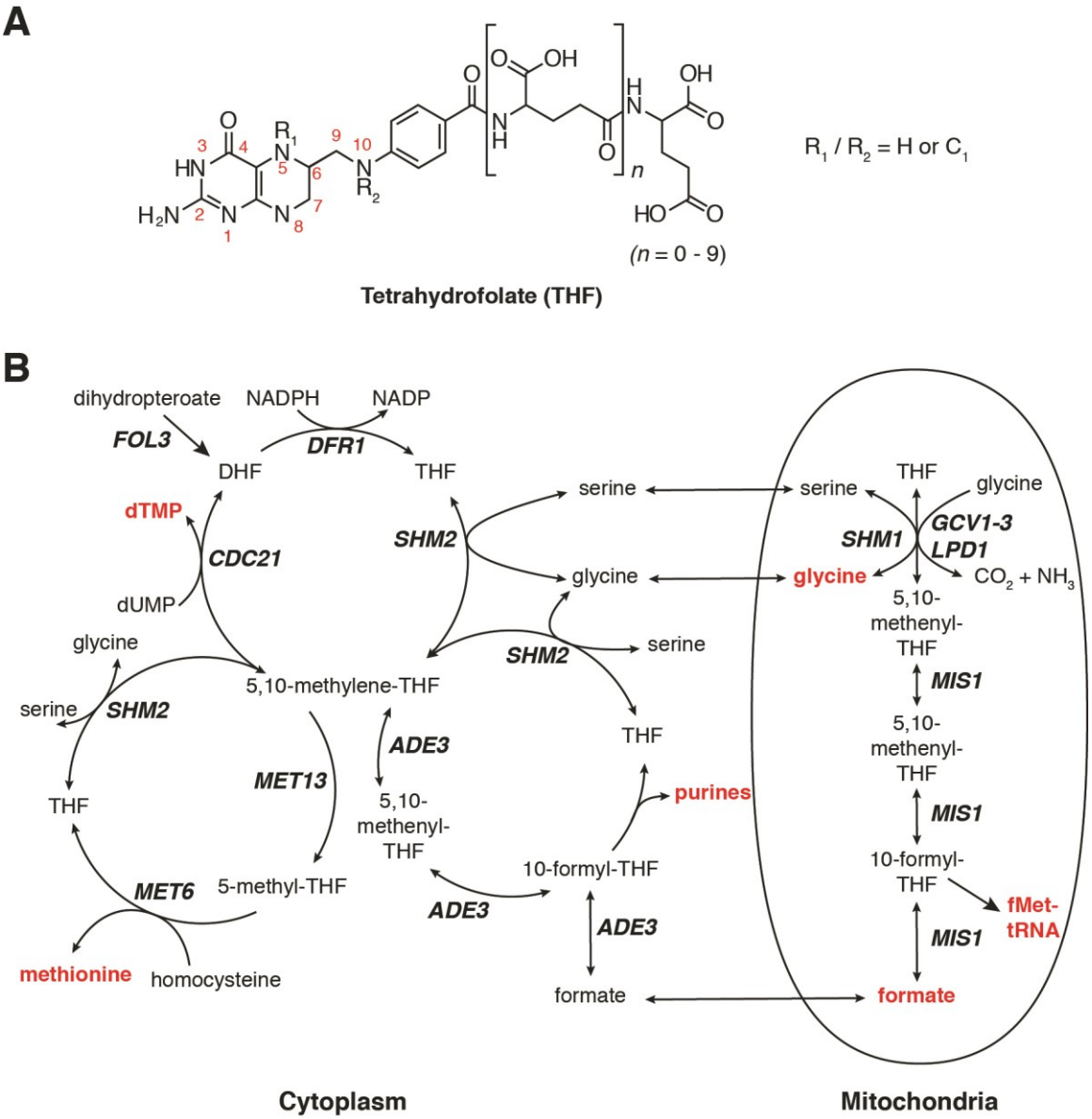

Fig. 1.8 The folate one-carbon metabolism in *S. cerevisiae*.
(A) Structure of tetrahydrofolate (THF). The one-carbon unit is bound either to N^5, N^{10} or both at the R_1 and R_2 position. Intracellular folates are polyglutamylated with variable chain length by FPGS to increase intracellular retention and affinity to folate metabolizing enzymes. (B) Model of folate one-carbon metabolism in *S. cerevisiae*. Folates are utilized in the cytoplasm and in the mitochondria. Metabolic genes are labels in bold and italic. Important products of folate one-carbon metabolism in each compartment are highlighted in bold and red.

1.9 Aim of the study

The interplay between DNA polymerases with high nucleotide selectivity and DNA proofreading functions and the post-replicative MMR mechanism enable cells to replicate their genomes with extremely high accuracy. Furthermore, the level of and balance between the different dNTPs, the building blocks of DNA, influences DNA polymerases' nucleotide selectivity and proofreading function. Defects in any of these DNA replication fidelity mechanisms increase the number of mutations generated during each round of DNA replication. Consequently, mutations in DNA polymerases and in MMR components increase cancer susceptibility (KUNKEL AND ERIE 2015). Moreover, inactivating mutations affecting the DNA polymerase proofreading domain and MMR components cause in human familial colorectal/ovarian cancer (BRIGGS AND TOMLINSON 2013; CHURCH *et al.* 2013; PALLES *et al.* 2013; SHLIEN *et al.* 2015) and the most frequent hereditary cancer predisposition Lynch syndrome (PELTOMAKI 2003; BOLAND AND GOEL 2010), respectively. The latter is characterized by increased mutagenesis in particular at repetitive sequences so called microsatellites. Thus, mutations caused by DNA replication errors are critical drivers of malignancies like cancer (TOMASETTI *et al.* 2017) but also enable evolution.

Interestingly, even though the majority of microsatellite-instable tumors can be linked to the inactivation of Mlh1, Msh2 or Msh6, around 5-10% of the tumors cannot be explained by mutations in or silencing of canonical MMR components (PELTOMAKI 2003) suggesting that additional factors may contribute to the suppression of frameshift mutations. In the past, powerful systematic screens in *S. cerevisiae* revealed many genes that prevent the accumulation of mutations (HUANG *et al.* 2003; SMITH *et al.* 2004), which were than further characterized in detail.

This work investigated DNA replication fidelity mechanisms focusing in particular on the identification of previously unrecognized genes that counteract the acquisition of mutations and moreover on the impact of deregulated dNTP pools on the generation of mutations.

In the first part of this study a genome-wide screen in budding yeast using a modified version of the synthetic genetic array (SGA) (TONG AND BOONE 2006) was performed to identify previously unrecognized non-essential genes that prevent the accumulation of base pair substitutions and frameshift mutations. For this, low-fidelity active-site mutants of the three major eukaryotic DNA polymerases Pol α, Pol δ and Pol ε (*pol1-L868M*, *pol2-M644G* and *pol3-L612M*, respectively) that confer a weak mutator phenotype by themselves were used as "sensitized mutator backgrounds" to detect mutational enhancers that are otherwise buffered in the WT background. Furthermore, according to the "division of labor" model of DNA replication (LUJAN *et al.* 2016), *pol1-L868M*/*pol3-L612M* and *pol2-M644G* are linked to lagging- and leading-strand replication, respectively. Therefore, the screen revealed specific mutator interactions with the leading and lagging-strand alleles that suggest differential dependencies of leading- and lagging strand DNA synthesis and repair on the identified genes. Thus, in the first part of this study, previously unrecognized non-essential genes that prevent the accumulation of mutations were identified and their contribution to DNA replication fidelity characterized.

The second part of this study aimed at elucidating the effect of imbalanced or elevated dNTP levels on DNA replication fidelity in *S. cerevisiae*. As the levels and balance of the dNTP pools influence DNA polymerases' nucleotide selectivity and proofreading activity, dNTP pool alterations cause

increased mutator phenotypes (CHABES *et al.* 2003; KUMAR *et al.* 2010). However, why certain dNTP pool alterations are more mutagenic than others is not understood. To address this question, a collection of PCR-mutagenized *rnr1* alleles was screened for increased mutagenesis under the assumption that the mutator phenotypes of these alleles were caused by alterations in the dNTP concentrations. Next, the effects of the identified mutagenic *rnr1* alleles on the dNTP pools were determined and their impact on DNA replication fidelity further characterized.

Taken together, this study identified previously unrecognized genes that contribute to DNA replication fidelity which potentially act as mini-drivers during human cancer evolution. Furthermore, this study improved the understanding on how different dNTP pool alterations influence DNA replication fidelity in *S. cerevisiae*.

2 MATERIALS

2 MATERIALS

2.1 Equipment

Table 2.1 List of equipment.

Equipment	Supplier
Autoclave Systec DE-65	Systec
Autoclave VAPOR-Line lite	VWR
BioShake XP, 96-Well Vortex	Scientific Industries
Bunsen burner Labogaz 470	Campingaz
Cellgard class III biological safety cabin	NuAire
Centrifuge J2-21M/E	Beckman
Centrifuge 5424	Eppendorf
Centrifuge Heraeus Fresco 21	Thermo Scientific
Centrifuge 5810 R	Eppendorf
Criterion Blotter	Bio-Rad
Disruptor Genie	Scientific Industries
Dri-block pB3	Techne
FACS CantoII	BD Biosciences
Forceps	Roth
Freezer	Liebherr
Fusion Solo S System	Vilber
Gelelectrophoresis chamber	Biozym
Gelelectrophoresis Power Supply, ST606	Gibco BRL Life Technologies
GelDoc system	Bio-Rad
Gene Pulser	Bio-Rad
Grinder	Severin
Ice machine	Hoshizaki
Imaging System	Bio-Rad
Incubator B6420	Hereaus
Incubator Heratherm	Thermo Scientific
Incubator shaker, Ecotron	Infors HT
Incubator shaker, Multitron Pro	Infors HT
Light microscope	Carl Zeiss
Liquidator (96-Well Pipet)	Mettler Toledo
Low temperature freezer	New Brunswick Scientific
Magnetic stirrer with heating, MR Hei-Standard	Heidolph
Microscale, PG 503-S	Mettler-Toledo
Microwave	AEG
Microwave	Sharp
Mini Protean® 3 System	Bio-Rad
Mini Protean® Tetra Cell	Bio-Rad
Multichannel pipette, 20 and 200 µL	Brand Tech Scientific
Multipette Plus	Eppendorf
Optimax TR X-ray film processor	Protec
Peristaltic pump Dosierfix	Welatec
Pharmaceutical refrigerator	Panasonic
pH-Meter, inoLab pH 720	WTW
Pipetboy	IBS Integra Bioscience
Pipetman pipettes 2 µl, 10 µl, 20 µl, 100 µl, 200 µl, 1000 µl	Gilson
Plate sealer (96-well)	4titude
PowerPac basic	Bio-Rad
Replica plating block	DKFZ
Reusable bottle top filter unit	Thermo Scientific Nalgene
Roller RM5 V-80	CAT
RoToR robot	Singer Instruments
Scale, BP 3100 S	neoLab
Scale, DL-501	Denver Instruments
Scalpel	neoLab
Shaker 3015	GFL
Sonicator - Sonifier 250	Branson
Sturdier vertical slab gel electrophoresis chamber	Hofer
Thermocycler C1000 Touch	Bio-Rad
Thermocycler GeneAmp PCR system 9700	Applied Biosystems
Thermomixer comfort and compact	Eppendorf

Transilluminator	Nippon Genetics
UV cabinet	Grant Instruments
UV/Vis Spectrometer, Pharmacia LKB Ultrospec III	Pharmacia
Vioflo II, 8 channel multipipette 12,5 µl	Integra Bioscience
Vortex Genie 2	Scientific Industries
Washing machine	Fagor

2.2 Software

Table 2.2 List of Software.

Software	Supplier
Adobe™ Illustrator™ CS6	Adobe Systems
BD FACSDiva™ Software	Becton Dickinson Biosciences
EndNote X7.7.1	Thomson Reuters, USA
FlowJo, v10.1	Tree Star Inc.
ImageJ, 1.47v	National Institute of Health, USA
Lasergene 12	DNASTAR
Office 2011	Microsoft
OligoCalc http://biotools.nubic.northwestern.edu/OligoCalc.html	Northwestern University
QuikChange® Primer Design Program https://www.genomics.agilent.com/primerDesignProgram.jsp	Agilent
R, v3.3.3	https://www.R-project.org/
Sigma plot	Systat Software Inc.

2.3 Consumables

Table 2.3 List of Consumables.

Consumables	Supplier
Cellulose nitrate filter, pore size 0.45 µm	Sartorius Stedim Biotech
Combitips advanced for Multipette Plus, 5 ml, 10 ml	Eppendorf
Cryotube vials, 1.8 mL	Thermo Scientific
Cuvettes	Brandt
Electroporation cuvettes, 2 mm	Steinbrenner
Filter pipette tips, 10 µL, 200 µL	Neptune
Filter pipette tips, 20 µL, 1000 µL	Greiner Bio-One
Falcon tubes, 14 ml	Greiner Bio-One
Falcon tubes, 50 ml	Greiner Bio-One
Gel Saver II Tip, 200µL	Starlab
Glass beads, 0.5 mm	Scientific Industries
Glass beads, acid wahsed	Sigma
Liquidator tips, 20 µl, 200 µl	Mettler-Toledo
Microscope cover glasses 18x18 mm	Menzel-Gläser
Microscope slides ca./env. 76x26 mm	Menzel-Gläser
4-15% Mini-PROTEAN TGX gels	Bio-Rad
Nitrile gloves	Microflex
PCR tubes 0.2 ml	Thermo Scientific
Petridishes, 60x15 mm	Sarstedt
Petridishes, 94x16 mm	Greiner Bio-One
Petridishes, 145x20 mm	Greiner Bio-One
Picks, flat	Kögler
Precision wipes	Kimtech Science
RoToR Plus Plates	Singer
PolyPrep® Chromatograhy column	Bio-Rad
Tips, 10 µl, 200 µl, 1000 µl	Starlab
Reaction tubes, 0.5 mL	Sarstedt
Reaction tubes, SafeSeal 1,5 ml, 2 ml	Sarstedt
Super RX-N Fuji medical x-ray films	Fujifilm
Tubes, round-bottom, 14 mL	Greiner Bio-One
96-Well Plate lids	Greiner Bio-One
96-well plate seal, aluminum	4titude
96-well plate seal, breathable	4titude

96-Well Plates, U-bottom	Greiner Bio-One
Chromatography paper 3MM Chr	Whatman

2.4 Kits

Table 2.4 List of Kits.

Kit	Order number	Supplier
Gentra Puregene Yeast/Bact. Kit B	158567	Qiagen
Immobilon Western chemiluminescent HRP substrate	WBKL S0500	Millipore
QIAprep Spin Miniprep Kit	27106	Qiagen
QIAquick Gel Extraction Kit	28706	Qiagen

2.5 Chemicals and reagents

Table 2.5 List of chemicals and reagents.

Name	Order number	Supplier
Acetic acid	A0820	AppliChem
Acrylamide-bisacrylamide solution, 40% (29:1)	10680	Serva Electrophoresis
Adenine	A8626	Sigma
Adenosine 5-triphosphate (ATP) disodium salt hydrate	A26209	Sigma
α-factor	RP01002	GenScript
Ammonium persulfate (APS)	13375	Serva Electrophoresis
Agar-agar, Kobe I	5210	Roth
Agarose	3810	Roth
Ampicilin	1046	Gerbu
Arginine	A5006	Sigma
Aspartic acid	A9256	Sigma
β-mercaptoethanol	M6250	Sigma
Butane / propane	CV470	Campingaz
cOmplete EDTA free protease inhibitor	1169749001	Roche Diagnostics
Bacto™ peptone	211820	Becton, Dickinson
Bacto™ yeast extract	212720	Becton Dickinson
Bovine serum albumin (BSA)	A7030	Sigma
Bromophenol blue	15375	Serva Electrophoresis
L-canavanine sulfate	C9758	Sigma
Coomassie brilliant blue G250	17524	Serva Electrophoresis
Cycloheximide	10700	Serva Electrophoresis
Difco™ agar	214530	Becton Dickinson
Difco™ nutrient broth	231000	Becton Dickinson
Difco™ yeast nitrogen base without amino acids	291930	Becton Dickinson
Difco™ yeast nitrogen base without amino acids without ammonium sulfate	233420	Becton Dickinson
Dimethyl sulfoxide (DMSO)	D8418	Sigma
dNTP sets, 100 mM each	M3015	Genaxxon
Dithiothreitol (DTT)	6908	Roth
Ethanol	E/0650DF/15	Fisher Scientific
Ethylenediaminetetraacetic acid (EDTA)	1034	Gerbu
5-Fluoroorotic acid monohydrate (5-FOA)	F5050	Biomol
GelRed™ nucleic acid gel stain	M3199	Genaxxon
Geneticin (G418) sulfate	sc-29065B	Santa Cruz Biotechnology
D(+)-glucose monohydrate	6887	Roth
Glycerol	15523	Sigma
Glycine	G7126	Sigma
Glutamic acid monosodium salt	49621	Sigma
Histidine	H8000	Sigma
Hydrochloric acid, 37%	20252	VWR Chemicals
Hydroxyurea, 98%	H8627	Sigma
Hygromycin B, 50 mg/mL	10687010	Thermo Scientific
Imidazole	I0125	Sigma
Isoleucine	I2752	Sigma
Isopropanol	6752	Roth
Kanamycin sulfate from *Streptomyces kanamyceticus*	K4000	Sigma

Leucine	L8000	Sigma
Lithium acetate dihydrate	L4158	Sigma
Lysine	L5501	Sigma
Magnesium chloride	M2670	Sigma
Methanol	M/4000/PC17	Fisher Scientific
Methionine	M9625	Sigma
Ni-NTA agarose	30210	Qiagen
Nocodazole	T2802	Target Molecule
Nourseothricin, clonNAT	5.0000	Werner BioAgents
NP-40, IGEPAL® CA-630	56741	Sigma
Phenol:Chloroform:Isoamylalcohol (25:24:1)	A156	Roth
Phenylalanine	P2126	Sigma
Phleomycin from *Streptomyces verticillus*	P9564	Sigma
Phenylmethylsulfonyl fluoride (PMSF)	6367	Roth
Poly(ethylene glycol), 3350	88276	Sigma
Potassium acetate	P1190	Sigma
Potassium dihydrogen phosphate	4873	Merck
Salmon sperm	AM9680	Invitrogen
Skim milk powder	70166	Sigma
Sodium acetate	106268	Merck
Sodium azide	S8032	Sigma
Sodium chloride	31434	Sigma
Sodium citrate	71405	Fluka
Sodium dodecyl sulfate (SDS)	1610302 / 20765	Bio-Rad / Serva Electrophoresis
Sodium hypochlorite solution, 12% Cl	9062	Roth
Sodium hydroxide	2020	Gerbu
Sodium dihydrogen phosphate	T878	Roth
di-Sodium hydrogen phosphate·2H_2O	4984	Roth
Sytox Green	S7020	Life Technologies
TEMED	T7024	Sigma
Threonine	T8625	Sigma
Trichloroacetic acid (TCA)	A1431	AppliChem
Triton X-100	T8787	Sigma
Trizma® base	T1503	Sigma
Tryptone	70172	Sigma
Tryptophan	T8941	Sigma
Tween-20	P1379	Sigma
Tyrosine	T3754	Sigma
Uracil	U0750	Sigma
Valine	V0500	Sigma

2.6 Markers for electrophoresis

Table 2.6 Markers for electrophoresis.

Marker	Order number	Supplier
GeneRuler 1Kb, ready-to-use	SM0313	Thermo Scientific
Precision Plus Protein™ Dual Color Standards	#1610394	Bio-Rad

2.7 Oligonucleotides

All oligonucleotides were purchased by Sigma, dissolved in HPLC-H_2O at a concentration of 100 µM.

Table 2.7 List of oligonucleotides.

HHP#	Name	Sequence 5'-3'
507	Can1Fx	GTTGGATCCAGTTTTTAATCTGTCGTC
508	Can1Rx	TTCGGTGTATGACTTATGAGGGTG
1018	Nat_fw1	CTAATCTCGAGGCGAATTTC
1036	Kan_K2	GTCAAGACTGTCAAGGAGGG
1037	kl-TRP1_rev	GACGTTGTTCGATTCTGGTG
1038	kl-TRP1_fw	CAACGGTTTGCAAACCACAC

1062	CYH2_3v	GGCTTCCAGATGTTAACTGC
1063	CYH2_fw	GAACAGTCATACTGTCTACTC
1100	rnr1_3v	GCGCATCCTGGGAATCTA
1276	POL1_L868M_fw	GTTTTAGTCATGGACTTTAATTCTATGTATCCATCTATTATCCAGGAATTT
1277	POL1_L868M_rev	AAATTCCTGGATAATAGATGGATACATAGAATTAAAGTCCATGACTAAAAC
1378	Kan_K3	CGCCTCGACATCATCTGCCC
1380	hph_JE345fw	GGCTGTGTAGAAGTACTCGCCG
1381	his3_5'test	CATTTGTAATACGCTTTACTAGGGC
1382	his3_3'test	CGCATTTTCTTGAAAGCTTTGCAGAG
1872	pRS425_GAL_PMS1-FLAG_rev	GCAAGTGTAGCGGTCACGC
1949	pMFA1_kl-LEU2_fw	AACTGTTTCTCGGATAAAACCAAAATAAGTACAAAGCCATCGAATAGAAATGTCTAAGAATATCGTTGTC
1950	pMFA1_kl-LEU2_rev	AGCGGAAAAGGAAGATAAAGGAGGGAGAACAACGTTTTTGTACGCAGAAATTAAGCCAAGATTTCCTTGA
1955	hom3-10.HIS3_fw	ATCCACCTTTCTTCTTCACTTTAATGATAGAATATTAATTTTCCCTTTATGAGCAGATTGTACTGAGAGTGCACC
1956	hom3-10.HIS3_rev	ATTAATATATATGTAAATATATGTGCGCGTATATATATATATATATATATCTCCTTACGCATCTGTGCGGTATTTC
2001	pMFA1-klLEU2.hphLYS2_rev	GGCGCGCCTTAATTAACCCGGGGATCCGTCGACCTGCAGCGTACGGATCCGCAGGCTAACCGGAA
2002	LYS2.hph_S1_300pb before ATG	GTCTATATTCATTGAAACTGATTATTCGATTTTCTTCTTGCTGACCGTACGCTGCAGGTCGAC
2003	LYS2.hph_S2_before ATG	TTGAAGAGTTTTCCTCGCTAAAACTGTGCGATGCCTCTAGAAGCGATCGATGAATTCGAGCTCG
2004	pMFA1-klLEU2.300pb_hphLYS2_fw	GTCTATATTCATTGAAACTGATTATTCGATTTTCTTCTTGCTGACCAGGATAGTGTGCAACGTGG
2197	URA3_5v	GGGAAGACAAGCAACGAAAC
2198	URA3_3v	GGAAACGCTGCCCTACAC
2201	kl-URA3_fw	TGATTTTGTGGACATGGTGC
2202	kl-URA3_rev	GTTGGCAGAGGACTTTTCG
2220	kl-URA3_downMlh2_fw	CTCTAATATTGCATTGTTACGACATCCTGTTGTCATGCGACTAAACAATACAACAGATCACGTG
2657	met7_S1	ATTGTCTTATTTCTGAAGCTCACTGAAGAACATTGCTTTATTATGCGTACGCTGCAGGTCGAC
2797	scPOL3_NotI_fw	CTGACTGCGGCCGCTCTTCGTTCAACTTGTTTTCCTTG
2798	scPOL3_SmaI_rev	GGTGACCCCGGGGTTTACAAATTACTGACAATAAA
2801	met7DM_S4	CAAAGAGTTTAGCGCAGTAACAGCGTCTCGATAAGTTTTTCCAACCATCGATGAATTCTCTGTCG
2876	URA3_fw	CGAAAGCTACATATAAGGAAC
2877	URA3_rev	TTAGTTTTGCTGGCCGCATC
2947	URA3_seq	GGAGCACAGACTTAGATTGG
2973	CAN1_rev	GAGCCAATGTAGAAGGTTAAG
2974	CAN1_fw2	CCTCTTTGATTAACGCTGCC
2976	RNR1_fw_promoter	CAGCTCAGTCACATGAGAC
3285	pRS315_rev	CGATTCATTAATGCAGCTGGC
3489	rnr1-R256Q_fw	GTATTGGTCTACATATCCATAACATTCAATCAACTGGTTCTTACATTGCTGG
3490	rnr1-R256Q_rev	CCAGCAATGTAAGAACCAGTTGATTGAATGTTATGGATATGTAGACCAATAC
3574	RNR1_D57N_fw	GGTGTCACAACAATCGAACTAAACAACTTAGCCGCTG
3575	RNR1_D57N_rev	CAGCGGCTAAGTTGTTTAGTTCGATTGTTGTGACACC
3678	CAN1_downstream_S1	ACCAAAGACTTTTTGGGACAAATTTTGGAATGTTGTAGCATAGATATGACCGTACGCTGCAGGTCGAC
3679	CAN1.downstream_S2	ATGAGGGTGAGAATGCGAAATGGCGTGGAAATGTGATCAAAGGTAATAAAACATCGATGAATTCGAGCTCG
3700	pRS_RNR1linked_fw	GTCGAATAATTTAACATGAACATTTTAAGCTGTCCTTGTAAGAAGGCGAGCAGATTGTACTGAGAGTGCACC
3701	pRS_RNR1linked_rev	CAATGTTGCCTAGACCCCATTTCGGGGCAGGGGGGAATCTGTATCATGCTCCTTACGCATCTGTGCGGTATTTC
3861	RNR1-I262V_fw	CATTCGTTCAACTGGTTCTTACGTTGCTGGTACAAACGGTACTTC
3862	RNR1-I262V_rev	GAAGTACCGTTTGTACCAGCAACGTAAGAACCAGTTGAACGAATG
3863	RNR1-N291D_fw	CCGTTATGTTGACCAGGGTGGTGATAAAAGACCTGGTGCGTTTGC
3864	RNR1-N291D_rev	GCAAACGCACCAGGTCTTTTATCACCACCCTGGTCAACATAACGG
4105	URA3_A4	TCATTACGACCGAGATTCC
4196	DUT1_promoter_BamHI_fw	CATGATGGATCCCATGCCCCATCTCCACGCTC
4197	DUT1_3v	CAGACCCTATTAGGAGCCC

4198	DUT1_G82S_fw	GAAAAACGGTATCCAAACCGGTGCTAGTGTTGTCGACAGAGATTACACCGG
4199	DUT1_G82S_rev	CCGGTGTAATCTCTGTCGACAACACTAGCACCGGTTTGGATACCGTTTTTC

2.8 Plasmids

All plasmids were stored in *E. coli TOP10F'* or *E. coli BL21 (DE3)* as glycerol stock at -80 °C. Minipreps were purified with QIAprep Spin Miniprep Kit and stored at -20 °C.

Table 2.8 Plasmids used in the study.

Name	Relevant genotype	*rnr1* base substitution (s)	Reference
pFA6a-hphNT1	*amp^r hphNT1*	none	(JANKE *et al.* 2004)
pFA6a-kanMX4	*amp^r kanMX4*	none	(WACH *et al.* 1994)
pFA6a-natNT2	*amp^r natNT2*	none	(JANKE *et al.* 2004)
pOM13	*amp^r loxP.klLEU2.loxP.6HA*	none	(GAUSS *et al.* 2005)
pRS303	*amp^r HIS3*	none	(SIKORSKI AND HIETER 1989)
pUG72	*amp^r loxP.klURA3.loxP*	none	(GUELDENER *et al.* 2002)
pUG73	*amp^r loxP.klLEU2.loxP*	none	(GUELDENER *et al.* 2002)
pYM22	*amp^r 3HA.klTRP1*	none	(JANKE *et al.* 2004)
pYM23	*amp^r 3Myc.klTRP1*	none	(JANKE *et al.* 2004)
pYM-N14	*amp^r kanMX4.pGPD*	none	(JANKE *et al.* 2004)
pYM-N15	*amp^r natNT2.pGPD*	none	(JANKE *et al.* 2004)
pHHB296	*pSIC1_SIC1(NTR)_3MYC_(GA)5 (ampR, natNT2, pSIC1-sic1^{NTR}(aa1-100)-3Myc-(GA)5)*	none	This study
pRS316	*amp^r CEN6 ARSH4 URA3*	none	(SIKORSKI AND HIETER 1989)
pHHB388	*pRS316-POL3* (*amp^r*, *CEN6, ARSH4, URA3*)	none	(SCHMIDT *et al.* 2017)
pHHB560	*pRS316-RNR1* (*amp^r*, *CEN6, ARSH4, URA3*)	none	This study
pRS315	*amp^r CEN6 ARSH4 LEU2*	none	(SIKORSKI AND HIETER 1989)
pHHB351	*pRS315-POL3 (amp^r*, *CEN6, ARSH4, LEU2*)	none	(SCHMIDT *et al.* 2017)
pHHB396	*pRS315-pol3-01 (amp^r*, *CEN6, ARSH4, LEU2*)	none	(SCHMIDT *et al.* 2017)
pHHB561	*pRS315-RNR1* (*amp^r*, *CEN6, ARSH4, LEU2*)	none	This study
pHHB649	*pRS315-rnr1-G8D,V278A* (*amp^r*, *CEN6, ARSH4, LEU2*)	c.23G > A, c.833T > C	This study
pHHB632	*pRS315-rnr1-F15S* (*amp^r*, *CEN6, ARSH4, LEU2*)	c.44T > C	This study
pHHB635	*pRS315-rnr1-D226G* (*amp^r*, *CEN6, ARSH4, LEU2*)	c.677A > G	This study
pHHB648	*pRS315-rnr1-D226V* (*amp^r*, *CEN6, ARSH4, LEU2*)	c.677A > T	This study
pHHB655	*pRS315-rnr1-S117P,D226N* (*amp^r*, *CEN6, ARSH4, LEU2*)	c.349T > C, c.676G > A	This study
pHHB650	*pRS315-rnr1-I231T,T244A* (*amp^r*, *CEN6, ARSH4, LEU2*)	c.692T > C, c.730A > G	This study
pHHB634	*pRS315-rnr1-S242T* (*amp^r*, *CEN6, ARSH4, LEU2*)	c.724T > A	This study
pHHB628	*pRS315-rnr1-K243E* (*amp^r*, *CEN6, ARSH4, LEU2*)	c.727A > G	This study
pHHB647	*pRS315-rnr1-T244I,V278A* (*amp^r*, *CEN6, ARSH4, LEU2*)	c.731C > T, c.833T > C	This study
pHHB651	*pRS315-rnr1-A245V,Q671R* (*amp^r*, *CEN6, ARSH4, LEU2*)	c.734C > T, c.2012A > G	This study
pHHB721	*pRS315-rnr1-A245V* (*amp^r*, *CEN6, ARSH4, LEU2*)	c.734C > T	This study
pHHB630	*pRS315-rnr1-R256H,Y779C* (*amp^r*, *CEN6, ARSH4, LEU2*)	c.767G > A, c.2336A > G	This study
pHHB667	*pRS315-rnr1-R256H* (*amp^r*, *CEN6, ARSH4, LEU2*)	c.767G > A	This study
pHHB668	*pRS315-rnr1-R256Q* (*amp^r*, *CEN6, ARSH4, LEU2*)	c.767G > A, c.768T > A	This study
pHHB642	*pRS315-rnr1-I262T,M275I* (*amp^r*, *CEN6, ARSH4, LEU2*)	c.785T > C, c.825G > A	This study
pHHB678	*pRS315-rnr1-I262V,N291D* (*amp^r*, *CEN6, ARSH4, LEU2*)	c.784A > G, c.871A > T	This study
pHHB677	*pRS315-rnr1-I262V,Q561L* (*amp^r*, *CEN6, ARSH4, LEU2*)	c.784A > G, c.1682A > T	This study
pHHB875	*pRS315-rnr1-I262V* (*amp^r*, *CEN6, ARSH4, LEU2*)	c.784A > G	This study
pHHB637	*pRS315-rnr1-T265A* (*amp^r*, *CEN6, ARSH4, LEU2*)	c.793A > G	This study
pHHB638	*pRS315-rnr1-G267C* (*amp^r*, *CEN6, ARSH4, LEU2*)	c.799G > T	This study
pHHB641	*pRS315-rnr1-S269P* (*amp^r*, *CEN6, ARSH4, LEU2*)	c.805T > C	This study
pHHB652	*pRS315-rnr1-G271S* (*amp^r*, *CEN6, ARSH4, LEU2*)	c.811G > A	This study
pHHB653	*pRS315-rnr1-P274L,N466S* (*amp^r*, *CEN6, ARSH4, LEU2*)	c.821C > T, c.1397A > G	This study
pHHB1000	*pRS315-rnr1-P274L* (*amp^r*, *CEN6, ARSH4, LEU2*)	c.821C > T	This study
pHHB636	*pRS315-rnr1-M275T* (*amp^r*, *CEN6, ARSH4, LEU2*)	c.824T > C	This study

pHHB633	*pRS315-rnr1-T282A* (*amp^r*, *CEN6, ARSH4, LEU2*)	c.844A > G	This study
pHHB676	*pRS315-rnr1-R21C,T282S* (*amp^r*, *CEN6, ARSH4, LEU2*)	c.61C > T, c.844A > T	This study
pHHB999	*pRS315-rnr1-T282S* (*amp^r*, *CEN6, ARSH4, LEU2*)	c.844A > T	This study
pHHB654	*pRS315-rnr1-A283V,S425L* (*amp^r*, *CEN6, ARSH4, LEU2*)	c.848C > T, c.1274C > T	This study
pHHB679	*pRS315-rnr1-Y285C* (*amp^r*, *CEN6, ARSH4, LEU2*)	c.854A > G	This study
pHHB876	*pRS315-rnr1-N291D* (*amp^r*, *CEN6, ARSH4, LEU2*)	c.871A > T	This study
pRS306	*amp^r URA3*	none	(SIKORSKI AND HIETER 1989)
pHHB97	*pRS306-pol1-L868M* (*amp^r*, *URA3*)	none	(SCHMIDT *et al.* 2017)
pHHB1093	*pRS306-DUT1* (*amp^r*, *URA3*)	none	This study
pHHB1094	*pRS306-dut1-1* (*amp^r*, *URA3, dut1-G82S*)	none	This study
pHHB424	*pRS306-RNR1* (*amp^r*, *URA3*)	none	This study
pHHB718	*pRS306-rnr1-F15S* (*amp^r*, *URA3*)	c.44T > C	This study
pHHB752	*pRS306-rnr1-D57N* (*amp^r*, *URA3*)	c.169G > A	This study
pHHB869	*pRS306-rnr1-S242T* (*amp^r*, *URA3*)	c.724T > A	This study
pHHB682	*pRS306-rnr1-K243E* (*amp^r*, *URA3*)	c.727A > G	This study
pHHB736	*pRS306-rnr1-A245V* (*amp^r*, *URA3*)	c.734C > T	This study
pHHB868	*pRS306-rnr1-R256H, Y779C* (*amp^r*, *URA3*)	c.767G > A, c.2336A > G	This study
pHHB933	*pRS306-rnr1-I262V, N291D* (*amp^r*, *URA3*)	c.784A > G, c.871A > T	This study
pHHB695	*pRS306-rnr1-Y285C* (*amp^r*, *URA3*)	c.854A > G	This study
pHHB118	*pET28c-Sic1 (kan^R, 6HIS-SIC1)*	none	Gift of G. Pereira

2.9 Enzymes

Table 2.9 List of enzymes.

Enzyme	Order number	Supplier
AccuPrime™ *Pfx* DNA polymerase, 2.5 U/µL	12344	Invitrogen
Ape I, 10 U/µL	M0282	NEB
BamHI-HF, 20 U/µL	R3136	NEB
BglII, 10 U/µL	R0144	NEB
Bsu36I, 10 U/µL	R0524	NEB
Exonuclease I, 20 U/µL	M0293	NEB
HindIII, 20 U/µL	R0104	NEB
KpnI-HF, 20 U/µL	R3142	NEB
Lysozyme	100834	MP Biomedicals
NcoI, 20 U/µL	R0193	NEB
NotI-HF, 20 U/µL	R3189	NEB
Phusion® High-Fidelity DNA polymerase 2 U/µL	M0530	NEB
Proteinase K	M3036	Genaxxon
Ribonuclease A	7156	Roth
Shrimp Alkaline Phosphatase (rSAP), 1 U/µL	M0371	NEB
SacII, 20 U/µL	R0157	NEB
SmaI, 20 U/µL	R0141	NEB
Taq DNA polymerase, 5 U / µL	M0273	NEB
Uracil-DNA Glycosylase (UDG)	M0280	NEB
Velocity DNA polymerase 2 U/µL	BIO-21098	Bioline
XcoI, 20 U/µL	R0146	NEB
Zymolase 100T, 10 mg/mL	Z1005	US biological

2.10 Antibodies

2.10.1 Primary antibodies

Primary antibodies are diluted in either 3% BSA or skim dry milk in PBS-T containing 0.02% sodium azide and 0.001% Thimerosal.

Table 2.10 List of primary antibodies for Western blotting.

Antigen	Species	Clone	Dilution	Order number	Source
Clb2	rabbit	polyclonal	1:1000	sc-9071	Santa Cruz Biotechnology
c-Myc	mouse	9E10	1:1000	05-419	Millipore
Pgk1	mouse	22C5D8	1:20000	459250	Invitrogen
Rad53	mouse	EL7.E1	1:1000	ab166859	Abcam
Rnr1	rabbit	polyclonal	1:60000	AS09576	Agrisera
Rnr2	rabbit	polyclonal	1:30000	AS09575	Agrisera
Rnr3	rabbit	polyclonal	1:1000	AS09574	Agrisera
Sic1	guinea pig	polyclonal	1:10000	-	this study
Tubulin/Rnr4	rat	YL1/2	1:40000	92092402	Sigma

2.10.2 Secondary antibodies

All secondary antibodies are linked to horseradish peroxidase (HRP) and used in a concentration of 1:10000 diluted in 0.5% skim dry milk in PBS-T.

Table 2.11 List of secondary antibodies for Western blotting.

Antigen	Species	Conjugate	Dilution	Order number	Source
guinea pig IgG	rabbit	HRP	1:10000	A60-211P	Bethyl Laboratories
mouse IgG	sheep	HRP	1:10000	NA9310	GE Healthcare
rabbit IgG	donkey	HRP	1:10000	NA934	GE Healthcare
anti-rat IgG	goat	HRP	1:10000	401416	Calbiochem

2.11 Buffers and solutions

If not other mentioned buffers and solutions are done in H_2O.

Table 2.12 List of buffers and solutions.

Buffer and solutions	Composition
APS	10% APS
Ampicillin, 1000x	100 mg/mL ampicillin
Buffer A	2% Triton X-100 1% SDS 100 mM NaCl 10 mM Tris-Hcl pH 8.0 1 mM EDTA pH 8.0
Coomassie destaining solution II	10% acetic acid 20% ethanol
Coomassie fixing and destaining I solution	10% acetic acid 40% ethanol
Coomassie staining solution stock I	0.2% brilliant blue G in 90% ethanol
Coomassie staining solution stock II	20% acetic acid
EDTA, 0.5 M, pH 8.0	0.5 M EDTA in H_2O, pH 8.0
Elution buffer, pH 8.0	50 mM NaH_2PO_4 x H_2O 600 mM NaCl 250 mM imidazole 10 mM β-mercaptoethanol
G418, 1000x	200 mg/mL geneticin
GSD buffer 3x	335 mM DTT 6.7% SDS 33% glycerol tip of bromophenol blue few drops 1M Tris pH 6.
GSD/TRIS buffer, 1x	2 volume GSD buffer, 3x

	1 volume Tris unbuffered 3 volumes H_2O
Kanamycin, 1000x	50 mg/mL kanamycin sulfate
LiAc, 10x	1 M LiAc, pH 7.5
Lysis buffer, pH 8.0	50 mM NaH_2PO_4 x H_2O 300 mM NaCl 20 mM imidazole 10 mM β-mercaptoethanol 0.1% Tween-20 1mM PMSF 1 tablet cOmplete, EDTA free 1 mg/mL Lysozyme
Magnesium chloride, 1M	1 M magnesium chloride
Nourseothricin, 1000x	100 mg/mL nouseothricin
PBS, 10x	1.37 M NaCl 27 mM KCl 82 mM Na_2HPO_4 x 2 H_2O 15 mM KH_2PO_4
PBS-T, 1x	1:10 dilution of 10x PBS in H_2O 0.05% Tween-20
PEG3350, 50%	50% (w/v) PEG3350
PMSF stock, 100x	0.2 M PMSF in isopropanol
Running buffer, 10x	250 mM Tris 1.9 M glycine 10% SDS
Salmon sperm	2 mg/mL salmon sperm 10 mM Tris/HCl, pH 8.0 1 mM EDTA
Sodium citrate, 50 mM	50 mM sodium citrate
SDS, 20%	20% SDS
Separating gel buffer, 4x	1.5 M Tris/HCl pH 8.8
TE, pH 7.5, 10x	1 M Tris/HCl 10 mM EDTA
Sodium azide, 1000x	20% sodium azide
Stacking buffer, 4x	0.5 M Tris/HCl, pH 6.8
TCA, 50%	50% (w/v) TCA
Thimerosal, 1000x	1% thimerosal
Washing buffer, pH 8.0	50 mM NaH_2PO_4 x H_2O 300 mM NaCl 20 mM imidazole 1mM PMSF
Western blot blocking solution	3% skim dry milk in 1x PBS-T
Western blot transfer buffer	25 mM Tris 190 mM glycine 20% (v/v) methanol
YEX buffer	1.95 NaOH 7.5% β-mercaptoethanol

2.12 Media

SD amino acid mix was prepared as described in (AMBERG *et al.* 2005). For the SGA screen, SD amino acid mix was prepared as described in (TONG AND BOONE 2006).

Table 2.13 List of media.

Medium	Composition
CAN plates	0.67% Difco yeast nitrogen base without amino acids 0.8 g/L arginine- amino acid dropout mix 60 mg/L canavanine 2% glucose 2% agar-agar
CAN plates + nourseothricin	0.17% yeast nitrogen base without amino acids and without ammonium sulfate 1 g/L glutamic acid mono sodium salt hydrate 0.8 g/L arginine- amino acid dropout mix 60 mg/L canavanine 100 µg/mL nourseothricin 2% glucose 2% agar-agar
5-FOA plates	0.67% Difco yeast nitrogen base without amino acids 0.8 g/L uracil- amino acid dropout mix 50 mg/L uracil 1 g/L 5-FOA 2% glucose 2% agar-agar
GCR plates	0.67% Difco yeast nitrogen base without amino acids 0.8 g/L arginine- uracil- amino acid dropout mix 60 mg/L canavanine 50 mg/L uracil 1 g/L 5-FOA 2% glucose 2% agar-agar
Minimal plates	0.67% Difco yeast nitrogen base without amino acids 2% glucose 2% agar-agar
SGA diploid selection medium	YPD plates + 200 mg/L G418 + 100 mg/L nourseothricin
SGA double mutant selection plates	SGA haploid selection plates + 1 g/L 5-FOA + 100 mg/L nourseothricin + 10 mg/L cycloheximide
SGA haploid selection plates	0.17% Difco yeast nitrogen base without amino acids and ammonium sulfate 1 g/L glutamic acid monosodium salt 2 g/L leucine- dropout mix (TONG AND BOONE 2006) 2% glucose 200 mg/L G418 2% Difco agar-agar
SGA presporulation plates	3% Difco nutrient broth 1% Bacto yeast extract 5% glucose 2% Difco agar-agar
SGA de-condensation plates	SGA haploid selection plates + 100 mg/L nourseothricin
SGA sporulation plates	1% potassium acetate 0.1% Bacto yeast extract 0.5 g/L glucose 0.05 g amino acid supplement powder for sporulation (mix of 2 g histidine, 10 g leucine, 2 g lysine and 2 g uracil) 50 mg/L G418 2% Difco agar-agar
Sporulation medium, pH 7.0	1% potassium acetate 0.19 g/L amino acid mix CSM
Synthetic dropout (SD) medium	0.67% yeast nitrogen base without amino acids 0.8 g/L amino acid dropout mix

	2% glucose
SD medium plates	SD medium with 2% agar-agar
SD medium for drugs	0.17% yeast nitrogen base without amino acids and without ammonium sulfate 1 g/L glutamic acid mono sodium salt hydrate 0.8 g/L amino acid dropout mix 2% glucose
SD medium plates for drugs	SD medium for drugs with 2% agar-agar
YPD	1% Bacto yeast extract 2% Bacto peptone 2% glucose
YPD plates	YPD with 2% agar-agar
YPG plates	1% Bacto yeast extract 2% Bacto peptone 3% glycerol 2% agar-agar

2.13 *E. coli* strains

Table 2.14 *E. coli* strains used in this work.

Strain	Genotype	Order number	Source
BL21 (DE3)	*E. coli B F- dcm ompT hsdS($r_b^-m_b^-$) galλ(DE3)*	200131	Agilent
TOP10F'	*F´{lac Iq Tn10 (TetR)} mcr A Δ (mrr-hsd RMS-mcr BC) Φ 80lac ZΔ M15 Δlac X74 rec A1 ara D139 Δ (ara-leu)7697 gal U gal K rps L end A1 nup G*	C303003	Invitrogen

2.14 *S. cerevisiae* strains

For the SGA, the non-essential gene deletion collection TKY3503 (Transomic technologies) was used. Yeast strains from this collection correspond to the BY4742 background with the following genotype: *Matα his3Δ1 leu2Δ0 ura3Δ lys2Δ yfg::kanMX4*.

Table 2.15 *S. cerevisiae* strains used in this work.

Name	Relevant genotype	Reference
RDKY3686	*Matα ura3-52 leu2∆1 trp1∆63 hom3-10 his3∆200 lys2-10A*	(AMIN *et al.* 2001)
RDKY5964	*Mata ura3-52 leu2∆1 trp1∆63 hom3-10 his3∆200 lys2-10A*	(HOMBAUER *et al.* 2011a)
HHY6484	RDKY5964 *MFA::klLEU2*	(SCHMIDT *et al.* 2017)
HHY6485	RDKY5964 *hph.300lys2-10A CAN1::URA3*	(SCHMIDT *et al.* 2017)
HHY6486	RDKY5964 *pMFA1-klLEU2.hph.300lys2-10A, can1::URA3*	(SCHMIDT *et al.* 2017)
HHY6487	*RDKY5964 cyh2-Q38K*	(SCHMIDT *et al.* 2017)
HHY6488	*HHY6487 hom3-10.HIS3*	(SCHMIDT *et al.* 2017)
HHY6489	RDKY3686 *pMFA1-klLEU2.hphNT1.lys2-10A, hom3-10.HIS3, cyh2-Q38K*	(SCHMIDT *et al.* 2017)
HHY6490	HHY6489 *MLH2.klURA3*	(SCHMIDT *et al.* 2017)
HHY5298	RDKY5964 *cyh2 Q38K hom3-10.HIS3 pMFA1-klLEU2.hphNT1.lys2-10A MLH2.klURA3 POL1.natNT2*	(SCHMIDT *et al.* 2017)
HHY5292	RDKY5964 *cyh2 Q38K hom3-10.HIS3 pMFA1-klLEU2.hphNT1.lys2-10A MLH2.klURA3 pol1-L868M.natNT2*	(SCHMIDT *et al.* 2017)
HHY5284	RDKY5964 *cyh2 Q38K hom3-10.HIS3 pMFA1-klLEU2.hphNT1.lys2-10A MLH2.klURA3 pol2-M644G.natNT2*	(SCHMIDT *et al.* 2017)
HHY5289	RDKY5964 *cyh2 Q38K hom3-10.HIS3 pMFA1-klLEU2.hphNT1.lys2-10A MLH2.klURA3 pol3-L612M.natNT2*	(SCHMIDT *et al.* 2017)
HHY6370	RDKY5964 *met7::kanMX4*	This study
HHY6441	RDKY5964 *kanMX4.pGPD-DUT1 met7::klTRP1*	This study
HHY6636	RDKY5964 *rev3::natNT2 met7::klTRP1*	This study
HHY6650	RDKY3686 *dut1-G82S*	This study
HHY6707	RDKY5964 *dut1-G82S*	This study

HHY1910	RDKY5964 *rfa1::TRP1 pKU1-t48 (LEU2)*	(CHEN AND KOLODNER 1999)
HHY1794	RDKY5964 *exo1::hphNT1*	(SCHMIDT *et al.* 2017)
HHY6372	RDKY5964 *gln3::HIS3*	(SCHMIDT *et al.* 2017)
HHY6378	RDKY5964 *rrm3::kanMX4*	(SCHMIDT *et al.* 2017)
HHY6374	RDKY5964 *shm2::kanMX4*	(SCHMIDT *et al.* 2017)
HHY6376	RDKY5964 *ura7::kanMX4*	(SCHMIDT *et al.* 2017)
HHY6425	RDKY5964 *dun1::hphNT1*	(SCHMIDT *et al.* 2017)
HHY6517	HHY6425 *gln3::HIS3*	(SCHMIDT *et al.* 2017)
HHY6519	HHY6425 *ura7::kanMX4*	(SCHMIDT *et al.* 2017)
HHY5746	HHY1794 *gln3::HIS3*	(SCHMIDT *et al.* 2017)
HHY5752	HHY1794 *rrm3::kanMX4*	(SCHMIDT *et al.* 2017)
HHY6415	HHY1794 *shm2::kanMX4*	(SCHMIDT *et al.* 2017)
HHY5743	HHY1794 *ura7::kanMX4*	(SCHMIDT *et al.* 2017)
HHY6505	RDKY5964 *msh2::HIS3*	(SCHMIDT *et al.* 2017)
HHY6507	RDKY5964 *msh2::natNT2 gln3::HIS3*	(SCHMIDT *et al.* 2017)
HHY5596	RDKY5964 *msh2::natNT2 rrm3::kanMX4*	(SCHMIDT *et al.* 2017)
HHY6509	RDKY5964 *msh2::natNT2 shm2::kanMX4*	(SCHMIDT *et al.* 2017)
HHY5749	RDKY5964 *msh2::natNT2 ura7::kanMX4*	(SCHMIDT *et al.* 2017)
HHY5195	RDKY5964 *msh3::HIS3*	(SCHMIDT *et al.* 2017)
HHY6511	HHY5195 *gln3::HIS3*	(SCHMIDT *et al.* 2017)
HHY2248	HHY5195 *rrm3::kanMX4*	(SCHMIDT *et al.* 2017)
HHY6513	HHY5195 *shm2::kanMX4*	(SCHMIDT *et al.* 2017)
HHY6515	HHY5195 *ura7::kanMX4*	(SCHMIDT *et al.* 2017)
HHY780	RDKY5964 *msh6::hphNT1*	(SCHMIDT *et al.* 2017)
HHY6419	HHY780 *gln3::HIS3*	(SCHMIDT *et al.* 2017)
HHY2246	HHY780 *rrm3::kanMX4*	(SCHMIDT *et al.* 2017)
HHY6421	HHY780 *shm2::kanMX4*	(SCHMIDT *et al.* 2017)
HHY6423	HHY780 *ura7::kanMX4*	(SCHMIDT *et al.* 2017)
HHY6252	RDKY5964 *pol1-L868M.natNT2*	(SCHMIDT *et al.* 2017)
HHY6428	HHY6252 *dun1::hphNT1*	(SCHMIDT *et al.* 2017)
HHY6379	HHY6252 *exo1::hphNT1*	(SCHMIDT *et al.* 2017)
HHY6381	HHY6252 *gln3::HIS3*	(SCHMIDT *et al.* 2017)
HHY6431	HHY6252 *gln3::HIS3 dun1::hphNT1*	(SCHMIDT *et al.* 2017)
HHY6399	HHY6252 *rrm3::kanMX4*	(SCHMIDT *et al.* 2017)
HHY6387	HHY6252 *shm2::kanMX4*	(SCHMIDT *et al.* 2017)
HHY6393	HHY6252 *ura7::kanMX4*	(SCHMIDT *et al.* 2017)
HHY6405	RDKY5964 *pol2-04.natNT2*	(SCHMIDT *et al.* 2017)
HHY6429	HHY6405 *dun1::hphNT1*	(SCHMIDT *et al.* 2017)
HHY6407	HHY6405 *gln3::HIS3*	(SCHMIDT *et al.* 2017)
HHY6433	HHY6405 *gln3::HIS3 dun1::hphNT1*	(SCHMIDT *et al.* 2017)
HHY6413	HHY6405 *rrm3::kanMX4*	(SCHMIDT *et al.* 2017)
HHY6409	HHY6405 *shm2::kanMX4*	(SCHMIDT *et al.* 2017)
HHY6411	HHY6405 *ura7::kanMX4*	(SCHMIDT *et al.* 2017)
HHY1993	RDKY5964 *pol2-M644G.natNT2*	(SCHMIDT *et al.* 2017)
HHY1947	HHY1993 *exo1::hphNT1*	(SCHMIDT *et al.* 2017)
HHY6383	HHY1993 *gln3::HIS3*	(SCHMIDT *et al.* 2017)
HHY6401	HHY1993 *rrm3::kanMX4*	(SCHMIDT *et al.* 2017)
HHY6389	HHY1993 *shm2::kanMX4*	(SCHMIDT *et al.* 2017)
HHY6395	HHY1993 *ura7::kanMX4*	(SCHMIDT *et al.* 2017)
HHY1996	RDKY5964 *pol3-L612M.natNT2*	(SCHMIDT *et al.* 2017)
HHY1943	HHY1996 *exo1::hphNT1*	(SCHMIDT *et al.* 2017)
HHY6385	HHY1996 *gln3::HIS3*	(SCHMIDT *et al.* 2017)
HHY6435	HHY1996 *gln3::HIS3 dun1::hphNT1*	(SCHMIDT *et al.* 2017)
HHY6497	HHY1996 *gln3::HIS3 rad30::hphNT1*	(SCHMIDT *et al.* 2017)

HHY6501	HHY1996 *gln3::HIS3 rev1::klTRP1*	(SCHMIDT *et al.* 2017)
HHY6163	HHY1996 *gln3::HIS3 rev3::kanMX4*	(SCHMIDT *et al.* 2017)
HHY6403	HHY1996 *rrm3::kanMX4*	(SCHMIDT *et al.* 2017)
HHY6391	HHY1996 *shm2::kanMX4*	(SCHMIDT *et al.* 2017)
HHY6397	HHY1996 *ura7::kanMX4*	(SCHMIDT *et al.* 2017)
HHY6437	HHY1996 *ura7::kanMX4 dun1::hphNT1*	(SCHMIDT *et al.* 2017)
HHY6495	HHY1996 *ura7::kanMX4 rad30::hphNT1*	(SCHMIDT *et al.* 2017)
HHY6503	HHY1996*ura7::kanMX4 rev1::klTRP1*	(SCHMIDT *et al.* 2017)
HHY6499	HHY1996 *ura7::kanMX4 rev3::hphNT1*	(SCHMIDT *et al.* 2017)
HHY6481	RDKY3686 *pol3::hphNT1* + pHHB388 (pRS316-*POL3*)	(SCHMIDT *et al.* 2017)
HHY6482	HHY6481 *ura7::kanMX4*	(SCHMIDT *et al.* 2017)
HHY6483	HHY6481 *msh2::HIS3*	(SCHMIDT *et al.* 2017)
HHY6526	HHY6481 *can1::klTRP1*	(SCHMIDT *et al.* 2017)
HHY6525	RDKY5964 *pol3::hphNT1* + pHHB388 (pRS316-*POL3*)	(SCHMIDT *et al.* 2017)
HHY6528	HHY6525 *CAN1.natNT2*	(SCHMIDT *et al.* 2017)
HHY6529	HHY6482 *can1::klTRP1*	(SCHMIDT *et al.* 2017)
HHY6530	HHY6525 *ura7::kanMX4*	(SCHMIDT *et al.* 2017)
HHY6531	HHY6531 *CAN1.natNT2*	(SCHMIDT *et al.* 2017)
HHY6521	MAT**a**/α *ura3-52/ura3-52, leu2Δ1/leu2Δ1, trp1Δ63/trp1Δ63, hom3-10/hom3-10, his3Δ200/his3Δ200, lys2-10A/lys2-10A, pol3::hphNT1/pol3::hphNT1* + pHHB388 (pRS316-*POL3*)	(SCHMIDT *et al.* 2017)
HHY6523	HHY6521 *ura7::kanMX4/ura7::kanMX4*	(SCHMIDT *et al.* 2017)
HHY6533	HHY6521 *can1::klTRP1/CAN1.natNT2*	(SCHMIDT *et al.* 2017)
HHY6535	HHY6521 *can1::klTRP1/CAN1.natNT2 ura7::kanMX4/ura7::kanMX4*	(SCHMIDT *et al.* 2017)
HHY1941	RDKY3686 *exo1::hphNT1*	This study
HHY6620	RDKY5964 *lig4::HIS3*	This study
HHY6551	RDKY5964 *rnr1::kanMX4* + pHHB560 (*pRS316-RNR1*)	This study
HHY6553	HHY6551 *dun1::hphNT1*	This study
TSY2941	HHY6551 *mrc1::natNT2*	This study
TSY2947	HHY6551 *rad9::natNT2*	This study
HHY6214	HHY6551 *exo1::hphNT1*	This study
HHY6555	HHY6551 *exo1::hphNT1 lig4::HIS3*	This study
HHY6556	HHY6551 *msh2::HIS3*	This study
HHY6558	HHY6551 *msh3::HIS3*	This study
HHY6560	HHY6551 *msh6::hphNT1*	This study
HHY6562	HHY6551 *pol2-04.natNT2*	This study
HHY6566	HHY6551 *pol3-01.natNT2*	This study
HHY6570	HHY6551 *rnr3::hphNT1*	This study
HHY6572	RDKY5964 *rnr1.HIS3*	This study
HHY6574	RDKY5964 *rnr1-F15S.HIS3*	This study
HHY6578	RDKY5964 *rnr1-D57N.HIS3*	This study
HHY6580	RDKY5964 *rnr1-S242T.HIS3*	This study
HHY6582	RDKY5964 *rnr1-K243E.HIS3*	This study
HHY6584	RDKY5964 *rnr1-A245V.HIS3*	This study
HHY6586	RDKY5964 *rnr1-R256H,Y779C.HIS3*	This study
HHY6588	RDKY5964 *rnr1-I262V,N291D.HIS3*	This study
HHY6596	RDKY5964 *rnr1-Y285C.HIS3*	This study
HHY6598	HHY1794 *rnr1-F15S.HIS3*	This study
HHY6602	HHY1794 *rnr1-D57N.HIS3*	This study
HHY6604	HHY1794 *rnr1-S242T.HIS3*	This study
HHY6606	HHY1794 *rnr1-A245V.HIS3*	This study
HHY6608	HHY1794 *rnr1-R256H,Y779C.HIS3*	This study
HHY6610	HHY1794 *rnr1-I262V,N291D.HIS3*	This study
HHY6618	HHY1794 *rnr1-Y285C.HIS3*	This study
HHY6634	RDKY5964 *rnr1-I262V,N291D.HIS3 ura3-52::URA3*	This study
RDKY6678	*Mata ura3-52 leu2Δ1 trp1Δ63 his3Δ200 hom3-10 lys2ΔBgl ade2Δ1 ade8 iYEL072W::hph can1::hisG yel072w::CAN1/URA3*	(PUTNAM *et al.* 2009)
HHY6491	RDKY3686 *iYEL072::hph can1::hisG yel072w::CAN1/URA3*	(SCHMIDT *et al.* 2017)
HHY6492	RDKY5964 *iYEL072::hph can1::hisG yel072w::CAN1/URA3*	(SCHMIDT *et al.* 2017)
HHY6493	HHY6491 *sml1::klTRP1*	(SCHMIDT *et al.* 2017)
HHY6494	HHY6492 *bar1::loxP.klLEU2.loxP*	(SCHMIDT *et al.* 2017)

HHY6443	RDKY5964 *iYEL072W::hph can1::hisG yel072w::CAN1/URA3 bar1::loxP.klLEU2.loxP*	(SCHMIDT *et al.* 2017)
HHY6537	RDKY3686 *iYEL072W::hph can1::hisG yel072w::CAN1/URA3 bar1::loxP.klLEU2.loxP*	(SCHMIDT *et al.* 2017)
HHY6445	HHY6443 *met7::kanMX4*	This study
HHY6447	HHY6443 *met7::klTRP1 natNT2.pGPD-DUT1*	This study
HHY6449	HHY6443 *met7::klTRP1 ung1::kanMX4*	This study
HHY6638	HHY6443 *natNT2.pGPD-DUT1*	This study
HHY6451	HHY6443 *ung1::kanMX4*	This study
HHY6640	HHY6443 *met7::klTRP1 natNT2.pGPD-DUT1 ung1::kanMX4*	This study
HHY6642	HHY6443 *natNT2.pGPD-met7ΔM*	This study
HHY6644	HHY6443 *met7-3Myc.klTRP1*	This study
HHY6646	HHY6443 *dut1-G82S*	This study
HHY6648	HHY6443 *dut1-G82S ung1::kanMX4*	This study
HHY6713	HHY6443 *dut1-G82S dcd1::natNT2*	This study
HHY6716	HHY6443 *dcd1::natNT2*	This study
TSY534	HHY6443 *natNT2.pSIC1-SIC1^{NTR}(aa1-100)-3Myc-(GA)5-RMI1*	This study
RDKY3615	*Mata ura3-52 leu2Δ1 trp1Δ63 his3Δ200 lys2ΔBgl hom3-10 ade2Δ1 ade8 yel069c::URA3*	(CHEN AND KOLODNER 1999)
HHY6477	RDKY3615 *met7::HIS3*	This study

3 METHODS

3 METHODS

3.1 Molecular biological methods

3.1.1 Agarose gel electrophoresis

PCR products or restriction digests were separated according to their size by agarose gel electrophoresis using 0.8% - 1.5% agarose gels stained with GelRed (1:20000 diluted). Prior to loading, DNA samples were mixed with 6x loading buffer. 1 kb GeneRuler DNA Ladder was used as a reference for size estimation of separated DNA fragments. Electrophoresis was carried out in 0.5 M TBE buffer in running chambers at constant voltage of 130 V.

3.1.2 Polymerase chain reaction (PCR)

To amplify specific sequences from genomic DNA, polymerase chain reaction (PCR) was used. For this, a reaction mix (Table 3.1) was pippeted into PCR stripes on ice, briefly mixed (vortex), spun down and transferred to the 95°C pre-heated PCR block. PCR run was run according to Table 3.2.

Table 3.1 PCR reaction mix for one reaction.

Reagent	TAQ PCR [µL]	Velocity PCR [µL]	Phusion PCR [µL]
TAQ DNA polymerase	0.25	-	-
Velocity DNA polymerase	-	0.5	-
Phusion DNA polymerase	-	-	0.5
TAQ standard buffer, 10x	2.5	-	-
Hi-Fi buffer, 5x	-	10	-
Phusion HF or GC buffer, 10x	-	-	5
dNTPs, 2 mM each	2.5	5	5
DMSO	-	1.5	1.5
primer mix, 5 µM each	2.5	5	5
genomic DNA	1	1	1
dH_2O	16.25	27	32
total volume	25	50	50

Table 3.2 PCR programs.

	TAQ PCR		Velocity or Phusion HF PCR	
Step#	Temperature [°C]	Time [min]	Temperature [°C]	Time [min]
1	95	5	98	3
2	95	1	98	1
3	55	1	55	1
4	72	1 / 1 kb length	72	1 / 1 kb length
5	72	10	72	10
6	4	∞	4	∞

Steps 2 – 4 were repeated for 30 cycles.

3.1.3 Colony polymerase chain reaction

Colony-PCR was used to test yeast transformants for the presence of the selection cassette at the expected genomic integration site. For this, yeast was transferred to PCR stripes, microwaved for 90 sec and PCR reaction components (Table 3.3) were added on ice. PCR was run as listed in Table 3.4.

Table 3.3 Colony-PCR reaction mix

Reagent	Colony-PCR [µL]
TAQ DNA polymerase	0.25
TAQ standard buffer, 10x	2.5
dNTPs, 2 mM each	2.5
primer mix, 5 µM each	2.5
colony	-
dH_2O	17.25
total volume	25

Table 3.4 Colony-PCR program.

Step#	Temperature [°C]	Time [min]
1	95	5
2	95	0.5
3	55	0.5
4	72	1
5	72	10
6	4	∞

Steps 2 – 4 were repeated for 30 cycles.

3.1.4 Cloning

To clone PCR products or subclone plasmid fragments into plasmids, restriction digest of DNA was performed at 37 °C for either 2 h or overnight. Reaction buffer was used as suggested by the manufacturer. The composition of the reaction mixture is listed in Table 3.5.

Table 3.5 Composition of restriction digestion mixture.

Reagent	Volume [µL]
PCR product / mini prep	50 / 10
restriction enzyme A	0.5
restriction enzyme B	0.5
Buffer X, 10x	10
dH_2O	up to 100
total volume	100

A small aliquot of the restriction digest was first checked by agarose gel electrophoresis, and then the remaining sample was loaded on a preparative agarose gel. Fragments of correct size were cut and extracted from the agarose using QIAquick Gel Extraction Kit following manufacturer's protocol. Purified fragments were run on an agarose gel to determine the volumes needed for a 3:1 ratio of insert to backbone in the ligation reaction. Ligation reaction was performed either for 1 h at RT or at 16 °C, overnight. The composition of the ligation reaction mixture is listed in Table 3.6. For every ligation reaction, a re-ligation control missing the insert was run in parallel under same conditions. Next, 3 µL of ligation reaction mix was transformed in electrocompetent bacteria as described in 3.1.6. Cultures of transformants were grown at 37 °C, overnight and plasmids were purified using QIAprep Spin Miniprep Kit following manufacturer's protocol. Presence of insert was checked by restriction test digestion and positive mini preps were sequenced (GATC).

Table 3.6 Composition of the ligation reaction mixture.

Reagent	Volume [µL]
T4 ligase	1
T4 ligase buffer, 10x	2
insert	x
backbone	y
dH_2O	up to 20
total volume	20

3.1.5 Site-directed mutagenesis

Plasmids containing specific point mutations were frequently generated by site-directed mutagenesis. Mutagenic primers were designed using QuikChange® Primer Design Program. Reagents for site-directed mutagenesis PCR were pipetted on ice as listed in Table 3.7 and PCR was run as depicted in Table 3.8.

Table 3.7 Site-directed mutagenesis PCR mix.

Reagent	Site-directed mutagenesis PCR [µL]
Accuprime Pfx DNA polymerase	1
Accuprime Pfx buffer, 10x	5
primer A, 100 µM	1
primer B, 100 µM	1
plasmid DNA (mini prep)	1
dH_2O	41
total volume	50

Table 3.8 Site-directed mutagenesis PCR program.

Step#	Temperature [°C]	Time [min]
1	95	5
2	95	0.5
3	55	1
4	68	1.5 / 1 kb plasmid DNA
6	4	∞

Steps 2 – 4 were repeated for 18 cycles.

Next, 10 µL PCR reaction was digested with 1 µL DpnI in a total volume of 50 µL 1x Cutsmart buffer (50 mM potassium acetate, 20 mM Tris-acetate, 10 mM magnesium acetate, 100 µg/ml BSA, pH 7.9) for 1 h at 37 °C. Finally, 3 µL DpnI-treated sample was transformed into electrocompetent cells as described in 3.1.6. Presence of the desired point mutation and absence of additional mutations were confirmed by sequencing (GATC).

3.1.6 Transformation of *E. coli*

Thawed electrocompetent *E. coli* TOP10F' were diluted 1:5 with cold dH_2O and 3 µL of ligation or site-directed mutagenesis reactions were added to 100 µL bacteria. The mix was incubated for 15 min on ice, transferred to a cuvette and electroporated at 2.48 V for 4 sec. Cells were resuspended in 1 mL LB medium and incubated for 1 h at 37 °C, shaking. Afterwards, cells were spun down, plated on solid LB medium containing the corresponding antibiotic and grown at 37 °C, overnight.

To retransform plasmid mini preps into bacteria, chemical competent *E. coli* were thawed on ice. 0.5 to 1 µL mini prep was added to competent cells and mix incubated on ice for 10 min. Cells were heat-shocked at 42 °C for 35 sec and incubated on ice for 5 min. Cells were resuspended in 1 mL LB medium and incubated at 37 °C for 1 h, shaking. Afterwards, cells were spun down, plated irregularly on solid LB medium containing the corresponding antibiotic and grown at 37 °C, overnight.

3.2 Protein biochemical methods

3.2.1 Yeast crude cell lysates

For yeast cell crude cell lysates, 500 µL overnight culture was added to 5 mL fresh medium and grown for 3 h at 30 °C, shaking. Cells were pelleted (3000 rpm, 10 min, RT), resuspended in 150 µL YEX buffer and transferred to a pre-chilled 1.5 mL reaction tube. Samples were incubated on ice for 10 min. Next, 150 µL 50% TCA was added to each sample. To mix the sample, the sample was vortexed and again incubated for 10 min on ice. To precipitate proteins, sample was spun down (14000 rpm, 10 min, 4°C) and the pellet was resuspended in 100 µL 1x GSD+Tris buffer. Samples were boiled for 5 min at 95 °C, spun down and either loaded on an SDS-PAGE gel or stored at -20 °C.

3.2.2 SDS polyacrylamide gel electrophoresis

Sodiumdodecylsulfate polyacrylamide gel electrophoresis (SDS-PAGE) was used to separate proteins according to their molecular weight. Yeast crude protein lysates were boiled for 5 min at 95 °C, spun down and loaded onto the prepared 7, 8, 10 or 12% SDS polyacrylamide gel (Table 3.9) or commercial 4-15% Mini-PROTEAN TGX gels. SDS-PAGE was run in 1x SDS running buffer at 80 V for approximately 20 min and then at 200 V until the running front reached the bottom of the gel. For protein size estimation, a prestained Precision Plus Protein™ Dual Color Standards protein marker was run on each gel.

Table 3.9 SDS-PAGE recipe for one SDS-PAGE gel.

Reagent	**Separating gel**				**Staking gel**
	7%	**8%**	**10%**	**12%**	**5%**
dH_20	5.65	5.4	4.9	4.4	3.125
separating buffer	2.5	2.5	2.5	2.5	0
stacking buffer	0	0	0	0	1.25
SDS, 10%	0.1	0.1	0.1	0.1	0.05
Acrylamide-Bis, 40%	1.75	2.0	2.5	3	0.625
APS, 10%	0,03	0.03	0,03	0.03	0.015
TEMED	0.015	0.015	0.015	0.015	0.0075

3.2.3 Coomassie staining

To visualize proteins with Coomassie brilliant blue G250, the SDS-PAGE gel was first incubated in fixing solution for 30 min, RT, shaking. Next, the gel was stained with Coomassie staining solution (a one to one mixture of stock solution I and II) for 20 min, RT, shaking. Afterwards, the gel was

destained in destaining solution I for 30 sec to 5 min and destainig solution II as long as needed. The destained gel was washed with dH_2O twice and imaged using a scanner.

3.2.4 Western blot

To transfer proteins present in the SDS-PAGE gel on a PVDF membrane a wet blotting system (Bio-Rad) was used. First, the PVDF membrane was activated with methanol. Next, the blotting cassette including sponges (one on each side), Whatman 3M paper (two on each side), the separating gel and the PVDF membrane was assembled and inserted in the blotting system. Transfer was performed for 1 to 4 h at 350 mA. After disassembling the apparatus, the membrane was washed with PBS-T once and blocked with in 3% milk dissolved in PBS-T for 1 h at RT with shaking. The membrane was washed once with PBS-T and incubated with the diluted primary antibody in either 3% milk or 3% BSA in PBS-T for 1 h at RT or overnight at 4 °C. After washing the membrane with PBS-T for 5 min at RT (repeat step three-times), the membrane was incubated with the secondary antibody coupled to horseradish peroxidase (HRP) in 0.5% milk diluted in PBS-T for 1 h at RT. Next, the membrane was again washed with PBS-T for 10 min at RT (repeat step three-times) and then incubated with Immobilon Western Chemiluminscent HRP substrate and imaged using Fusion Solo S System or Super RX-N Fuji medical x-ray films and an Optimax TR X-ray film processor. All antibodies used for Western blot analysis (including used dilutions) are listed in Table 2.10 and 2.11.

3.2.5 Sic1 antibody generation

To raise antibodies against yeast Sic1 in guinea pigs, first, 6xHis-tagged full-length Sic1 was expressed from pET28c-Sic1 (kind gift from Dr. Gislene Pereira) in *E. coli BL21 (DE3)* and purified using Ni-NTA agarose affinity purification. For this, the overnight culture was diluted 1:50 in 1 L LB+Kan and growth at 37 °C, shaking (230 rpm) was followed by measuring OD_{595}. At an OD_{595} of 0.8 Sic1 expression was induced by addition of IPTG (c_{final} = 1mM). After 4 h of incubation at 37 °C, 230 rpm, the culture was spun down by centrifugation in a Beckman centrifuge (JA-10 rotor, 5000rpm, 15 min, 4 °C) and the mass of the wet pellet was measured. Pellets were resuspended in PBS, transferred in one 50 mL Falcon tubes and centrifuged again (4000 rpm, 15 min, 4 °). Cell pellet was resuspended in lysis buffer, lysozyme was added to a final concentration of 1 mg/mL and sample was incubated for 30 min on ice. Next, the sample was sonicated on ice for six 10 sec bursts with 1 min cooling period between each burst. The lysate was transferred to a centrifugation flask and centrifuged at 10000 x g for 30 min at 4 °C to pellet cellular debris. The supernatant was transferred to a 50 mL Falcon tube and magnesium chloride and ATP was added to the supernatant to a final concentration of 10 mM and 2 mM, respectively. 2 mL 50% Ni-NTA slurry was added to a 50 mL Falcon tube and washed twice with 1 mL lysis buffer (1500 rpm, 4 °C, 5 min). All subsequent steps are carried out in the cold room. The supernatant was added to the prepared Ni-NTA slurry and mixed gently on a rotary wheel for 2 h at 4 °C. The lysate Ni-NTA mixture was loaded into a PolyPrep® Chromatograhy column, the bottom cap was removed and flow through was collected. Column was washed with 4 mL wash buffer, twice and wash fractions

were collected. Finally, Ni-NTA-bound proteins were eluted by adding 8 times 250 µL elution buffer. All eluates were collected in individual tubes and analyzed by SDS-PAGE followed by Coomassie staining. The concentration of purified Sic1 in each eluate was estimated using a BSA standard. The different steps of the Ni-NTA affinity purification of 6xHis-Sic1 is shown in Fig. 3.1A. At the DKFZ core facility for monoclonal antibodies, two guinea pigs were immunized with 6xHis-Sic1. Specificity of serum was tested by immunoblotting (Fig. 3.3B).

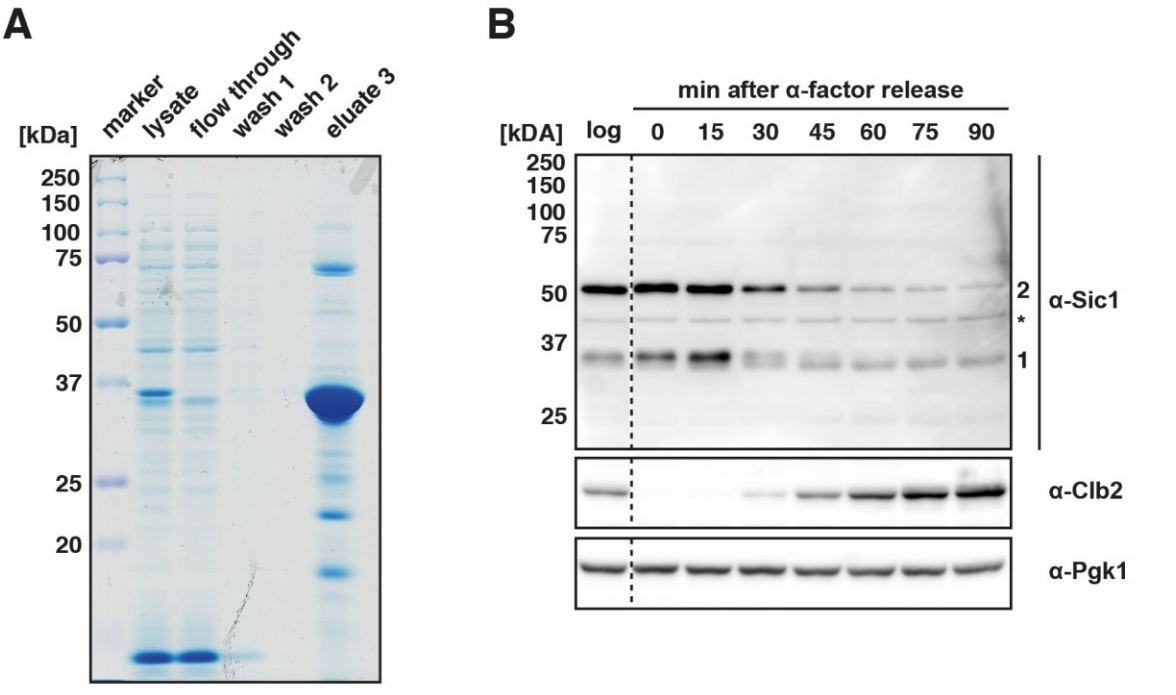

Fig. 3.1 Sic1 purification and α-Sic1 serum test.
(A) Proteins in lysate, flow through, washes and eluate 3 (the most concentrated eluate) were separated on a 12% SDS-PAGE and stained with Coomassie. (B) α-factor release experiment of TSY534 to test for specificity of the α-Sic1 serum. Cells were arrested in G1 by α-factor and released in fresh medium. Samples were taken every 15 min. The α-Sic1 serum recognizes Sic1 (1), the Sic1-NTR-Rmi1 fusion protein (2) expressed under the control of the Sic1 promoter, as well as one unspecific band (*). Clb2 was used as G2 marker and Pgk1 was used as loading control. Cropping of the image is shown as dotted lane.

3.3 *S. cerevisiae* methods

3.3.1 Growth conditions

S. cerevisiae strains were grown at 30°C either in yeast extract-peptone-dextrose (YPD) media, or in synthetic dropout (SD) media. For plates, media contained 2% agar-agar. Yeast extract-peptone-glycerol (YPG) media was used to test for *petite* phenotype (dysfunctional mitochondria). Mutator plates and growth medium used to measure mutation rates in strains with plasmid-borne *rnr1* alleles were prepared as described above but lacking leucine (Leu) to select for the *rnr1* plasmid (*ARS-CEN*, *LEU2*). Antibiotics were used at the following final concentrations (unless otherwise specified): 200 µg/mL geneticin (G418), 300 µg/mL hygromycin B (hph), 100 µg/mL nourseothricin (nat) and 10 µg/mL cycloheximide. The DNA damaging agents Hydroxyurea (HU) and Phleomycin from *Streptomyces verticillus* were used in the indicated concentrations in YPD medium.

3.3.2 Generation of competent yeast cells

To generate competent yeast cells, 2 mL of a saturated overnight culture was added to 50 mL fresh media and incubated for 4 h at 30 °C with shaking. Cells were pelleted (3000 rpm, 10 min, RT), washed once with 1x LiAc/TE buffer and resuspended in 600 µL LiAc/TE. Cells were incubated at 30 °C in a shaking incubator for 15 min and stored up to one week at 4 °C.

3.3.3 Yeast transformation

To transform a PCR product or a plasmid into competent yeast cells, competent cells were pelleted. DNA, 40% PEG, 10x LiAc and salmon sperm was added to the pelleted cells (Table 3.10). Transformation mix was resuspended and incubated for 30 min at 30 °C followed by 20 min at 42 °C. Cells were washed once with sterile dH_2O and plated on YPD or drop-out plates. In case of a transformation of an antibiotic resistance cassette as selection marker, cells were replica plated onto an YPD plate containing the antibiotic next day. Alternatively, cells were directly resuspended in 5 mL liquid YPD after the transformation, grown for 5 h at 30 °C and plated on YPD containing the antibiotic.

Table 3.10 Yeast transformation mix.

Reagents	PCR product [µL]	Plasmid [µL]
competent cells	200	30
PCR product	25	-
plasmid mini prep	-	0.5 - 1
PEG3350, 50% w/v	240	60
LiAc, 1M	36	9
salmon sperm, 2mg/mL	25	5

3.3.4 Sporulation and random spore analysis

To obtain diverse genetically modified yeast strain combinations yeast mating followed by random spore isolation was used. Mata and Matα haploid yeast cells were mated and diploids were selected either following auxotrophic and resistance markers or by testing for mating type with mating type tester strains. 1 mL of the diploid overnight culture was washed once with dH_2O and resuspendend in 3 mL sporulation medium. Cells were incubated at 30 °C with shaking for 5-7 days, and sporulation was checked visually using light microscopy. To purify spores, 1 mL sporulated culture was pelleted. Cells were resuspended in 40 µL zymolase (c = 0.5 mg/mL) and incubated at 30 °C for 30 min. 500 µL sterile dH_2O was added to the sample and cells were pelleted. 70 µL dH_2O was added to the sample and the sample was subsequently vortexed in a disruptor genie for 5 min, RT. Supernatant was removed using vacuum and cells were washed 6 times with 1 mL dH_2O. Finally, 1 mL dH_2O containing 0.01% NP-40 was added to the sample and cells were vortexed for 1 min, RT. Depending on the sporulation efficiency different volumes were plated on selection medium plates. Purified spores were patched on YPD agar and tested for the presence of auxotrophic/drug resistance markers linked to specific genetic modifications according to the desired genotype.

3.3.5 α-factor arrest and release

α-factor arrest and release experiments were performed in a *bar1Δ* background. Cells were grown in YPD overnight. The logarithmically growing control cultures were prepared as described in (3.2.1). To arrest cells in G1 with α-factor, 2 mL of the overnight culture was washed with sterile water twice and then resuspended in 20 mL YPD medium containing 0.1 µg/mL α-factor followed by incubation at 30 °C for 3 h with shaking. Next, cells were washed twice with sterile water, released in 20 mL YPD medium containing 15 µg/mL nocodazole and grown at 30 °C with shaking. Samples for DNA content analysis and cell lysates were taken every 10 min. Cell cycle progression was analyzed by DNA content using flow cytometry and by SDS-PAGE/immunoblotting.

3.3.6 Spotting on solid media

Proliferation of different yeast strains was compared using the “spotting assay” in which serial dilutions of a yeast culture are spotted in a solid media agar plate. Yeast cultures were grown overnight in YPD. Next day, cultures were normalized to the lowest OD_{595} and spotted in 10-fold serial dilution on solid YPD plates, YPG plates and on YPD plates containing phleomycin from *Streptomyces verticillus* in the indicated concentration. Plates were incubated at 30 °C and imaged using the GelDoc system.

3.3.7 Proliferation assay

Saturated overnight cultures were diluted to OD_{600} = 0.1 in fresh YPD. Growth at 30 °C was followed by OD_{600} measurement every hour. For each genotype at least two independent isolates were used and determination were done at least in triplicates. The OD_{600} mean with standard deviation was plotted in a log2 scale against incubation time.

3.3.8 DNA content analysis

For DNA content analysis, saturated overnight cultures were diluted 1:20 in fresh YPD and grown for 3 h at 30 °C with shaking. 200 µL culture aliquot was washed with cold dH_2O. Cells were resuspended in 300 µL cold dH_2O and transferred to a 14 mL culture tube. While constantly vortexing, cells were fixed by adding 700 µL cold absolute ethanol. Fixed cells were incubated for 1 h at RT and then either stored at 4 °C or further processed. To prepare cells for DNA content analysis, cells were resuspended in 50 mM sodium citrate buffer and sonicated (5 pulses, 1 sec break; 30% output). Samples were treated with 1 mg/mL proteinase K and 0.25 mg/mL ribonuclease A in 50 mM sodium citrate overnight at 37 °C. Next day, cells were pelleted, resuspended in 50 mM sodium citrate containing 1 µM sytox green and incubated in the dark at RT for at least 1 h. DNA content was measured at FACS CantoII. 30000 events were recorded per sample. Data was analyzed using FlowJo and the percentage of cells in S phase was determined using FlowJo cell cycle analysis plug-in.

3.3.9 Purification of genomic DNA

Genomic DNA was prepared either using Qiagen Puregene Yeast / Bact. Kit B following manufacturer's protocol or using phenol-chloroform extraction (HOFFMAN AND WINSTON 1987). For the latter, a saturated 5 mL yeast overnight culture was spun down and resuspended in 200 µL buffer A. 200 µL TE was added and mixture was transferred to 2 mL safe-lock reaction tube containing 400 µL glass beads. In the fume hood, 200 µL phenol-chloroform-isoamyl alcohol (25:24:1) was added to the sample, followed by vortexing for 3 min at RT using a disrupter genie. Samples were centrifuged (14000 rpm, 10 min, 4 °C) and 50 µL of the upper aqueous phase, which contains the genomic DNA, was transferred to a fresh 1.5 mL reaction tube.

3.3.10 Plasmid rescue from yeast cells

For plasmid rescue from yeast cells, DNA was purified as described in 3.3.9, but instead of 50 µL 300 µL of the DNA containing aqueous phase was transferred to a new 1.5 reaction tube. To precipitate DNA, 1 mL 96% ethanol was added, the sample mixed by inverting the tube and centrifuged at 14000 rpm for 2 min. The supernatant was discarded and pellet resuspended in 400 µL TE. Next, 15 µL 3 M sodium acetate, pH 5.2 was added to the sample, mixed (vortex), followed by the addition of 1 mL 96% ethanol and vortexing. Sample was centrifuged at 14000 rpm for 2 min. The supernatant was removed carefully and pellet air-dried for 10 min. DNA was resuspended in 50 µL TE and either incubated at 65 °C for 1 h or at RT, overnight. Finally, 3 µL DNA was electroporated into electrocompetent TOP10F' following protocol 3.1.6.

3.3.11 Uracil accumulation assay

Uracil accumulation assay was mainly done as described (SEIPLE *et al.* 2006). Genomic DNA was isolated from logarithmic cultures using Puregene Yeast / Bact. Kit B. Genomic DNA was incubated overnight at 37 °C in the presence or absence of 10 U uracil DNA glycosylase from *E. coli* (UDG) and 20 U human AP endonuclease (APE I) in 1x NEBuffer 4 (50 mM potassium acetate, 20 mM Tris-acetate, 10 mM magnesium acetate, 1 mM DTT, pH 7.9). DNA was precipitated and loaded on a 0.8% agarose gel stained with GelRed. Images were taken using the GelDoc system.

3.3.12 Determination of NTP and dNTP pools

NTP and dNTPs were measured in Dr. Chabes lab as described in (RENTOFT *et al.* 2016; SCHMIDT *et al.* 2017).

3.3.13 Synthetic lethal interaction with polymerase mutants by plasmid shuffling

To test for potential lethal interactions between *ura7Δ* and the DNA proofreading-deficient *pol3-01* allele, plasmid shuffling was performed. For this, first the *POL3* vectors were cloned. The *POL3* gene, including 1 kb upstream and 200 bp downstream of *POL3*, was amplified from genomic DNA with primers HHP2797 and HHP2798, introducing a NotI and a SmaI sites to clone the amplified fragment into pRS315 and pRS316 (SIKORSKI AND HIETER 1989) to generate pHHB351 (pRS315-

POL3) and pHHB388 (pRS316-*POL3*), respectively. To generate pRS315-*pol3-01*, plasmids RDK3097 (DATTA *et al.* 2000) and pHHB351 were digested with NcoI and BglII. The 2015 bp *pol3* fragment of RDK3097 plasmid containing *D321A* and *E323A* mutations, and the 8479 bp fragment of pHHB351 were gel extracted and ligated to generate pHHB396 (pRS315-*pol3-01*). All plasmid inserts and junctions were sequenced. Next, the strains used for the DNA polymerase plasmid shuffling experiments were generated by mating RDKY3686 and RDKY5964. In this diploid wild-type strain an *hphNT1* cassette (amplified from *pFA6a-hphNT1*) was used to replace one of the two *POL3* alleles. Next, strains were transformed with pHHB388 (pRS316-*POL3*) and sporulated to generate HHY6481. In HHY6481, *URA7* was deleted with a *kanMX4* cassette (amplified from *pFA6a-kanMX4*) and *MSH2* with a *HIS3* cassette (amplified from pRS303) to generate HHY6482 and HHY6483, respectively. HHY6481, HHY6482 and HHY6483 were transformed with pHHB351 and pHHB396. To check for synthetic lethality, transformants (Ura^+Leu^+) were streaked on 5-FOA plates (to select for the loss of WT-*POL3-URA3* plasmid) and in SD media lacking Ura and Leu (as control). The *msh2Δ pol3Δ* strain (HHY6483) transformed with pHHB396 (pRS315-*pol3-01*) was used as a positive control for a synthetic lethal interaction (TRAN *et al.* 1999). Strains were imaged after 3 days of growth with a GelDoc system. Homozygous diploid strains HHY6521 and HHY6523 were generated by mating and used for plasmid shuffling as described above.

3.3.14 Synthetic lethal interactions between *rnr1* mutants and DNA replication fidelity or checkpoint-compromised mutants by plasmid shuffling

To investigate genetic interactions between *rnr1*- and replication fidelity or checkpoint-compromised mutants by plasmid shuffling, different plasmid shuffling queries were generated by mating. All these queries lack the essential *RNR1* gene, but are complemented by a low copy plasmid expressing WT-*RNR1* (pHHB560, pRS316-*RNR1*) in addition to the indicated additional gene deletion/mutation. Plasmids either expressing the *WT-RNR1* or mutant *rnr1* alleles (*ARSH4-CEN6, LEU2*) were transformed into the query strains. Overnight cultures were spotted in serial dilutions on media lacking Leu, in the presence or absence of 5-FOA. Plates were incubated for 4 days at 30 °C, imaged and scored visually.

3.3.15 Determination of mutation rates in haploid cells

Mutation rates for the *CAN1* inactivation assay, the *lys2-10A* and *hom3-10* frameshift reversion assay and the standard and post-duplication gross-chromosomal rearrangement (GCR) assay were measured by fluctuation analysis as described previously (MARSISCHKY *et al.* 1996; AMIN *et al.* 2001; PUTNAM AND KOLODNER 2010). Mutation rates were determined based on two biological isolates and at least 14 independent cultures. 95% confidence intervals were calculated for all fluctuation tests.

3.3.16 Determination of mutation rates in diploid cells

CAN1 inactivation rates in diploid strains were determined by fluctuation analysis in HHY6533 and HHY6535 strains after plasmid shuffling as previously described (HERR *et al.* 2014). Both, HHY6533 and HHY6535 were transformed with either pHHB351 (pRS315-*POL3*) or pHHB396 (pRS315-*pol3-01*). The transformants were streaked out for single colonies on Leu- medium containing 5-FAO and nat to select for loss of the plasmid expressing WT-*POL3* (pHHB388, pRS316-*POL3*). Mutation rates for the *CAN1* inactivation assay were determined by fluctuation analysis as previously described with the modification that cells were grown in YPD media containing nat, plated on YPD containing nat and or *CAN1* inactivation assay plates containing nat. Each mutation rate was determined by using two biological isolates and at least 14 independent cultures.

3.3.17 *CAN1* and *URA3* mutation spectra analysis

To determine *CAN1* mutation spectra in different yeast genetic backgrounds, individual colonies were patched on YPD and replicated on *CAN1* mutator plates. Can^R clones were re-streaked on SD plates containing canavanine and single independent colonies were used for genomic DNA isolation. *CAN1* gene was amplified with Phusion High-Fidelity DNA polymerase using primers HHP507 and HHP508. PCR product was checked by agarose gel electrophoresis and sequenced with primers HHP2973 and HHP2974 by GATC. Sequences were analyzed using Lasergene 12 (or more recently, Lasergene 15) and mutations were annotated in the *CAN1* sequence. A mutational hotspot was defined as a specific mutation found in more than 5% of all sequenced Can^R clones of the genotype. Mutations rates for specific positions were calculated by multiplying the overall Can^R mutation rate of the strain with the percentage of the specific mutation relative to the overall observed mutations. Mutation spectra distributions and mutational hotspots were compared with Fisher's exact test in R.

To determine the *URA3* mutation spectrum of the *rnr1-I262V, N291D* mutant, two isogenic strains (HHY6634 and HHY6635) were generated, in which the *ura3-52* allele was replaced by a WT-*URA3* gene by transforming an *URA3* cassette lacking the ATG, amplified from pRS306 with primers HHP2876 and HHP2877. Next, individual colonies were patched on YPD and replica plated on 5-FOA containing plates. $5\text{-}FOA^R$ colonies were re-streaked on 5-FOA plates. Single $5\text{-}FOA^R$ colonies were used for genomic DNA isolation. The *URA3* gene was amplified with Phusion High-Fidelity DNA polymerase using primers HHP2197 and HHP2198 and sequenced with primers HHP4105 and HHP2947 by GATC. Sequences were analyzed using Lasergene 12 (or 15) and mutations were annotated in the *URA3* sequence. *URA3* spectrum was compared to WT *URA3* mutation spectrum reported by (LANG AND MURRAY 2008) using Fisher's exact test in R.

3.3.18 Strain construction

Gene deletions and gene-tagging were performed using standard PCR-based recombination methods, followed by confirmation by PCR (WACH *et al.* 1994; JANKE *et al.* 2004). Alternatively, strains carrying combination of different genetic alterations were generated by mating and

sporulation as described in 3.3.4. Correct insertion of tags, promoters or point mutations, as well as absence of additional unwanted mutations, were confirmed by sequencing.

To generate HHY6642, which overexpresses the cytoplasmic *met7ΔM* allele that lacks the mitochondrial leader sequence (DESOUZA *et al.* 2000), a constitutive *GPD* promoter was introduced directly upstream of *MET7* methionine 63 in HHY6443 using PCR-based recombination method with pYM-N15 (JANKE *et al.* 2004) as PCR template and primers HHP2657 and HHP2801. Promoter and junction were confirmed by sequencing.

Specific mutations were introduced by pop-in/pop-out strategy (polymerase alleles and *rnr1* alleles) or PCR-based recombination methods (*cyh2-Q38K)* and the presence of the desired mutations, as well as the absence of additional mutations, were verified by sequencing.

DNA Polymerase active-site mutations: *pol2-M644G* (PURSELL *et al.* 2007) and *pol3-L612M* (LI *et al.* 2005) were introduced in RDKY5964 by pop-in/pop-out strategy as previously described in (HOMBAUER *et al.* 2011a). The *pol1-L868M* mutation was introduced in RDKY5964 following the same strategy, but with BamHI linearized plasmid pHHB97. pHHB97 was generated by site-directed mutagenesis using primers HHP1276 and HHP1277 and pRS306-*POL1* as DNA template, which contains the full-length wild-type *POL1* gene, including 1 kb of the 5'-UTR and 738 bp of the 3'-UTR, cloned in between the KpnI and SacII sites of pRS306.

To generate strains expressing *dut1-1* mutant allele integrated at the chromosomal *DUT1* locus, the *DUT1* gene, including 1 kb upstream and 752 nt downstream of *DUT1* was amplified with primers HHP4196 and HHP4197 from genomic DNA isolated from RDKY5964. The introduced BamHI site in combination with an XhoI site downstream of *DUT1* was used to clone the amplified fragment into pRS306 (SIKORSKI AND HIETER 1989) to generate pHHB1093 (pRS306-*DUT1*). The *dut1-G82S* mutation (GUILLET *et al.* 2006) was introduced in pHHB1093 by site-directed mutagenesis using primers HHP4198 and HHP4199 to generate pHHB1094 (pRS306-*dut1-1*). Next, the HindIII linearized pHHB1094 was used to introduce the *dut1-1* allele (*dut1-G82S*) at the chromosomal *DUT1* locus of RDKY3686 by pop-in/pop-out strategy generating HHY6650. The presence of the desired *dut1-G82S* mutation, as well as the absence of unwanted mutations, was confirmed by sequencing. Next, HHY6650 was crossed against HHY6441 and HHY6451 to generate HHY6707 and HHY6646, respectively.

To integrate *rnr1* alleles into the *RNR1* chromosomal locus by pop-in/pop-out strategy, first the *RNR1* gene (including promoter and 3' UTR) was amplified from genomic DNA with primers HHP1100 and HHP2976, digested with KpnI and partially with BglII, gel extracted and cloned into pRS306 (SIKORSKI AND HIETER 1989) to generate pHHB424 (pRS306-*RNR1*). pHHB424 contains the WT-*RNR1* gene, 786 nt of the promoter and 135 nt downstream of the *RNR1* STOP codon. Second, the desired *rnr1* mutations were introduced using site-directed mutagenesis or subcloning. The resulting integrative plasmids encoding for the specific *rnr1* mutations were linearized with BglII or with Bsu36I in case of pHHB718 and pHHB752 prior to transformation. To mark the mutant *rnr1* alleles a *HIS3* cassette (amplified from pRS303 (SIKORSKI AND HIETER 1989) with primers HHP3700 and HHP3701) was integrated 232 nt downstream of the *RNR1* STOP codon.

3.3.19 Strain construction post-GCR

The post-duplication GCR strain HHY6443 was generated in three steps. First, RDKY6678 (PUTNAM *et al.* 2009) containing the post-duplication gross chromosomal rearrangement reporter was crossed against RDKY3686 (AMIN *et al.* 2001) containing the *lys2-10A* allele to generate HHY6491 and HHY6492. Next, a *TRP1* cassette from *Kluyveromyces lactis* (*klTRP1*) was amplified from pYM22 (JANKE *et al.* 2004) and introduced at the *SML1* locus in HHY6491 to generate HHY6493. In parallel, a *LEU2* cassette from *Kluyveromyces lactis* (*klLEU2*) flanked by loxP sites was amplified from pUG73 (GUELDENER *et al.* 2002) and introduced at the *BAR1* locus in HHY6492 to generate HHY6494. Finally, HHY6493 was crossed against HHY6494 and sporulated to generate HHY6443.

3.3.20 Strain construction to measure mutation rates in diploids

HHY6533 and HHY6535 were used as query strains to measure mutation rates in diploids as described in 3.3.16. HHY6533 was generated as follows: First, a *TRP1* cassette from *Kluyveromyces lactis* (*klTRP1*) was amplified from pYM22 (JANKE *et al.* 2004) and introduced at the *CAN1* locus in HHY6481 to generate HHY6526. Second, a *natNT2* cassette was amplified from pFA6a-natNT2 (JANKE *et al.* 2004) using primers HHP3678 and HHP3679 and introduced 7 nt downstream of the *CAN1* STOP codon in the *CAN1* 3'UTR of HHY6525 (a Mat**a** version of HHY6481) to generate HHY6528. Third, HHY6526 was crossed with HHY6528 to generate HHY6533.

HHY6535 was generated as described for HHY6533, with the modification that the initial *CAN1* deletion and the integration of the natNT2 cassette were done in HHY6482 and HHY6530, respectively.

3.3.21 SGA query strain construction

Due to the incompatibility of the selectable markers used in the query of the original SGA protocol (TONG AND BOONE 2006) with the genetic markers required for the mutator assays the query was modified as follows: First, because the *CAN1* inactivation assay requires a functional *CAN1* gene and strains carrying the *lys2-10A* allele depend on the lysine permease Lyp1 for survival, canavanine and thialysine could not be used to kill diploids cells. Thus, to kill diploids a combination of cycloheximide and 5-FOA was used. For this, the cycloheximide-resistant mutation (*cyh2-Q38K*) (KAUFER *et al.* 1983) was introduced at the *CYH2* locus and a *URA3* cassette from *Kluyveromyces lactis* (*klURA3*) was integrated downstream of *MLH2* by PCR-based recombination method. Second, the *LEU2* gene from *Kluyveromyces lactis* (*klLEU2*) under the control of the mating type a specific *MFA1* promoter and an *hphNT1* cassette were introduced upstream of the *lys2-10A* allele. The pMFA1-LEU2 cassette allows the selection of haploid *Mata* progeny, whereas the hph resistance marker is used to select for those strains carrying the *lys2-10A* reporter. Third, downstream of the DNA polymerase mutant alleles (*pol1-L868M*, *pol2-M644G* and *pol3-L612M*) and the wild-type *POL1* gene a *natNT2* cassette was integrated, which allows selection for mutant or wild-type polymerase alleles by nourseothricin resistance.

In detail, the query strains were generated as follows. First, the *klLEU2* open reading frame (ORF) and 143 nt of the 3'-untranslated region (3'-UTR) was amplified with primers HHP1949 and HHP1950 from pOM13 (GAUSS *et al.* 2005) and the PCR product was used to replace the *MFA1* ORF in RDKY5964 generating HHY6484. In parallel, a hygromycin B resistance cassette (*hphNT1*) from pFA6a-hphNT1 (JANKE *et al.* 2004) was amplified with primers HHP2002 and HHP2003 and inserted upstream of the *lys2-10A* allele in HHY5218 resulting in HHY6485. Second, the *MFA1* promoter and the *klLEU2* gene (*pMFA1-klLEU2*) were amplified with primers HHP2001 and HHP2004 from genomic DNA of HHY6484. This *pMFA1-klLEU2* cassette was than inserted directly upstream the *hphNT1* cassette in HHY6485 to generate HHY6486.
In parallel, the cycloheximide-resistance *cyh2-Q38K* mutation was introduced into RDKY3686 by transformation of a PCR product amplified from genomic DNA from RDKY7593 (which harbors the *cyh2-Q38K* mutation, generously provided by C.D. Putnam and R. D. Kolodner, Ludwig Institute for Cancer Research, San Diego) with primers HHP1062 and HHP1063 creating HHY6487. Then, a *HIS3* cassette amplified from pRS303 (SIKORSKI AND HIETER 1989) with primers HHP1955 and HHP1956 was integrated in the 3'-UTR of the *hom3-10* allele in strain HHY6487 to generate HHY6488. Third, HHY6486 was crossed against HHY6488 and sporulated to generate HHY6489. Fourth, a *klURA3* cassette was amplified from pUG72 (GUELDENER *et al.* 2002) with primers HHP2220 and HHP2221 and introduced in the 3'-UTR of *MLH2* resulting in HHY6490. Fifth, the active-site polymerase mutations were introduced in RDKY5964 by pop-in/pop-out as described in 3.3.18. Next, a *natNT2* cassette was amplified from pFA6a-natNT2 (JANKE *et al.* 2004) and integrated in the 3'-UTR of DNA polymerase active-site mutant alleles or wild-type *POL1*. Finally, these strains were crossed against HHY6490 to generate the *pol1-L868M*, *pol2-M644G*, *pol3-L612M* and WT-*POL1* SGA queries (HHY5292, HHY5284, HHY5289 and HHY5298, respectively).

3.3.22 SGA

All the steps until the freezing of the generated double mutant cells were done using RoToR robot. The four SGA query strains HHY5298, HHY5292, HHY5984 and HHY5289 (grown on YPD + hph agar plates) were crossed to an array of the quadruplicated non-essential BY4742 gene deletion collection TKY3503 by pinning onto fresh YPD agar plates. After 1 day of growth at 30 °C, cells were subjected to two rounds of pinning onto SGA diploid selection medium and grown for 2 days and 1 day, respectively at 30 °C. Afterwards, cells were pinned onto SGA presporulation medium and grown for 1 day at 30 °C.
Next, cells were pinned onto SGA sporulation medium and incubated for 7 days at 23-25 °C. Spores were pinned onto SGA haploid selection medium and grown for 5 days at 30 °C followed by two rounds of pinning on SGA double mutant selection medium (in the second round of pinning medium contained additional 50 µg/mL hph) for 1 day at 30 °C. Next, cells were de-condensed from 1536- to 384-format by pinning onto SGA de-condensation medium and grown for 2 days at 30 °C. Finally, cells were transferred to 96-well plates containing liquid SD medium without Leu containing 15% glycerol, G418 and nat, grown for 2 days at 30 °C and stored at -80 °C.
The generated double mutants were spotted on YPD-agar using Liquidator 96, grown for 2 days at 30 °C. Then, plates were imaged using the GelDoc system for documentation and replica-plated

onto two mutator plates, either lacking lysine (for *lys2-10A* frameshift reversion assay) or lacking Arg and supplemented with canavanine (*CAN1* inactivation assay). After 4 days of growth at 30 °C, mutator plates were imaged and scored visually. Positive hits were re-checked and those mutants that confer an increased mutator phenotype were generated in S288C background (RDKY5964 and HHY6443) for further analysis.

3.3.23 Strain construction for *RNR1* random mutagenesis screen

The *RNR1* random mutagenesis screen was performed in HHY6555, which was complemented by pHHB560 (pRS316-*RNR1*) plasmid. To generate HHY6555, we inactivated the *LIG4* gene (to prevent non-homologous end joining events) with a *HIS3* cassette (amplified from pRS303) in RDKY5964 (HOMBAUER *et al.* 2011a) and crossed it with HHY1941. In the resulting diploid strain one of the two *RNR1* alleles was replaced by a *kanMX4* cassette, amplified from *pFA6a-kanMX4*. The heterozygous diploid strain was transformed with pHHB560 (*pRS316-RNR1*) and sporulated to obtain HHY6555. HHY6124 and HHY6551, which were used for further analysis, were generated following the same strategy.

3.3.24 Construction of a *rnr1* mutation library

To generate an *rnr1* mutant library, the *RNR1* gene was amplified from pHHB424 (pRS306-*RNR1*) using primers HHP3285 and HHP1872 with standard Taq polymerase (3'-5' exonuclease-deficient) for 12 cycles under standard conditions (3.1.2) in 52 independent reactions. Next, all PCR reactions were pooled and purified using QIAquick Gel Extraction Kit. The *rnr1* PCR products were co-transformed with a purified 6 kb fragment of HindIII and NotI digested pHHB561 into HHY6555 for *in vivo* gap repair. Transformants containing the gap-repaired plasmids were selected by growth on SD plates lacking Leu and replica plated on SD plates lacking Leu but containing 5-FOA to select for the loss of pHHB560 (pRS316-*RNR1*).

3.3.25 Screening for mutator phenotypes, plasmid rescue and identification of *rnr1* mutations

To screen for mutator phenotypes in the *hom3-10* and *lys2-10A* frameshift reversion assay as well as in the *CAN1* inactivation assay, the colonies obtained after plasmid shuffling (Leu^+ + $5\text{-}FOA^R$) were replica-plated on SD media lacking threonine (Thr) or lysine (Lys) or lacking Arg containing canavanine. Cells were grown for 3 days at 30 °C. Colonies, which showed increased papillation in at least two mutator assays or multiple small canavanine-resistant colonies were re-tested for mutator phenotype. Clones that confer an increased mutator phenotype after re-testing, were inoculated for DNA extraction with subsequent plasmid rescue as described in (3.3.10). Plasmids were prepared using QIAprep Spin Miniprep Kit and transformed into competent HHY6214. After plasmid shuffling in SD media lacking Leu and containing 5-FOA, clones were screened for increased mutator phenotypes in the *hom3-10* and *lys2-10A* frameshift reversion assay as well as in the *CAN1* inactivation assay. Plasmids that consistently increased the mutator phenotype were

sequenced to identify *rnr1* mutation(s). Next, yeast strains expressing *rnr1* mutant alleles were used for mutations rate analysis as described in 3.3.15. The identified *rnr1* alleles were also expressed in a WT-*EXO1* background (HHY6551) and the obtained strains were qualitatively tested for mutator phenotype.

4 RESULTS

4 RESULTS

4.1 A genome-wide screen reveals genes that prevent the accumulation of mutations.

To identify non-essential genes that contribute to replication fidelity, a genome-wide screen in *S. cerevisiae* was performed. For this, four query strains expressing either the WT or one of the low-fidelity DNA polymerase alleles *pol1-L868M*, *pol2-M644G* and *pol3-L612M* were crossed against the quadruplicated yeast non-essential gene deletion collection (~4800 different gene deletions) following a modified version of the synthetic genetic array (SGA) (TONG AND BOONE 2006)(Fig 4.1A).

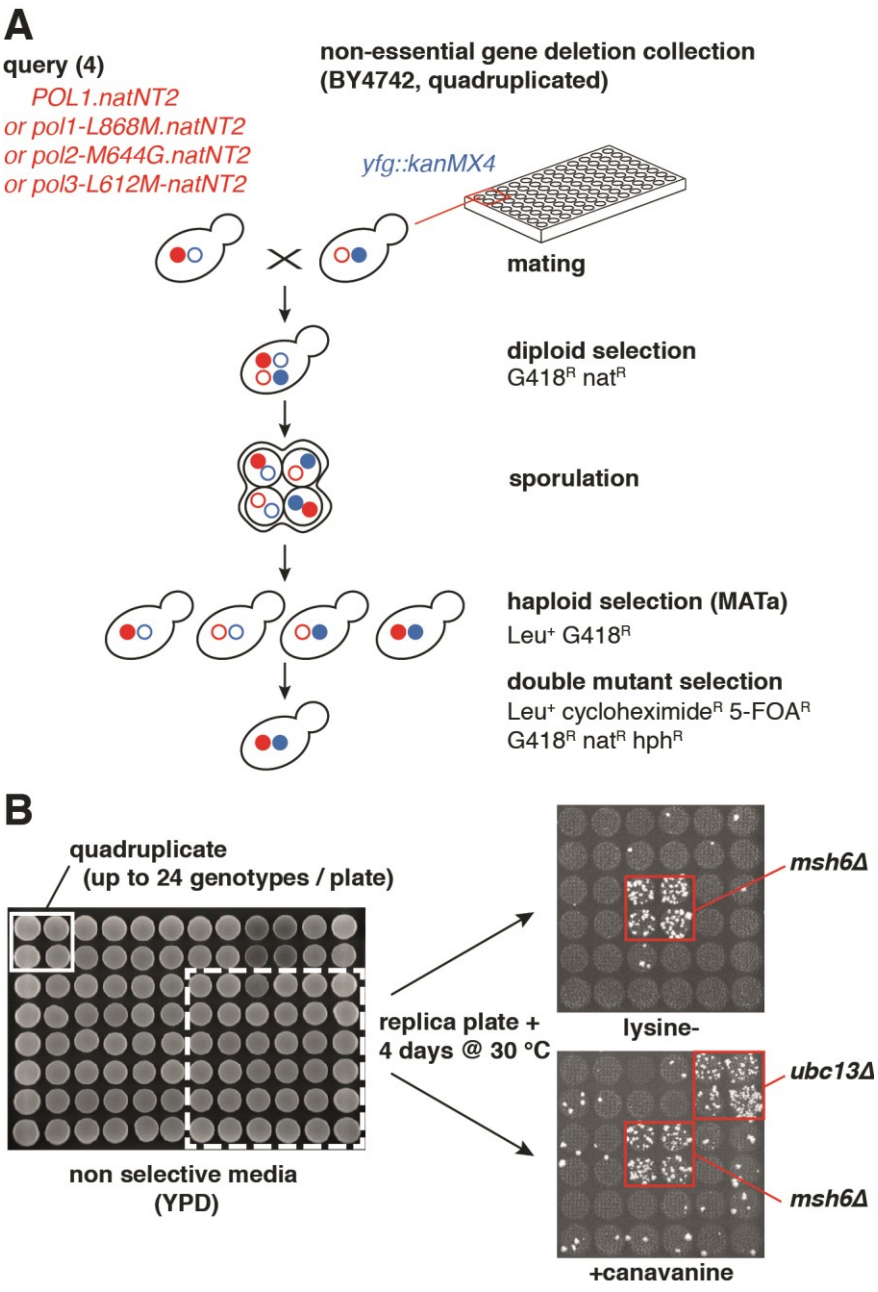

Fig. 4.1 Genome-wide screen reveals genes that affect DNA replication fidelity in *S. cerevisiae*. (A) Strategy used to cross the nonessential gene deletion collections against DNA polymerase active-site mutants and the WT. (B) The forward *CAN1* inactivation assay (+canavanine) and the *lys2-10A* frameshift reversion assay (lysine-) were used to screen for mutator phenotypes in 96-well format. Cells were spotted on YPD, grown and replica plated on mutator plates. The number of colonies is indicative for the strength of the mutator phenotype. In the zoom-in on the right side, *msh6Δ* shows elevated papillation in the frameshift-specific mutator assay and the general *CAN1* inactivation assay, whereas *ubc13Δ* showed increased number of colonies exclusively in the *CAN1* inactivation assay. Figure was adapted from (SCHMIDT *et al.* 2017).

Table 4.1 List of single gene deletions resulting in increased mutator phenotypes.

Gene	*lys2-10A*	*CAN1*	WT function	Reference
CCS1		X	Copper chaperone, oxidative stress response	1
CSM2		X	Component of Shu complex, error-free DNA repair	1, 2
ELG1	X	X	Subunit of RFC1-like complex, DNA replication and genome integrity	1, 2
EXO1	X	X	5'-3' exonuclease and flap endonuclase, DSB repair, error-free PRR and MMR	3
MET7		X	Folylpolyglutamate synthetase	this study
MLH1	X	X	MMR	1, 2
MLH3	X		MMR, meiotic recombination	4
MMS2		X	Ubiquitin-conjugating enzyme, error-free PRR	1, 2
MPH1		X	DNA helicase	2
MRE11		X	Nuclease subunit of MRX complex in DSB	1, 2
MSH2	X	X	MMR	1, 2
MSH3	X	X	MMR	2
MSH6	X	X	MMR	1, 2
OGG1		X	8-oxoguanine DNA glycosylase, BER	1, 2
PIF1		X	DNA helicase	1
PMS1	X	X	MMR	1
PSY3		X	Component of Shu complex, error-free DNA repair	1
RAD1		X	Single-stranded DNA endonuclease, NER, DSB	2
RAD4		X	NER	5
RAD5		X	DNA helicase, PRR	1, 2
RAD10		X	Single-stranded DNA endonuclease, NER, DSB	6
RAD14		X	NER	7
RAD17		X	DNA damage checkpoint	8
RAD18		X	E3 ubiquitin ligase, PRR	1, 2
RAD27		X	5' to 3' exonuclease, 5' flap endonuclease, DNA replication and repair	1, 2
RAD50		X	Subunit of MRX complex, DSB repair	1
RAD51		X	DSB repair	1
RAD52		X	DSB repair	1, 2
RAD54		X	DSB repair	1, 2
RAD55		X	DSB repair	1
RAD57		X	DSB repair	1, 2
RNH203		X	Ribonucleotide H2 subunit, ribonucleotide excision repair	1
SHU1		X	Component of Shu complex, error-free DNA repair	1, 2
SHU2		X	Component of Shu complex, error-free DNA repair	1
TSA1		X	Thioredoxin peroxidase, oxidative stress response	1, 2
UBC13		X	E2 ubiquitin-conjugating enzyme, error-free PRR	9
UNG1		X	Uracil-DNA glycosylase, BER	1, 2
XRS2		X	Subunit of MRX complex, DSB repair	1
YAP1		X	Transcription factor, oxidative stress response	1

The following mutants including: *sli15Δ*, *ygr050cΔ*, *yhl005cΔ*, *yml083c, ymr166cΔ*, and *zwf1Δ* were identified as false positives. Abbreviations: base excision repair (BER), double-strand break (DSB), mismatch repair (MMR), nucleotide excision repair (NER), post-replicative repair (PRR). References: 1 (HUANG *et al.* 2003); 2 (SMITH *et al.* 2004); 3 (TISHKOFF *et al.* 1997); 4 (FLORES-ROZAS AND KOLODNER 1998); 5 (HOWLETT AND SCHIESTL 2004); 6 (BERTRAND *et al.* 1998); 7 (SCOTT *et al.* 1999); 8 (COLLURA *et al.* 2012); 9 (BRUSKY *et al.* 2000).

The generated double mutants were subsequently screened in a “semi-high-throughput” 96-well format for increased mutator phenotypes in the *lys2-10A* frameshift reversion assay and the forward *CAN1* inactivation assay (Fig. 4.1B). The *lys2-10A* assay is specific to one A:T nucleotide deletion events in a mononucleotide run of 10 A:T (TRAN *et al.* 1997). The *CAN1* inactivation assay is a general forward mutation reporter assay (WHELAN *et al.* 1979) and scores for events that inactivate the *CAN1* gene facilitating resistance to the toxic arginine analog canavanine. These inactivating events can be base pair substitutions and frameshift mutations, but also more complex genetic alterations and gross chromosomal rearrangements (GCRs).

The active-site mutant alleles of the three major DNA polymerases used in the screen confer a mild mutator phenotype (NIIMI *et al.* 2004; PAVLOV *et al.* 2006; VENKATESAN *et al.* 2006; PURSELL *et al.* 2007; NICK MCELHINNY *et al.* 2008) but do not interfere with Pol2/Pol3 DNA proofreading function. In the screen, the low-fidelity alleles serve as “sensitized backgrounds” to identify previously unrecognized genes that contribute to DNA replication fidelity. Furthermore, due to the postulated role in leading- and lagging-strand DNA replication according to the “division of labor” model, the comparison of the genetic mutator interactions may reveal mechanistic differences between leading- and lagging-strand replication and repair as previously reported for the 5’-3’ double-stranded exonuclease Exo1 (HOMBAUER *et al.* 2011a; LIBERTI *et al.* 2013).

In the WT polymerase background 8 single gene deletions were identified that showed an elevated frameshift mutator phenotype in the *lys2-10A* reporter assay (Table 4.1). All of them have been previously reported (FLORES-ROZAS AND KOLODNER 1998; TISHKOFF *et al.* 1998; HUANG *et al.* 2003; SMITH *et al.* 2004) and most of them are well-characterized MMR components (REYES *et al.* 2015). Given that the screen identified not only mutations resulting in strong (*mlh1Δ*, *pms1Δ* and *msh2Δ*) but also in weak mutator phenotypes (*elg1Δ*, and *mlh3Δ*), it is unlikely that additional non-essential single deletion mutants may cause an increased frameshift mutator phenotype.

Analysis of the *CAN1* reporter assay plates revealed 38 single gene deletions that resulted in increased *CAN1* inactivation in the presence of WT DNA polymerases. Most of them have been previously identified in two genome-wide screens (HUANG *et al.* 2003; SMITH *et al.* 2004) and have known roles in DNA replication and DNA repair (Table 4.1). Interestingly, one gene deletion *met7Δ* has not been previously linked to an increased *CAN1* mutator phenotype. Therefore, the role of Met7 in mutation avoidance and genome stability was further investigated. A detailed analysis is described in section 4.2.

Analysis of the qualitative mutator phenotypes in the presence of low-fidelity DNA polymerase alleles revealed a group of genes (*EXO1*, *GLN3*, *RRM3*, *SHM2* and *URA7*) that showed synergistic mutator interactions with at least two of the low-fidelity DNA polymerase alleles in the *CAN1* reporter assay (three representative examples of the screening plates are shown in Fig. 4.2). However, besides the previously reported synergistic interaction between low-fidelity DNA polymerase alleles and *exo1Δ* (HOMBAUER *et al.* 2011a; LIBERTI *et al.* 2013), no additional gene mutation caused an elevated frameshift mutator phenotype in the presence of the low-fidelity DNA polymerase alleles, arguing again for no additional, unrecognized single-gene deletion that increases frameshift mutations in the subset of the non-essential yeast genes (Fig. 4.2). Interestingly, none of the identified gene deletions, except *exo1Δ*, caused an increased mutator

phenotype in the presence of WT DNA polymerases. Moreover, these identified genes have not been previously linked to the suppression of mutations. Thus, this group of genes was further examined in respect to their role in replication fidelity and the results are described in section 4.3.

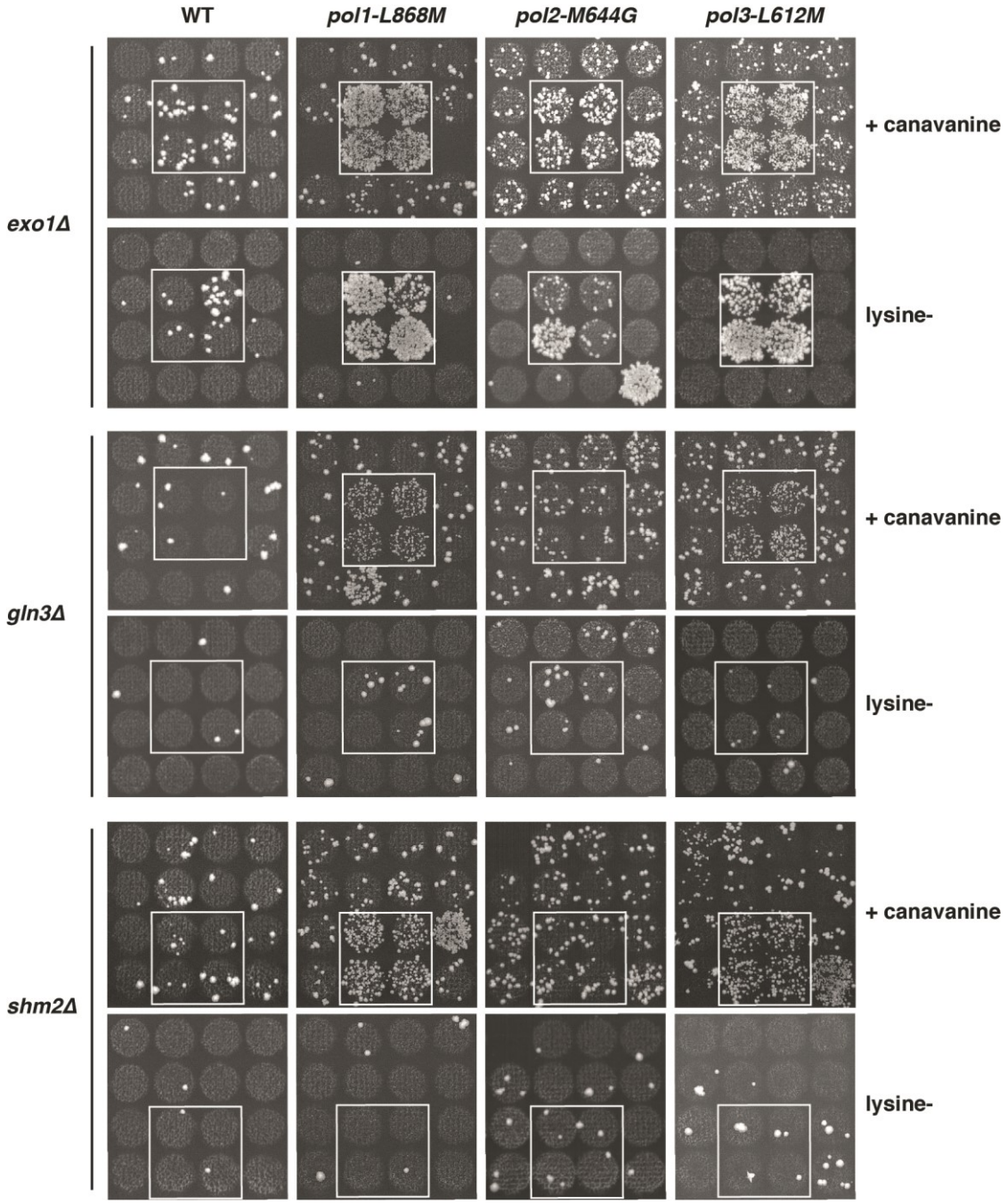

Fig. 4.2 Representative images of mutator plates (zoom-in) illustrating the synergistic mutator interactions in some *S. cerevisiae* double mutants.
Inactivation of *EXO1*, *GLN3* or *SHM2* in combination with the lagging-strand DNA polymerase active-site mutants (*pol1-L868M* and *pol3-L612M*) results in a strong increase in the number of colonies on *CAN1* mutator assay plates (+canavanine), whereas increased papillation on the frameshift reporter plates (-lysine) was exclusively observed in *exo1Δ* double mutants. Figure was adapted from (SCHMIDT *et al.* 2017).

4.2 The folylpolyglutamate synthetase Met7 prevents uracil accumulation and genome instability.

4.2.1 Met7 prevents the accumulation of mutations and GCRs.

The genome-wide screen identified *MET7* as the only previously unrecognized gene that prevents the accumulation of mutations. *MET7* encodes for the cytoplasmic and mitochondrial folylpolyglutamate synthetase (FPGS) in *S. cerevisiae* (DESOUZA *et al.* 2000). FPGS catalyzes the ATP-dependent addition of a glutamate to the terminal glutamate of folates (Fig. 1.8A). Polyglutamylated folate show increases cellular retention and higher affinity to their metabolizing enzymes (SCHIRCH AND STRONG 1989). In *S. cerevisiae*, inactivation of *MET7* has been shown to result in mitochondrial dysfunction (*petite* phenotype) (CHEREST *et al.* 2000; MERZ AND WESTERMANN 2009), methionine auxotrophy (MASSELOT AND DE ROBICHON-SZULMAJSTER 1975), short telomeres (ASKREE *et al.* 2004; GATBONTON *et al.* 2006), a non-homologous end-joining defect and dNTP imbalance (RUBINSTEIN *et al.* 2014). However, inactivation of *MET7* has not been linked to increased mutator phenotypes. Thus, to validate the initial qualitative *met7Δ* mutator phenotype identified in the genome-wide screen, *MET7* was inactivated in a WT strain and the *CAN1* mutation rate was measured. Indeed, loss of Met7 resulted in a 9-fold increase in the *CAN1* inactivation assay over the WT (Table 4.2). As the *CAN1* gene can be inactivated not only by base substitutions and frameshifts, but also by GCRs, Met7's role in the suppression of GCRs was investigated using two different GCR assays. These GCR reporters score for the simultaneous deletion of a *CAN1-URA3* cassette integrated at two different locations in the left arm of chromosome V (PUTNAM AND KOLODNER 2017). Inactivation of *MET7* caused a 38- and 177-fold increase over WT in the standard (CHEN AND KOLODNER 1999) and post-duplication GCR assay (PUTNAM *et al.* 2009), respectively (Table 4.2). Thus, Met7 not only suppresses the accumulation of mutations, but is also required to prevent GCRs.

Table 4.2 *met7Δ* results in accumulation of mutations and gross chromosomal rearrangements (GCRs).

Relevant genotype	Mutation Rate Can^R (fold increase)[a]	Standard GCR (fold increase)[b]	Post-duplication GCR (fold increase)[b]
WT	7.2 [5.7-9.0] x 10^{-8} (1)	5.1 [0.0-38.0] x 10^{-11} (1)	5.6 [3.7-8.3] x 10^{-8} (1)
met7Δ	6.4 [4.2-8.8] x 10^{-7} (9)	2.0 [1.0-3.6] x 10^{-9} (38)	9.9 [7.4-13.7] x 10^{-6} (177)
pGPD-DUT1 met7Δ	2.9 [1.9-5.5] x 10^{-7} (4)	not determined	4.6 [3.6-7.4] x 10^{-7} (8)
ung1Δ met7Δ	not determined	not determined	2.6 [2.0-3.5] x 10^{-6} (46)
pGPD-met7Δm	not determined	not determined	6.3 [4.5-8.1] x 10^{-8} (1)
dut1-1	1.3 [1.0-2.5] x 10^{-7} (2)	not determined	1.2 [0.4-1.6] x 10^{-7} (2)
rev3Δ met7Δ	3.0 [2.5-3.7] x 10^{-7} (4)	not determined	not determined

[a] Median rates of inactivation of *CAN1* gene (Can^R) with 95% confidence interval in square brackets and fold increase relative to the WT in parentheses.
[b] Median rates of accumulating Can^R $5\text{-}FOA^R$ progeny in standard and post-duplication GCR with 95% confidence interval in square brackets and fold increase relative to the WT in parentheses.

4.2.2 Loss of *MET7* activates the DNA damage response.

In the absence of Met7, cells confer a slow growth phenotype (DESOUZA *et al.* 2000; KOREN *et al.* 2010). To investigate, whether *met7Δ* cells also showed an activated DNA damage response (DDR), whole cell lysates of WT and *met7Δ* cells were analyzed by Western blotting. In the absence of Met7, the checkpoint kinase Rad53 showed slower electrophoretic mobility, characteristic of Rad53 phosphorylation, and thus the activation of the DDR. Moreover, strong induction of the DNA damage inducible alternative large RNR subunit Rnr3 was detected (Fig. 4.3A). Furthermore, DNA content analysis of logarithmically growing WT and *met7Δ* cells by flow cytometry revealed that cells in the absence of Met7 showed an altered cell cycle profile with cells accumulating in S phase (Fig. 4.3B)(KOREN *et al.* 2010).

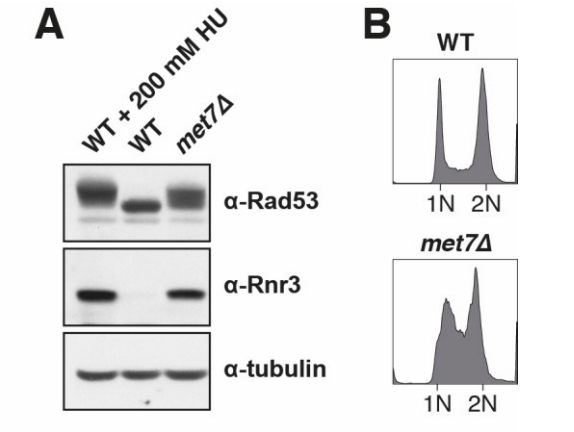

Fig. 4.3 Inactivation of *MET7* causes activation of the DNA damage checkpoint.
(A) Whole cell lysates of logarithmically growing WT and *met7Δ* were analyzed by SDS-PAGE and immunoblotting against Rad53, Rnr3 and tubulin. As positive control for the activation of the DNA damage response, WT cells treated for 3 h with 200 mM hydroxyurea (HU) were used. (B) DNA content profiles of logarithmically grown WT and *met7Δ* cells

These observations open up the possibility that Met7 function might be primarily required during S phase and that Met7 expression levels may be potentially regulated across the cell cycle. To test whether Met7 expression levels are changing during the cell cycle, the *MET7* gene was C-terminal tagged with 3xMyc tag to follow Met7 protein levels throughout the cell cycle by Western blotting. The results indicate that Met7 expression levels were stable throughout the cell cycle (Fig 4.4).

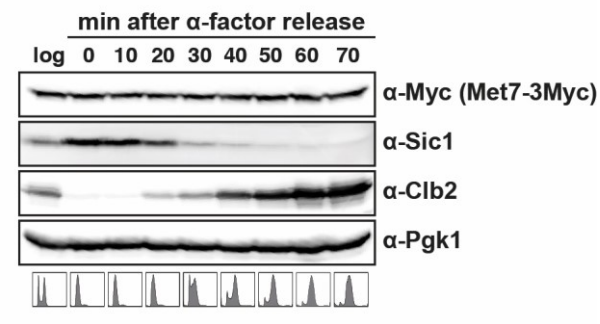

Fig. 4.4 Met7 is present throughout the cell cycle.
Cells expressing C-terminal tagged Met7-3Myc from the endogenous chromosomal locus were arrested in G1 with α-factor and released in YPD containing nocodazole. Samples were taken every 10 min for whole cell lysates and DNA content profiles. Samples were analyzed by SDS-PAGE and immunoblotting against Myc for Met7-3xMyc, Sic1 as G1 marker, Clb2 as G2 marker and Pgk1 as loading control.

In summary, inactivation of *MET7* results in DNA damage checkpoint activation and accumulation of cells in S phase. However, Met7 expression levels were not increased in S phase and relatively stable throughout the cell cycle.

4.2.3 Inactivation of *MET7* results in a dNTP imbalance and dUTP accumulation.

The slow growth phenotype of *met7Δ* strains (CHEREST *et al.* 2000; DESOUZA *et al.* 2000; MERZ AND WESTERMANN 2009) and the accumulation of cells in S phase in the absence of Met7 (Fig.

4.3B)(KOREN *et al.* 2010) suggested that Met7 supports metabolic reactions important for S phase progression. A previous study described a cytoplasmic *met7ΔM* allele that lacks the N-terminal mitochondrial leader sequence, which when overexpressed suppressed the *petite* phenotype described for *met7Δ* strains (DESOUZA *et al.* 2000). To test in which compartment Met7 is required to suppress DDR activation and GCRs, the cytoplasmic *met7ΔM* allele was expressed under the control of a strong constitutive *GPD* promoter. This neither resulted in an increased post-duplication GCR rate (Table 4.2), nor in accumulation of cells in S phase or DNA damage checkpoint activation (Fig. 4.7A,B). These findings suggested that the cytoplasmic FPGS activity and presumably cytoplasmic folate pools are sufficient to prevent the slow growth phenotype and potentially the mutator phenotype in the absence of Met7. As cytoplasmic folate pools are required for nucleotide biosynthesis and dNTPs are essential for DNA replication during S phase, NTP and dNTP concentrations were determined in logarithmically growing WT and *met7Δ* mutant strains (collaboration with Chabes lab, Umeå University).

Table 4.3 NTP and dNTP concentrations of *met7Δ* mutants.

A

Relevant genotype	CTP	UTP	ATP	GTP
WT	2374 ± 16 (1.0)	5605 ± 32 (1.0)	11339 ± 48 (1.0)	3987 ± 67 (1.0)
met7Δ	2206 ± 5 (0.9)	4109 ± 60 (0.7)	13697 ± 153 (1.2)	4514 ± 3 (1.1)
met7Δ pGPD-DUT1	2242 ± 9 (0.9)	3915 ± 13 (0.7)	13676 ± 57 (1.2)	4601 ± 15 (1.2)

B

Relevant genotype	dCTP	dTTP	dATP	dGTP	dUTP
WT –hDUT1	114 ± 4 (1.0)	203 ± 6 (1.0)	125 ± 4 (1.0)	82 ± 4 (1.0)	not detectable
WT + hDUT1	104 ± 1 (0.9)	203 ± 7 (1.0)	123 ± 4 (1.0)	81 ± 1 (1.0)	not detectable
met7Δ - hDUT1	302 ± 7 (2.7)	125 ± 5 (0.6)	497 ± 1 (4.0)	49 ± 4 (0.6)	9 ± 2
met7Δ + hDUT1	282 ± 3 (2.5)	125 ± 6 (0.6)	490 ± 9 (3.9)	49 ± 6 (0.6)	not detectable
met7Δ pGPD-DUT1 - hDUT1	314 ± 1 (2.8)	95 ± 2 (0.5)	463 ± 1 (3.7)	38 ± 2 (0.5)	not detectable
met7Δ pGPD-DUT1 + hDUT1	284 ± 1 (2.5)	95 ± 1 (0.5)	444 ± 5 (3.6)	40 ± 2 (0.5)	not detectable

NTP (A) and dNTP (B) concentrations (pmol per 10^8 cells) are the average of two biological replicates ± standard deviation with the fold increase over WT in parentheses. Extracts of + hDUT1 samples were treated for 1 h at 37 °C with 1ng/µL recombinant human DUT1 prior the measurement. NTP and dNTP concentrations were measured in collaboration with Chabes lab.

In the absence of Met7, NTP purine pools were mildly increased (up to 20%) and NTP pyrimidine pools decreased (up to 30%) (Table 4.3A). dNTP concentration measurements revealed that inactivation of *MET7* caused 2.7-fold increased dCTP and 4-fold increased dATP pools and 40% decreased dTTP and dGTP pools, relative to WT levels (Fig. 4.5A, Table 4.3B). The dNTP pool measurements were similar to previously dNTP concentrations in *met7Δ* cells (RUBINSTEIN *et al.* 2014). Interestingly, the dNTP pools measured in the absence of Met7 were similar to dNTP pools measured in mammalian cells upon antifolate treatment (TATTERSALL AND HARRAP 1973; RITTER *et al.* 1980; YOSHIOKA *et al.* 1987). Antifolates inhibit folate-dependent metabolic reactions (VAN TRIEST *et al.* 2000; VISENTIN *et al.* 2012) suggesting that the dNTP pool alterations measured in

met7Δ are presumably a consequence of folate depletion due to the absence of Met7. As mammalian cells treated with antifolates show not only dNTP imbalance but also dUTP accumulation (VAN TRIEST *et al.* 2000), the consequences of *MET7* inactivation on dUTP pools was investigated. dUTP pool accumulation is normally efficiently counteracted by the dUTPase Dut1, which dephosphorylates dUTP to dUMP (GADSDEN *et al.* 1993). Consequently, dUTP concentrations in WT cycling cells are extremely low. However, analysis of cell extracts obtained from *met7Δ* strains revealed 9 ± 2 pmol dUTP per 10^8 cells were measured, whereas dUTP concentrations in WT was below the detection limit (Fig. 4.5 A, Table 4.3 B).

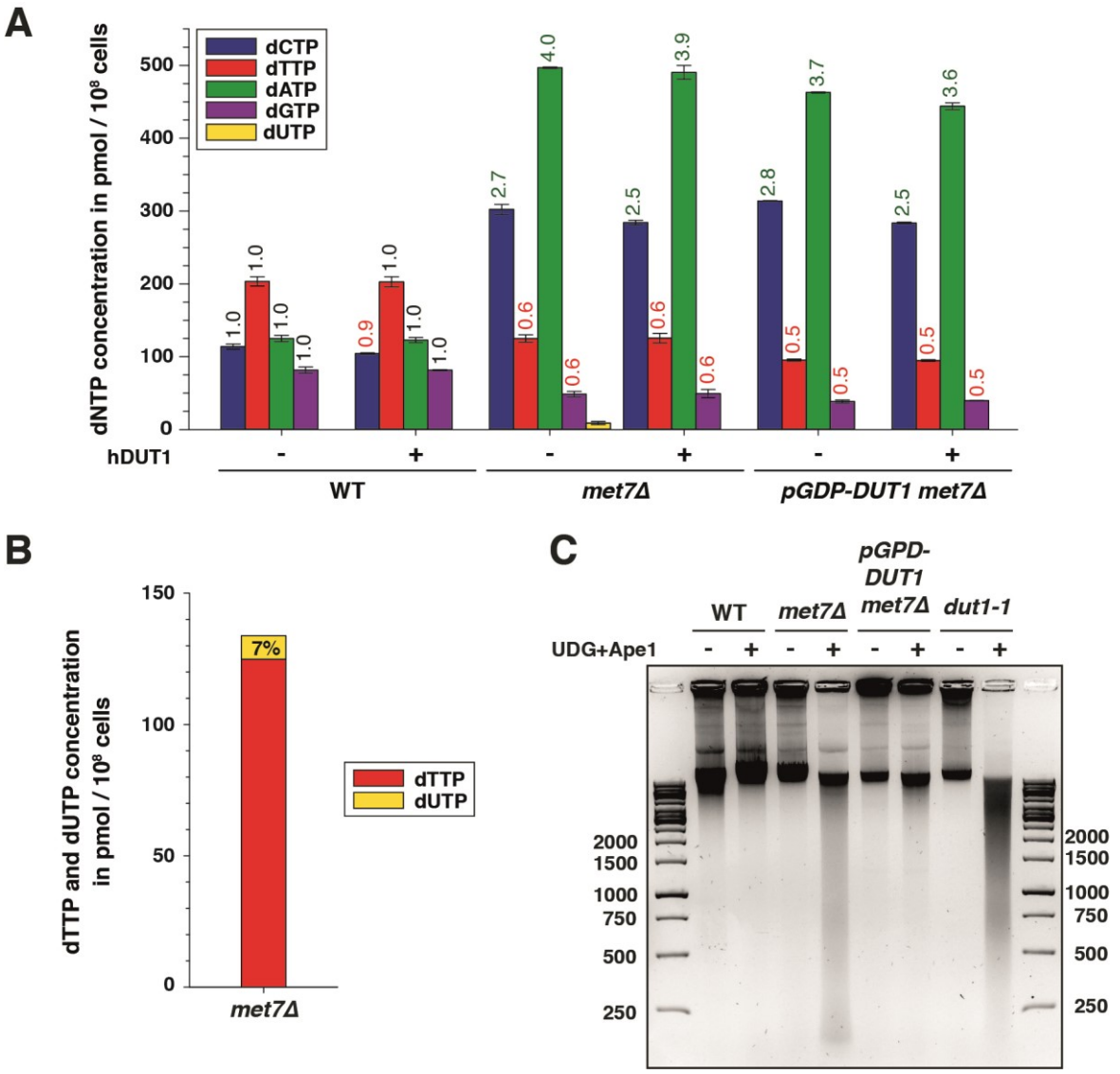

Fig. 4.5 Loss of Met7 results in a dNTP imbalance, accumulation of dUTP and increased uracil incorporation.
(A) dNTP concentration measurement in the indicated strains (Table 4.3B). Error bars represent standard deviation (SD). The fold over WT is indicated above each bar and color-coded green or red for increased and decreased fold over WT, respectively. Extracts were treated ± recombinant human dUTPase hDUT1 prior to the measurement. (B) Total dTTP and dUTP pools in *met7Δ*. (C) Uracil accumulation assay. Genomic DNA of logarithmically growing WT, *met7Δ*, *met7Δ pGPD-DUT1* and *dut1-1* cells were treated ± recombinant E. coli UDG and human Ape1 and analyzed by agarose gel electrophoresis. Presence of uracil in DNA results in fragmentation of the genomic DNA and appears as a smear of lower molecular weight fragments. To enrich for genomic uracil the experiment was performed in an *ung1Δ* background.

To verify that the measured dUTP concentration in *met7Δ* cells was truly dUTP, cellular extracts were treated or not with recombinant human DUT1 (hDUT1) prior to the dNTP measurement. Strikingly, dUTP was no longer detectable in the hDUT1 treated *met7Δ* sample, whereas no major changes were observed in the other dNTP pools (Fig. 4.5A, Table 4.3B). Likewise, *met7Δ* cells overexpressing the *DUT1* gene (*pGPD-DUT1*) presented undetectable levels of dUTP and otherwise identical dNTP concentrations as measured in the *met7Δ* strain (Fig. 4.5A, Table 4.3B). As DNA polymerases cannot discriminate between dTTP and dUTP, the balance between dTTP and dUTP directly determines which dNTP will be incorporated during DNA synthesis (SHLOMAI AND KORNBERG 1978; WARNER *et al.* 1981; TINKELENBERG *et al.* 2002). According to the dNTP concentration measurements in *met7Δ* cells, dUTP contributes to 7% of the total dTTP and dUTP pool (Fig. 4.5B). Previous studies have shown that the alterations in the dUTP/dTTP balance (e.g. caused by antifolate treatment) can lead to increased dUTP incorporation into genomic DNA (SHLOMAI AND KORNBERG 1978; WARNER *et al.* 1981; TINKELENBERG *et al.* 2002). These observations and the altered dUTP/dTTP balance detected *met7Δ* strains suggest that *met7Δ* cells may incorporate dUTP into genomic DNA.

To test this idea, uracil accumulation in genomic DNA of WT, *met7Δ*, *met7Δ pGPD-DUT1* and *dut1-1* cells was analyzed. As uracil is efficiently removed from DNA by the BER system (BOITEUX AND JINKS-ROBERTSON 2013), the analysis was performed in an uracil deglycosylase-deficient background (*ung1Δ*) (SEIPLE *et al.* 2006). Genomic DNA of logarithmically growing cells was purified, treated (or not) with recombinant *E. coli* uracil-DNA glycosylase (UDG) and human apurinic/apyrimidinic (AP) endonuclease 1 (hAPE 1) and separated by agarose gel electrophoresis. Incorporated uracil results in fragmentation of genomic DNA and appears as smear of lower molecular weight fragments. In line with low dUTP concentrations (Fig. 4.5A, Table 4.3B), no fragmentation was observed in genomic DNA isolated from WT cells. However, in the absence of Met7, genomic DNA was strongly fragmented and fragments up to sizes below 250 nt were observed (Fig. 4.5C). In agreement with the dUTP measurements (Fig. 4.5A, Table 4.3B), overexpression of *DUT1* in *met7Δ* cells strongly suppressed DNA fragmentation. The previously reported *dut1-1* allele, which confers reduced dUTPase activity and causes increased genomic uracil accumulation (GUILLET *et al.* 2006) was included in the experiment as positive control and showed in line with the previous report massive fragmentation of the genomic DNA (Fig. 4.5C). Thus, loss of Met7 induces a dNTP imbalance, dUTP accumulation and increased uracil incorporation during DNA replication.

4.2.4 The *met7Δ* GCR phenotype is driven by dUTP accumulation and processing of genomic uracil.

In order to test whether *met7Δ*'s GCR phenotype is driven by dUTP accumulation, GCR rate was measured in *met7Δ pGPD-DUT1* cells, in which neither elevated dUTP pools (Fig. 4.5A, Table 4.3B) nor accumulation of genomic uracil species (Fig. 4.5C) could be detected. Strikingly, the GCR rate was suppressed from 177- to 8-fold over WT in *met7Δ* cells that overexpressed *DUT1* (Table 4.2) arguing that the GCRs generated in the absence of Met7 were largely consequence of the increased dUTP levels.

As previously mentioned, genomic uracil is recognized and repaired by BER (BOITEUX AND JINKS-ROBERTSON 2013). The uracil glycosylase Ung1 removes the uracil base and creates an abasic site. AP endonucleases introduce a single-strand DNA break at the abasic site followed by either short or long patch repair. Therefore, a high amount of incorporated uracil may not only result in transient single-strand breaks but also DSBs, that can eventually result in GCRs. Consequently, inhibiting repair of genomic uracil by inactivation of *UNG1* should counteract *met7Δ*'s GCR phenotype. Indeed, inactivation of *UNG1* in the absence of Met7 partially suppressed the post-duplication GCR rate by almost 75% (Table 4.2). This indicates that the processing of genomic uracil in the presence of an increased dUTP/dTTP ratio results in futile-repair cycles that may lead to GCRs. Therefore, the increased GCRs observed in the absence of Met7 are a consequence of dUTP pool accumulation followed by futile-repair cycles.

4.2.5 Increased mutations in the absence of Met7 are a consequence of a dNTP pool imbalance and dUTP accumulation.

Inactivation of *MET7* not only resulted in elevated GCRs, but also in an increased *CAN1* inactivation rate (Table 4.2). Abasic sites, as for example produced by the repair of genomic uracil, lead to stalled replication forks and recruitment of specialized translesion synthesis (TLS) DNA polymerases, such as Polζ (Rev3) (MCCULLOCH AND KUNKEL 2008; LANGE *et al.* 2011). These TLS DNA polymerases are error-prone and may therefore contribute to the mutator phenotype observed in *met7Δ*. In line with this assumption, the *CAN1* mutation rate was approximately 50% reduced in the *met7Δ rev3Δ* double mutant in comparison to *met7Δ* (Table 4.2).

Table 4.4 *CAN1* mutation spectrum of *met7Δ*.

Relevant genotype	Insertion / deletion			Base change		Complex
		Mutation	Occurrence	Mutation	Occurrence	Occurrence
WT	ΔA	A6 → A5	1 (1)	A-T → G-C	6 (7)	8 (9)
	ΔT	T6 → T5	2 (2)	G-C → A-T	18 (20)	
		T2 → T1	2 (2)	G-C → T-A	29 (32)	
	ΔC	C2 → C1	1 (1)	A-T → C-G	3 (3)	
		C1 → C0	2 (2)	A-T → T-A	7 (8)	
	+T	T6 → T7	3 (3)	C-G → G-C	6 (7)	
		T2 → T3	3 (3)			
	+G	G2 → G3	1 (1)			
			15 (16)		**69 (75)**	**8 (9)**
met7Δ	ΔA	A3 → A2	1 (1)	A-T → G-C	5 (3)	19 (10)
	ΔT	T6 → T5	4 (2)	G-C → A-T	54 (29)	
		T4 → T3	4 (2)	G-C → T-A	40 (22)	
		T3 → T2	2 (1)	A-T → C-G	11 (6)	
		T1 → T0	3 (2)	A-T → T-A	14 (8)	
	ΔG	G4 → G3	2 (1)	C-G → G-C	19 (10)	
		G2 → G1	2 (1)			
		G1 → G0	1 (1)			
	ΔC	C3 →C2	2 (1)			
		C2 → C1	1 (1)			
	+T	T6 → T7	1 (1)			
			23 (12)		**143 (77)**	**19 (10)**

The *CAN1* mutation spectra based on DNA sequencing of individual Can^R mutants, shown as the number of clones containing the indicated mutations, and in parenthesis as the percentage relative to the total (Fig. S7.1 and Fig. S7.2).

Moreover, overexpression of *DUT1* in *met7Δ* suppressed the *CAN1* inactivation rate to a similar degree as the *met7Δ rev3Δ* double mutant (Table 4.2). Both results together support the idea that dUTP accumulation also contributes to the generation of *CAN1* inactivation events.

To further characterize the type of events that lead to *CAN1* inactivation, *CAN1* mutation spectra analysis were performed in WT and *met7Δ* strains (Table 4.4). Interestingly, the *met7Δ CAN1* mutation spectrum was not significantly different to the WT *CAN1* spectrum (Fisher's exact test, p value 0.2275) and no mutational hotspots could be identified. However, increased amount of G-C to A-T mutations and decreased G-C to T-A mutations in the *met7Δ CAN1* mutation spectrum were in line with elevated dATP and dCTP pools and reduced dTTP and dGTP pools (Table 4.3B). Hence, in addition to dUTP accumulation, the general dNTP imbalance seems to contribute to the *CAN1* inactivation.

4.2.6 A DSB repair defect is required for dUTP-driven GCRs.

Both, inactivation of *MET7* and reduced dUTPase activity (*dut1-1*) (GUILLET *et al.* 2006) caused increase uracil incorporation during DNA replication (Fig. 4.5C). Surprisingly, in contrast to *met7Δ* cells, *dut1-1* expressing cells showed neither an increased *CAN1* inactivation rate nor an elevated post-duplication GCR rate (Table 4.2) suggesting that uracil incorporation alone is not sufficient to cause increased mutations and elevated GCR rates. To search for potential differences that may explain the apparent discrepancy between *met7Δ* and *dut1-1* phenotypes, dNTP concentrations were measured. Interestingly, *dut1-1* expressing cells had slightly elevated, but balanced dNTP pools (Fig. 4.6A). Unexpectedly, dUTP was not detectable in *dut1-1* samples using the same methodology as in Fig. 4.5A (data not shown) presumably due to insufficient sensitivity of the method. Furthermore, RNR subunits were not induced in *dut1-1* (Fig. 4.6B) and no accumulation of cells in S phase was observed (Fig. 4.6C). This is in agreement with the absence of dNTP pool limitations observed in the *dut1-1* strain.

The difference between *met7Δ* and *dut1-1* cells could arise from an overall milder and more specific defect in the *dut1-1* mutant (Fig. 1.6). As dNTP pools in *met7Δ* cells are severely imbalanced and dTTP and dGTP levels are below WT (Fig. 4.6A), *met7Δ* cells might be unable to sufficiently increase dNTP pools for DNA repair. Moreover, the low dTTP levels in the absence of Met7 contribute presumably to an increased dUTP/dTTP ratio. In order to test whether the combination of dUTP accumulation and low dTTP and dGTP levels is required to cause a dUTP-driven GCR phenotype, *DCD1* was inactivated in *dut1-1* cells. *DCD1* is the dCMP deaminase in budding yeast, which converts dCMP to dUMP, which is further metabolized to dTTP (Fig. 1.6)(MCINTOSH AND HAYNES 1984). Previous work in fission yeast suggested that Dcd1 contributes to 75% of the produced dTTP, as *dcd1Δ* cells showed decreased dTTP levels and strongly increased dCTP levels (SANCHEZ *et al.* 2012). Hence, inactivation of *DCD1* in *dut1-1* expressing cells presumably further increases the dUTP/dTTP ratio. In a qualitative post-duplication GCR mutator assay the *dcd1Δ dut1-1* double mutant showed increased papillation (indicative for an elevated GCR phenotype) in comparison to WT and *dut1-1* cells, however less than *met7Δ* cells (Fig. 4.6D). Interestingly, *dcd1Δ dut1-1* cells did not induce RNR subunits (Fig 4.6B) suggesting that even in the presence of both mutations, there is no substantial reduction in dNTP pools to trigger activation of the DDR. Moreover, DNA content analysis of logarithmically growing *dcd1Δ*

dut1-1 cells revealed no accumulation of cells in S phase, but a strongly increased population of cells in G1 (Fig. 4.6C) arguing for a problem in the G1-S transition.

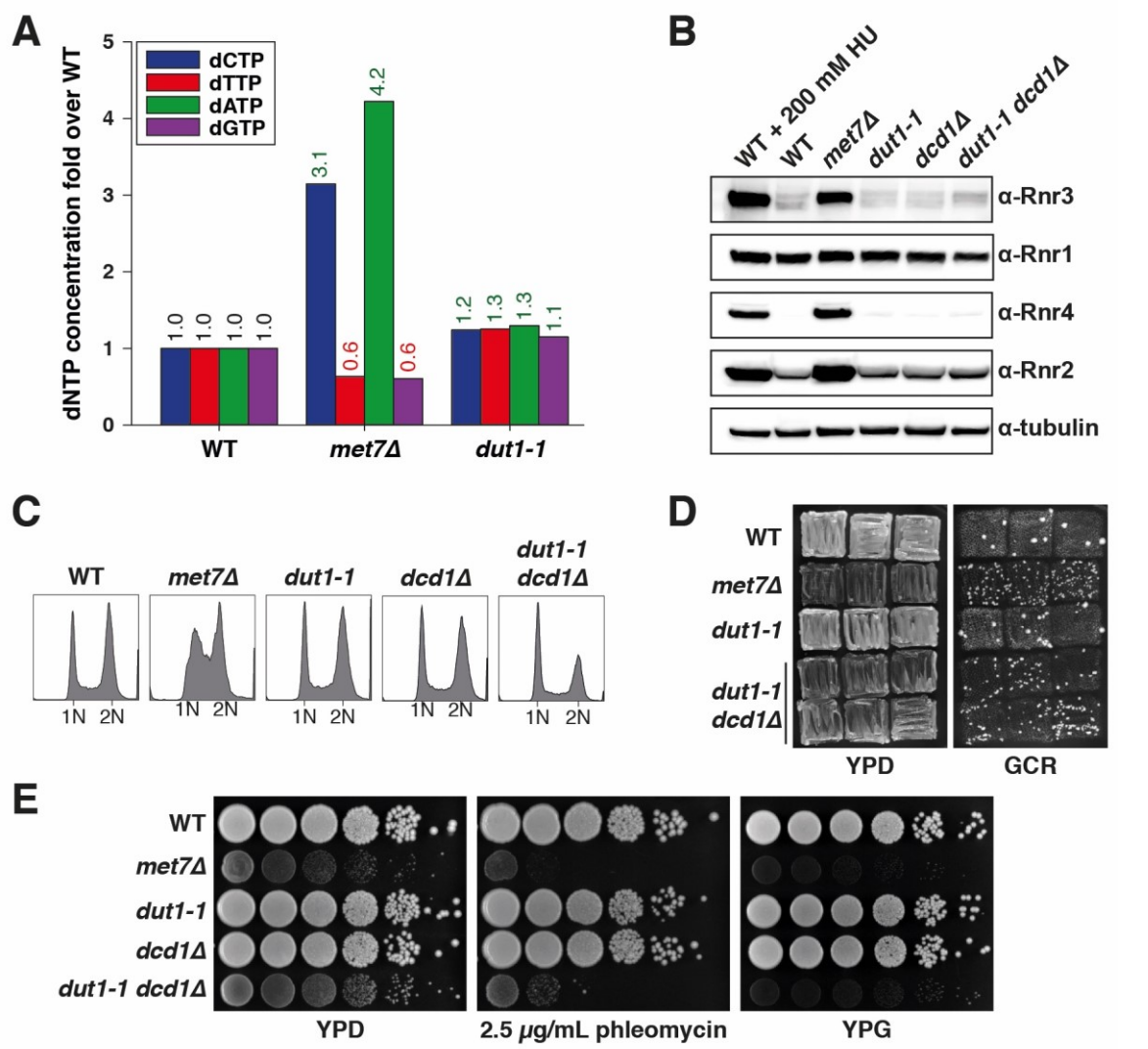

Fig. 4.6 Strains expressing the dUTPase mutant *dut1-1* depend on Dcd1 to prevent genome instability. (A) dNTP concentration measurement in the indicated strains represented as fold over WT. Fold increases are colored in green, whereas decreased levels are labeled red. (B) Whole cell lysates of logarithmically growing indicated strains were analyzed by SDS-PAGE and immunoblotting against Rnr1-4 and tubulin. WT cells treated for 3 h with 200 mM HU were used as positive control for the activation of the DNA damage response. (C) DNA content profiles of logarithmically growing strains of the indicated genotypes. (D) Patch test of the indicated strains. Increased papillation is indicative of an increased GCR phenotype. (E) Spotting assay of the indicated strains in 10-fold serial dilutions on YPD ± the DNA double-strand break inducing agent phleomycin and on YPG to test for mitochondrial dysfunction (*petite*).

As *met7Δ* and *dcd1Δ dut1-1* mutant strains both showed an increased GCR phenotype and DSB are required for GCR formation, the GCR phenotype might be linked to a DSB repair defect in both backgrounds. To test this, the sensitivity of *met7Δ* and *dut1-1 dcd1Δ* cells to the DSB-inducing agent phleomycin was investigated. In line, with the previously reported NHEJ defect of *met7Δ* cells (RUBINSTEIN *et al.* 2014), the absence of Met7 caused extreme sensitivity to phleomycin. While *dut1-1* and *dcd1Δ* cells showed no sensitivity to phleomycin, *dcd1Δ dut1-1* double mutant cells were sensitive to phleomycin, similar to *met7Δ* cells (Fig. 4.6E). Furthermore, as *met7Δ* cells, *dcd1Δ dut1-1* cells conferred a slow growth phenotype and dysfunctional mitochondria (Fig 4.6E).

Thus, the *dcd1Δ dut1-1* double mutant partially recapitulates *met7Δ* phenotypes, suggesting that a combination of dUTP accumulation and DSB repair defect is required to cause uracil-driven GCRs. The DSB repair defect might result from dNTP pool alterations and/or defects associated to the *petite* phenotype.

4.2.7 dUTP accumulation in *met7Δ* is not responsible for the DNA damage checkpoint activation, phleomycin sensitivity and short telomeres.

Inactivation of *MET7* causes pleiotropic effects including slow growth, DNA damage checkpoint activation, DSB repair defects and short telomeres, among others. In order to investigate the role of uracil accumulation in these phenotypes, the consequence of either overexpressing *DUT1* or inactivating *UNG1* in *met7Δ* cells were examined.

First, the impact of dUTP accumulation on DDR activation and growth in the absence of Met7 was investigated. Neither the *met7Δ* double mutant overexpressing *DUT1* nor the *met7Δ* double mutant deficient in *UNG1* could rescue the altered cell cycle distribution of logarithmically growing *met7Δ* cells (Fig. 4.6A). Moreover, *met7Δ* single and double mutants both activate the DNA damage checkpoint according to the increased Rad53 phosphorylation and Rnr3 induction (Fig. 4.6B). Furthermore, all three *met7Δ* strains showed a slow growth phenotype. Even though *pGPD-DUT1 met7Δ* cells grew slightly better than *met7Δ*, the *met7Δ ung1Δ* strain grew worse than *met7Δ* (Fig. 4.6C). Thus, the altered cell cycle, the slow growth phenotype and DNA damage checkpoint activation in *met7Δ* strains is not driven by dUTP accumulation or futile-repair attempts to remove uracil from DNA.

Second, the effect of dUTP accumulation on phleomycin sensitivity was examined. In the absence of Met7, cells confer a NHEJ defect (RUBINSTEIN *et al.* 2014) and were sensitive to the DSB-inducing agent phleomycin (Fig. 4.6). The DSB repair defect in *met7Δ* cells could originate from an inability to increase dNTP pools to sufficient levels to support DSB repair (CHABES *et al.* 2003). Alternatively, inefficient DSB repair could result from the saturation of the DSB repair machinery. One possible explanation for this might be the combination of frequent misincorporation and removal of uracil together with DSBs induced by phleomycin treatment. To investigate whether the phleomycin sensitivity in *met7Δ* is due to saturation of the DSB repair machinery, *met7Δ* cells with inactivated *UNG1* or overexpressing *DUT1* were tested for phleomycin sensitivity. Both double mutants were as sensitive to phleomycin as the *met7Δ* single mutant (Fig. 4.6C). Therefore, the DSB repair defect of *met7Δ* cells is not caused by uracil accumulation in DNA. This indicates that the DSB repair defect of *met7Δ* cells might be linked to the *petite* phenotype and/or be a consequence of the inability to increase dNTP pools in the absence of Met7 to sufficient levels to facilitate DSB repair.

Third, the contribution of genomic uracil to the short telomere phenotype (ASKREE *et al.* 2004; GATBONTON *et al.* 2006; RUBINSTEIN *et al.* 2014) of cells lacking Met7 was tested. As budding yeast telomeres consist of 5'-C_{1-3}A/TG_{1-3}-3' repeats (WELLINGER AND ZAKIAN 2012) the accumulation of dUTP and an increased dUTP/dTTP ratio should also facilitate uracil incorporation into telomeric DNA. Futile-repair cycles of genomic uracil at telomeric regions may cause DSBs at telomeric

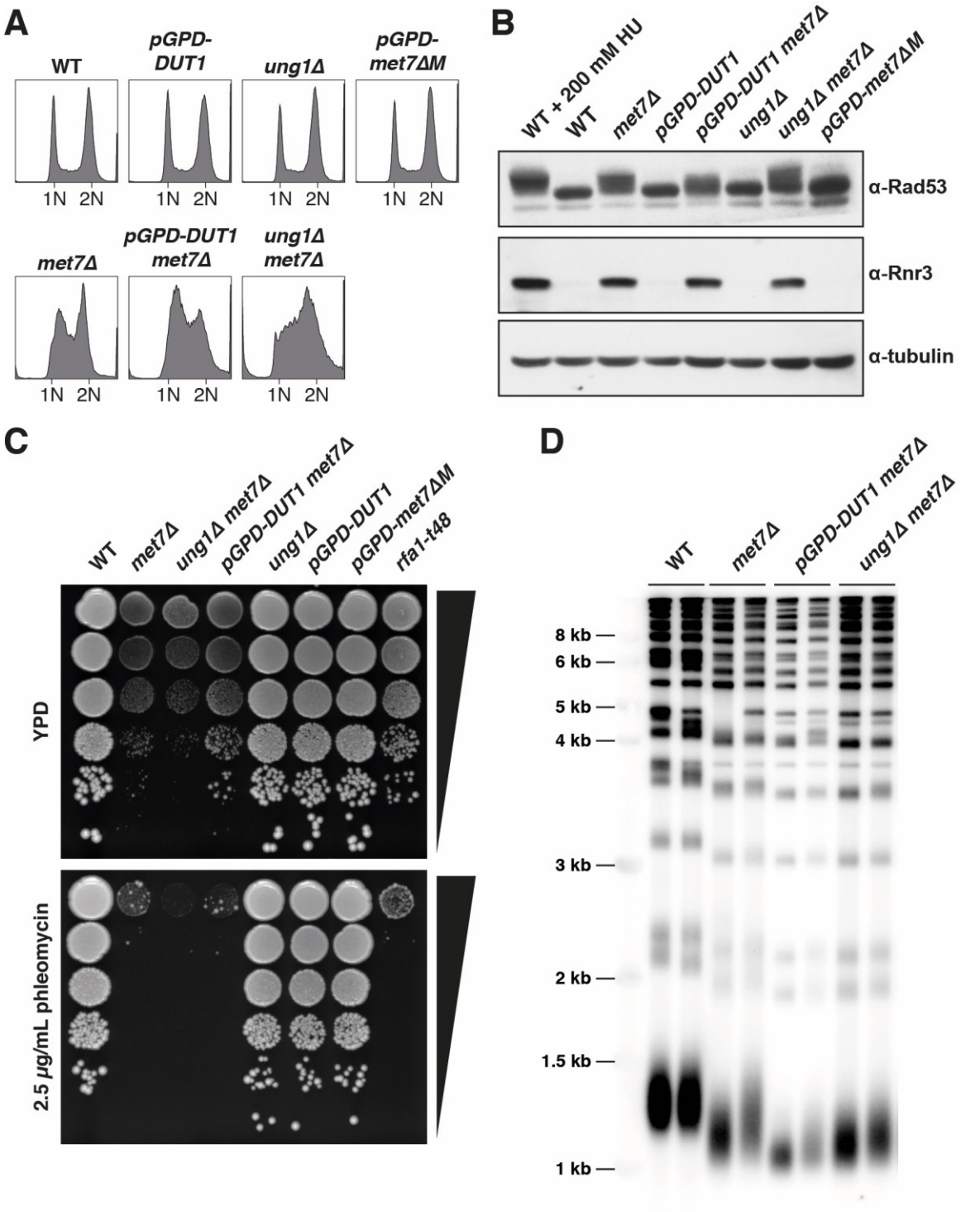

Fig. 4.7 DNA damage checkpoint activation, phleomycin sensitivity and short telomere phenotype in the absence of Met7 is not driven by dUTP accumulation.
(A) DNA content profiles of logarithmically growing strains of the indicated genotypes. (B) Whole cell lysates of logarithmically growing indicated strains were analyzed by SDS-PAGE and immunoblotting against Rad53, Rnr3 and tubulin. As positive control for the activation of the DNA damage response, WT cells treated for 3 h with 200 mM HU were used. (C) Spotting assay of the indicated strains in 10-fold serial dilutions on YPD ± phleomycin. (D) Telomere-specific Southern blot for the indicated genotypes (collaboration Luke lab).

regions leading to telomere shortening. To test the contribution of dUTP accumulation and processing of genomic uracil to the short telomere length phenotype observed in *met7Δ*, telomere

length was compared in WT, *met7Δ*, *pGPD-DUT1 met7Δ* and *ung1Δ met7Δ* (Fig. 4.6D)(collaboration with B. Luke lab, IMB). The *met7Δ* single and double mutants had shorter telomeres compared to the WT. However, no difference in telomere length was observed between the *met7Δ* single and double mutants. Thus, the short telomere phenotype in the absence of Met7 is not driven by uracil accumulation.

Taken together, these results indicate that neither the DDR activation, the slow growth phenotype, the phleomycin sensitivity nor the short telomere length observed in the absence of Met7 were triggered by dUTP accumulation and processing of genomic uracil.

4.3 Alterations in cellular metabolism triggered by *URA7* or *GLN3* inactivation cause imbalanced dNTP pools and increased mutagenesis.

4.3.1 Genome-wide screen reveals genes that are critically important if DNA polymerase fidelity is impaired.

The low-fidelity active-site mutant DNA polymerase alleles *pol1-L868M*, *pol2-M644G* and *pol3-L612M* were used as "sensitized mutator background" in the genome-wide screen to identify previously unrecognized genes that contribute to replication fidelity. A group of genes was identifed whose deletion caused an enhanced *CAN1* mutator phenotype in the presence of the low-fidelity polymerase alleles (Fig. 4.2 and Table 4.5).

Table 4.5 Mutation rate analysis of the mutants identified in this screen in combination with DNA polymerase active-site mutant alleles.

	Mutation Rate (fold increase)* Can^R			
Relevant genotype	**WT**	***pol1-L868M***	***pol2-M644G***	***pol3-L612M***
WT	7.2 [5.7-9.0] x 10^{-8} (1)	3.9 [3.3-4.9] x 10^{-7} (5)	8.4 [7.3-10.6] x 10^{-7} (12)	9.3 [7.7-11.6] x 10^{-7} (13)
exo1Δ	7.4 [6.3-9.8] x 10^{-7}(10)	5.7 [3.1-8.1] x 10^{-6} (80)	1.9 [1.1-2.9] x 10^{-6} (26)	6.5 [3.6-10.8] x 10^{-6} (91)
gln3Δ	1.0 [0.8-1.2] x 10^{-7} (1)	2.1 [1.4-4.5] x 10^{-5} (293)	3.3 [2.6-6.0] x 10^{-7} (5)	9.1 [7.3-18.2] x 10^{-6} (127)
shm2Δ	1.2 [1.1-1.7] x 10^{-7} (2)	1.7 [1.0-2.0] x 10^{-6} (23)	5.5 [3.9-7.3] x 10^{-7} (8)	3.6 [2.1-4.7] x 10^{-6} (50)
ura7Δ	1.0 [0.9-1.5] x 10^{-7} (1)	2.3 [1.3-4.1] x 10^{-5} (323)	1.1 [0.7-1.5] x 10^{-6} (15)	1.6 [1.1-2.6] x 10^{-5} (218)
rrm3Δ	1.1 [0.8-1.5] x 10^{-7} (2)	3.5 [2.1-4.4] x 10^{-7} (5)	2.8 [1.9-4.8] x 10^{-6} (40)	3.6 [2.6-6.0] x 10^{-6} (50)

* Median rates of inactivation of *CAN1* gene (Can^R) with 95% confidence interval in square brackets and fold increase relative to the WT in parentheses. Table was adapted from (Schmidt *et al.* 2017).

This group includes the double-stranded DNA exonuclease *EXO1* (TISHKOFF *et al.* 1997), the DNA helicase *RRM3* (IVESSA *et al.* 2000) and the three metabolic genes *GLN3* (COURCHESNE AND MAGASANIK 1988), *SHM2* (MCNEIL *et al.* 1994) and *URA7* (OZIER-KALOGEROPOULOS *et al.* 1991). The transcription factor Gln3 controls nitrogen metabolism and is negatively regulated by target of rapamycin (TOR) (BECK AND HALL 1999; CRESPO *et al.* 2002). *SHM2* encodes for the cytoplasmic serine hydroxymethyltransferase and is part of the folate one-carbon metabolism (Fig. 1.8)(MCNEIL *et al.* 1994), whereas Ura7 is the major CTP synthetase in *S. cerevisiae* converting UTP into CTP under the consumption of ATP and glutamine (OZIER-KALOGEROPOULOS *et al.* 1991; OZIER-KALOGEROPOULOS *et al.* 1994)(Fig. 1.6). Remarkably, with the exception of *EXO1*, which is a mild mutator by its own (TISHKOFF *et al.* 1997), inactivation of all other identified genes did not result in a mutator phenotype in the presence of WT DNA polymerases (Table 4.5), suggesting that the potential defects might be buffered by WT DNA polymerases. However, in the presence of low-fidelity DNA polymerases, strong synergistic increases in the *CAN1* mutation rates were measured. The strongest mutator interactions were observed in the absence of Gln3 or Ura7 in combination with *pol1-L868M* and *pol3-L612M* (Table 4.5). For example, the *pol1-L868M ura7Δ* double mutant showed a 323-fold and 65-fold increased *CAN1* mutation rate over the WT and the *pol1-L868M* single mutant, respectively. Interestingly, loss of Exo1, Gln3, Shm2 or Ura7 caused strong

synergistic increases in the *CAN1* inactivation rate in combination with the lagging-strand DNA polymerase alleles *pol1-L868M* and *pol3-L612M*, but not with the leadings-strand allele *pol2-M644G* (Table 4.5). In contrast, inactivation of *RRM3* caused increased mutagenesis exclusively in combination with *pol2-M644G* and *pol3-L612M*, but not with *pol1-L868M* (Table 4.5).

To test, whether error-prone TLS DNA polymerases (Polζ, Polη, Rev1) (MCCULLOCH AND KUNKEL 2008; LANGE *et al.* 2011) contribute to the synergistic mutator interactions measured in *gln3Δ* and *ura7Δ pol3-L612M* double mutants, *CAN1* mutation rates in the absence of Polζ (*rev3Δ*), Polη (*rad30Δ*) and Rev1 (*rev1Δ)* were determined (Table 4.6). *CAN1* inactivation rate measured in the triple mutants in comparison to the *gln3Δ* or *ura7Δ pol3-L612M* double mutants were not reduced. Thus, the synergistic mutator interactions between *gln3Δ* and *ura7Δ* and the low-fidelity lagging-strand DNA polymerase mutant *pol3-L612M* are independent of TLS DNA polymerases.

Table 4.6 Mutation rate analysis (*CAN1* inactivation) in *pol3-L612M gln3Δ* or *pol3-L612M ura7Δ* strains lacking TLS DNA polymerases.

Relevant genotype	Mutation Rate (fold increase)* Can^R
pol3-L612M gln3Δ	9.1 [7.3-18.2] x 10^{-6} (127)
pol3-L612M gln3Δ rev1Δ	2.9 [2.3-3.4] x 10^{-5} (399)
pol3-L612M gln3Δ rev3Δ	2.3 [1.3-3.3] x 10^{-5} (327)
pol3-L612M gln3Δ rad30Δ	1.8 [0.9-2.8] x 10^{-5} (247)
pol3-L612M ura7Δ	1.6 [1.1-2.6] x 10^{-5} (218)
pol3-L612M ura7Δ rev1Δ	3.7 [2.7-4.9] x 10^{-5} (521)
pol3-L612M ura7Δ rev3Δ	1.9 [1.3-4.0] x 10^{-5} (264)
pol3-L612M ura7Δ rad30Δ	4.3 [3.4-6.2] x 10^{-5} (597)

* Median rates of inactivation of *CAN1* gene (Can^R) with 95% confidence interval in square brackets and fold increase relative to the WT in parentheses. Table was adapted from (Schmidt *et al.* 2017).

4.3.2 Loss of Gln3 or Ura7 results in a mutational potential that is buffered by DNA polymerase proofreading and MMR.

The active-site mutations in the low-fidelity DNA polymerase alleles used in the screen compromise primarily the nucleotide selectivity of the DNA polymerases. However, besides nucleotide selectivity also DNA proofreading of Pol δ and Pol ε and MMR contribute to high-fidelity DNA replication (Fig. 1.2) (KUNKEL 2009; KUNKEL AND ERIE 2015). The observed mutator interactions could be specific for the low-fidelity DNA polymerases alleles used in the screen or related to DNA replication fidelity-compromised backgrounds. To test this idea, the identified genes were inactivated in DNA proofreading defective (*pol2-04*)(MORRISON *et al.* 1991), or mutant backgrounds that confer a partial (*exo1Δ*, *msh3Δ* and *msh6Δ*)(MARSISCHKY *et al.* 1996; TISHKOFF *et al.* 1997) or complete MMR defect (*msh2Δ*) (REENAN AND KOLODNER 1992) and mutation rates were determined (Table 4.7). Loss of either Gln3 or Ura7 strongly increased the *CAN1* mutation rate in all tested DNA replication fidelity-compromised backgrounds except for *msh3Δ* (Table 4.7). For example, inactivation of *URA7* in an *exo1Δ* background resulted in a *CAN1* mutation rate 261- and 26-fold increased over WT and the *exo1Δ* single mutant, respectively. *GLN3* inactivation in *msh6Δ* caused a 334- and 26-fold over WT and the *msh6Δ* single mutant, respectively. In contrast, *SHM2* and

RRM3 inactivation resulted in only a mild increase in the measured *CAN1* inactivation rate in an *msh6Δ* background and no increase was observed in the absence of *EXO1* (Table 4.7).

Loss of Gln3, Shm2, Ura7 or Rrm3 in a completely MMR-deficient *msh2Δ* background caused an increased *CAN1* mutation rate in all double mutants which were, except for the *shm2Δ msh2Δ* double mutant, significantly higher than the *msh2Δ* single mutant (based on 95% confidence intervals) (Table 4.7). Thus, the identified genes prevent mutations not only in the presence of the low-fidelity active-site DNA polymerase mutant alleles, but also in genetic backgrounds with compromised DNA proofreading or MMR.

Table 4.7 Mutation rate analysis of the mutants identified in this screen in combination with proofreading or partial MMR-defective alleles.

	Mutation Rate (fold increase)*		
Relevant genotype	**Can^R**	**Lys$^+$**	**Thr$^+$**
WT	7.2 [5.7-9.0] x 10^{-8} (1)	1.5 [0.8-2.2] x 10^{-8} (1)	2.1 [1.4-3.2] x 10^{-9} (1)
gln3Δ	1.0 [0.8-1.2] x 10^{-7} (1)	1.6 [1.1-3.7] x 10^{-8} (1)	2.4 [1.7-3.7] x 10^{-9} (1)
shm2Δ	1.2 [1.1-1.7] x 10^{-7} (2)	3.1 [1.2-5.0] x 10^{-8} (2)	2.6 [1.7-5.6] x 10^{-9} (1)
ura7Δ	1.0 [0.9-1.5] x 10^{-7} (1)	1.4 [1.0-2.5] x 10^{-8} (1)	1.9 [1.2-5.6] x 10^{-9} (1)
rrm3Δ	1.1 [0.8-1.5] x 10^{-7} (2)	2.4 [1.3-3.0] x 10^{-8} (2)	4.6 [2.6-7.9] x 10^{-9} (2)
exo1Δ	7.4 [6.3-9.8] x 10^{-7} (10)	1.4 [0.9-1.8] x 10^{-7} (10)	8.7 [6.1-15.0] x 10^{-9} (4)
exo1Δ gln3Δ	1.1 [0.8-1.4] x 10^{-5} (146)	1.2 [0.7-1.6] x 10^{-6} (83)	3.5 [2.7-5.0] x 10^{-7} (170)
exo1Δ shm2Δ	8.4 [7.1-10.1] x 10^{-7} (12)	3.5 [2.4-5.1] x 10^{-7} (24)	1.8 [1.1-2.5] x 10^{-8} (9)
exo1Δ ura7Δ	1.9 [0.8-2.4] x 10^{-5} (261)	1.3 [0.7-1.9] x 10^{-6} (89)	6.6 [4.9-8.3] x 10^{-7} (319)
exo1Δ rrm3Δ	6.3 [4.3-7.6] x 10^{-7} (9)	1.3 [1.0-1.8] x 10^{-7} (9)	2.5 [2.0-3.1] x 10^{-8} (12)
msh2Δ	5.4 [4.4-7.2] x 10^{-6} (75)	9.9 [8.1-10.8] x 10^{-5} (6771)	6.3 [5.2-12.8] x 10^{-6} (3053)
msh2Δ gln3Δ	1.3 [0.8-2.1] x 10^{-5} (177)	8.7 [6.9-14.9] x 10^{-5} (5972)	4.5 [3.1-6.5] x 10^{-6} (2149)
msh2Δ shm2Δ	7.4 [4.8-8.6] x 10^{-6} (104)	1.4 [1.1-2.1] x 10^{-4} (9737)	6.1 [4.4-8.2] x 10^{-6} (2918)
msh2Δ ura7Δ	3.5 [2.6-4.2] x 10^{-5} (492)	6.1 [4.7-8.8] x 10^{-5} (4161)	5.7 [4.1-8.5] x 10^{-6} (2738)
msh2Δ rrm3Δ	1.7 [1.2-2.6] x 10^{-5} (234)	1.1 [0.9-1.2] x 10^{-4} (7198)	1.6 [1.1-2.4] x 10^{-5} (7491)
msh3Δ	1.1 [0.8-1.2] x 10^{-7} (1)	2.5 [2.0-3.0] x 10^{-7} (17)	2.7 [2.0-4.2] x 10^{-8} (13)
msh3Δ gln3Δ	1.6 [1.1-2.6] x 10^{-7} (2)	1.9 [1.4-2.3] x 10^{-7} (13)	1.8 [1.5-1.9] x 10^{-8} (9)
msh3Δ shm2Δ	1.5 [1.3-2.9] x 10^{-7} (2)	1.2 [1.3-2.6] x 10^{-7} (12)	2.7 [1.7-3.7] x 10^{-8} (13)
msh3Δ ura7Δ	1.5 [1.3-2.0] x 10^{-7} (2)	1.2 [0.8-2.1] x 10^{-7} (8)	1.7 [1.1-3.0] x 10^{-8} (8)
msh3Δ rrm3Δ	2.6 [1.9-3.4] x 10^{-7} (4)	3.7 [3.5-4.3] x 10^{-7} (25)	6.1 [4.9-8.3] x 10^{-8} (30)
msh6Δ	9.6 [7.8-11.7] x 10^{-7} (13)	1.3 [0.9-1.6] x 10^{-6} (86)	1.3 [0.9-1.6] x 10^{-8} (6)
msh6Δ gln3Δ	2.4 [1.7-3.4] x 10^{-5} (334)	1.2 [0.7-4.0] x 10^{-6} (80)	1.0 [0.6-1.6] x 10^{-7} (48)
msh6Δ shm2Δ	2.1 [1.3-2.6] x 10^{-6} (30)	1.0 [0.9-1.3] x 10^{-6} (71)	3.5 [2.7-5.4] x 10^{-8} (17)
msh6Δ ura7Δ	3.8 [3.2-8.5] x 10^{-5} (524)	8.6 [6.6-20.6] x 10^{-7} (59)	9.2 [4.5-26.2] x 10^{-8} (44)
msh6Δ rrm3Δ	4.9 [3.6-7.3] x 10^{-6} (68)	9.1 [6.1-13.8] x 10^{-7} (62)	5.5 [3.9-6.8] x 10^{-8} (26)
pol2-04	6.2 [4.3-7.6] x 10^{-7} (6)	nd	nd
pol2-04 gln3Δ	1.1 [0.9-1.6] x 10^{-5} (154)	nd	nd
pol2-04 shm2Δ	1.5 [1.1-2.3] x 10^{-6} (22)	nd	nd
pol2-04 ura7Δ	2.5 [1.8-5.2] x 10^{-5} (354)	nd	nd
pol2-04 rrm3Δ	1.4 [0.9-1.8] x 10^{-6} (19)	nd	nd

* Median rates of inactivation of *CAN1* gene (Can^R) and *lys2-10A* (Lys$^+$) and *hom3-10* (Thr$^+$) reversion with 95% confidence interval in square brackets and fold increase relative to the WT in parentheses. "nd" indicates not determined. Table was adapted from (Schmidt *et al.* 2017).

According to the qualitative frameshift mutator analysis (*lys2-10A*), most of the identified gene deletions (with the exception of *exo1Δ*) did not caused an inceased frameshift mutator phenotype. Moreover, inactivation of the identified genes in MMR-compromised backgrounds did not result in strongly increased frameshift mutator phenotypes according to the *lys2-10A* and *hom3-10* reporter assay (Table 4.7). Two exceptions were the *gln3Δ exo1Δ* and *ura7Δ exo1Δ* double mutants that resulted in a 170- and 319-fold increase over WT in the *hom3-10* frameshift assay, respectively. To confirm that the *hom3-10* assay is specifically reverted by a single T:A deletion event in a 7 T:A mononucleotide run (starting at nucleotide position 646) and not due to base pair or complex mutations, the *hom3-10* reporter of 50 independent *ura7Δ exo1Δ hom3-10* revertants were sequenced. In line with literature (MARSISCHKY *et al.* 1996) only single T:A deletions events in the 7 T:A mononucleotide run gave rise to *hom3-10* reversion. In conclusion, loss of Ura7 in an *exo1Δ* background causes a mild *hom3-10* frameshift mutator phenotype, which is equivalent to 10% of a complete MMR-defect (*msh2Δ*) and presumably a consequence of saturation of MMR due to increased base pair substitutions.

To test whether mutations induced in the absence of the identified genes are corrected by Pol2 proofreading activity, *GLN3*, *SHM2*, *URA7* and *RRM3* were inactivated in the Pol2 proofreading-deficient background *pol2-04* and *CAN1* mutation rates were measured. Whereas only mild increases of 3- to 4-fold over *pol2-04* were detected in the *shm2Δ pol2-04* and *rrm3Δ pol2-04* double mutants, loss of either Gln3 or Ura7 increased the *CAN1* mutation rates 26- and 59-fold over *pol2-04,* respectively.

Despite several attempts the *URA7* deletion could not be combined with the Pol3 proofreading defective *pol3-01* allele (MORRISON *et al.* 1993). Therefore, the possibility of a synthetic growth defect or synthetic lethality was investigated by plasmid shuffling. For this, the chromosomal *POL3* gene was inactivated in *URA7* or *ura7Δ* haploid (n) cells, which were complemented with WT-*POL3* expressed from a low copy number plasmid (*URA3*-WT-*POL3*). Next, cells were transformed with either WT-*POL3* or *pol3-01* expressing low copy number plasmids (*LEU2*-WT-*POL3*/*pol3-01*). Striking on 5-FOA containing media selected for loss of the *URA3*-WT-*POL3* plasmid and growth in the presence of *POL3* or *pol3-01* was evaluated. Indeed, the *ura7Δ pol3Δ* mutant complemented with a *pol3-01* expressing plasmid showed a severe growth defect (Fig. 4.8A). In yeast cells, very high mutation rates, which are for example observed in mutants with combined DNA proofreading defects and complete MMR deficiency, can result in lethality due to “error-induced extinction” (TRAN *et al.* 1999; GREENE AND JINKS-ROBERTSON 2001; WILLIAMS *et al.* 2013). Under these circumstances, cells die because of the extremely elevated mutation rate that results in the inactivation of at least one essential gene is inactivated per cell cycle (1×10^{-3} mutations per cell division in haploid yeast cells)(HERR *et al.* 2014). In line with this, no growth was observed in an *msh2Δ pol3Δ* mutant complemented with a *pol3-01* expressing plasmid (Fig. 4.8A). To evaluate, whether the observed slow growth phenotype of the *ura7Δ* + *pol3-01* double mutant is linked to the high mutational load, homozygous diploid (2n) *URA7 pol3Δ* or *ura7Δ pol3Δ* plasmid shuffling strains hemizygous for *CAN1* (*CAN1/can1Δ*) were generated. In comparison to the very slowly growing haploid *ura7Δ* + *pol3-01* cells, the homozygous diploid *ura7Δ* + *pol3-01* cells grew better, which is

in line with an approximately 10-fold higher error extinction threshold in diploid cells (Fig. 4.8B). However, diploid *ura7Δ* + *pol3-01* cells still grew slower than diploid *ura7Δ* + *POL3* cells (Fig 4.8B).

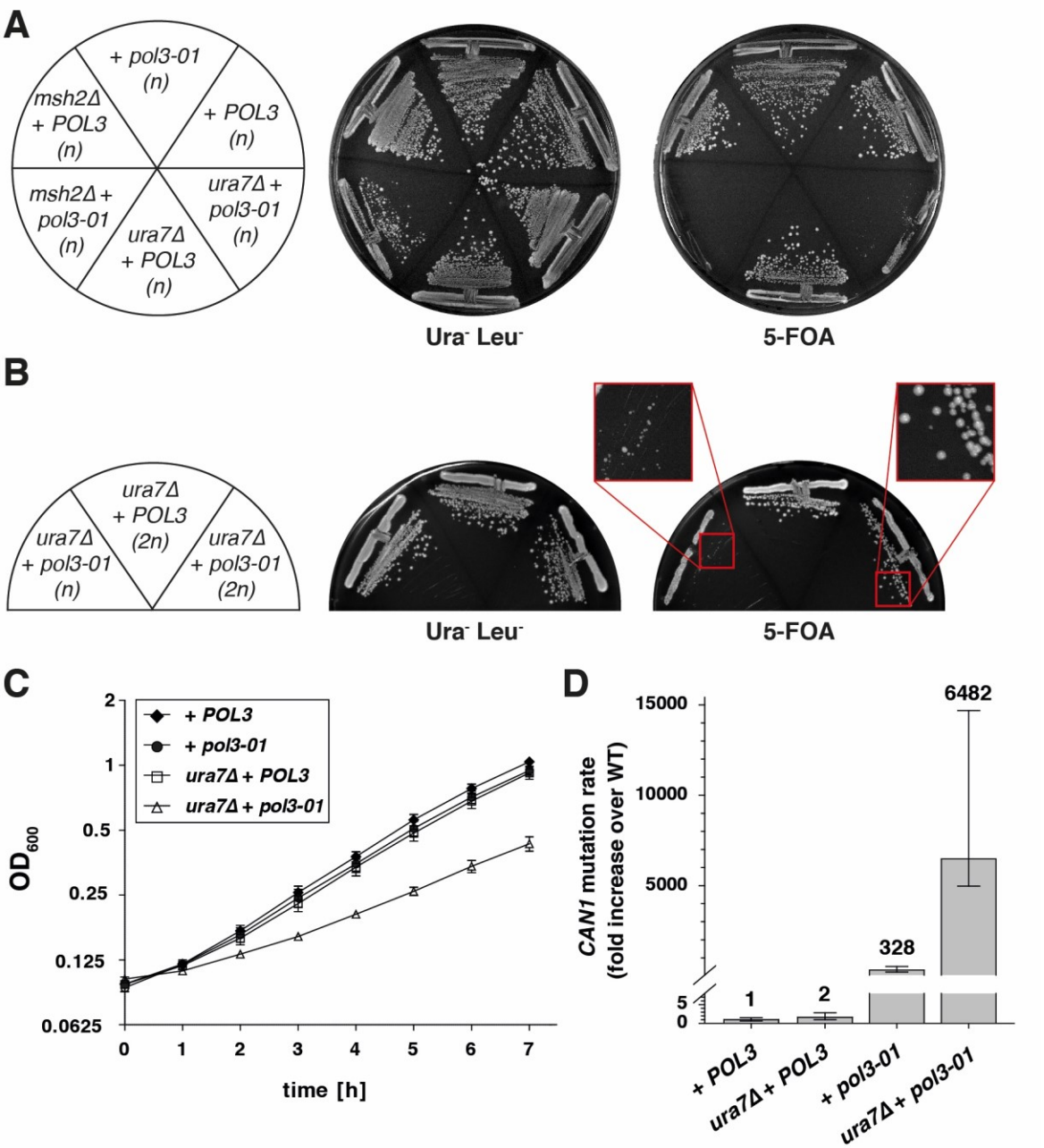

Fig. 4.8 *URA7* inactivation in Pol3 proofreading-defective background results in severe growth defect and synergistic increase in the mutations rate.
(A) Plasmid shuffling assay in haploid *pol3Δ*, *pol3Δ ura7Δ* and *pol3Δ msh2Δ* complemented with a WT-*POL3-URA3* plasmid and transformed with either WT-*POL3-LEU2* or *pol3-01-LEU2* plasmid. Cells were streaked out on Ura-Leu- SD plates (growth control) and on 5-FOA containing SD plates to counterselect for the WT-*POL3-URA3* plasmid. The *msh2Δ pol3-01* double mutant serves as positive control for a synthetic lethal interaction. (B) Haploid (n) or diploid homozygous (2n) *pol3Δ ura7Δ* cells expressing either WT-*POL3* or *pol3-01* were grown as in A. (C) Proliferation curve of homozygous diploids of the indicated genotypes after plasmid shuffling. Proliferation was followed by OD_{600} measurement and the values were plotted as mean of three independent isogenic strains ± SD in a $\log_2$ scale. (D) Quantification of *CAN1* mutation rates in diploids hemizygous for the *CAN1* locus and homozygous for *pol3Δ* or *pol3Δ ura7Δ* complemented with WT-*POL3* or *pol3-01* on a *LEU2* plasmid. Error bar represent 95% confidence intervals (CIs) and the number on top represents the fold increase in the mutation rate over the WT diploid strain (2.4×10^{-7} Can^R mutants per cell division). Figure was adapted from (SCHMIDT *et al.* 2017).

To compare proliferation of diploid homozygous *pol3Δ* or *pol3Δ ura7Δ* strains either complemented with WT-*POL3* or *pol3-01* expressed from a low copy number plasmid, growth was followed over time (Fig. 4.8C). In agreement with the previous qualitative growth analysis (Fig. 4.8B), the diploid *pol3Δ ura7Δ* strains complemented with the *pol3-01* plasmid grew slower than the diploid *pol3Δ ura7Δ* strains complemented with the WT-*POL3* plasmid and the diploid *pol3Δ* strains complemented with WT-*POL3* or *pol3-01* plasmids. Next, the *CAN1* mutation rates were measured in the *ura7Δ* + *pol3-01* diploids hemizygous for the *CAN1* reporter (Fig. 4.8D). Strikingly, the *ura7Δ* + *pol3-01* diploid showed a *CAN1* inactivation rate of 1.6 x 10^{-3} (6482-fold increase over the WT). This mutation rate is at the error-induced extinction threshold for haploid cells (1.0 x 10^{-3} mutations per cell division in haploid yeast cells), but below the threshold reported for diploid cells (1.0 x 10^{-2} mutations per cell division in diploid yeast cells). Taken together, mutations induced in the absence of *GLN3* or *URA7* and to a lesser degree in *shm2Δ* and *rrm3Δ* are counteracted by MMR and Pol2 proofreading. Moreover, inactivation of *URA7* in the absence of Pol3 proofreading results in a hypermutator phenotype that compromises cell viability.

4.3.3 Inactivation of *GLN3* or *URA7* results in activation of the DNA damage response.

Three of the here identified gene deletions (*gln3Δ*, *rrm3Δ* and *ura7Δ*) have been previously reported to show a prolonged S phase (KOREN *et al.* 2010). An extended S phase can be caused by either replication stress or DNA damage (ROUSE AND JACKSON 2002; PARDO *et al.* 2017). Upon these stress conditions, the Rad53 kinase is phosphorylated on multiple sites, resulting in Rad53 activation and Dun1 phosphorylation. Dun1 phosphorylates the negative regulators of RNR Sml1, Crt1 and Dif1 and marks them for degradation. Consequently, the expression of RNR subunits and the activity of RNR is increased which leads to elevated dNTP levels (Fig. 4.9A). To investigate whether the reported extended S phase in *gln3Δ* and *ura7Δ* is due to activation of the DNA damage response (DDR), whole cell lysates of logarithmically growing cells were analyzed by immunoblotting for Rad53 phosphorylation (represented by a smear in the Rad53 electrophoretic mobility) and induction of the RNR subunits. Indeed, the absence of Ura7 and to a lesser degree of Gln3 activated the DDR. Loss of Shm2 did not result in Rad53 phosphorylation and Rnr3 induction, but to a mild increase in Rnr2 and Rnr4 expression levels. Interestingly, in contrast to the *pol2-M644G* mutant, which was previously reported to depend on DDR activation and concomitant elevated dNTP pools for survival (WILLIAMS *et al.* 2015), the lagging strand DNA polymerase mutant alleles (*pol1-L868M* and *pol3-L612M*) did not activate the DDR. In agreement with the Western blotting results, DNA content analysis of logarithmically growing cells revealed that *pol1-L868M*, *pol3-L612M* and *shm2Δ* did not show accumulation of cells in S phase, whereas *pol2-M644G*, *gln3Δ* and *ura7Δ* cells did (Fig. 4.9C). Thus, loss of Gln3 or Ura7 causes activation of the DDR and accumulation of cells in S phase.

Next, to test whether the observed synergistic mutator interaction between DNA replication fidelity-compromised backgrounds and *gln3Δ* or *ura7Δ* are dependent on the activation of the DNA damage checkpoint, *CAN1* mutation rates were measured in the absence of Dun1 (Zhou and Elledge 1993). Remarkably, inactivation of *DUN1* strongly suppressed the mutator phenotypes (Table 4.8). For example, loss of Dun1 reduced the *CAN1* mutation rates from 293- to 4-fold and

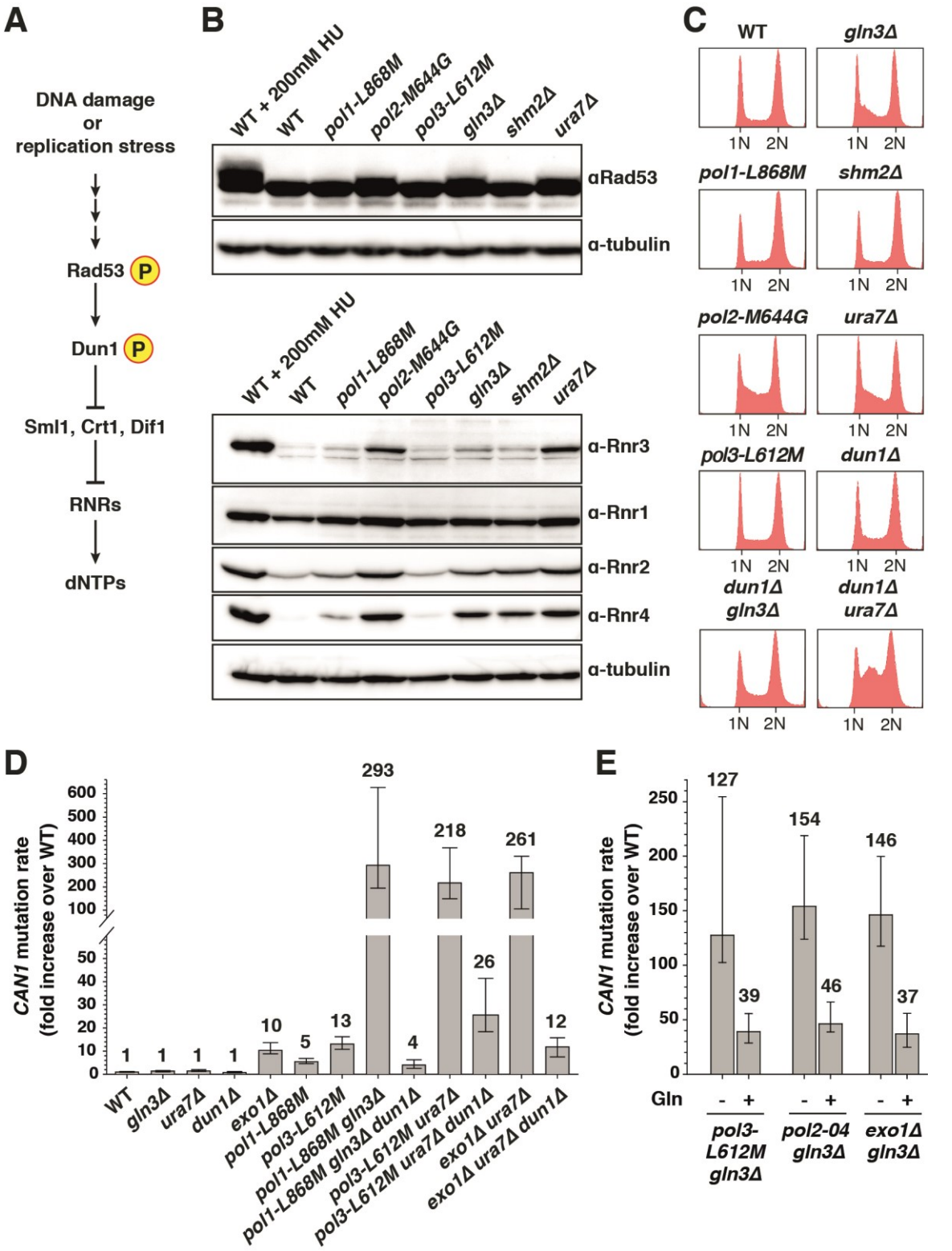

Fig. 4.9 Inactivation of *GLN3* or *URA7* causes DNA damage checkpoint activation.
(A) Simplified scheme of the DNA damage response in *S. cerevisiae*. (B) Whole cell lysates of logarithmically growing cells were analyzed by SDS-PAGE and immunoblotting against Rad53, Rnr3 and tubulin. As positive control for the activation of the DNA damage response, WT cells treated for 3 h with 200 mM HU were used. (C) DNA content profiles of logarithmically growing strains with the indicated genotypes. (D) *CAN1* mutation rates in mutant strains in the presence or absence of *DUN1* (Table 4.8). (E) *CAN1* mutation rate in the indicated strains grown in YPD supplemented or not with 5 mM glutamine (Gln). Error bars represent the 95% CI, and numbers on top are the fold increase in the mutation rate over WT. Figure was adapted from (SCHMIDT *et al.* 2017).

from 218- to 26-fold over WT in *pol1-L868M gln3Δ* and *pol3-L612M ura7Δ*, respectively (Fig. 4.9D, Table 4-8). Moreover, the *CAN1* inactivation rate of the *exo1Δ ura7Δ* double mutant was suppressed from 261- to 12-fold over WT in the absence of Dun1 (Fig. 4.9D, Table 4-8). These findings suggest that the absence of Dun1 increases DNA replication fidelity in *gln3Δ* and *ura7Δ* double mutants. Strikingly, this phenotype is not restricted to DNA polymerase mutant allele combinations and most likely caused by the constant activation of the negative regulators of RNR and consequently lower dNTP pools (FASULLO *et al.* 2010). Accordingly, the *dun1Δ ura7Δ* double mutant showed an even stronger S phase delay in the DNA content analysis, whereas no difference was observed in the *dun1Δ gln3Δ* double mutant (Fig. 4.9C).

Table 4.8 Mutation rate analysis in *gln3Δ* and *ura7Δ* double mutants in the presence or absence of *DUN1*.

	Mutation Rate (fold increase)*		
Relevant genotype	**Can^R**	**Lys$^+$**	**Thr$^+$**
WT	7.2 [5.7-9.0] x 10^{-8} (1)	1.5 [0.8-2.2] x 10^{-8} (1)	2.1 [1.4-3.2] x 10^{-9} (1)
gln3Δ	1.0 [0.8-1.2] x 10^{-7} (1)	1.6 [1.1-3.7] x 10^{-8} (1)	2.4 [1.7-3.7] x 10^{-9} (1)
ura7Δ	1.0 [0.9-1.5] x 10^{-7} (1)	1.4 [1.0-2.5] x 10^{-8} (1)	1.9 [1.2-5.6] x 10^{-9} (1)
dun1Δ	5.6 [4.2-9.1] x 10^{-8} (1)	2.1 [0.9-3.5] x 10^{-8} (1)	2.4 [1.7-5.2] x 10^{-9} (1)
exo1Δ	7.4 [6.3-9.8] x 10^{-7} (10)	1.4 [0.9-1.8] x 10^{-7} (10)	8.7 [6.1-15.0] x 10^{-9} (4)
exo1Δ ura7Δ	1.9 [0.8-2.4] x 10^{-5} (261)	1.3 [0.7-1.9] x 10^{-6} (89)	6.6 [4.9-8.3] x 10^{-7} (319)
exo1Δ ura7Δ dun1Δ	8.5 [5.4-11.3] x 10^{-7} (12)	2.6 [1.8-3.6] x 10-7 (18)	8.3 [4.7-10.7] x 10^{-9} (4)
pol2-04	6.2 [4.3-7.6] x 10^{-7} (6)	nd	nd
pol2-04 gln3Δ	1.1 [0.9-1.6] x 10^{-5} (154)	nd	nd
pol2-04 dun1Δ	9.4 [6.5-17.4] x 10^{-8} (1)	nd	nd
pol2-04 gln3Δ dun1Δ	8.6 [6.4-16.5] x 10^{-8} (1)	nd	nd
pol1-L868M	3.9 [3.3-4.9] x 10^{-7} (5)	nd	nd
pol1-L868M dun1Δ	9.6 [5.4-15.0] x 10^{-8} (1)	nd	nd
pol1-L868M gln3Δ	2.1 [1.4-4.5] x 10^{-5} (293	nd	nd
pol1-L868M gln3Δ dun1Δ	2.9 [1.9-4.5] x 10^{-7} (4)	nd	nd
pol3-L612M	9.3 [7.7-11.6] x 10^{-7} (13)	nd	nd
pol3-L612M gln3Δ	9.1 [7.3-18.2] x 10^{-6} (127)	nd	nd
pol3-L612M gln3Δ dun1Δ	3.1 [1.8-4.0] x 10^{-6} (43)	nd	nd
pol3-L612M ura7Δ	1.6 [1.1-2.6] x 10^{-5} (218)	nd	nd
pol3-L612M ura7Δ dun1Δ	1.8 [1.3-3.0] x 10^{-6} (26)	nd	nd

* Median rates of inactivation of *CAN1* gene (Can^R) and *lys2-10A* (Lys$^+$) and *hom3-10* (Thr$^+$) reversion with 95% confidence interval in square brackets and fold increase relative to the WT in parentheses. "nd" indicates not determined. Table was adapted from (Schmidt *et al.* 2017).

The GATA transcription factor Gln3 activates genes upon glutamine limitation (BECK AND HALL 1999; CRESPO *et al.* 2002). Glutamine is an important cellular metabolite for energy production, but also for purine and pyrimidine biosynthesis, among others. Thus, to test whether defects due to glutamine starvation in *gln3Δ* are responsible for the synergistic mutator interactions observed in *gln3Δ* double mutants, *CAN1* mutation rates were measured in YPD medium or in YPD medium supplemented with 5 mM glutamine. Strikingly, glutamine supplementation suppressed the *CAN1* mutation rates by 70-75% in *pol3-L612M gln3Δ*, *pol2-04 gln3Δ* and *exo1Δ gln3Δ* (Fig. 4.9E). Thus, at one stage during the growth of the culture glutamine becomes limiting, even if the culture is

grown in nutrient-rich YPD medium. Normally, cells would respond to glutamine limitation by activation of Gln3, but in the absence of Gln3 the cells cannot counteract the metabolic imbalance resulting in increased mutagenesis.

4.3.4 Gln3 and Ura7 are critical to maintain balanced NTP and dNTP pools.

The reported metabolic function of Gln3 (BECK AND HALL 1999; CRESPO *et al.* 2002) and Ura7 (OZIER-KALOGEROPOULOS *et al.* 1991; OZIER-KALOGEROPOULOS *et al.* 1994), together with the activation of the DDR in the absence of both genes (Fig. 4.9B,C)(KOREN *et al.* 2010) and the suppression of the mutator phenotypes by inactivation of *DUN1* (Table 4.8), suggested that inactivation of either one of these two genes may affect nucleotide pool homeostasis. To test this hypothesis, NTP and dNTP pools were measured by HPLC (Fig. 4.10, Table 4-9) (collaboration with Chabes lab, Umeå University). Inactivation of *GLN3* and *URA7* reduced CTP levels to 50% and 30%, respectively (Fig. 4.10A, Table 4.9A). Additionally, 1.7-fold increased UTP levels were measured in *gln3Δ* cells. In contrast, the NTP pools in the absence of Shm2 and in the presence of the active-site mutant DNA polymerase alleles did not strongly change.

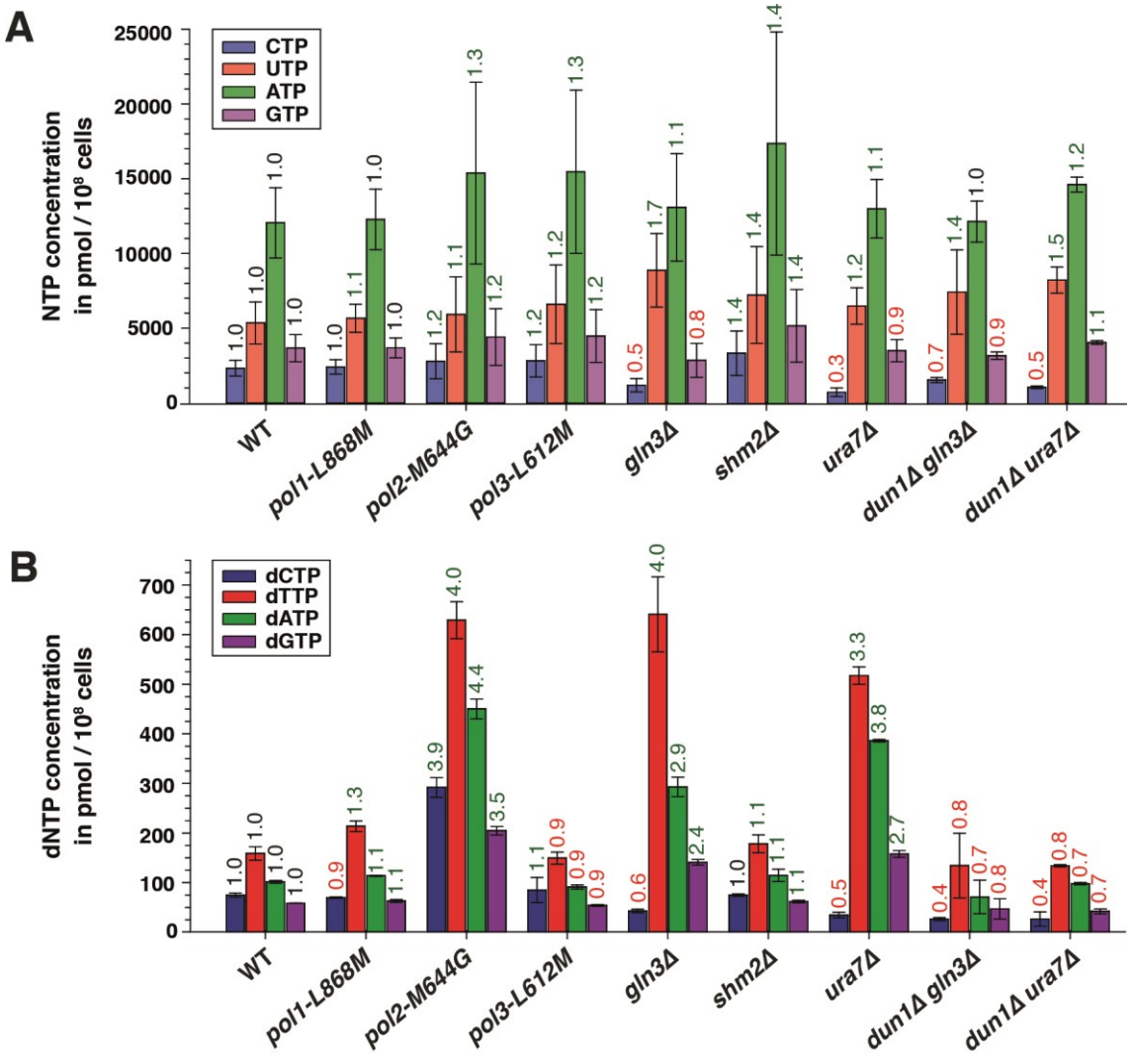

Fig. 4.10 Inactivation of *GLN3* or *URA7* induces an NTP and dNTP imbalance.
(A) NTP and (B) dNTP concentration measurements in the indicated strains (Table 4.9). Error bars represent SD and the number on top of each bar indicates the folds over WT. Fold increases are colored in green,

whereas decreased levels are labeled red. NTP and dNTP concentrations were measured by the Chabes lab. Figure was adapted from (Schmidt et al. 2017).

Table 4.9 NTP and dNTP concentrations measured in polymerase, *gln3Δ*, *shm2Δ* and *ura7Δ* mutants.

A

Relevant genotype	CTP	UTP	ATP	GTP
WT	2360 ± 532 (1.0)	5384 ± 1406 (1.0)	12088 ± 2351 (1.0)	3705 ± 912 (1.0)
pol1-L868M	2440 ± 483 (1.0)	5704 ± 942 (1.1)	12310 ± 2029 (1.0)	3719 ± 669 (1.0)
pol2-M644G	2825 ± 1171 (1.2)	5959 ± 2511 (1.1)	15418 ± 6078 (1.3)	4443 ± 1902 (1.2)
pol3-L612M	2870 ± 1085 (1.2)	6654 ± 2626 (1.2)	15524 ± 5465 (1.3)	4529 ± 1765 (1.2)
gln3Δ	1267 ± 443 (0.5)	8957 ± 2458 (1.7)	13167 ± 3592 (1.1)	2929 ± 1130 (0.8)
shm2Δ	3411 ± 1485 (1.4)	7302 ± 3243 (1.4)	17439 ± 7467 (1.4)	5243 ± 2429 (1.4)
ura7Δ	808 ± 288 (0.3)	6575 ± 1225 (1.2)	13080 ± 1958 (1.1)	3587 ± 745 (1.0)
*dun1Δ gln3Δ**	1645 ± 172 (0.7)	7533 ± 2824 (1.4)	12246 ± 1371 (1.0)	3272 ± 246 (0.9)
*dun1Δ ura7Δ**	1160 ± 81 (0.5)	8338 ± 874 (1.5)	14723 ± 502 (1.2)	4151 ± 119 (1.1)

B

Relevant genotype	dCTP	dTTP	dATP	dGTP
WT	75 ± 4 (1.0)	159 ± 14 (1.0)	102 ± 3 (1.0)	59 ± 0 (1.0)
pol1-L868M	70 ± 1 (0.9)	214 ± 11 (1.3)	114 ± 1 (1.1)	63 ± 3 (1.1)
pol2-M644G	292 ± 20 (3.9)	629 ± 37 (4.0)	450 ± 20 (4.4)	205 ± 9 (3.5)
pol3-L612M	85 ± 25 (1.1)	149 ± 12 (0.9)	91 ± 4 (0.9)	54 ± 2 (0.9)
gln3Δ	43 ± 3 (0.6)	641 ± 76 (4.0)	293 ± 20 (2.9)	141 ± 6 (2.4)
shm2Δ	75 ± 2 (1.0)	178 ± 18 (1.1)	115 ± 12 (1.1)	62 ± 3 (1.1)
ura7Δ	35 ± 6 (0.5)	517 ± 17 (3.3)	386 ± 3 (3.8)	158 ± 7 (2.7)
*dun1Δ gln3Δ**	27 ± 3 (0.4)	134 ± 65 (0.8)	71 ± 34 (0.7)	47 ± 20 (0.8)
*dun1Δ ura7Δ**	27 ± 14 (0.4)	134 ± 2 (0.8)	98 ± 2 (1.0)	42 ± 5 (0.7)

NTP (A) and dNTP (B) concentrations (pmol per 10^8 cells) are the average of two biological replicates ± standard deviation with the fold increase over WT in parentheses. NTP and dNTP concentrations were measured by the Chabes lab. Table was adapted from (Schmidt *et al.* 2017).
* NTP and dNTP concentrations were measured at a different time point and normalized according to a WT strain included in the same run.

To examine whether the low CTP levels in *gln3Δ* and *ura7Δ* cells affect dCTP pools, dNTP concentrations were measured. The dCTP pools in *gln3Δ* and *ura7Δ* cells were reduced by 40% and 50%, respectively, in comparison to the WT, whereas the other dNTPs were strongly increased (2.4- to 4.0-fold over WT) (Fig. 4.10B, Table 4.9B). In agreement with a previous report (WILLIAMS *et al.* 2015), and the observed accumulation of cells in S phase (Fig. 4.9C), the *pol2-M644G* mutant strain showed an overall increase in dNTP pools. Moreover, neither *SHM2* inactivation nor the lagging strand DNA polymerase alleles caused major dNTP pool alterations (Fig. 4.10B, Table 4.9B). Taken together, loss of Gln3 or Ura7 causes low CTP pools for which neither RNR nor any mechanism downstream RNR can compensate, resulting in a severe dNTP imbalance which is characterized by limiting dCTP pools and elevated dTTP, dATP and dGTP pools.

As the inactivation of *DUN1* suppressed the *CAN1* mutation rates in *gln3Δ* and *ura7Δ* double mutants, NTP and dNTP concentrations were also measured in *dun1Δ gln3Δ* and *dun1Δ ura7Δ*. Whereas NTP pools in these double mutants were similar to the levels measured in *gln3Δ* and

ura7Δ single mutants (Fig. 4.10A, Table 4.9A), the overall dNTP pools were strongly decreased (Fig. 4.10B, Table 4.9B). The dCTP concentrations in *dun1Δ* double mutants were still comparable to the dCTP concentrations measured in the presence of Dun1 (40% to 60% of dCTP WT levels in *dun1Δ gln3Δ* to *gln3Δ* and 40% to 50% of dCTP WT levels in *dun1Δ ura7Δ* to *ura7Δ*, respectively). However, the contribution of dCTP to the total dNTP pool was strongly increased in the *dun1Δ* double mutants. For example, dCTP pools in *ura7Δ* contributed 3% to the total dNTP pool (19% in the WT), whereas dCTP in the *dun1Δ ura7Δ* double mutant contributed to 9% of the total dNTP pool. Moreover, the ratio between dCTP to dTTP changed from 1:15 in *ura7Δ* cells to 1:5 in *dun1Δ ura7Δ* cells (1:2 in WT cells). Therefore, the lower overall dNTP pools and the less extreme ratios between the different dNTP pools might explain the observed increase in DNA replication fidelity upon inactivation of *DUN1* in *gln3Δ* and *ura7Δ* double mutants.

4.3.5 Inactivation of *GLN3* or *URA7* results in a *CAN1* mutation spectrum dominated by G-C to A-T transitions.

In order to investigate whether the measured dNTP pool imbalance in the absence of Gln3 or Ura7 impacts on the type of replication errors generated, *CAN1* mutation spectra analysis was performed. Based on the results obtained in the mutator assay (Table 4.5 and 4.7), mostly base substitution events were expected in *gln3Δ*, *shm2Δ* and *ura7Δ* mutations spectra. Therefore, and to avoid potential correction by MMR, the mutation spectra analysis was performed in the absence of Msh6, which forms together with Msh2 the mismatch recognition complex primarily responsible for the recognition of base pair substitutions (MARSISCHKY *et al.* 1996).

Table 4.10 *CAN1* mutation spectra analysis in WT, *msh6Δ, msh6Δ gln3Δ*, *msh6Δ shm2Δ* and *msh6Δ ura7Δ* mutants.

	WT	*msh6Δ*	*msh6Δ gln3Δ*	*msh6Δ shm2Δ*	*msh6Δ ura7Δ*
Can^R clones sequenced	91	110	94	95	110
Mutations overall *	92 (100)	111 (100)	96 (100)	96 (100)	110 (100)
Base substitutions	69 (75)	102 (92)	95 (99)	95 (99)	109 (99)
A-T → G-C	6 (7)	9 (8)	1 (1)	1 (1)	0 (0)
G-C → A-T	18 (20)	60 (54)	92 (96)	77 (80)	104 (95)
G-C → T-A	29 (32)	27 (24)	0 (0)	14 (15)	5 (5)
A-T → C-G	3 (3)	2 (2)	0 (0)	3 (3)	0 (0)
A-T → T-A	7 (8)	1 (1)	0 (0)	0 (0)	0 (0)
C-G → G-C	6 (7)	3 (3)	2 (2)	0 (0)	0 (0)
Transitions	24 (26)	69 (62)	93 (97)	78 (81)	104 (95)
Transversions	45 (49)	33 (30)	2 (2)	17 (18)	5 (5)
One-base-pair frameshifts	15 (16)	7 (6)	1 (1)	1 (1)	1 (1)
Complex mutations†	8 (9)	2 (2)	0 (0)	0 (0)	0 (0)

Mutation spectra analysis based on DNA sequencing of the *CAN1* gene in independent Can^R mutants, shown as the number of clones containing the indicated mutations, and in parenthesis as the percentage relative to the total (Fig. S 7.1 and Fig. S 7.3-6). Table was adapted from (Schmidt *et al.* 2017).

*In few cases (about 1-2% of the sequenced clones) two simultaneous *CAN1* mutations (more than 100 bp apart) were found. These mutations were included in the analysis and considered as independent mutational events.

† includes: multiple mutations within 10 nucleotides, insertions or deletions of more than 1 nucleotide and duplication events.

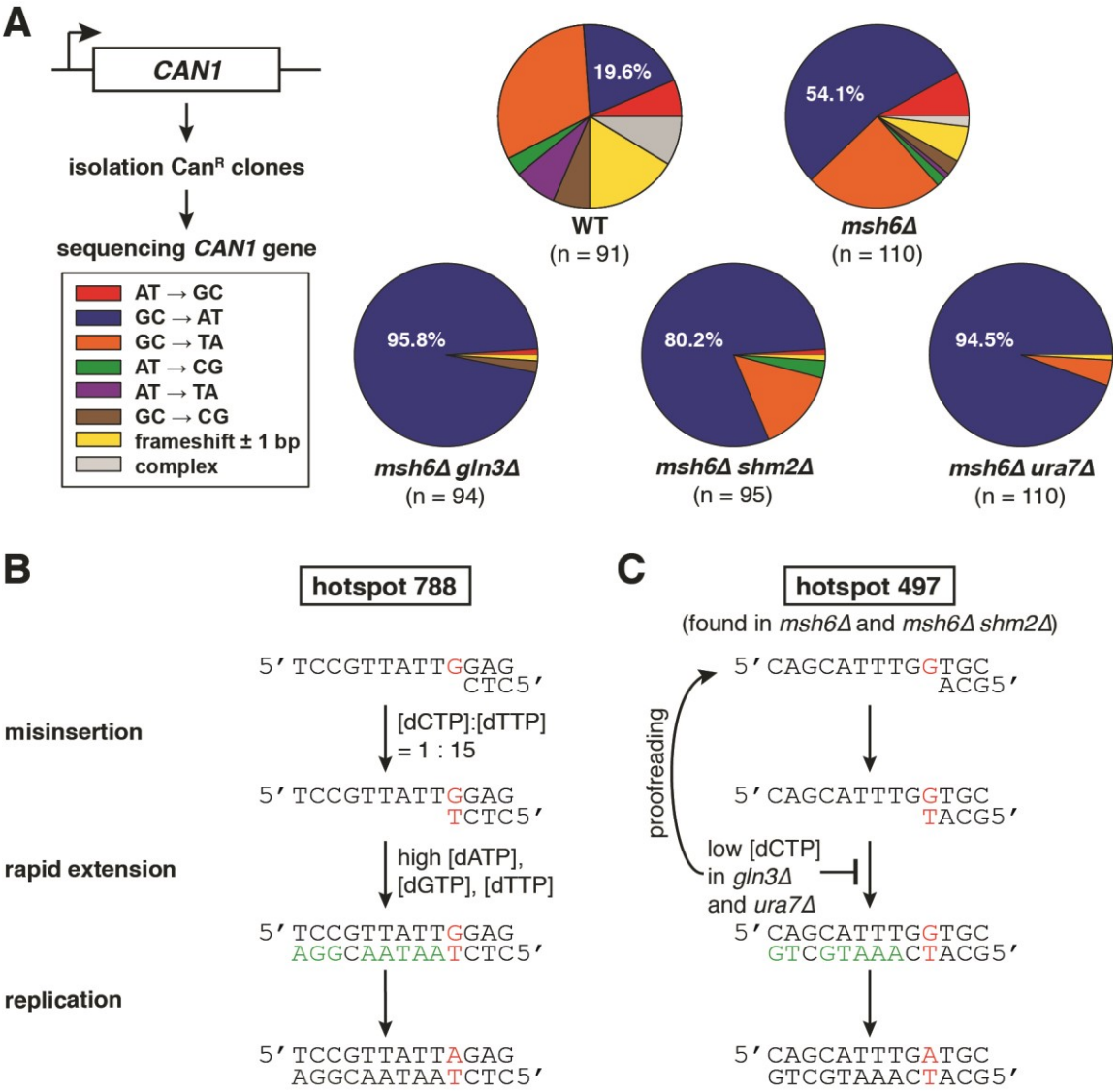

Fig. 4.11 The *CAN1* mutation spectrum in the absence of Ura7 or Gln3 is dominated by G-C to A-T transitions.
(A) Independent Can^R clones (n ≥ 91 per genotype) were sequenced for *CAN1* mutations. The graphs represent the type of the identified mutations in percentage (Table 4.10). (B) The G-to-A mutational hotspot at nucleotide 788 was frequently found in *msh6Δ gln3Δ*, *msh6Δ shm2Δ* and *msh6Δ ura7Δ* strains. Predicted mutation is noted in red. Nucleotides marked in green are more abundant in *gln3Δ* and *ura7Δ* than in the WT and facilitate rapid extension of the mispair. (C) The G-to-A mutational hotspot at nucleotide 497 was frequently found in *msh6Δ* and *msh6Δ shm2Δ*, but not in *msh6Δ gln3Δ* or *msh6Δ ura7Δ*. Here, immediately after the predicted G-dT mispair a dCTP needs to be incorporated, which is less abundant in *gln3Δ* and *ura7Δ* strains and thus, unlikely to support rapid mismatch extension. Figure was adapted from (SCHMIDT *et al.* 2017)

Sequencing of the *CAN1* gene in independent canavanine resistant clones (Can^R) (n ≥ 91 per genotype) revealed that the *msh6Δ* single and double mutant mutation spectra were dominated by base substitutions. In the WT 75% of all sequenced mutation events were base substitutions, whereas in *msh6Δ* and *msh6Δ* double mutants base substitutions were found in 92% and 99% of all sequenced events, respectively (Table 4.10). The *msh6Δ CAN1* mutation spectrum was in comparison to the WT strongly enriched for G-C to A-T transitions (54.1% in *msh6Δ* compared to 19.6% in WT), suggesting that this type of replication error is efficiently repaired by MMR in the WT background. The additional knockout of *SHM2, URA7* or *GLN3* in the *msh6Δ* background further

increased G-C to A-T mutations, which accounted for 80.2%, 94.5% and 95.8% of all sequenced Can^R events, respectively.

Statistical analysis of the *CAN1* spectra revealed that the double mutant *CAN1* mutation spectra were significantly different to the *msh6Δ* spectrum (Fisher's exact test, p value 0.0005 for *msh6Δ shm2Δ*, 4.0 x 10^{-12} for *msh6Δ gln3Δ* and 1.3 x 10^{-10} for *msh6Δ ura7Δ*). Further analysis revealed mutational hotspots, in which specific mutational events were observed at least in 5% of all sequenced clones (Table 4.11).

Table 4.11 Mispair base substitution hotspots identified in *msh6Δ gln3Δ*, *msh6Δ ura7Δ* and *msh6Δ shm2Δ* mutants.

Position	Mutation	No of occurrences (% of total)	Mutation rate (x10^{-8})	Fold increase over *msh6Δ*	Predicted intermediate
gln3Δ: 0.6 x dCTP, 4.0 x dTTP, 2.9 x dATP, 2.4 dGTP					
overall		96	2400	25.0	
788	G → A	15 (15.6)	375.0	434	5′TCCGTTATTGGAG, AGGCAATAATCTC5′
806	G → A	5 (5.2)	125.0	≥145	5′CAGGTGCCTGGGG, GTCCACGGATCCC5′
980	G → A	18 (18.8)	450.0	87	5′TTGTTTTCCGTAT, AACAAAAGGTATA5′
1018	G → A	13 (13.5)	325.0	94	5′TTATTCATTGGAC, AATAAGTAATCTG5′
1622	G → A	5 (5.2)	125.0	≥145	5′TAGCTGTTTGGAT, ATCGACAAATCTG5′
ura7Δ: 0.5 x dCTP, 3.3 x dTTP, 3.8 x dATP, 2.7 dGTP					
overall		110	3800	39.6	
268	C → T	6 (5.5)	207.3	240	5′AAGTAAAGACATA, TTCGTTTCTGTAT5′
670	G → A	11 (10.0)	380.0	439	5′AAATATTACGGTG, TTTATAATGTCAC5′
788	G → A	16 (14.5)	552.7	633	5′TCCGTTATTGGAG, AGGCAATAATCTC5′
980	G → A	14 (12.7)	483.6	92	5′TTGTTTTCCGTAT, AACAAAAGGTATA5′
1018	G → A	11 (10.0)	380.0	110	5′TTATTCATTGGAC, AATAAGTAATCTG5′
shm2Δ: 1.0 x dCTP, 1.1 x dTTP, 1.1 x dATP, 1.1 dGTP					
overall		96	210	2.2	
497	G → A	6 (6.3)	13.1	2	5′CAGCATTTGGTGC, GTCGTAAACTACG5′
670	G → A	7 (7.3)	15.3	18	5′AAATATTACGGTG, TTTATAATGTCAC5′
788	G → A	7 (7.3)	15.3	18	5′TCCGTTATTGGAG, AGGCAATAATCTC5′
980	G → A	10 (10.4)	21.9	4	5′TTGTTTTCCGTAT, AACAAAAGGTATA5′

Mutations are shown relative to the coding strand. The predicted mutation is noted in red. Nucleotides following the mutation and which dNTP pools are increased in the mutants in comparison to WT are noted in green. dNTP levels are shown as fold over the WT (Table 4.9B). The mutation spectra analysis was done in an *msh6Δ* background. A mutation hotspot is defined as a specific mutation found in more than 5% of all sequenced CAN^R clones in the indicated genotype. Mutation hotspots that are significant different to the *msh6Δ* control (Fisher's exact test, p-value ≤ 0.05) are shown in bold. Table was adapted from (Schmidt *et al.* 2017).

All mutational hotspots in *msh6Δ gln3Δ* and *msh6Δ ura7Δ* strains were most likely driven by the altered dCTP to dTTP ratio (1:15 in the mutants in comparison to 1:2 in WT), which favored dTTP incorporation opposite of a template G. Furthermore, all identified hotspots in *msh6Δ gln3Δ* and *msh6Δ ura7Δ* are in agreement with a rapid mispair extension, promoted by increased dTTP, dATP and dGTP pools (Table 4.11). A frequent mutational hotspot in *msh6Δ gln3Δ* and *msh6Δ ura7Δ CAN1* mutation spectra was the misinsertion of dTTP opposite of the template G at position 788 (Fig. 4.11B). In these backgrounds, the misinsertion is presumably driven by the dCTP to dTTP ratio and the high levels of the dNTPs required to extend the mispair (next-nucleotide effect). In contrast, misinsertion of a dTTP opposite of the template G at position 497 was frequently identified in the *msh6Δ* and *msh6Δ shm2Δ CAN1* mutation spectra, but not in *msh6Δ gln3Δ* and *msh6Δ ura7Δ CAN1* mutation spectra (Fig. 4.11C). To continue DNA replication after the mispair at position 497, dCTP is required. Therefore, low dCTP pools, like in *gln3Δ* or *ura7Δ*, may counterselect for rapid extension giving more time for DNA proofreading. Taken together, the absence of Gln3 or Ura7 induces a severe dNTP imbalance that favors G-C to A-T mutations and shapes the *CAN1* mutation spectra.

4.3.6 Pol δ and Pol ε contribute to DNA replication in the absence of Ura7.

In the course of this work, an alternative model for DNA replication was proposed by the Prakash lab, in which Pol δ replicates the leading and lagging DNA strands, and Pol ε functions primarily during origin assembly, S-phase checkpoint activation and proofreading of the leading strand (JOHNSON *et al.* 2015). The here presented genome-wide screen identified a group of genes (*GLN3*, *SHM2*, *URA7* and *EXO1*) that exclusively interacted with the proposed lagging strand DNA polymerase alleles *pol1-L868M* and *pol3-L612M*, but not with the leading strand allele *pol2-M644G* (Table 4.5). One explanation for the observed bias could be that *pol2-M644G* does not contribute to genome replication in the absence of the identified genes. To investigate this possibility and to further characterize the basis for the observed synergistic mutator interactions, *CAN1* mutation spectra analysis was performed in WT, *ura7Δ*, *pol2-M644G*, *pol2-M644G ura7Δ*, *pol3-L612M* and *pol3-L612M ura7Δ* (Table 4.12). In agreement with the *msh6Δ ura7Δ CAN1* mutation spectrum (Table 4.10), more base substitution events were observed in the *ura7Δ CAN1* mutation spectrum (75% in WT and 87.1% in *ura7Δ*). Even in the presence of high-fidelity DNA polymerases and functional MMR, G-C to A-T mutations in *ura7Δ* were 2 times more abundant than in the WT and represented 53% of all observed base pair substitution events (Table 4.12). Statistical comparison of WT and *ura7Δ CAN1* mutation spectra revealed that the type of replication errors produced were significantly different in the presence and absence of Ura7 (Fisher's exact test, p value 0.0016).
In line with previous reports (PURSELL *et al.* 2007; NICK MCELHINNY *et al.* 2008) specific mutational signatures were observed in *pol2-M644G* and *pol3-L612M* expressing cells (Table 4.12). The *pol2-M644G* allele favors T-T mispairs (PURSELL *et al.* 2007) and consequently A-T to T-A mutations were 9-fold more abundant in the *pol2-M644G* spectrum than in the WT (Table 4.12). In contrast, a 3-fold increase in G-C to A-T mutations was detected in the *pol3-L612M CAN1* mutation spectrum (Table 4.12)(NICK MCELHINNY *et al.* 2008).

Consistent with reduced dCTP levels in the absence of Ura7 (Table 4.9B), inactivation of *URA7* in *pol3-L612M* further increased the fraction of G-C to A-T mutations from 58.3% in *pol3-L612M* to 71.4% of all sequenced Can^R events in *pol3-L612M ura7Δ*. Interestingly, in the *pol3-L612M ura7Δ* mutation spectrum one-base-pair frameshifts were also increased (23.1% in *pol3-L612M ura7Δ* in comparison to 12.5% in *pol3-L612M*). Moreover, the type of one-base-pair frameshifts varied between WT, *pol3-L612M* and *pol3-L612M ura7Δ.* Whereas the one-base-pair frameshifts detected in the WT or *pol3-L612M* were dominated by A:T deletions or insertions (73% in WT and 92% in *pol3-L612M*), which were most frequently found in longer mononucleotide runs, the *pol3-L612M ura7Δ CAN1* mutation spectrum showed an increased fraction of G:C one-base-pair frameshifts (68% of the total one-base-pair frameshifts). These G:C one-base-pair frameshifts were located all over the spectrum and were found primarily at single nucleotides or short mononucleotide runs ($n < 3$). Both, *pol3-L612M* and *pol3-L612M ura7Δ* shared the mutational hotspot at position 788 and 1018 (Table 4.13). Interestingly, the mutational hotspot 671 was exclusively found in *pol3-L612M* but was not mutated in *pol3-L612M ura7Δ*, which instead showed a mutational hotspot at position 670 (Table 4.13). The difference can be explained by the mutational sequence context and the altered dNTP pools. Rapid mismatch extension at position 671 requires dCTP directly following the misinsertion.

Table 4.12 *CAN1* mutation spectra of *ura7Δ* and polymerase mutants.

	WT	***ura7Δ***	***pol2-M644G***	***pol2-M644G ura7Δ***	***pol3-L612M***	***pol3-L612M ura7Δ***
Can^R clones sequenced	91	91	94	95	96	95
Mutations overall*	92 (100)	93 (100)	94 (100)	95 (100)	96 (100)	95 (100)
Base substitutions	69 (75.0)	81 (87.1)	82 (87.2)	82 (86.3)	81 (84.4)	72 (75.8)
A-T to G-C	6 (6.5)	4 (4.3)	2 (2.1)	1 (1.1)	12 (12.5)	2 (2.2)
G-C to A-T	18 (19.6)	43 (46.2)	9 (9.6)	20 (21.1)	56 (58.3)	68 (71.4)
G-C to T-A	29 (31.5)	19 (20.4)	5 (5.3)	10 (10.5)	8 (8.3)	1 (1.1)
A-T to C-G	3 (3.3)	7 (7.5)	1 (1.1)	1 (1.1)	2 (2.1)	1 (1.1)
A-T to T-A	7 (7.6)	1 (1.1)	62 (66.0)	49 (51.6)	2 (2.1)	0 (0.0)
C-G to G-C	6 (6.5)	7 (7.5)	3 (3.2)	1 (1.1)	1 (1.0)	0 (0.0)
Transitions	24 (26.1)	47 (50.5)	11 (11.7)	21 (22.1)	68 (70.8)	70 (73.6)
Transversions	45 (48.9)	34 (36.6)	71 (75.5)	61 (64.2)	13 (13.5)	2 (2.2)
One-base-pair frameshifts	15 (16.3)	8 (8.6)	8 (8.5)	11 (11.6)	12 (12.5)	22 (23.1)
Complex mutations†	8 (8.7)	4 (4.3)	4 (4.3)	2 (2.1)	3 (3.1)	1 (1.1)

Mutation spectra analysis based on DNA sequencing of the *CAN1* gene in independent Can^R mutants, shown as the number of clones containing the indicated mutations, and in parenthesis as the percentage relative to the total. (Fig. S7.1 and Fig. S7.7-11)

*In few cases (about 1-2% of the sequenced clones) two simultaneous *CAN1* mutations (more than 100 bp apart) were found. These mutations were included in the analysis and considered as independent mutational events.

† includes: multiple mutations within 10 nucleotides, insertions or deletions of more than 1 nucleotide and duplication events.

Table 4.13 Mispair base substitution hotspots identified in *ura7Δ* and polymerase mutants.

Position	Mutation	No of occurrences (% of total)	Mutation rate ($x10^{-8}$)	Fold increase over WT	Predicted intermediate
		ura7Δ: 0.5 x dCTP, 3.3 x dTTP, 3.8 x dATP, 2.7 dGTP			
overall		91	10	1.4	
1018	G → A	11 (12.1)	1.2	≥15.3	5′TTATTCATTGGAC AATAAGTAATCTG5′
		pol2-M644G: 3.9 x dCTP, 4.0 x dTTP, 4.4 x dATP, 3.5 dGTP			
overall		94	84	11.7	
103	A → T	19 (20.2)	17.0	≥214.6	5′CACTGACGTGGGT GTGTCTGCACCCA5′
271	A → T	5 (5.3)	4.5	≥56.5	5′CAATGACATATTG GTTTCTGTATAAC5′
475	A → T	13 (13.8)	11.6	≥146.8	5′CAATGATTCCTTT GTTTCTAAGGAAA5′
1417	A → T	14 (14.9)	12.5	158.1	5′ATCTGATTTATGC TAGTCTAAATACG5′
		ura7Δ pol2-M644G: not determined			
overall		95	110	15.3	
103	A → T	8 (8.4)	9.3	≥117.1	5′CACTGACGTGGGT GTGTCTGCACCCA5′
475	A → T	8 (8.4)	9.3	≥117.1	5′CAATGATTCCTTT GTTTCTAAGGAAA5′
1018	G → A	6 (6.3)	6.9	≥87.8	5′TTATTCATTGGAC AATAAGTAATCTG5′
1417	A → T	17 (17.9)	19.7	≥248.8	5′ATCTGATTTATGC TAGTCTAAATACG5′
		pol3-L612M: 1.1 x dCTP, 0.9 x dTTP, 0.9 x dATP, 0.9 dGTP			
overall		96	93	12.9	
671	G → A	6 (6.3)	5.8	≥73.5	5′AAATATTACGGTGA TTTATAATGCTACT5′
788	G → A	5 (5.2)	4.8	≥61.2	5′TCCGTTATTGGAG AGGCAATAATCTC5′
1018	G → A	14 (14.6)	13.6	≥171.4	5′TTATTCATTGGAC AATAAGTAATCTG5′
		ura7Δ pol3-L612M: not determined			
overall		95	1560	218	
670	G → A	7 (7.4)	114.9	≥1452.8	5′AAATATTACGGTG TTTATAATGTCAC5′
788	G → A	14 (14.7)	229.9	≥2905.6	5′TCCGTTATTGGAG AGGCAATAATCTC5′
1018	G → A	13 (13.7)	213.5	≥2698.1	5′TTATTCATTGGAC AATAAGTAATCTG5′

Mutations are shown relative to the coding strand. The predicted mutation is noted in red. Nucleotides following the mutation and which dNTP pools are increased in the mutants in comparison to WT are noted in green. dNTP levels are shown as fold over the WT (Table 4.9B). For *ura7Δ* double mutants, in which dNTP pools were not determined, the predicted intermediates are color-coded as if dCTP pools were limiting. A mutation hotspot is defined as a specific mutation found in more than 5% of all sequenced CAN^R clones in the indicated genotype. Mutation hotspots that are significant different to the WT control (Fisher's exact test, Benjamini and Hochberg corrected p-value ≤ 0.05) are shown in bold.

Therefore, the low dCTP levels in the absence of Ura7 presumably counteract rapid extension and facilitate proofreading. In contrast, rapid extension of a misinsertion at position 670 is supported on the expense of proofreading by the high abundance of dTTP, dATP and dGTP required for the synthesis of the next 11 nucleotides following the misinsertion (position 669-659). Thus, the dNTP

imbalance induced by the *URA7* inactivation facilitates the existing mutational bias of the *pol3-L612M* allele and this combination may cause the hypermutator phenotype.

Inactivation of *URA7* in *pol2-M644G* reduced the fraction of A-T to T-A mutations from 66% in *pol2-M644G* to 51.6% of all identified events in *pol2-M644G ura7Δ*. G-C to A-T mutations were increased 2-fold in the *pol2-M644G ura7Δ* double mutant in comparison to the *pol2-M644G CAN1* mutation spectrum, presumably due to the dNTP imbalance in *ura7Δ* cells (Table 4.9B). However, statistical analysis revealed that the *pol2-M644G ura7Δ CAN1* mutation spectrum was not significantly different to the *pol2-M644G* spectrum (Fisher's exact test, p value 0.155) supporting the role of *pol2-M644G* as replicating DNA polymerase even in the absence of Ura7. Furthermore, the strong A to T mutational hotspots at position 103, 475 and 1417 identified in *pol2-M644G* were also found in *pol2-M644G ura7Δ*. However, the relative contribution of the individual hotspot to the total spectrum changed. For example, the hotspots at position 103 and 475 were identified less frequently in *pol2-M644G ura7Δ* than in *pol2-M644G*, presumably because dCTP levels are reduced in *ura7Δ* strains and dCTP is required at these hotspots for rapid mispair extension (even though not as direct adjacent nucleotide) (Table 4.13). Furthermore, as in the *ura7Δ* single mutant, a G to A mutation hotspot at position 1018 was detected that most likely originated from lagging strand replication and was presumably driven by low dCTP levels. Thus, the *CAN1* mutation spectrum analysis of *pol2-M644G ura7Δ* suggests that the absence of a synergistic mutator interaction between *pol2-M644G* and *ura7Δ* is not due to absent DNA replication by *pol2-M644G*, but rather that the mutational bias of *pol2-M644G* is not supported by the *ura7Δ* induced dNTP imbalance. Nevertheless, the dNTP imbalance influences the relative frequency of mutational hotspots produced by *pol2-M644G* and impacts also on lagging-strand replication fidelity.

4.4 A *RNR1* random mutagenesis screen reveals specific residues in *RNR1* with crucial functions for dNTP homeostasis and uncovers a highly mutagenic dNTP imbalance.

4.4.1 *RNR1* screen identifies key residues for dNTP homeostasis and genome stability.

The genome-wide screen had identified two genes *GLN3* and *URA7* that when absent caused a dNTP imbalance (Fig. 4.10B, Table 4.9B) by affecting the concentration of one substrate required for dNTP biosynthesis (Fig. 4.10A, Table 4.9A). The mutational potential of this dNTP imbalance was normally buffered by DNA polymerase nucleotide selectivity and proofreading as well as MMR but resulted in a hypermutator phenotype if any of the aforementioned processes were defective (Table 4.5 and 4.7). Similar synergistic mutator interactions between dNTP pool alterations and defects in other DNA replication fidelity mechanisms have been previously described. However, several open questions remain to be answered: Why certain dNTP pool alterations are more mutagenic than others? Which dNTP pool alterations favor frameshift mutations *in vivo* and which type of dNTP pool alteration is the most detrimental in *S. cerevisiae*? To address these questions and to further investigate the mutagenic potential of different dNTP pool alterations an *RNR1* random mutagenesis screen was conducted. Mutagenesis of *RNR1* and mutator screening in an *exo1Δ* background was performed based on three lines of evidence: First, Rnr1 is the major large subunit of RNR, the master regulator of dNTP pools. Rnr1 does not only contain the C-site, but also the two allosteric regulatory sites making Rnr1 a critical determinant of dNTP pools homeostasis (Fig. 1.7) (NORDLUND AND REICHARD 2006). Second, previous studies have described a small number of *rnr1* mutant alleles, some of them only viable in the presence of a second suppressed WT-*RNR1* copy, with different dNTP pool alterations and effects on DNA replication fidelity (CHABES *et al.* 2003; KUMAR *et al.* 2010) suggesting that additional, previously unrecognized *rnr1* alleles exist that affect dNTP pool homeostasis. Third, a chemical mutagenesis screen in budding yeast revealed besides MMR mutant alleles also one *rnr1* allele (*rnr1-G271S*) as an *exo1Δ*-dependent mutator. However, the *rnr1-G271S* allele was not characterized in detail at that time (AMIN *et al.* 2001). Taken together, these evidence suggested that the *exo1Δ* background might be used, similar to the low-fidelity DNA polymerase backgrounds in the genome-wide screen (SCHMIDT *et al.* 2017), as “sensitized mutator background” in a plasmid-based *RNR1* random mutagenesis screen. This screen may reveal novel *rnr1* alleles resulting in elevated mutator phenotypes driven by dNTP pool alterations.

To identify novel *rnr1* alleles that increase mutagenesis in an *exo1Δ* background, a library of different *rnr1* alleles was generated using error-prone PCR followed by *in vivo* gap repair and screening for increased mutagenesis using three different mutator assays (*CAN1* inactivation assay and *hom3-10* and *lys2-10A* frameshift reversion assay) (Fig. 4.12A). In this plasmid-based screen approximately 39,000 Leu^+ transformants were tested. Finally, 24 different *rnr1* alleles were identified that conferred an increased mutator phenotype in the absence of Exo1 (Fig. 4.12B and C, Table 4.14). 11 of the 24 alleles were found more than once. For example, the *rnr1-S269P*, *rnr1-Y285C* and *rnr1-K243E* alleles were found 14, 10 and 10 times, respectively.

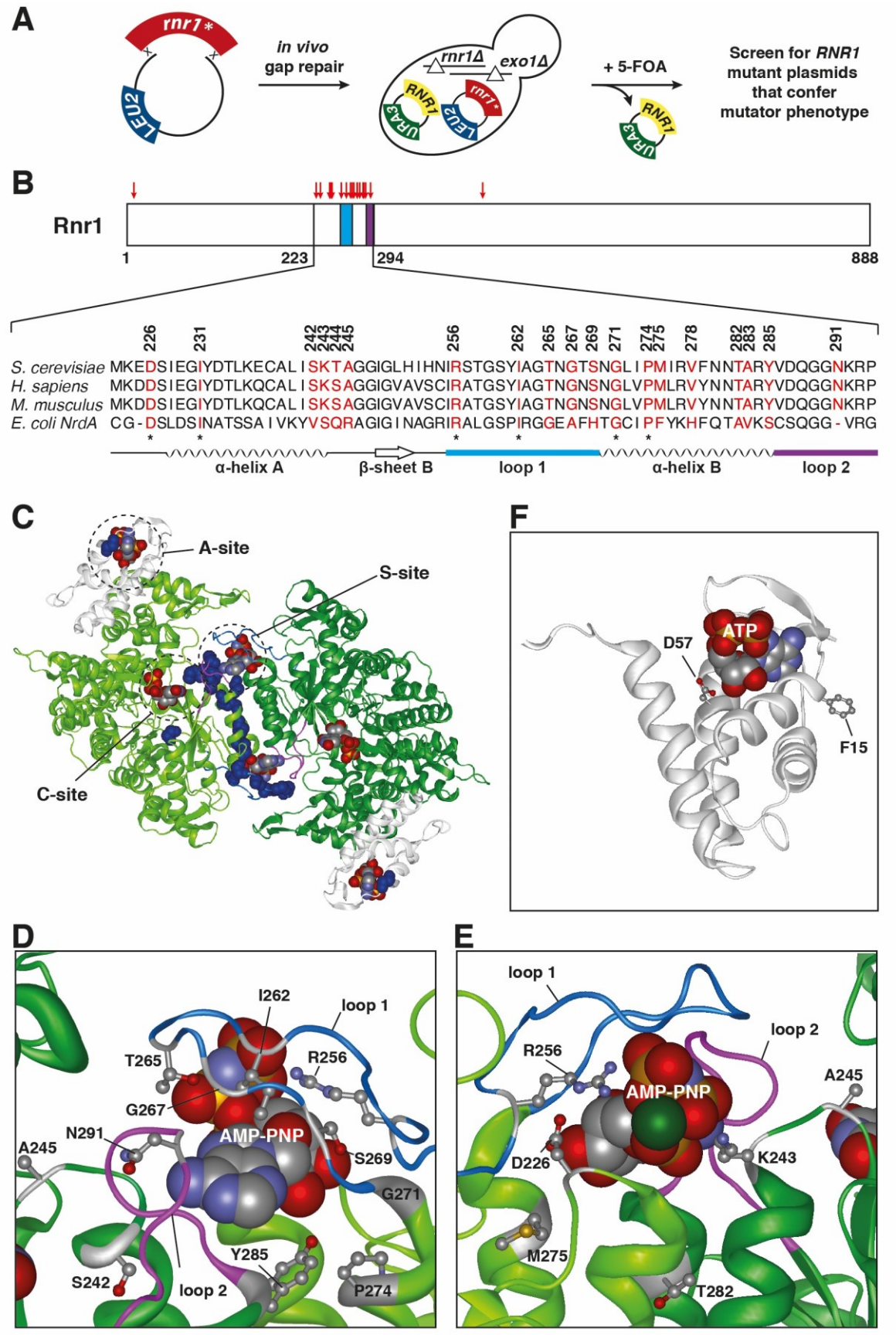

Fig. 4.12 *rnr1* mutations identified in a *RNR1* random mutagenesis screen cluster in the S-site.
(A) Schematic representation of the *rnr1* random mutagenesis screening strategy. Briefly, a PCR-mutagenized *rnr1* was co-transfected with a linearized plasmid (*CEN6*, *ARSH4*, *LEU2*) in HHY6555 for in vivo gap repair. The WT-*RNR1-URA3* plasmid was counterselected by replica-plating on SD media containing 5-FOA followed

by screening for increased papillation on three mutator assay plates (*hom3-10*, *lys2-10A* and *CAN1* inactivation assay). (B) Schematic representation of the Rnr1 protein. The positions of identified mutations are shown as red arrows. Loop 1 and loop 2 are shown as light blue and violet boxes, respectively. Below a sequence alignment of *S. cerevisiae* Rnr1 (aa 223-294) with human, mouse and *E. coli* homologs is shown. Identified mutations are colored red. Mutated residuals that are conserved from *E. coli* to human are labeled with an asterisk. (C) Model of the Rnr1-Rnr1 homodimer based on crystal structure (PDB 2vvv in green and 3hne superimposed in white). Identified mutations are shown as blue spheres in one subunit. (D) and (E) Zoom-in in the S-site (PDB 2cvv). Mutated amino acids are shown as balls and sticks model. (F) Zoom-in in the A-site (PDB 3hne). The mutated Phe15 and the previously described Asp57 are shown as balls and sticks model.

This indicates a good saturation of the screen and suggests that under the screening conditions used not many other *rnr1* alleles can be identified.

Interestingly, most of the identified mutations (21 of the 24) clustered between amino acid (aa) 226 and 291 of Rnr1 (Fig. 4.12B,C). This region forms the S-site and based on the available crystal structure of *S. cerevisiae* Rnr1 (XU *et al.* 2006a) some of the identified residuals form direct or indirect interactions with the bound effector nucleotide (Fig. 4.12C-E). Furthermore, two mutations (*A245V* and *S425L*) were located closer to the C-site and two mutations (*G8D* and *F15S*) were identified at the N-terminal A-site (Fig. 4.12 F).

Taken together, this comprehensive *rnr1* random mutagenesis screen identified 24 different mutagenic *rnr1* alleles, most of them affecting residues located at the S-site between aa 226 and 291.

4.4.2 *rnr1* mutant alleles confer *exo1Δ*-dependent and *exo1Δ*-independent mutator phenotypes.

To validate the mutator phenotypes of the identified *rnr1* alleles, mutation rates of *exo1Δ rnr1Δ* cells expressing the *rnr1* alleles on a centromeric plasmid were determined using the *CAN1* inactivation assay as well as the *lys2-10A* and *hom3-10* frameshift reversion assay (Table 4.14). Some *rnr1* alleles like *rnr1-A245V*, *rnr1-I262V*, *rnr1-G271S, rnr1-M275T*, and *rnr1-T282A* conferred only a weak mutator phenotype (*CAN1* inactivation rate < 10-fold). Others, like *rnr1-D226G/V/N*, *rnr1-K243E*, *rnr1-I262V,M275T* and *rnr1-S269P* caused strongly increased mutator phenotypes with up to 80-fold increases in the *CAN1* mutation rates (Table 4.14). Remarkably, some of the *rnr1* alleles in the absence of Exo1 were even stronger mutators than a completely MMR-deficient strain (*msh2Δ* + WT-*RNR1*) (Table 4.14).

To examine whether the *rnr1* alleles conferred a mutator phenotype in the presence of Exo1, *rnr1* alleles were expressed on a centromeric plasmid in WT-*EXO1 rnr1Δ* strains and the *lys2-10A* frameshift mutator phenotype was qualitatively evaluated (Fig. 4.13). Most of the *rnr1* alleles did not cause increased *lys2-10A* reversion (as evaluated by increased papillation on -lysine mutator plates). However, three *rnr1* alleles *rnr1-K243E*, *rnr1-I262T,M275I* and *rnr1-I262V,N291D* resulted in strongly increased *lys2-10A* mutator phenotypes even in the presence of Exo1. This finding suggests that the presumed dNTP pool alteration in the presence of these alleles is extremely mutagenic and overwhelms the buffer capacity of the cellular DNA replication fidelity machinery.

Moreover, to test whether the identified *rnr1* alleles also increase mutagenesis in other partially MMR-defective backgrounds (MARSISCHKY *et al.* 1996), the WT-*RNR1* and four *rnr1* alleles (*rnr1-*

Table 4.14 Mutation rates caused by *rnr1* mutations expressed on a centromeric plasmid in the *exo1Δ rnr1Δ* mutant.

	Mutation Rate (fold increase)*		
Allele†	**Can^R**	**Thr$^+$**	**Lys$^+$**
+ *RNR1-WT*	1.7 [1.5-3.0] x 10^{-6} (1)	2.4 [1.8-3.2] x 10^{-8} (1)	2.2 [1.6-3.0] x 10^{-7} (1)
+ *rnr1-G8D,V278A*	3.5 [3.1-4.9] x 10^{-6} (2)	2.5 [1.6-3.5] x 10^{-7} (10)	4.0 [2.8-8.6] x 10^{-6} (19)
+ *rnr1-F15S*	2.6 [1.9-3.9] x 10^{-5} (16)	3.8 [2.7-5.0] x 10^{-6} (158)	3.2 [2.6-5.8] x 10^{-6} (15)
+ *rnr1-D226G*	1.3 [0.4-1.8] x 10^{-4} (80)	1.8 [0.9-3.5] x 10^{-4} (7523)	9.3 [5.3-25.9] x 10^{-5} (424)
+ *rnr1-D226V*	1.1 [0.5-1.7] x 10^{-4} (66)	1.9 [0.7-3.2] x 10^{-4} (7737)	1.6 [0.7-2.8] x 10^{-4} (753)
+ *rnr1-S117P‡,D226N*	4.5 [3.0-9.0] x 10^{-5} (27)	1.1 [0.4-2.8] x 10^{-4} (4612)	1.4 [1.0-1.9] x 10^{-4} (645)
+ *rnr1-I231T,T244A*	8.4 [6.9-11.0] x 10^{-6} (5)	3.3 [2.3-5.2] x 10^{-6} (137)	3.3 [2.9-4.5] x 10^{-5} (150)
+ *rnr1-S242T*	4.5 [3.1-7.7] x 10^{-5} (27)	9.5 [6.4-16.3] x 10^{-6} (396)	1.6 [1.3-2.8] x 10^{-4} (750)
+ *rnr1-K243E*	1.0 [0.7-1.2] x 10^{-4} (63)	3.9 [2.6-8.1] x 10^{-5} (1613)	2.6 [1.8-4.9] x 10^{-4} (1185)
+ *rnr1-T244I,V278A*	1.4 [0.9-2.5] x 10^{-5} (8)	1.0 [0.8-2.1] x 10^{-5} (423)	5.7 [1.3-11.0] x 10^{-5} (262)
+ *rnr1-A245V*	1.3 [0.9-2.3] x 10^{-5} (8)	5.0 [2.8-11.7] x 10^{-6} (207)	3.4 [2.1-6.6] x 10^{-6} (16)
+ *rnr1-R256H,Y779C*	2.3 [1.3-3.6] x 10^{-5} (14)	2.9 [1.9-5.6] x 10^{-5} (1214)	1.6 [0.9-2.4] x 10^{-4} (741)
+ *rnr1-I262T,M275I*	1.1 [0.8-1.9] x 10^{-5} (69)	2.0 [0.7-2.6] x 10^{-4} (8165)	4.5 [3.0-11.2] x 10^{-4} (2077)
+ *rnr1-I262V,N291D*	6.4 [4.5-9.6] x 10^{-5} (39)	1.7 [1.0-2.8] x 10^{-5} (711)	1.8 [1.2-2.8] x 10^{-4} (815)
+ *rnr1-I262V*	2.8 [2.1-3.4] x 10^{-6} (2)	2.8 [2.2-3.1] x 10^{-7} (12)	3.3 [1.8-6.3] x 10^{-6} (15)
+ *rnr1-T265A*	6.3 [3.9-7.9] x 10^{-6} (4)	1.9 [0.9-4.1] x 10^{-6} (81)	3.3 [1.1-5.9] x 10^{-5} (153)
+ *rnr1-G267C*	3.9 [2.2-7.8] x 10^{-5} (23)	1.0 [0.6-2.0] x 10^{-5} (428)	2.1 [1.8-2.8] x 10^{-4} (957)
+ *rnr1-S269P*	8.4 [6.6-13.0] x 10^{-5} (51)	2.1 [1.2-4.1] x 10^{-4} (8595)	2.8 [2.0-4.3] x 10^{-4} (1276)
+ *rnr1-G271S*	3.7 [3.4-4.5] x 10^{-6} (2)	1.1 [0.9-1.3] x 10^{-6} (47)	1.7 [1.4-3.6] x 10^{-6} (8)
+ *rnr1-P274L*	5.9 [3.9-10.2] x 10^{-6} (4)	9.4 [5.5-11.5] x 10^{-7} (39)	2.7 [1.7-3.9] x 10^{-5} (123)
+ *rnr1-M275T*	1.8 [1.0-2.4] x 10^{-6} (1)	2.6 [2.0-4.1] x 10^{-7} (11)	2.1 [1.3-6.3] x 10^{-6} (9)
+ *rnr1-T282A*	2.9 [2.4-4.6] x 10^{-6} (2)	1.0 [0.8-1.5] x 10^{-7} (4)	2.0 [1.6-2.2] x 10^{-6} (9)
+ *rnr1-T282S*	3.3 [2.4-6.4] x 10^{-6} (2)	3.3 [2.3-6.4] x 10^{-7} (14)	3.0 [1.5-5.5] x 10^{-5} (138)
+ *rnr1-A283V,S425L*	8.2 [6.4-9.4] x 10^{-6} (5)	1.1 [0.9-1.5] x 10^{-6} (48)	3.1 [2.1-6.4] x 10^{-5} (140)
+ *rnr1-Y285C*	1.1 [0.8-1.3] x 10^{-5} (7)	4.5 [3.5-7.1] x 10^{-6} (187)	7.7 [6.4-13.0] x 10^{-5} (35)
msh2Δ + *RNR1-WT*	4.0 [2.4-6.2] x 10^{-5} (24)	4.3 [2.4-7.9] x 10^{-5} (1792)	2.3 [1.5-2.7] x 10^{-4} (1045)

* Median rates for the *CAN1* (Can^R) inactivation assay and for *hom3-10* (Thr$^+$) and *lys2-10A* (Lys$^+$) frameshift reversion assays with 95% confidence interval in square brackets and fold increase in parentheses, relative to *rnr1Δ exo1Δ* strain complemented with the WT-*RNR1* plasmid. † Allele expressed on a low-copy number plasmid in an *rnr1Δ exo1Δ* strain. As reference for total MMR deficiency an *rnr1Δ msh2Δ* strain complemented with the WT-*RNR1* plasmid was included. Site directed mutagenesis (or subcloning) was used to independently generate *rnr1* single point mutants for all plasmids containing more than one mutation. Passenger mutations are indicated with ‡.

F15S, *rnr1-S242T*, *rnr1-I262V,N291D* and *rnr1-Y285C*) that differed in the strength of the mutator phenotypes in *exo1Δ* and *EXO1* backgrounds, were expressed on centromeric plasmids in *msh3Δ rnr1Δ* and *msh6Δ rnr1Δ* cells and mutation rates were determined (Table 4.15). In comparison to the WT-*RNR1* increased mutation rates were measured for all tested *rnr1* alleles in these partially mismatch recognition-compromised backgrounds. In agreement with a primary role of Msh6 in mispair recognition and Msh3 in the detection of insertions and deletions (MARSISCHKY *et al.* 1996), increased *CAN1* inactivation were predominantly found in *msh6Δ* double mutants and *hom3-10* reversions were more abundant in *msh3Δ* double mutants

Thus, the here identified *rnr1* alleles presumably induce dNTP pool alterations that not only facilitates misinsertions, but also slippage events, leading to increased mutagenesis in MMR-compromised backgrounds. Remarkably, three *rnr1* alleles caused presumably such a mutagenic

dNTP pool alteration that increased frameshift mutations were detected even in an MMR-proficient WT background.

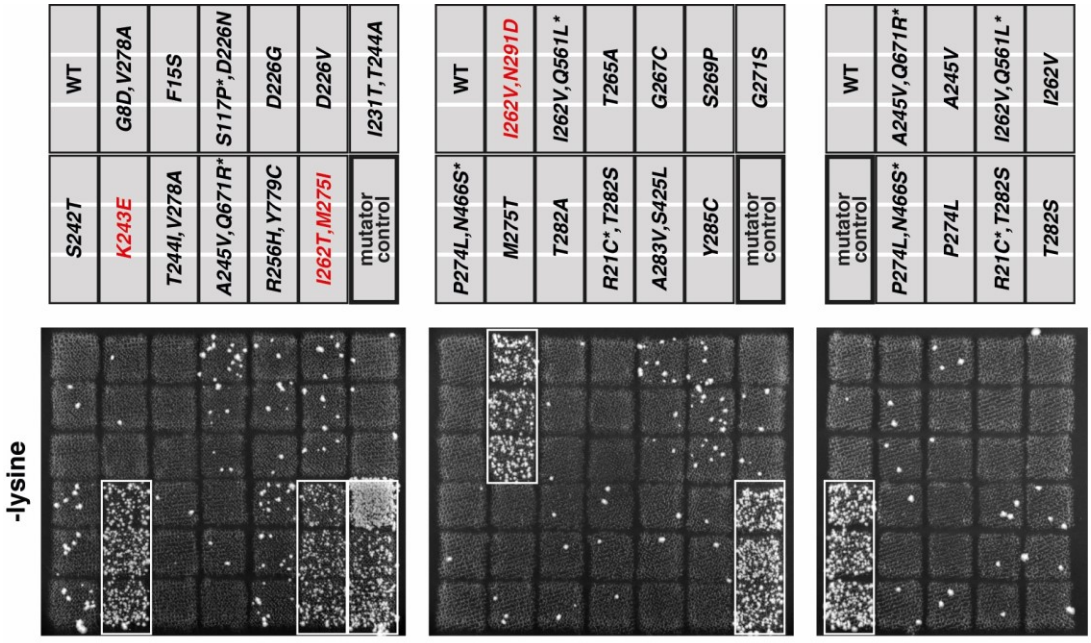

Fig. 4.13 *rnr1* mutation screen identifies *exo1Δ*-dependent and independent mutator phenotypes. Qualitative patch test of *rnr1Δ* strains expressing WT-*RNR1* or *rnr1* mutant alleles on a centromeric *LEU2* plasmid. Increased papillation is indicative for an elevated frameshift mutator phenotype. Three colonies per genotype were patched. *rnr1* alleles which confer a strong frameshift mutator phenotype in the WT *rnr1Δ* background are colored in red. Passenger mutations are labeled with asterisks. As positive mutator control *rnr1Δ exo1Δ* complemented with *rnr1-G271S* expressed from a centromeric *LEU2* plasmid was used.

Table 4.15 Mutation rates of *rnr1* mutants expressed from a centromeric plasmid in an *msh3Δ rnr1Δ* and *msh6Δ rnr1Δ* background.

	Mutation Rate (fold increase)*		
Allele†	**Can^R**	**Thr$^+$**	**Lys$^+$**
WT + *RNR1-WT*	2.8 [1.9-3.2] x 10^{-7} (1)	5.3 [3.5-7.1] x 10^{-9} (1)	1.6 [0.9-3.2] x 10^{-8} (1)
msh2Δ + *RNR1-WT*	4.0 [2.4-6.2] x 10^{-5} (145)	4.3 [2.4-7.9] x 10^{-5} (8090)	2.3 [1.5-2.7] x 10^{-4} (14470)
msh3Δ + *RNR1-WT*	8.4 [6.6-13.1] x 10^{-7} (3)	2.4 [2.0-3.7] x 10^{-7} (46)	1.1 [0.9-2.3] x 10^{-6} (72)
msh3Δ + *rnr1-F15S*	4.4 [2.6-6.1] x 10^{-6} (16)	9.0 [6.4-14.4] x 10^{-7} (169)	1.3 [0.7-1.6] x 10^{-6} (81)
msh3Δ + *rnr1-S242T*	6.3 [3.5-11.2] x 10^{-6} (23)	3.9 [2.3-6.8] x 10^{-6} (726)	5.7 [3.6-8.2] x 10^{-6} (365)
msh3Δ + *rnr1-I262V,N291D*	1.9 [1.4-2.4] x 10^{-5} (69)	1.2 [0.8-1.5] x 10^{-5} (2332)	3.1 [2.0-4.2] x 10^{-5} (2011)
msh3Δ + *rnr1-Y285C*	1.5 [1.1-2.5] x 10^{-5} (55)	2.0 [1.6-2.6] x 10^{-6} (385)	2.5 [1.2-3.7] x 10^{-6} (160)
msh6Δ + *RNR1-WT*	1.3 [1.0-2.0] x 10^{-5} (47)	1.2 [0.6-1.5] x 10^{-7} (22)	2.6 [1.5-4.3] x 10^{-6} (169)
msh6Δ + *rnr1-F15S*	8.3 [6.0-12.0] x 10^{-5} (298)	5.9 [2.9-9.4] x 10^{-7} (111)	1.8 [1.2-4.1] x 10^{-6} (116)
msh6Δ + *rnr1-S242T*	6.4 [4.2-11.8] x 10^{-5} (232)	2.7 [1.6-6.4] x 10^{-6} (514)	2.4 [1.2-3.7] x 10^{-5} (1564)
msh6Δ + *rnr1-I262V,N291D*	1.2 [0.4-1.5] x 10^{-4} (436)	1.3 [0.9-2.4] x 10^{-6} (248)	4.4 [1.4-5.7] x 10^{-5} (2827)
msh6Δ + *rnr1-Y285C*	1.3 [1.0-1.7] x 10^{-4} (453)	2.6 [1.9-3.5] x 10^{-6} (495)	9.4 [6.8-24.9] x 10^{-6} (606)

* Median rates of inactivation of *CAN1* gene (Can^R) and *lys2-10A* (Lys$^+$) and *hom3-10* (Thr$^+$) frameshift reversion with 95% confidence interval in square brackets and fold increase in parentheses, relative to the WT-*RNR1* plasmid.

† Allele expressed from a low copy number plasmid in *rnr1Δ msh3Δ* or *rnr1Δ msh6Δ* background.

4.4.3 *rnr1* mutant alleles rely differentially on DNA damage response, DNA proofreading and MMR.

Mutations in *RNR1* can severely compromise RNR catalytic activity, so that cells depend on an active S-phase checkpoint and expression of the alternative large RNR subunit *RNR3* to produce sufficient amounts of dNTP for DNA replication (KUMAR *et al.* 2010). Moreover, as observed for the *ura7Δ* + *pol3-01* (Fig. 4.8), the combination of mutagenic dNTP pool alterations and the absence of DNA proofreading or MMR can result in hypermutator phenotypes that severely impair viability leading to growth defects (GD) or even synthetic lethality (SL). Thus, the dependency of the *rnr1* mutants on functional DDR, as well as potential GD/SL genetic interactions with DNA proofreading and MMR mutants were investigated using plasmid shuffling (Fig. 4.14, 4.15).

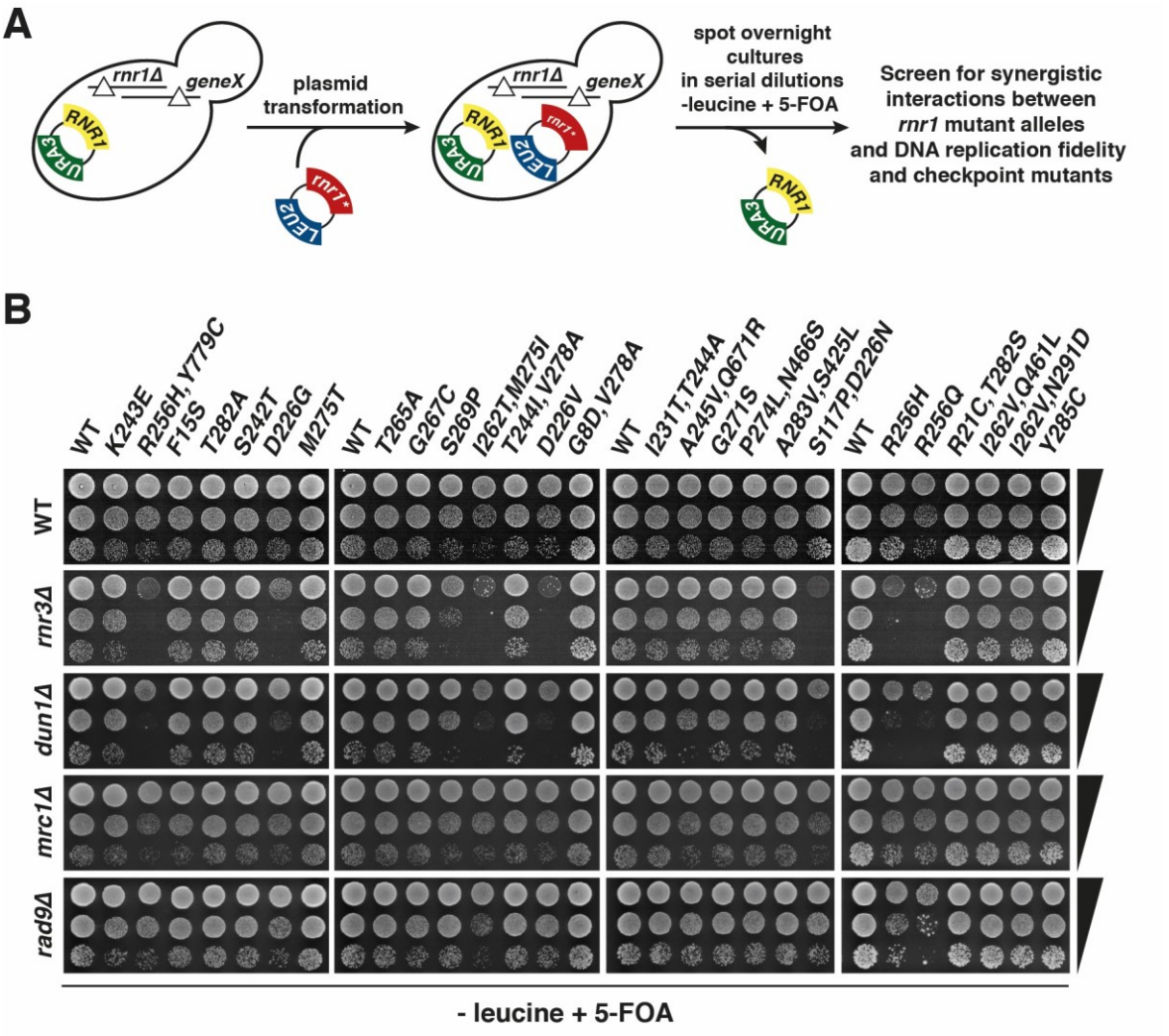

Fig. 4.14 Specific *rnr1* mutant alleles depend on DNA damage checkpoint for survival.
(A) Schematic representation of the experimental outline to investigate genetic interactions by plasmid shuffling. Centromeric *LEU2* plasmids encoding the WT and mutant *rnr1* alleles were transformed in WT and DNA damage checkpoint- or DNA replication fidelity-compromised *rnr1Δ* backgrounds complemented with WT-*RNR1-URA3* plasmid. Overnight cultures were spotted in serial dilution on SD medium lacking Leu and containing 5-FOA to counterselect for the WT-*RNR1-URA3* plasmid and screened for synthetic interactions. (B) Representative images of yeast strains of the indicated genotypes (complemented by WT or mutant *rnr1* plasmids), serially diluted and spotted onto Leu- +5-FOA containing media. Images were taken after 4 days at 30 °C.

In the absence of Rnr3 SL interactions were observed in the *rnr1-D226G/V/N*, *rnr1-R256H,Y779C* and *rnr1-I262T,M275I* and a GD was detected for *rnr1-S269P* (Fig. 4.14B). Similar dependency of these alleles was observed for the DDR kinase Dun1, which is required to inactivate the negative regulators of RNR. Previous reports suggested two branches of the S-phase checkpoint, one Rad9- and the other Mrc1-dependent (PARDO *et al.* 2017). To test, whether the identified *rnr1* alleles relied more on one or the other branch, plasmid shuffling was performed in backgrounds either deficient for Rad9 or Mrc1. No *rnr1* allele conferred severe GD in the absence of Rad9 or Mrc1 suggesting that both checkpoint mediators can compensate for each other and support growth of the Rnr3-dependent *rnr1* alleles even if one of them is absent (Fig. 4.14B).

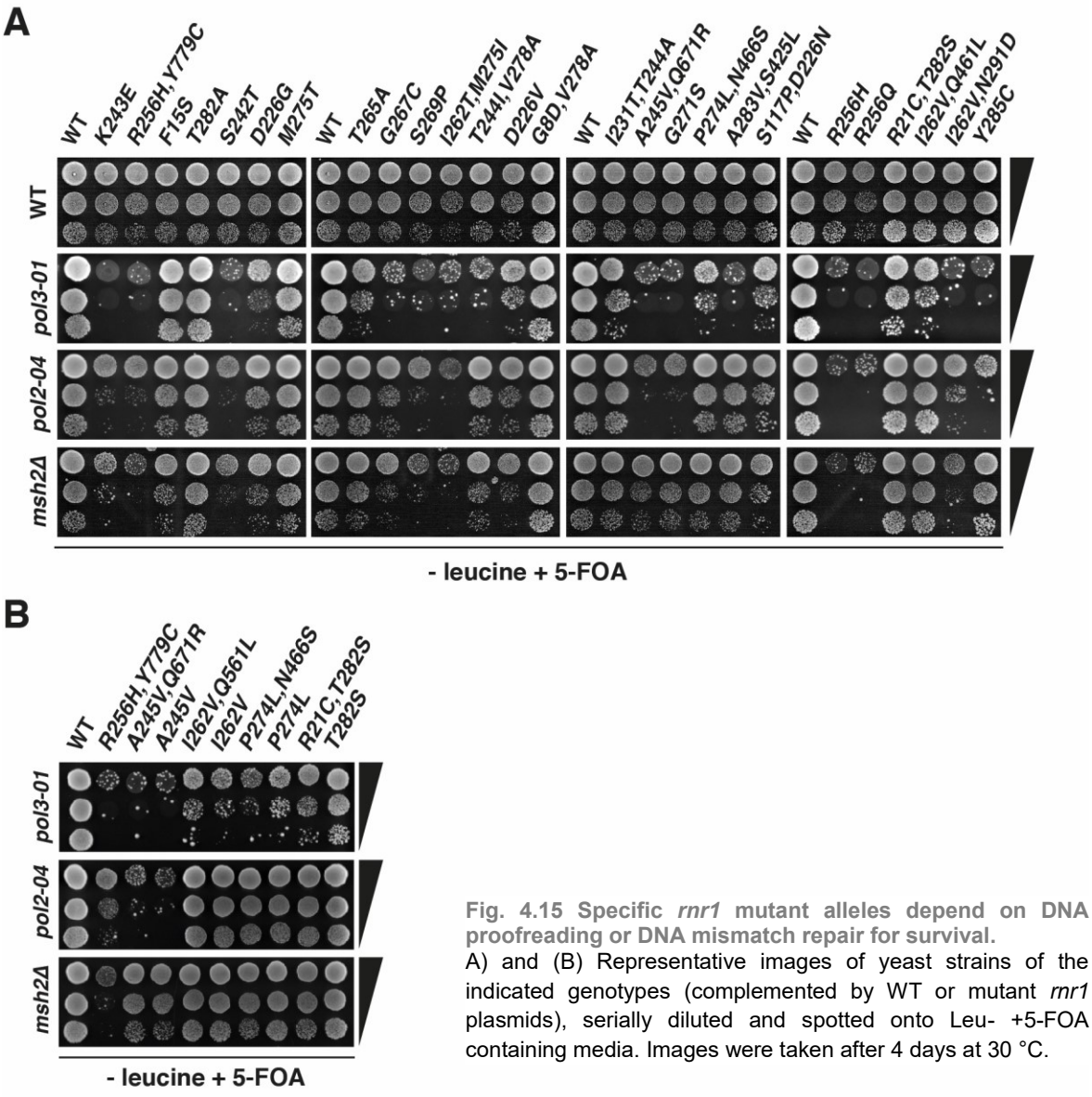

Fig. 4.15 Specific *rnr1* mutant alleles depend on DNA proofreading or DNA mismatch repair for survival.
A) and (B) Representative images of yeast strains of the indicated genotypes (complemented by WT or mutant *rnr1* plasmids), serially diluted and spotted onto Leu- +5-FOA containing media. Images were taken after 4 days at 30 °C.

The identified genetic interactions between the *rnr1* alleles and DNA polymerase proofreading-defective strains (*pol3-01* and *pol2-04*) and MMR-deficient mutant (*msh2Δ*) (Fig. 4.15), in combination with the mutator phenotypes in the presence (Fig. 4.13) or absence of Exo1 (Table 4.14) were used to categorize the identified *rnr1* alleles in four groups (summarized in Table 4.16).

Table 4.16 Summary of *rnr1* mutant alleles identified in this study, including their genetic interactions and mutator phenotypes.

Allele*	synthetic growth defect/lethality				*CAN1* mutator phenotype in *exo1Δ (1)*	frameshift mutator phenotype in *EXO1*-WT *(2)*
	rnr3Δ‡	*pol3-01*	*pol2-04*	*msh2Δ*		
group 1 (no interaction or just with *pol3-01*)						
rnr1-G8D,V278A	-	-	-	-	weak	-
rnr1-F15S	-	-	-	-	strong	-
rnr1-I231T,T244A	-	-	-	-	weak	-
rnr1-T244I,V278A	-	SL	-	-	moderate	-
rnr1-I262V	-	-	-	-	weak	-
rnr1-T265A	-	GD	-	-	weak	-
rnr1-P274L	-	GD	-	-	weak	-
rnr1-M275T	-	-	-	-	weak	-
rnr1-T282A	-	-	-	-	weak	-
rnr1-T282S	-	-	-	-	weak	-
rnr1-A283V,S425L	-	SL	-	-	weak	-
group 2 (interaction with *pol2-04* and *pol3-01*)						
rnr1-A245V	-	SL	GD	-	moderate	-
rnr1-G271S	-	SL	GD	-	weak	-
rnr1-Y285C	-	SL	GD	-	moderate	-
group 3 (interaction with *pol2-04, pol3-01* and *msh2Δ*)						
rnr1-D226G	SL	GD	GD	GD	strong	-
rnr1-D226V	SL	GD	GD	GD	strong	-
rnr1- D226N‡*,S117P*	SL	GD	GD	GD	strong	-
rnr1-S242T	-	SL	GD	GD	strong	-
rnr1-R256H,Y779C	SL	SL	GD	GD	strong	-
rnr1-G267C	-	SL	GD	GD	strong	-
rnr1-S269P	GD	SL	GD	GD	strong	-
group 4 (interaction with *pol2-04, pol3-01* and *msh2Δ* and mutator in *EXO1*-WT*)*						
rnr1-K243E	-	SL	GD	GD	strong	mutator
rnr1-I262T,M275I	SL	SL	GD	GD	strong	mutator
rnr1-I262V,N291D	-	SL	GD	GD	strong	mutator

* Indicated allele expressed on a low-copy number plasmid was used for complementation studies in strains lacking the chromosomal *RNR1* gene in addition to the indicated mutations. Passenger mutations are marked with †. "-" indicates growth similar to WT-*RNR1*; "GD", growth defect; "SL", synthetic lethality. ‡*rnr1* alleles showing GD or SL in the absence of *RNR3* also showed GD or SL in the absence of *DUN1*.

(1) mutator phenotype according to the *CAN1* inactivation rate (Table 1) fold increase over *WT-RNR1* (in *rnr1Δ exo1Δ*): 2-5 = weak; 6-10 = moderate; ≥ 11 = strong.

(2) frameshift mutator phenotype (*lys2-10A* assay) in *EXO1*-WT *rnr1Δ* background (Fig. 4.13).

Group 1 consists of *rnr1* alleles that did not interact with any of the tested alleles or just with *pol3-01* (*rnr1-G8D,V278A*, *rnr1-F15S*, *rnr1-I231T,T244A*, *rnr1-T244I,V278A*, *rnr1-I262V*, *rnr1-T265A*, *rnr1-P274L*, *rnr1-M275T*, *rnr1-T282A*, *rnr1-T282S* and *rnr1-A283V,S425L*). Most of the *rnr1* alleles in this group caused weak mutator phenotypes in the absence of Exo1 (≤5-fold in *CAN1* inactivation). Group 2 *rnr1* alleles showed GD/SL exclusively with the DNA proofreading defective alleles (*pol3-01* and *pol2-04*), but not in the absence of MMR (*rnr1-A245V*, *rnr1-G271S* and *rnr1-*

Y285C). These *rnr1* alleles conferred weak or moderate mutator phenotypes in the absence of Exo1 (≤10-fold in *CAN1* inactivation). Group 3 contains the *rnr1* alleles that showed GD/SL in the absence of DNA proofreading and MMR (*rnr1-D226G/V/N*, *rnr1-S242T*, *rnr1-R256H,Y779C*, *rnr1-G267C* and *rnr1-S269P*). The mutator phenotype of the *rnr1* alleles in this group was strong in the absence of Exo1, but no elevated frameshift mutator phenotype was observed in the presence of Exo1. Finally, group 4 includes the *rnr1* alleles that showed GD/SL in the absence of DNA proofreading and MMR and strongly increased mutagenesis in the absence and presence of Exo1 (*rnr1-K243E*, *rnr1-I262T,M275I* and *rnr1-I262V,N291D*). This distinct dependencies on DNA proofreading and MMR suggest that replication errors caused by the potentially dNTP pool alterations rely differentially on DNA proofreading and MMR for repair.

4.4.4 *rnr1* mutants cause either overall increased or imbalanced dNTP pools.

To validate that the measured increased mutator phenotypes and the detected genetic interactions of the *rnr1* alleles were caused by altered dNTP pools, NTP and dNTP concentrations were measured by HPLC (collaboration with Chabes lab, Umeå University) for those *rnr1* alleles above a defined mutator threshold (>5-fold increase in *CAN1* assay or >40-fold increase in *hom3-10* assay

Table 4.17 NTP concentrations in strains expressing *rnr1* mutant alleles on a centromeric plasmid.

	NTP concentration (pmol per 10^8 cells)*			
Allele	**CTP**	**UTP**	**ATP**	**GTP**
+ WT-*RNR1*	2139 ± 165 (1.0)	4249 ± 130 (1.0)	13792 ± 870 (1.0)	3232 ± 197 (1.0)
group 1 (no interaction or just with *pol3-01*)				
+ *rnr1-F15S*	2073 ± 50 (1.0)	3926 ± 8 (0.9)	14255 ± 40 (1.0)	2753 ± 86 (0.9)
+ *rnr1-I231T,T244A*	2105 ± 72 (1.0)	3734 ± 36 (0.9)	14223 ± 34 (1.0)	2854 ± 81 (0.9)
+ *rnr1-T244I,V278A*	2066 ± 7 (1.0)	3810 ± 32 (0.9)	14108 ± 8 (1.0)	2888 ± 15 (0.9)
+ *rnr1-T265A*	2122 ± 1 (1.0)	3912 ± 197 (0.9)	14480 ± 448 (1.0)	2947 ± 42 (0.9)
+ *rnr1-A283V,S425L*	2143 ± 37 (1.0)	4050 ± 118 (1.0)	13975 ± 383 (1.0)	2610 ± 61 (0.8)
group 2 (interaction with *pol2-04* and *pol3-01*)				
+ *rnr1-A245V*	1930 ± 56 (0.9)	4132 ± 119 (1.0)	15154 ± 182 (1.1)	3450 ± 37 (1.1)
+ *rnr1-G271S*	2267 ± 39 (1.1)	4218 ± 6 (1.0)	15307 ± 11 (1.1)	3674 ± 50 (1.1)
+ *rnr1-Y285C*	2100 ± 105 (1.0)	3904 ± 80 (0.9)	14817 ± 173 (1.1)	2907 ± 62 (0.9)
group 3 (interaction with *pol2-04, pol3-01* and *msh2Δ*)				
+ *rnr1-D226G*	2202 ± 61 (1.0)	3913 ± 114 (0.9)	14276 ± 518 (1.0)	2870 ± 56 (0.9)
+ *rnr1-D226V*	2096 ± 26 (1.0)	3809 ± 33 (0.9)	13770 ± 124 (1.0)	2921 ± 47 (0.9)
+ *rnr1-S117P,D226N*	2029 ± 70 (0.9)	3728 ± 281 (0.9)	13955 ± 1034 (1.0)	3047 ± 81 (0.9)
+ *rnr1-S242T*	2185 ± 14 (1.0)	3849 ± 193 (0.9)	14395 ± 462 (1.0)	2915 ± 55 (0.9)
+ *rnr1-R256H,Y779C*	2103 ± 60 (1.0)	4101 ± 88 (1.0)	13750 ± 58 (1.0)	3005 ± 41 (0.9)
+ *rnr1-G267C*	2182 ± 2 (1.0)	4068 ± 8 (1.0)	14103 ± 105 (1.0)	2828 ± 15 (0.9)
+ *rnr1-S269P*	1922 ± 35 (0.9)	4154 ± 136 (1.0)	14738 ± 1198 (1.1)	3013 ± 233 (0.9)
group 4 (interaction with *pol2-04, pol3-01* and *msh2Δ* and mutator in *EXO1*-WT)				
+ *rnr1-K243E*	2173 ± 9 (1.0)	4177 ± 114 (1.0)	14350 ± 222 (1.0)	2703 ± 18 (0.8)
+ *rnr1-I262T,M275I*	2075 ± 22 (1.0)	3905 ± 54 (0.9)	13932 ± 242 (1.0)	2843 ± 52 (0.9)
+ *rnr1-I262V,N291D*	2110 ± 15 (1.0)	4432 ± 136 (1.0)	15045 ± 131 (1.1)	2970 ± 51 (0.9)

* NTP concentrations (pmol per 10^8 cells) are the average of two biological replicates ± standard deviation with the fold increase over WT in parentheses. NTP concentrations were measured by the Chabes lab.

or >150-fold increase in the *lys2-10A* assay (the difference in the mutator thresholds takes into consideration the different linear range of the used assays)). In agreement with a function of Rnr1 downstream of NTP biosynthesis, NTP concentrations were largely unchanged in comparison to the WT (Table 4.17). All *rnr1* alleles caused altered dNTP pools (Fig. 4.16A, Table 4.18) supporting the idea that the observed phenotypes in DNA replication fidelity-compromised backgrounds were due to dNTP pool alterations. Except for one *rnr1* allele (*rnr1-F15S*) that caused overall increased dNTP levels (in average 6.5-fold over WT), all other alleles induced dNTP pool imbalances. All dNTP imbalances were characterized by elevated pyrimidine levels, relatively low dATP levels and either low or increased dGTP pools. In contrast to the dCTP/dTTP ratio, which was relatively stable (0.9-1.6 fold) between the different mutants, the *rnr1* alleles differed strongly in the dGTP/dATP ratio (0.6-13.4 fold), which was primarily a consequence of the altered dGTP levels (Table 4.18).

Table 4.18 dNTP concentrations in strains expressing *rnr1* mutant alleles on a centromeric plasmid.

	dNTP concentration (pmol per 10^8 cells)*			
Allele	**dCTP**	**dTTP**	**dATP**	**dGTP**
+ WT-*RNR1*	117 ± 17 (1.0)	260 ± 17 (1.0)	170 ± 20 (1.0)	73 ± 4 (1.0)
group 1 (no interaction or just with *pol3-01*)				
+ *rnr1-F15S*	866 ± 34 (7.4)	1439 ± 129 (5.5)	1125 ± 156 (6.6)	461 ± 31 (6.3)
+ *rnr1-I231T,T244A*	525 ± 17 (4.5)	1065 ± 78 (4.1)	287 ± 59 (1.7)	256 ± 24 (3.5)
+ *rnr1-T244I,V278A*	783 ± 12 (6.7)	1377 ± 22 (5.3)	352 ± 2 (2.1)	255 ± 7 (3.5)
+ *rnr1-T265A*	436 ± 62 (3.7)	833 ± 61 (3.2)	205 ± 0 (1.2)	164 ± 7 (2.3)
+ *rnr1-A283V,S425L*	370 ± 17 (3.2)	741 ± 61 (2.8)	314 ± 19 (1.8)	682 ± 49 (9.4)
group 2 (interaction with *pol2-04* and *pol3-01*)				
+ *rnr1-A245V*	524 ± 84 (4.5)	1005 ± 105 (3.9)	123 ± 21 (0.7)	30 ± 7 (0.4)
+ *rnr1-G271S*	711 ± 106 (6.1)	1426 ± 97 (5.5)	343 ± 59 (2.0)	101 ± 10 (1.4)
+ *rnr1-Y285C*	950 ± 76 (8.1)	1662 ± 43 (6.4)	166 ± 40 (1.0)	74 ± 4 (1.0)
group 3 (interaction with *pol2-04, pol3-01* and *msh2Δ*)				
+ *rnr1-D226G*	521 ± 43 (4.5)	896 ± 73 (3.4)	204 ± 18 (1.2)	238 ± 22 (3.3)
+ *rnr1-D226V*	565 ± 11 (4.8)	945 ± 8 (3.6)	200 ± 0 (1.2)	235 ± 8 (3.2)
+ *rnr1-S117P,D226N*	338 ± 44 (2.9)	599 ± 66 (2.3)	149 ± 4 (0.9)	169 ± 23 (2.3)
+ *rnr1-S242T*	559 ± 30 (4.8)	1033 ± 39 (4.0)	87 ± 3 (0.5)	358 ± 51 (4.9)
+ *rnr1-R256H,Y779C*	1155 ± 80 (9.9)	1771 ± 80 (6.8)	121 ± 3 (0.7)	303 ± 13 (4.2)
+ *rnr1-G267C*	548 ± 18 (4.7)	1030 ± 28 (4.0)	141 ± 7 (0.8)	583 ± 39 (8.0)
+ *rnr1-S269P*	2135 ± 273 (18.3)	3032 ± 338 (11.6)	340 ± 70 (2.0)	312 ± 2 (4.3)
group 4 (interaction with *pol2-04, pol3-01* and *msh2Δ* and mutator in *EXO1*-WT)				
+ *rnr1-K243E*	765 ± 36 (6.6)	1331 ± 76 (5.1)	259 ± 7 (1.5)	968 ± 61 (13.3)
+ *rnr1-I262T,M275I*	720 ± 50 (6.2)	1163 ± 87 (4.5)	168 ± 6 (1.0)	536 ± 86 (7.4)
+ *rnr1-I262V,N291D*	404 ± 35 (3.5)	852 ± 22 (3.3)	140 ± 14 (0.8)	780 ± 16 (10.7)

* dNTP concentrations (pmol per 10^8 cells) are the average of two biological replicates ± standard deviation with the fold increase over WT in parentheses. dNTP concentrations were measured by the Chabes lab.

To examine whether the observed genetic interactions could be correlated to the measured dNTP pools, the log2 of the dGTP/(dCTP+dTTP) ratio normalized to the WT was plotted against the relative fraction of dATP to the total dNTP pool (Fig. 4.16B). As all *rnr1* alleles, except *rnr1-F15S*, showed a relative decrease in the fraction of dATP to the total dNTP pool in comparison to the WT,

the ratio between dGTP and pyrimidines can discriminate between an equal increase and a relatively stronger increase in either dGTP or pyrimidines. Thus, alleles, which caused an equal increase in dGTP and pyrimidines were plotted on the x-axis (y = 0), whereas alleles that resulted in relatively stronger increases of dGTP or pyrimidines were plotted above (y > 0) and below (y < 0) the x-axis, respectively. Interestingly, *rnr1* alleles that interacted exclusively with the proofreading-deficient alleles (group 2, colored in blue) caused at least a 4-fold stronger increase in pyrimidines than in dGTP (y < -2). In contrast, the *rnr1* alleles that showed GD/SL in DNA proofreading and MMR-deficient backgrounds (group 3 (orange) and group 4 (red)) clustered in a region defined by less than 12% dATP of the total dNTP pool and a dGTP/pyrimidine ratio > 0.25. In comparison to group 3, group 4 mutants, that additionally caused a frameshift mutator phenotype in the presence of Exo1, showed the strongest increases in the dGTP pools. One exception is the *rnr1-G267C* allele, which was almost indistinguishable from the *rnr1-I262T,M275I* allele in terms of dNTP pool alterations, but did not caused a frameshift mutator phenotype in the presence of Exo1. This discrepancy might be explained by differences in cell cycle progression and Rnr3 dependency (Fig. 4.14B, Table 4.16).

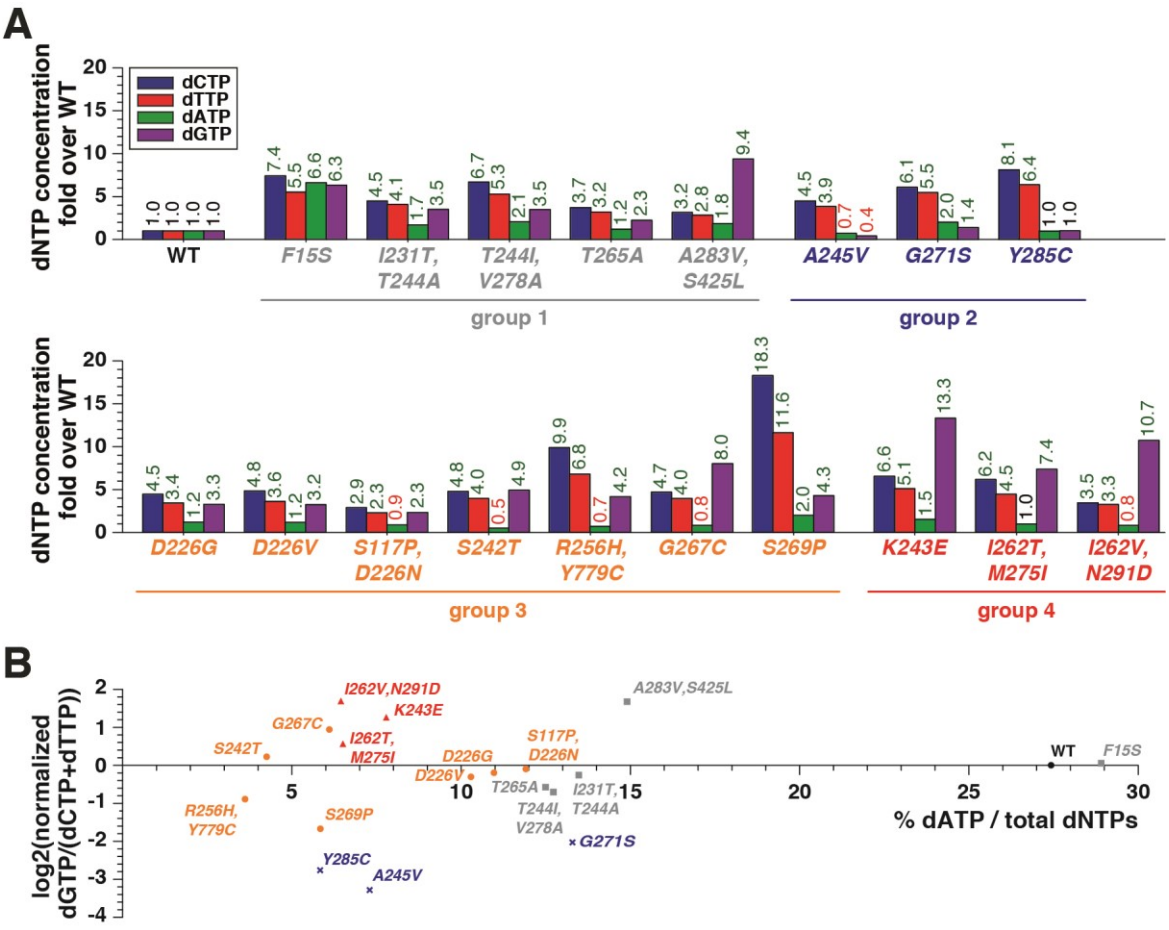

Fig. 4.16 Identified *rnr1* mutant alleles cause increased dNTP pools or dNTP pool imbalances.
(A) dNTP concentration measurement in the indicated *rnr1Δ* strains after plasmid shuffling (Table 4.18). Data is shown as fold over WT. The numbers on top represent the fold over WT. Fold increases are colored in green, whereas decreased levels are labeled red. *rnr1* alleles are grouped and color-coded according to genetic interactions (Table 4.16). (B) Graphical representation of the $\log_2$ of the ratio between dGTP and the sum of dCTP and dTTP normalized to the WT against the %dATP of the total dNTP pool. *rnr1* alleles are color-coded according to genetic interactions (Table 4.16)

Taken together, the *rnr1* alleles identified in the *RNR1* random mutagenesis screen caused four different types of dNTP pool alterations with distinct genetic interactions: First, overall increased but balanced dNTP pools (*rnr1-F15S*) did not cause any genetic interactions (part of group 1, grey). Second, a dNTP imbalance characterized by elevated pyrimidine pools and low purine pools ("low purines" or "2 out of 4") depended on DNA proofreading but not MMR for survival (group 2, blue). Third, low dATP pools and increased pyrimidine and dGTP pools ("low dATP" or "3 out 4") characterized the *rnr1* alleles that were dependent on DNA proofreading and MMR (group 3, orange). Fourth, dNTP imbalances with low dATP pools, elevated pyrimidines and strongly increased dGTP pools ("low dATP + high dGTP" or "3 out 4 + high dGTP"). These alleles were dependent on DNA proofreading and MMR for survival and conferred a mutator phenotype in the presence of Exo1 (group 4, red).

4.4.5 *rnr1* alleles expressed at the endogenous locus cause dNTP pool alteration, checkpoint activation and increased mutagenesis.

To further characterize the identified *rnr1* alleles and their dNTP pool alterations, two representative examples of each type of dNTP pool alteration were integrated at the endogenous chromosomal locus. As only one *rnr1* allele (*rnr1-F15S*) was identified in the screen that caused an overall increased dNTP pool, the previously reported *rnr1-D57N* allele, which is refractory to dATP inhibition at the A-site, resulting in overall increased dNTPs (CHABES *et al.* 2003), was included in the analysis. For the "low purine" type of dNTP imbalance the *rnr1* alleles with the lowest purine pools were selected (*rnr1-A245V* and *rnr1-Y285C*). For the "low dATP" type of dNTP imbalance the *rnr1-S242T* and *rnr1-R256H,Y779C* were chosen, representing a Rnr3-independent and -dependent allele, respectively. Finally, for the "low dATP + high dGTP" type of dNTP pool imbalance the two alleles (*rnr1-K243E* and *rnr1-I262V,N291D*) with the highest increases in dGTP were integrated at the endogenous locus. Next, mutation rates were determined in the presence and absence of Exo1 (Table 4.19). Only mild mutator phenotypes were measured in the WT background (1-4 fold increase in *CAN1* inactivation rate), except for *rnr1-K243E* and *rnr1-I262V,N291D*. The latter mutants caused 92- and 164-fold higher *CAN1* inactivation rates compared to WT, respectively. Remarkably, these high *CAN1* mutation rates are 1.5- and 2.6-fold higher than in a completely MMR-deficient *msh2Δ* strain (Table 4.19). Moreover, both *rnr1* alleles caused strong frameshift mutator phenotype in the range of a complete MMR-defect. Thus, in line with the results obtained with *rnr1* alleles expressed on centromeric plasmids (Fig. 4.13), only *rnr1-K243E* and *rnr1-I262V,N291D* caused strong mutator phenotypes in a WT background and the mutagenic potential of the other *rnr1* alleles was buffered by other DNA replication fidelity mechanisms.

In the absence of Exo1, strong increases in all three mutator assays were observed for all *rnr1* alleles except for the *rnr1-D57N* allele (Table 4.19). Even though *rnr1-F15S* and *rnr1-D57N* caused similar increases in the *CAN1* inactivation assay in the presence of Exo1 (4- and 3-fold, respectively), only *rnr1-F15S* showed synergistically increased mutation rates in combination with *exo1Δ* suggesting that the dNTP pool alteration in *rnr1-F15S* is more severe in comparison to *rnr1-D57N*. Furthermore, the *rnr1-K243E exo1Δ* double mutant could not be obtained by mating in

several attempts presumably due to the high mutational load in the double mutant or due to DNA replication-independent defects.

Table 4.19 Mutation rates caused by *rnr1* mutations integrated at the *RNR1* genomic locus in Exo1-proficient and Exo1-deficient backgrounds.

	Mutation Rate (fold increase)*		
Relevant genotype	**Can^R**	**Thr$^+$**	**Lys$^+$**
WT	8.7 [7.2-10.0] x 10^{-8} (1)	2.0 [1.1-3.0] x 10^{-9} (1)	2.1 [1.8-2.3] x 10^{-8} (1)
exo1Δ	7.4 [6.3-9.8] x 10^{-7} (9)	8.7 [6.1-15.0] x 10^{-9} (4)	1.4 [0.9-1.8] x 10^{-7} (7)
msh2Δ	5.4 [4.4-7.2] x 10^{-6} (62)	6.4 [5.2-12.9] x 10^{-6} (3200)	9.9 [8.1-10.8] x 10^{-5} (4714)
"overall increased"			
rnr1-F15S	3.5 [2.8-4.2] x 10^{-7} (4)	5.3 [4.4-7.6] x 10^{-9} (3)	2.0 [1.6-2.6] x 10^{-8} (1)
rnr1-F15S exo1Δ	5.1 [3.9-6.3] x 10^{-6} (59)	6.5 [4.0-8.9] x 10^{-7} (330)	1.9 [1.3-2.3] x 10^{-6} (93)
rnr1-D57N	2.2 [2.0-3.7] x 10^{-7} (3)	4.2 [2.5-7.5] x 10^{-9} (2)	1.6 [1.3-2.3] x 10^{-8} (1)
rnr1-D57N exo1Δ	6.5 [4.0-9.1] x 10^{-7} (7)	1.6 [1.2-1.8] x 10^{-8} (8)	4.6 [3.5-6.4] x 10^{-8} (2)
"low purines"			
rnr1-A245V	1.1 [0.8-1.4] x 10^{-7} (1)	3.1 [2.1-4.2] x 10^{-8} (16)	3.8 [2.2-5.3] x 10^{-8} (2)
rnr1-A245V exo1Δ	2.0 [1.1-3.7] x 10^{-6} (22)	1.1 [0.6-2.1] x 10^{-5} (5405)	1.3 [0.8-3.1] x 10^{-5} (634)
rnr1-Y285C	3.2 [1.8-5.1] x 10^{-7} (4)	4.8 [3.7-8.7] x 10^{-8} (24)	1.6 [0.9-2.0] x 10^{-7} (8)
rnr1-Y285C exo1Δ	1.6 [1.1-3.2] x 10^{-5} (184)	4.6 [3.0-7.8] x 10^{-5} (23037)	1.9 [1.6-5.5] x 10^{-4} (9139)
"low dATP"			
rnr1-S242T	2.6 [2.0-5.1] x 10^{-7} (3)	1.6 [1.1-3.1] x 10^{-8} (8)	1.3 [0.8-2.7] x 10^{-7} (6)
rnr1-S242T exo1Δ	2.4 [1.9-4.0] x 10^{-5} (273)	9.4 [5.8-18.5] x 10^{-6} (4743)	1.7 [1.3-3.0] x 10^{-4} (8017)
rnr1-R256H,Y779C	9.5 [7.1-16.0] x 10^{-8} (1)	2.6 [1.4-4.0] x 10^{-8} (13)	9.2 [7.2-11.6] x 10^{-8} (4)
rnr1-R256H,Y779C exo1Δ	2.2 [1.5-3.3] x 10^{-6} (25)	3.2 [2.1-3.2] x 10^{-6} (1619)	7.3 [5.4-8.8] x 10^{-6} (351)
"low dATP + high dGTP"			
rnr1-K243E†	8.1 [4.4-11.3] x 10^{-6} (92)	1.5 [1.1-2.4] x 10^{-5} (7362)	2.7 [2.0-4.6] x 10^{-5} (1319)
rnr1-I262V,N291D	1.4 [0.9-2.4] x 10^{-5} (164)	5.4 [3.8-8.3] x 10^{-6} (2731)	6.7 [4.5-10.8] x 10^{-5} (3216)
rnr1-I262V,N291D exo1Δ	4.3 [3.1-7.1] x 10^{-5} (489)	1.9 [0.7-3.0] x 10^{-5} (9366)	2.1 [0.9-3.4] x 10^{-4} (10103)

* Median rates of inactivation of *CAN1* gene (Can^R) and *hom3-10* (Thr$^+$) and *lys2-10A* (Lys$^+$) frameshift reversion, with 95% confidence interval in square brackets and fold increase relative to WT strain in parentheses. Strains with partial or total loss of mismatch repair activity (*exo1Δ* and *msh2Δ,* respectively) were included as reference.
† The *rnr1-K243E exo1Δ* strain could not be obtained by mating.

Next, NTP and dNTP concentrations of the *rnr1* mutant alleles integrated at the endogenous *RNR1* locus were measured by HPLC (Table 4.20). NTP levels were indistinguishable from WT levels (Table 4.20A). The dNTP concentration of *rnr1* mutant alleles integrated at the endogenous *RNR1* locus (Fig. 4.17A, Table 4.20B) were in agreement with the dNTP concentrations measured in cells expressing *rnr1* alleles on a centromeric plasmid (Table 4.18). Minor changes might be based on the difference between the expression from the endogenous chromosomal locus and from a low copy number plasmid. In line with the literature report (CHABES *et al.* 2003), the *rnr1-D57N* allele showed an overall increase in dNTP pools (in average 3.6-fold over WT), but the increase was approximately 50% weaker than in *rnr1-F15S* suggesting indeed that the lack of interaction with *exo1Δ* is due to the less severe dNTP pool alteration.

In some of the *rnr1* mutants, like *rnr1-A245V* and *rnr1-R256H,Y779C*, dNTP pools below the WT levels were found (Figure 4.17A, Table 4.20B). To evaluate the cell cycle and DDR activation, the

DNA content and induction of RNR subunits were analyzed in logarithmically growing cells. DNA content analysis by flow cytometry revealed that overall increased dNTP pools did not severely alter the cell cycle, whereas reductions of 30% and more in one individual dNTP pool resulted in an accumulation of cells in S phase (Fig. 4-17A,B). Furthermore, cells with a "low dATP and high dGTP" type of dNTP imbalance did not accumulate in S phase, but nevertheless showed an altered cell cycle distribution and an accumulation of cells in G2 phase (Fig. 4.17B).

Table 4.20 NTP and dNTP concentrations in strains containing *rnr1* mutant alleles integrated at the endogenous *RNR1* locus

A

Relevant genotype	CTP	UTP	ATP	GTP
WT	2195 ± 18 (1.0)	5449 ± 93 (1.0)	11386 ± 363 (1.0)	3473 ± 10 (1.0)
"overall increased"				
rnr1-F15S	2110 ± 103 (1.0)	5411 ± 111 (1.0)	11773 ± 169 (1.0)	3519 ± 42 (1.0)
rnr1-D57N	2167 ± 12 (1.0)	5376 ± 212 (1.0)	11754 ± 178 (1.0)	3455 ± 64 (1.0)
"low purines"				
rnr1-A245V	1997 ± 33 (0.9)	5384 ± 152 (1.0)	11725 ± 165 (1.0)	3730 ± 4 (1.1)
rnr1-Y285C	2004 ± 34 (0.9)	5322 ± 84 (1.0)	11916 ± 77 (1.0)	3702 ± 132 (1.1)
"low dATP"				
rnr1-S242T	2125 ± 14 (1.0)	5804 ± 62 (1.1)	11751 ± 96 (1.0)	3246 ± 47 (0.9)
rnr1-R256H, Y779C	2325 ± 22 (1.1)	5094 ± 124 (0.9)	11370 ± 251 (1.0)	3468 ± 30 (1.0)
"low dATP + high dGTP"				
rnr1-K243E	2283 ± 6 (1.0)	5312 ± 803 (1.0)	12946 ± 1484 (1.1)	2953 ± 85 (0.9)
rnr1-I262V,N291D	1907 ± 435 (0.9)	5039 ± 333 (0.9)	14892 ± 12222 (1.3)	3152 ± 118 (0.9)

B

Relevant genotype	dCTP	dTTP	dATP	dGTP
WT	146 ± 18 (1.0)	292 ± 27 (1.0)	158 ± 17 (1.0)	80 ± 7 (1.0)
"overall increased"				
rnr1-F15S	972 ± 99 (6.7)	1672 ± 116 (5.7)	1151 ± 145 (7.3)	522 ± 58 (6.6)
rnr1-D57N	521 ± 181 (3.6)	984 ± 250 (3.4)	640 ± 236 (4.0)	294 ± 99 (3.7)
"low purines"				
rnr1-A245V	1057 ± 71 (7.2)	1712 ± 130 (5.9)	69 ± 2 (0.4)	54 ± 4 (0.7)
rnr1-Y285C	1304 ± 48 (8.9)	2226 ± 62 (7.6)	139 ± 2 (0.9)	114 ± 2 (1.4)
"low dATP"				
rnr1-S242T	935 ± 44 (6.4)	1596 ± 66 (5.5)	133 ± 14 (0.8)	762 ± 45 (9.6)
rnr1-R256H, Y779C	481 ± 20 (3.3)	784 ± 16 (2.7)	80 ± 3 (0.5)	221 ± 3 (2.8)
"low dATP + high dGTP"				
rnr1-K243E	1796 ± 123 (12.3)	2891 ± 292 (9.9)	536 ± 7 (3.4)	1656 ± 28 (20.8)
rnr1-I262V,N291D	404 ± 88 (2.8)	869 ± 10 (3.0)	190 ± 1 (1.2)	1365 ± 290 (17.1)

NTP (A) and dNTP (B) concentrations (pmol per 10^8 cells) are the average of two biological replicates ± standard deviation with the fold increase over WT in parentheses. NTP and dNTP concentrations were measured by the Chabes lab.

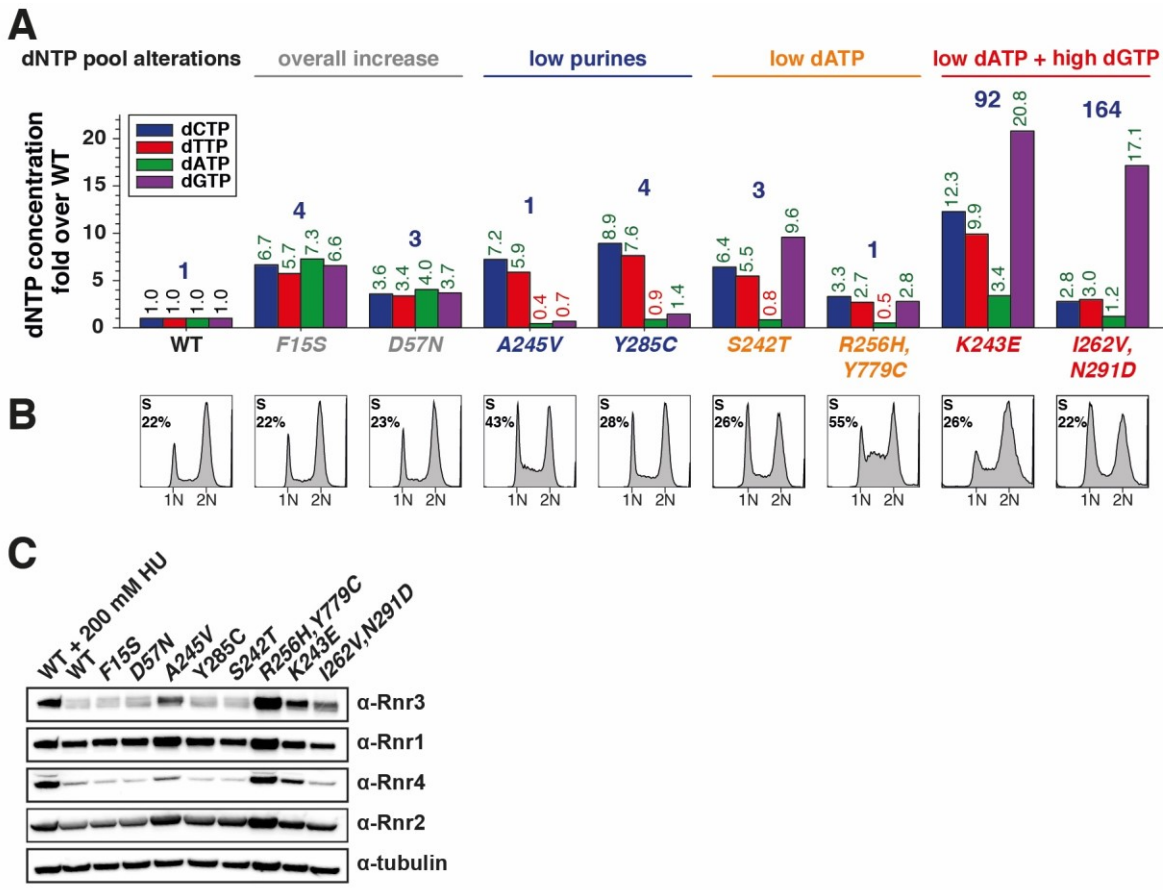

Fig. 4.17 *rnr1* mutant alleles expressed at the endogenous chromosomal locus cause dNTP pool alterations and DNA damage checkpoint activation.
(A) dNTP concentration measurement in the indicated strains (Table 4.20B). Data is shown as fold over WT. The numbers on top of each bar represent the fold over WT. Fold increases are colored in green, whereas decreased levels are labeled red. The blue number represents the fold over WT in the *CAN1* mutation rate measured in the rnr1 WT-*EXO1* strains (Table 4.19). *rnr1* alleles are grouped and color-coded according to genetic interactions, type of dNTP pool alteration and mutator phenotype (Table 4.16). (B) DNA content profiles of logarithmically growing strains of the indicated genotypes in A. Cells in S phase were approximated using FlowJo's cell cycle plugin. (C) Whole cell lysates of logarithmically growing indicated strains were analyzed by SDS-PAGE and immunoblotting against Rnr1-4 and tubulin. As positive control for the activation of the DNA damage response, WT cells treated for 3 h with 200 mM HU were used.

In agreement with the strongest accumulation of cells in S phase, the highest RNR subunit expression levels were found in *rnr1-R256H,Y779C* and though to a lesser extend in *rnr1-A245V* expressing cells (Fig. 4.17C). No RNR induction was observed for cells expressing the *rnr1-F15S*, *rnr1-D57N*, *rnr1-S242T* or *rnr1-Y285C* alleles. All of them had in common that no individual dNTP was reduced more than 20% compared to WT levels (Fig. 4.17A) and no strong accumulation of cells in S phase was observed (Fig. 4.17B). Interestingly, the *rnr1-K243E* expressing cells activated the DDR (Fig. 4.17C) showing neither dNTP levels below the WT (Fig. 4.17A, Table 4.20B) nor strong accumulation of cells in S phase (Fig. 4.17B). Moreover, *rnr1-I262V,N291D* belonging to the same type of dNTP imbalance with low dATP and very high dGTP pools, slightly induced Rnr3, but not Rnr1, Rnr2 or Rnr4. Thus, the altered DNA content profiles and the DDR activation in these mutants might suggest that the very high dGTP pools in these mutants interfere with processes outside S phase.

Taken together, the analysis of *rnr1* alleles expressed from the endogenous *RNR1* locus revealed first, that dNTP imbalances characterized by low dATP and high dGTP (3 out of 4 + high dGTP) were the most mutagenic dNTP imbalances resulting in very high mutation rates even in the presence of high-fidelity DNA polymerases and functional MMR and second, that limitation in one individual dNTP pool of at least 30% activated the DDR.

4.4.6 Elevation of "3 out of 4" dNTPs promotes base pair mutations and frameshifts.

To examine whether the three different types of dNTP imbalances influence the type of replication error generated, *CAN1* mutation spectra analysis in WT, *rnr1-Y285C*, *rnr1-R256H,Y779C* and *rnr1-I262V,N291D* strains was performed (Fig. 4.18A, Table 4.21). All *rnr1* mutation spectra were significantly different to the WT (Fisher's exact test, p value 2.5×10^{-11} for *rnr1-Y285C*, 0.0029 for *rnr1-R256,Y779C* and $<2.2 \times 10^{-16}$ for *rnr1-I262V,N291D*).

Table 4.21 *CAN1* mutation spectra in strains carrying *rnr1* mutant alleles.

	WT‡	***rnr1-Y285C***	***rnr1-R256H,Y779C***	***rnr1-I262V,N291D***
Mutants sequenced	91	93	96	96
Mutations total*	92 (100)	94 (100)	96 (100)	98 (100)
Base substitutions	69 (75.0)	80 (85.1)	55 (57.3)	18 (18.4)
A-T → G-C	6 (6.5)	14 (14.9)	9 (9.4)	13 (13.3)
G-C → A-T	18 (19.6)	9 (9.6)	17 (17.7)	2 (2.0)
G-C → T-A	29 (31.5)	5 (5.3)	6 (6.3)	0 (0.0)
A-T → C-G	3 (3.3)	20 (21.3)	6 (6.3)	1 (1.0)
A-T → T-A	7 (7.6)	28 (29.3)	6 (6.3)	2 (2.0)
C-G → G-C	6 (6.5)	4 (4.3)	11 (11.5)	0 (0.0)
Transitions	24 (26.1)	23 (24.5)	26 (27.1)	15 (15.3)
Transversions	45 (48.9)	57 (60.6)	29 (30.2)	3 (3.1)
One-base-pair frameshifts	15 (16.3)	12 (12.8)	30 (31.3)	80 (81.6)
ΔA/T	5 (5.4)	9 (9.6)	25 (26.0)	79 (80.6)
ΔG/C	3 (3.3)	3 (3.2)	4 (4.2)	0 (0.0)
+A/T	6 (6.5)	0 (0.0)	1 (1.0)	1 (1.0)
+G/C	1 (1.1)	0 (0.0)	0 (0.0)	0 (0.0)
Complex†	8 (8.7)	2 (2.1)	11 (11.5)	0 (0.0)

Mutation spectra analysis based on DNA sequencing of the *CAN1* gene in independent Can^R mutants, shown as the number of clones containing the indicated mutations, and in parenthesis as the percentage relative to the total. (Fig. S7.1 and Fig. S7.12-14)

*In few cases (about 1-2% of the sequenced clones) two simultaneous *CAN1* mutations (more than 100 bp apart) were found. These mutations were included in the analysis and considered as independent mutational events.

† includes: multiple mutations within ten nucleotides, insertions or deletions of more than one nucleotide and duplication events.

‡*CAN1* mutation spectrum of WT strain was taken from (SCHMIDT *et al.* 2017).

In the *rnr1-Y285C* mutant with low purine and elevated pyrimidine pools increased base pair substitutions were detected in comparison to the WT (85.1% vs. 75.0%). The *CAN1* spectrum was dominated by A-T to C-G and A-T to T-A mutations, which were 6.5 and 3.9 times more frequently found than in WT and approximately detected in half of all sequenced Can^R clones (10.9% in WT). Hotspots at position 538, 680 and 946 were frequently mutated in *rnr1-Y285C* (Table 4.22). For

example, hotspot 538 is presumably driven by low levels of dATP and increased dCTP pools, which result in a dATP/dCTP ratio of 1:9 (1:0.9 in WT) supporting the misincorporation of dCTP opposite of the template T. The elevated dCTP and dTTP levels present in *rnr1-Y285C* facilitate rapid mispair extension over proofreading (Fig. 4.18B).

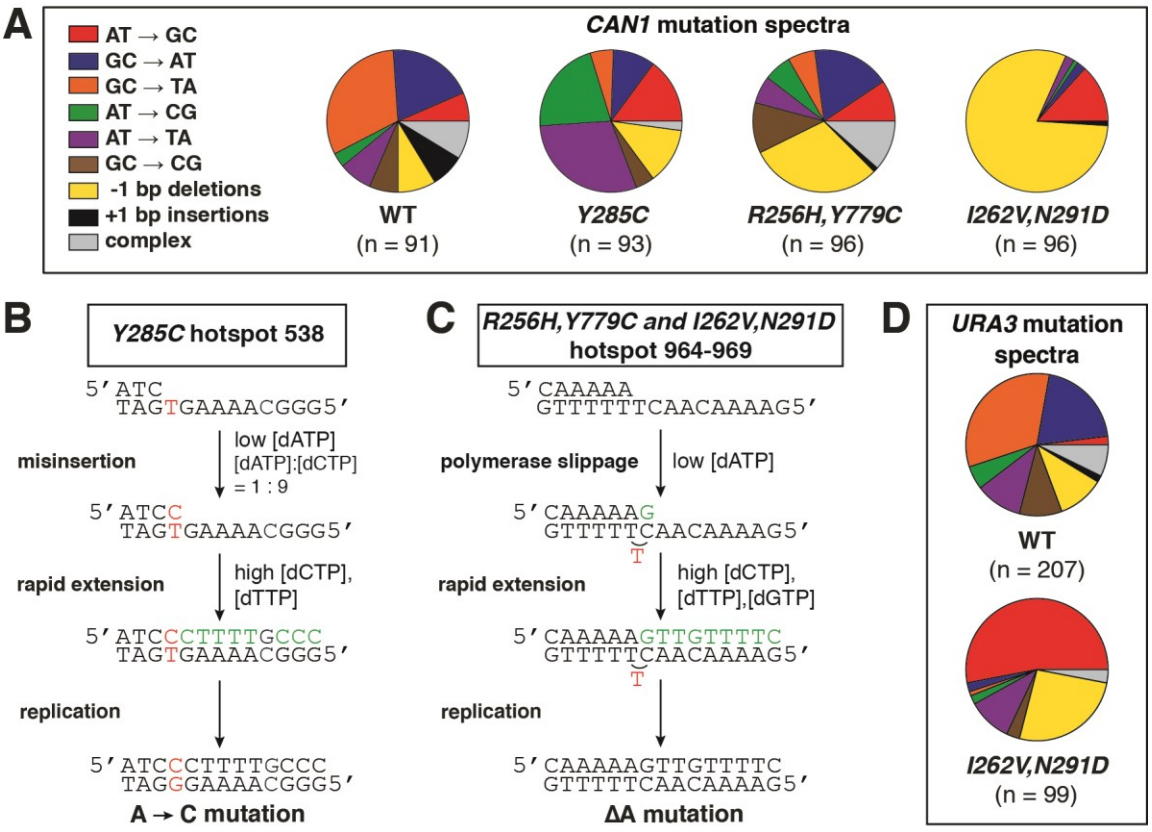

Fig. 4.18 dNTP imbalances caused by *rnr1* mutants shape mutation spectra.
(A) Independent Can^R clones (n ≥ 91 per genotype) were sequenced for *CAN1* mutations. The graphs represent the type of the identified mutations in percentage (Table 4.21). (B) The A-to-C mutation hotspot at nucleotide 538 identified in *rnr1-Y285C*. Predicted mutation is noted in red. Nucleotides marked in green are more abundant in *rnr1-Y285C* than in the WT and facilitate rapid extension of the mispair. (C) The ΔA mutation at nucleotide 964-969 was frequently identified in *rnr1-I262V,N291D*. Predicted slippage event is noted in red. Nucleotides marked in green are more abundant in *rnr1-I262V,N291D* than in the WT and facilitate rapid extension of the mismatch. (D) Independent 5-FOA^R clones (n ≥ 99 per genotype) were sequenced for *URA3* mutations. The graphs represent the type of the identified mutations in percentage (Table 4.23). WT mutational spectrum was taken from (LANG AND MURRAY 2008).

The *CAN1* mutation spectra in *rnr1-R256H,Y799C* and *rnr1-I262V,N291D* strains one-base-pair frameshifts were 3.5 and 9.3 times more frequently detected than in the WT and consisted in large of A:T deletion events (Table 4.21). Moreover, the only hotspots identified in those two mutants were in two 6 A:T mononucleotide runs at position 964-969 and 1381-1386, the latter only identified in *rnr1-R256H,Y779C* (Table 4.22). The ΔA mutation hotspot at position 964-969 is presumably facilitated by low dATP pools in *rnr1-R256H,Y779C* and *rnr1-I262V,N291D*, which favor polymerase slippage events in the mononucleotide run of 6 A, followed by insertion of a dGTP directly after the mononucleotide run, strand misalignment and rapid extension due to elevated dCTP, dTTP and dGTP levels (Fig. 4.18C). Remarkably, the mutational hotspot at position 964-969 was detected in about 2/3 of all sequenced *rnr1-I262V,N291D* clones, suggesting that under the dNTP imbalance present in *rnr1-I262V,N291D* DNA polymerases are especially error-prone at this

sequence context. Even though base substitution events contributed only 18.4% to all observed Can^R events in *rnr1-I262V,N291D*, 72% of the base pair substitutions were A-T to G-C mutations presumably as consequence of the increased dGTP:dATP ratio (7:1 in *rnr1-I262V,N291D* to 0.5:1 in WT). To investigate the effect of the "low dATP + high dGTP" dNTP imbalance on the generation of replication errors in more detail the *URA3* gene of individual 5-FOA resistant *rnr1-I262V,N291D* clones was sequenced and the *URA3* mutation spectra was analyzed (Table 4.23). As already observed in the *CAN1* mutations spectrum, base pair substitutions in the *rnr1-I262V,N291D URA3* mutation spectrum were dominated by A-T to G-C mutations (53% of all observed mutations and 75% of all base pair substitutions). In comparison to the WT (LANG AND MURRAY 2008), the *rnr1-I262V,N291D URA3* mutation spectrum was significantly different (Fisher's exact test, p value $< 2.2 \times 10^{-16}$) and A-T to G-C mutations were detected 28 times more frequent in *rnr1-I262V,N291D*. Remarkably, also in the *URA3* mutation spectrum one-base-pair deletions and ΔA/T frameshifts were found 2.5 and 4.7 times more frequent in *rnr1-I262V,N291D* than in WT. Thus, the "low dATP + high dGTP" type of dNTP imbalance facilitates not only base pair substitutions, but also one-base-pair deletions independently of the used mutational reporter.

Table 4.22 *CAN1* mutation hotspots identified in strains carrying *rnr1* mutant alleles.

Position	Mutation	No of occurrences / total	Mutation rate (x10^{-8})	Fold increase over WT	Predicted intermediate
rnr1-Y285C: 8.9 x dCTP, 7.6 x dTTP, 0.9 x dATP, 1.4 dGTP; CAN^R = 3.2 x 10^{-7} (4)					
538	A → C	10 / 94	3.4	≥36	5′ ATCCCTTTTTGCCC TAGTGAAAACGGG 5′
680	A → T	10 / 94	3.4	≥36	5′ TCGTGTTCTGGGT AGCTCAAGACCCA 5′
946	T → C	5 / 94	1.7	≥18	5′ CCCAGAAAATCCG GGGTCTTTTTGGGC 5′
rnr1-R256H,Y779C: 3.3 x dCTP, 2.7 x dTTP, 0.5 x dATP, 2.8 dGTP; CAN^R = 9.5 x 10^{-8} (1)					
964-969	ΔA	6 / 96	0.6	6	5′ CAAAAAGTTGTTTTTC GTTTTTCAACAAAAG 5′ T
1381-1386	ΔT	9 / 96	0.9	9	T 5′ GTTGCAGGCTTTTTG CAACGTCCGAAAAAC 5′
rnr1-I262V,N291D: 2.8 x dCTP, 3.0 x dTTP, 1.2 x dATP, 17.1 dGTP; CAN^R = 1.4 x 10^{-5} (164)					
964-969	ΔA	63 / 98	900	9517	5′ CAAAAAGTTGTTTTTC GTTTTTCAACAAAAG 5′ T

Mutations are shown relative to the coding strand. The predicted mutation is noted in red. Nucleotides incorporated after the mutation from dNTPs at higher concentrations than WT, are shown in green. dNTP levels are shown as fold over WT and *CAN1* inactivation rate as median, with fold increase relative to WT in parentheses. A mutation hotspot is defined as a specific mutation found in more than 5% of all sequenced CAN^R clones in the indicated genotype. Mutation hotspots that are significant different to the WT control (Fisher's exact test, Benjamini and Hochberg corrected p-value ≤ 0.05) are shown in bold.

Taken together, mutation spectra analysis of *rnr1* alleles revealed that distinct dNTP pool imbalances shape the mutation spectra in agreement with the observed genetic interactions (Table 4.16). The "low purines" type of dNTP pool imbalances generated primarily base pair substitutions (Table 4.21) and exclusively relied on DNA proofreading, but not on MMR for survival (Table 4.16). In contrast, "low dATP" and "low dATP + high dGTP" type of dNTP pool imbalances favored base

pair substitutions and one-base-pair deletions (Table 4.21 and 4.23). Consequently, these types of dNTP pool imbalances relied on DNA proofreading and MMR for survival (Table 4.16).

Table 4.23 *URA3* mutation spectrum in *rnr1-I262V,N291D* mutant strain.

	WT‡	***rnr1-I262V,N291D***
Mutants sequenced	207	131
Mutations total*	207 (100)	100 (100)
Base substitutions	167 (80.7)	71 (71.0)
A-T → G-C	4 (1.9)	53 (53.0)
G-C → A-T	42 (20.3)	2 (2.0)
G-C → T-A	68 (32.9)	1 (1.0)
A-T → C-G	11 (5.3)	2 (2.0)
A-T → T-A	22 (10.6)	10 (10.0)
C-G → G-C	20 (9.7)	3 (3.0)
Transitions	46 (22.2)	55 (55.0)
Transversions	121 (58.5)	16 (16.0)
One-base-pair frameshifts	25 (12.1)	26 (26.0)
ΔA/T	11 (5.3)	25 (25.0)
ΔG/C	11 (5.3)	1 (1.0)
+A/T	2 (1.0)	0 (0.0)
+G/C	1 (0.5)	0 (0.0)
Complex†	15 (7.2)	3 (3.0)

Mutation spectra analysis based on DNA sequencing of the *URA3* gene independent 5-FOA^R mutants, shown as the number of clones containing the indicated mutations, and in parenthesis as relative percentage (Fig. S7.15).
*In few cases (about 1-2% of the sequenced clones) two simultaneous *URA3* mutations (more than 100 bp apart) were found. These mutations were included in the analysis and were considered as independent mutational events.
† includes: multiple mutations within ten nucleotides, insertions or deletions of more than one nucleotide and duplication events.
‡ *URA3* mutation spectrum of WT strain was taken from (LANG AND MURRAY 2008).

5 DISCUSSION

5 DISCUSSION

5.1 A genome-wide screen identifies genes that prevent the accumulation of mutations.

Genome-wide screens in *S. cerevisiae* are powerful tools to uncover genetic interactions as well as to investigate phenotypes on a genome-wide level. Here, the yeast non-essential gene deletion collection was screened in a "semi-high-throughput" 96-well format for increased mutagenesis using the *CAN1* forward inactivation assay and the frameshift-specific *lys2-10A* reporter. The screen was performed in a WT background as well as in the presence of low-fidelity active-site mutants (*pol1-L866M*, *pol2-M644G*, *pol3-L612M*) of the three major eukaryotic DNA polymerases (Fig. 4.1). In the WT background, 39 single-gene deletions were identified that caused increased mutator phenotypes (Table 4.1). With the exception of *MET7*, all other identified genes have known roles in DNA replication and repair and have been previously linked to increased mutagenesis. In comparison to a previous screen scoring for increased *CAN1* inactivation in a WT background (HUANG *et al.* 2003), only two of the reported genes (*SOD1* and *SKN7*) were not identified in the here presented screen, whereas both screens share 28 genes. Moreover, the here performed screen unraveled 11 additional genes that have not been identified in the first screen (HUANG *et al.* 2003). However, with the exception of *MET7*, all other gene deletions were previously linked to increased mutagenesis (TISHKOFF *et al.* 1997; BERTRAND *et al.* 1998; FLORES-ROZAS AND KOLODNER 1998; SCOTT *et al.* 1999; BRUSKY *et al.* 2000; HOWLETT AND SCHIESTL 2004; SMITH *et al.* 2004; COLLURA *et al.* 2012). By making use of the *lys2-10A* frameshift reversion assay all known MMR components, except of *mlh2Δ* that shows a mutator phenotype almost indistinguishable from WT (HARFE *et al.* 2000; CAMPBELL *et al.* 2014), were identified. Consistent with a previous report (HUANG *et al.* 2003), inactivation of *ELG1*, that promotes the unloading of PCNA (KUBOTA *et al.* 2013), also caused increased frameshift mutations most likely by affecting PCNA levels on chromatin. Thus, these findings suggest that the here performed screen not only in large recapitulated previous results obtained by different genome-wide screens (HUANG *et al.* 2003; SMITH *et al.* 2004) and other studies (TISHKOFF *et al.* 1997; BERTRAND *et al.* 1998; FLORES-ROZAS AND KOLODNER 1998; SCOTT *et al.* 1999; BRUSKY *et al.* 2000; HOWLETT AND SCHIESTL 2004; COLLURA *et al.* 2012) but also was sensitive enough to identify one previously unrecognized gene (*MET7*). A potential explanation why *MET7* has not been identified in previous screens may lay in the severe growth defect characteristic of *met7Δ* strains (DESOUZA *et al.* 2000). Thus, the identification of *MET7* in this screen suggest that in the subset of genes present in the yeast non-essential gene deletion collection used, no additional unrecognized gene deletions may exist that confer a *CAN1* and/or *lys2-10A* mutator phenotype in a WT background. Nevertheless, it cannot be excluded that additional genes may exist that prevent the accumulation of mutations due to the following reasons: First, some gene deletions may cause similar to *met7Δ* severe growth defects (MERZ AND WESTERMANN 2009). The initial qualitative mutator phenotype screening depends on growth so that mutants may not be detected due to severely compromised growth. Second, some gene deletions have reported defects in mating and sporulation (DEUTSCHBAUER *et al.* 2002; ENYENIHI AND SAUNDERS 2003), so that their mutator phenotype cannot be investigated because the

finally tested strains cannot be generated by the SGA protocol. Third, approximately 8.5% of the non-essential genes have a homologue in the yeast genome (GIAEVER *et al.* 2002) and this homologue may compensate the defect of the gene deletion. Fourth, the used collection may lack the gene deletion. The budding yeast genome consists of approximately 6131 genes of which 4803 are inactivated in the BY4742 non-essential gene deletion collection (GIAEVER *et al.* 2002). During the construction of the collection the deletion of roughly 215 genes failed and consequently these genes are not part of the deletion collection (GIAEVER *et al.* 2002). To screen a more comprehensive collection, 65 of those genes were manually inactivated by the Hombauer lab and included in the screen. Fifth, as part of this screen, only non-essential gene deletions were investigated, remaining essential genes excluded from the analysis. Indeed, a screen that tested 813 mutant alleles of 525 essential genes revealed 47 alleles in 38 essential genes that conferred increased *CAN1* inactivation (STIRLING *et al.* 2014) highlighting that both non-essential and essential genes prevent genome instability. As a frameshift mutational reporter has not been used systematically in the subset of essential genes it might be informative to screen alleles of essential genes (temperature sensitive-, DAmP- or Tet-OFF-collections)(MNAIMNEH *et al.* 2004; BEN-AROYA *et al.* 2008; BRESLOW *et al.* 2008) for increased frameshift mutator phenotypes. Sixth, some gene deletions may cause increased mutator phenotypes but are not supporting growth on canavanine containing mutator plates or plates lacking lysine and are therefore not found in this screen. For example, Can^R mutants require a functional arginine biosynthesis pathway to grow on canavanine containing mutator plates, which lack arginine. Similarly, *lys2-10A* mutator plates lack lysine and cells that require external lysine supplementation will not grow even in the presence of a reverted *lys2-10A* allele. One example for this is *CCS1* (previously called *LYS7* (CULOTTA *et al.* 1997)), a copper chaperone for *SOD1* playing a role in the oxidative stress response (LAMB *et al.* 2000). In the absence of *CCS1* and in the presence of oxygen, cells require lysine and methionine for growth (CULOTTA *et al.* 1997). Inactivation of *CCS1* results in an increased *CAN1* mutator phenotype (Table 4.1) (HUANG *et al.* 2003) and a mildly increased frameshift reversion rate (3-fold increase over WT in *hom3-10* frameshift reversion rate (HUANG *et al.* 2003)). However, as *ccs1Δ* cells require lysine in the presence of oxygen, no conclusion about the *lys2-10A* frameshift mutator phenotype in this mutant can be made under standard growth conditions. Consequently, *CCS1* was not found in the screen as a gene that suppresses frameshift mutations. To avoid these potential restrictions for the frameshift assay, initially the SGA generated mutants should be tested for increased frameshift mutations not only in the *lys2-10A* but also in the *hom3-10* frameshift reversion assay. For this, a *HIS3* cassette was integrated downstream of the *hom3-10* reporter in all four SGA query strains. However, as a subset of the non-essential gene deletion collection was *HIS3* and not *his3Δ1*, the *HIS3* selection marker could not be used to follow the *hom3-10* reporter. Consequently, the mutator phenotype of the SGA generated mutants were exclusively evaluated based on the *lys2-10A* and the *CAN1* reporter. Thus, to complement the here performed screen in the subset of non-essential genes, a second screen using the *hom3-10* frameshift reversion assay and the *URA3* forward inactivation assay that scores for 5-FOA resistant events (BOEKE *et al.* 1984) could be performed. However, it is questionable whether additional previously unrecognized genes that suppress mutations might be identified in a WT background using these two alternative

mutator assays. Due to the shorter mononucleotide run in the *hom3-10* reporter, the *hom3-10* frameshift reversion rate in a WT strain is approximately 7-fold lower than the *lys2-10A* frameshift reversion rate (Table 4.7). Therefore, to be detected as mutator in a qualitative *hom3-10* mutator screening, mutants have to confer a relatively strong frameshift mutator phenotype. This makes it in comparison to the *lys2-10A* assay less likely to identify weak mutators with the *hom3-10* assay. All in all, it is therefore unlikely that within the used non-essential gene deletion collection additional single gene deletions exist that cause base pair substitutions and frameshift mutations in a WT background.

An additional approach to screening in a WT background is to use DNA replication fidelity-compromised backgrounds as "sensitized mutator backgrounds". In the here described genome-wide screen low-fidelity active-site mutants of the three major DNA polymerases were successfully used as "sensitized mutator backgrounds" to identify gene deletions (*gln3Δ*, *rrm3Δ*, *shm2Δ* and *ura7Δ*) that showed strong synergistic mutator interactions with some of the DNA polymerase alleles (Table 4.5) (discussed in section 5.3). Importantly, inactivation of none of the four genes conferred a mutator phenotype in the presence of high-fidelity DNA polymerases suggesting that the defects are buffered under WT conditions by DNA polymerases and MMR (Table 4.5). Thus, screening in different DNA replication fidelity-compromised backgrounds may reveal additional mutational enhancers and improve the understanding of this second layer of genome stability genes, which become critically important for genome stability when DNA replication fidelity is compromised.

5.2 The folylpolyglutamate synthetase Met7 suppresses dUTP accumulation and genome instability.

5.2.1 Genomic uracil is a prerequisite, but not sufficient to cause GCRs in *S. cerevisiae*.

The genome-wide screen performed in the WT background identified Met7 as a suppressor of mutations according to the *CAN1* inactivation assay (Table 4.2). Furthermore, the absence of Met7 not only resulted in increased *CAN1* inactivation, but also in elevated GCRs (Table 4.2). Thus, this work showed that the yeast folylpolyglutamate synthetase (FPGS) Met7 is an integral part of the cellular genome stability network and characterized how Met7 suppresses mutation and GCRs. Moreover, this study highlights how metabolic defects due to the absence of Met7 cause a complex genome instability phenotype characterized by increased mutations and GCRs as well as short telomeres (Fig. 5.1). Met7 catalyzes the polyglutamylation of folates in budding yeast (DESOUZA *et al.* 2000) which increases the cellular retention of folates and their affinity to folate-metabolizing enzymes (SCHIRCH AND STRONG 1989). Consequently, in the absence of FPGS intracellular folate pools are depleted (MCBURNEY AND WHITMORE 1974; RAZ *et al.* 2016). Folates serve as cofactors in different metabolic pathways including dTMP, purine and methionine biosynthesis (APPLING 1991; DUCKER AND RABINOWITZ 2017). In agreement with a previous study (RUBINSTEIN *et al.* 2014), inactivation of *MET7* caused a dNTP imbalance that is characterized by low dTTP and dGTP pools and elevated dCTP and dATP pools (Fig. 4.5A, Table 4.3B). Given that dNTP levels peak during S phase (CHABES *et al.* 2003) and *met7Δ* cells showed in comparison to the WT an accumulation of cells in S phase (Fig. 4.3B)(KOREN *et al.* 2010), dNTP pools measured in *met7Δ* cells are

approximately 2-3-fold overrepresented. This suggests that normalized to a WT cell cycle distribution, the dTTP and dGTP pool reductions would be even more severe in *met7Δ* cells. Thus, cells lacking Met7 present a severe dNTP imbalance with strongly reduced dTTP and dGTP pools. Remarkably, dNTP pool measurements in mammalian cells treated with either the antifolate methotrexate or the antimetabolites 5-fluorouracil or 5-fluorodeoxyuridine (the latter two both targeting thymidylate synthase), revealed very similar dNTP pool imbalances as Met7-deficient yeast cells. In the presence of these drugs, dTTP and dGTP pools were strongly reduced, dATP pools were elevated and dCTP pools were either stable or increased (TATTERSALL AND HARRAP 1973; RITTER *et al.* 1980; YOSHIOKA *et al.* 1987). Thus, these measurements suggest that the dNTP pool alteration observed in the absence of Met7 is likely a consequence of folate deficiency. Due to the absence of folate polyglutamylation in *met7Δ* cells, folate pools are depleted. Consequently, dTMP biosynthesis, as one major folate requiring metabolic pathway (FOX AND STOVER 2008), is reduced resulting in low dTTP levels. Interestingly, binding of dTTP to the allosteric S-site in RNR primes RNR's C-site for reduction of GDP to dGDP (BROWN AND REICHARD 1969), suggesting that the low dGTP concentrations in the absence of Met7 or upon antifolate treatment might be a consequence of low dTTP levels that may not be sufficient to trigger dGDP production. This idea is further supported by dNTP pool measurements in fission yeast cells deficient for the dCMP deaminase *DCD1* (SANCHEZ *et al.* 2012). In agreement with converting dCMP to dUMP, which is further metabolized to dTTP (Fig. 1.6), dCTP pools were 30-fold increased and dTTP pools were 4-fold decreased in the absence of Dcd1. Moreover, dGTP pools were decreased ~2-fold and dATP levels were 2.5-fold increased suggesting that the decrease in dGTP and presumably also the increase in dATP is a general consequence of reduced dTTP levels.

Inhibition of dTMP biosynthesis not only results in reduced dTTP pools and a dNTP imbalance, but also in an accumulation of the thymidylate synthase substrate dUMP and of the upstream metabolite dUTP (VAN TRIEST *et al.* 2000; LONGLEY *et al.* 2003). Indeed, dUTP strongly accumulated in the absence of Met7 (Fig. 4.5). WT yeast counteract the accumulation of dUTP by the action of the dUTPase Dut1 (GADSDEN *et al.* 1993; GUILLET *et al.* 2006) and consequently dUTP pools under normal growth conditions are extremely small and difficult to quantify (ZHANG *et al.* 2011). The finding that dUTP was no longer detectable in *met7Δ* cells that overexpress the dUTPase *DUT1* (Fig. 4.5A), suggests that the dUTP accumulation in the absence of Met7 is so severe that the catalytic capacity of endogenous Dut1 is saturated. Consequently, the dUTP/dTTP ratio in the absence of Met7 is dramatically shifted and dUTP contributes to 7% of the total dUTP and dTTP pool (Fig. 4.5B). This is in particular detrimental for DNA replication fidelity, as DNA polymerases cannot discriminate between dTTP and dUTP as substrates (SHLOMAI AND KORNBERG 1978; WARNER *et al.* 1981; TINKELENBERG *et al.* 2002). Thus, the ratio between dUTP and dTTP directly determines which nucleotide is incorporated opposite of a template A during DNA replication. Therefore, under the assumption that nucleotides are randomly distributed according to their average occurrence in the budding yeast genome (approximately 31% As and Ts, and 19% Gs and Cs) (GOFFEAU *et al.* 1996), in the absence of Met7 in average two dUTPs will be incorporated every 100 nucleotides polymerized. In line with the increased dUTP/dTTP ratio in the absence of Met7 (Fig. 4.5B), strong uracil accumulation was detected in an uracil accumulation

assay, in which the observed fragments ranged from high molecular weight species to fragments below 250 nt (Fig. 4.5C). Reasons for the difference in fragment size can be for example different nucleotide distributions within the genetic sequence, like GC-rich regions, preferential incorporation of dUTP in actively-transcribed genes (KIM AND JINKS-ROBERTSON 2009) and the acquisition of suppressor mutations during the growth of the culture in a subset of cells, which than accumulate less uracil. Overexpression of *DUT1* in *met7Δ* cells not only suppressed dUTP accumulation (Fig. 4.5A) and genomic uracil incorporation (Fig. 4.5C), but also the GCR phenotype (Table 4.2). This finding suggests that GCRs in the absence of Met7 are triggered by dUTP accumulation. Moreover, the GCR phenotype in *met7Δ* cells could be partially suppressed by the inactivation of Ung1 (Table 4.2). This indicates that first, accumulation of genomic uracil alone is a prerequisite but not sufficient to induce GCRs in budding yeast and second, that processing of genomic uracil and presumably subsequent futile-repair cycles contribute to the GCR phenotype in the absence of Met7. This idea is further supported by the finding that cells expressing the *dut1-1* allele, a *DUT1* allele with reduced dUTPase activity (~95% reduction in dUTPase activity) (GUILLET *et al.* 2006), conferred neither a *CAN1* mutator nor a GCR phenotype (Table 4.2) despites showing strong genomic uracil accumulation (Fig. 4.5C). The absence of any mutator phenotype in the presence of *dut1-1* was unexpected as a previous study (GUILLET *et al.* 2006) reported a 45-fold increase over WT in the *CAN1* mutation rate. Furthermore, the *dut1-1* expressing cells of the previous report showed a growth defect and altered cell cycle progression (GUILLET *et al.* 2006), phenotypes that were not observed for the here investigated *dut1-1* expressing cells (Fig.4.6C,D). The discrepancy between the previous study and the here presented results may originate from additional mutations present in the initially *dut1-1* expressing cells. The former study identified the *dut1-1* allele in a UV mutagenesis screen. As result of this random mutagenesis screen, it is possible that the identified clone carrying the *dut1-G82S* mutation (*dut1-1*) contains additional mutations that may contribute to the observed phenotype. In contrast to this previous study, in the here presented work the *dut1-G82S* mutation was integrated at the endogenous *DUT1* locus using a non-mutagenic approach (pop-in/pop-out strategy) followed by mating. Neither the initial *dut1-1* strain nor spores obtained from different individual crosses showed increased mutagenesis or growth defects. Thus, it is likely that the mutator phenotype and growth defect described in the previous study result from a combinational effect of the *dut1-G82S* mutation and other co-occuring mutations. Alternatively, it is also possible that the observed differences are the result of different yeast backgrounds used in both studies.

5.2.2 A DSB repair defect is required for dUTP-driven GCRs.

The observations that first, the GCR phenotype in *met7Δ* cells is triggered by dUTP accumulation and second, *dut1-1* expressing cells show no GCR phenotype despite uracil accumulation in genomic DNA, argues for additional requirements to induce a dUTP-driven GCR phenotype in budding yeast. In comparison to cells lacking Met7, *dut1-1* expressing cells neither induced a dNTP imbalance nor activated the DNA damage checkpoint. Moreover, *dut1-1* cells did not accumulate in S phase and did not show increased sensitive to phleomycin or a *petite* phenotype (Fig. 4.6). Despite *dut1-1* cells accumulated uracil into the genome (Fig. 4.5C), dUTP concentrations were

below the detection limit of the used HPLC method, suggesting that dUTP levels in *dut1-1* cells are lower than in *met7Δ* cells. Moreover, in addition to increased dUTP pools also reduced dTTP pools were found in *met7Δ* cells, resulting in a presumably more severe dUTP/dTTP ratio. To investigate the effect of a higher dUTP/dTTP ratio on genome stability, the dCMP deaminase *DCD1* was inactivated in *dut1-1*, which should presumably result in lower dTTP pools (SANCHEZ *et al.* 2012). Supporting this idea, similar to *met7Δ* strain, the *dut1-1 dcd1Δ* double mutant showed an elevated GCR phenotype in a qualitative patch test (Fig. 4.6D), increased sensitivity to phleomycin and a *petite* phenotype (Fig. 4.6E). However, *dut1-1 dcd1Δ* double mutant cells neither activated the DDR (Fig. 4.6B) nor accumulated in S phase (Fig. 4.6C). The latter findings suggest that the presumed reduction in either dTTP or any other dNTP is not severe enough to active the DDR. Analysis of dNTP pools and S-phase checkpoint activation in *gln3Δ*, *ura7Δ* (Fig. 4.9B-C, Table 4.9B) and *rnr1* mutant cells (Fig. 4.17, Table 4.20B) revealed that a reduction of dCTP or dATP to levels below dGTP concentrations in WT cells were required to activate the S-phase checkpoint. This would suggest that the dTTP concentration in *dut1-1 dcd1Δ* cells is still higher than the dGTP concentrations measured in WT or in other words dTTP pools are reduced less than 60%. Moreover, the finding that *dut1-1 dcd1Δ* cells accumulate in G1 phase may hint to a problem in G1 to S phase transition. A delayed G1 to S phase transition has been previously linked to increased dNTP pools in G1 (CHABES AND STILLMAN 2007; FRANZOLIN *et al.* 2013) suggesting that *dut1-1 dcd1Δ* cells presumably showed elevated dNTP pools in G1. Thus, to complement these observations it would be informative to measure dNTP concentrations in *dut1-1 dcd1Δ* cells.

Interestingly, as *met7Δ* cells, *dut1-1 dcd1Δ* cells also showed a *petite* phenotype (Fig. 4.6E). A previous study proposed that the reduced dTTP production in the absence of Met7 results in dysfunctional mitochondria based on the finding that the *petite* phenotype in a special *met7Δ* background could be suppressed by external supplementation of the media with dTMP (DESOUZA *et al.* 2000). Potential reasons for the rescue of the *petite* phenotype of *met7Δ* with constant dTMP supplementation are: First, incorporation and processing of mitochondrial uracil results in the *petite* phenotype of *met7Δ* cells. Thus, dTMP supplementation of *met7Δ* cells decreases the dUTP/dTTP ratio leading to less uracil incorporation in genomic and mitochondrial DNA, preventing loss of mitochondrial DNA. Second, low dGTP levels interfere with mitochondrial genome stability. dTMP supplementation increases dTTP pools. dTTP binds to RNR's S-site and promotes dGTP production. In contrast to the nucleus where dGTP pools represent the smallest dNTP pool, dGTP is the most abundant dNTP pool in mitochondria (SONG *et al.* 2005; NIKKANEN *et al.* 2016) suggesting that high dGTP pools, presumably due to the oxidative environment, are required for mitochondrial genome maintenance. Third, dTMP supplementation allows the production of fMet-tRNA and mitochondrial protein biosynthesis. In contrast to mammalian cells, budding yeast cells can synthesize folates *de novo* (CHEREST *et al.* 2000). Thus, supplementation with dTMP may reduce the cellular need for folates dramatically, so that the *de novo* generated folates are sufficient to produce enough fMet-tRNA to maintain mitochondrial protein biosynthesis and consequently functional mitochondria. For cells lacking Met7, none of the possibilities can be excluded and eventually several of these explanations may contribute to the *petite* phenotype.

However, for *dut1-1 dcd1Δ* cells it is rather unlikely that defects in mitochondrial protein biosynthesis are accounting for the observed *petite* phenotype as neither Dut1 nor Dcd1 directly affect the cellular folate pools (Fig. 1.6). Thus, the *petite* phenotype of *dut1-1 dcd1Δ* cells suggests that altered dNTP pools, most likely an increased dUTP/dTTP ratio, are sufficient to induce mitochondrial dysfunction, presumably also in cells lacking Met7.

Both, cells in the absence of Met7 and *dut1-1 dcd1Δ* cells showed increased sensitivity to the DSB inducing agent phleomycin (Fig. 4.6E) suggesting that both mutant backgrounds have problems in DSB repair. The finding that *met7Δ* cells either overexpressing *DUT1* or deficient for Ung1 were as sensitive as *met7Δ* cells to phleomycin (Fig. 4.7C) argues for the hypothesis that the phleomycin sensitivity of *met7Δ* cells is not driven by dUTP accumulation and processing of genomic uracil. Upon DNA damage, such as DSB, budding yeast cells activate the DDR which results among others, in elevated dNTP pools (PARDO *et al.* 2017). In *met7Δ* and *met7Δ pGPD-DUT1* cells, the DDR is constantly activated (Fig. 4.7A-B) still dTTP and dGTP pools were reduced (Fig. 4.5A, Table 4.3B). Thus, one explanation for the observed phleomycin sensitivity in the absence of Met7 may be that *met7Δ* cells are unable to increase dTTP and dGTP pools to sufficiently high levels to facilitate DSB repair. However, *dut1-1 dcd1Δ* cells did not show a constitutively activated checkpoint (Fig. 4.6B). Presumably, *dut1-1 dcd1Δ* cells can increase dNTP pools by activating the DDR, but were anyway sensitive to phleomycin. Thus, at least in *dut1-1 dcd1Δ* cells the inability to increase dNTP pools is most likely not the cause for the detected phleomycin sensitivity. An alternative explanation for the phleomycin sensitivity in *met7Δ* and *dut1-1 dcd1Δ* cells may be the *petite* phenotype. Mitochondrial dysfunction has been previously shown to cause defects in iron-sulfur cluster biogenesis (LILL AND MÜHLENHOFF 2008). Iron-sulfur clusters are required for various proteins including DNA polymerases and DNA repair proteins (VEATCH *et al.* 2009) and consequently for genome stability (DIRICK *et al.* 2014). Thus, inactivation of *MET7* (or *dut1-1 dcd1Δ*) causes, most likely induced by the increased dUTP/dTTP ratio, the loss of mitochondrial DNA that results in a *petite* phenotype and defective iron-sulfur cluster biogenesis. Defects in the biosynthesis of iron-sulfur clusters compromises the activity of DNA polymerases and DNA repair proteins, which results in DSB repair defects and sensitivity to phleomycin. Moreover, the DSB repair defects induced by iron-sulfur cluster deficiency may explain why in *met7Δ* cells uracil incorporation into DNA is toxic and causes increased GCRs, whereas *dut1-1* expressing cells can handle genomic uracil accumulation without compromising genome stability (Table 4.2). Thus, to test the hypothesis that the GCR phenotype of *met7Δ* cells is caused by the combination of uracil incorporation into DNA and a DSB defect due to the *petite* phenotype, it would be interesting to investigate the GCR phenotype of *dut1-1* expressing cells depleted of mitochondrial DNA (e.g. *rho*^{0} cells obtained after treatment with high doses of ethidium bromide (DIRICK *et al.* 2014)).

5.2.3 DDR activation and short telomeres in the absence of Met7 are not driven by dUTP accumulation.

Similar to the phleomycin sensitivity, the DDR activation and the telomere phenotype of *met7Δ* was neither suppressed by overexpression of *DUT1* nor by inactivating *UNG1* (Fig. 4.7). This findings

suggest that the DDR activation in *met7Δ* cells is not driven by uracil-induced damage, but as *met7Δ* and *met7Δ pGPD-DUT1* cells showed reduced dTTP and dGTP levels (Fig. 4.5A, Table 4.3B) rather by limiting dTTP and/or dGTP pools. This is in agreement with other mutants characterized in this study (*gln3Δ*, *ura7Δ* and *rnr1* mutants), which induced dNTP pool imbalances with limiting dNTPs (Fig. 4.10B, 4.17A) and DDR activation (Fig. 4.9B,C, 4.17C).

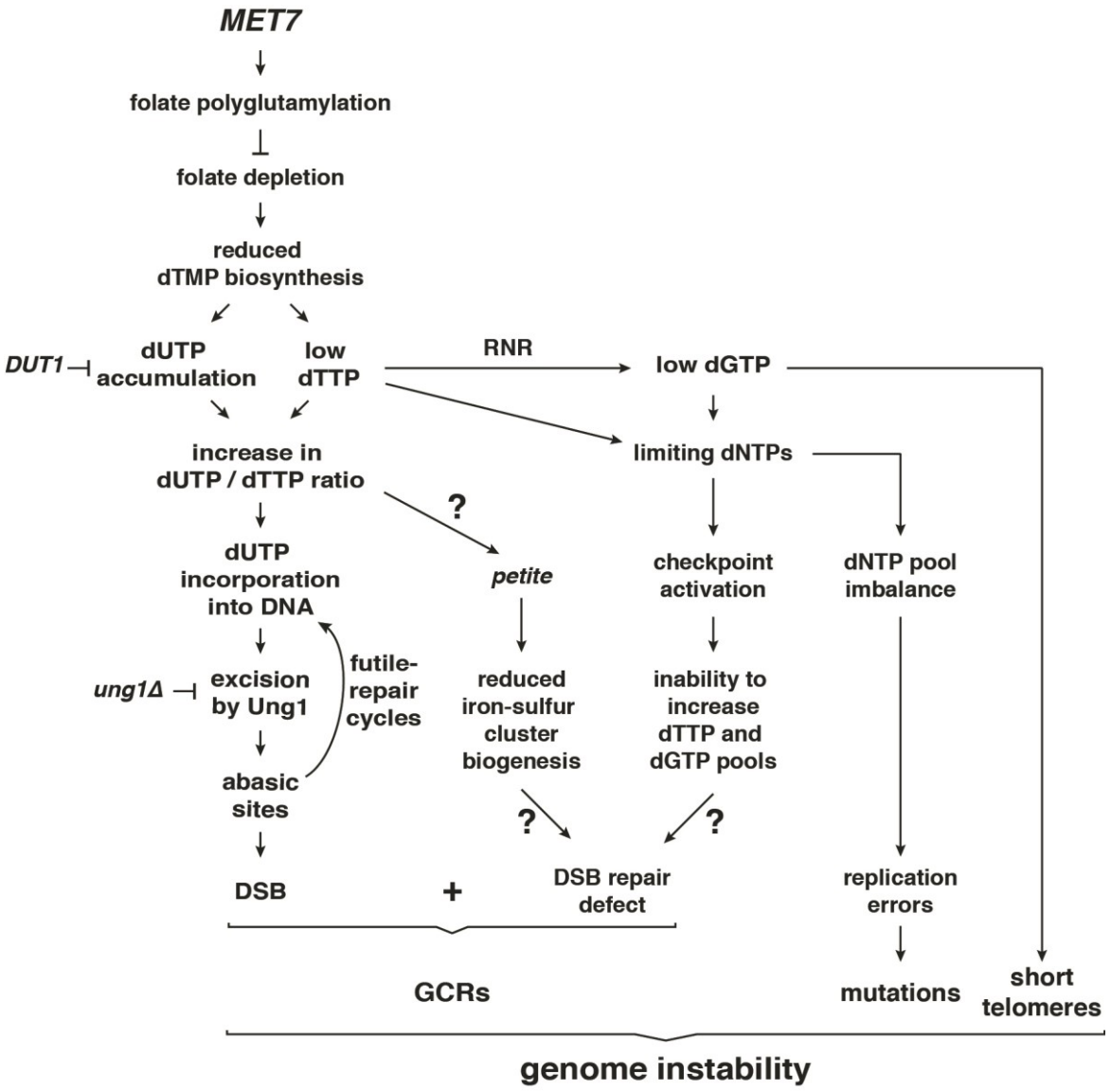

Fig. 5.1 Met7 prevents folate depletion and genome instability.
The absence of Met7 results in folate depletion, a dNTP imbalance characterized by low dTTP and dGTP levels, dUTP accumulation and an increase in the dUTP/dTTP ratio, which favors dUTP incorporation into DNA. Processing of genomic uracil by Ung1 results in transient abasic sites causing under these conditions either futile-repair cycles or double-strand breaks (DSB) and finally due to potential DNA double strand repair defect gross-chromosomal rearrangements (GCRs). Moreover, the dNTP imbalance and the low dGTP pools cause increased replication errors and short telomeres, respectively.

The increased uracil incorporation into the genome did not account for the short telomere phenotype in the absence of Met7 because neither overexpression of *DUT1* nor inactivating *UNG1* increased the telomere length (Fig. 4.7D). Previous reports have correlated increased dGTP pools with increased telomere length (GUPTA *et al.* 2013; MAICHER *et al.* 2017). According to the model

low dGTP pools reduce telomerase activity and prevent re-elongation of short telomeres. Strikingly, the dGTP levels of *met7Δ* and *met7Δ pGDP-DUT1* cells were reduced (Fig. 4.5A, Table 4.3B) suggesting that the short telomere phenotype in the absence of Met7 is indeed a consequence of the very low dGTP pools.

Taken together, this work on Met7 emphasizes the importance of folate polyglutamylation for the cellular metabolism and characterizes the detrimental consequences on genome stability when this process is compromised (Fig. 5.1). As the absence of Met7 in yeast mimics folate depletion and antifolate treatment, inhibitors of human FPGS might be an interesting alternative drug to target the folate-one-carbon metabolism in cancer cells. Moreover, this work may help to dissect different consequences of therapeutically applied antifolates. For example, based on the observed phleomycin sensitivity of *met7Δ* cells, the combination therapy of antifolates and DSB-inducing drugs or ionizing radiation may be beneficial for the treatment outcome. Indeed, these combinations are already in use in the clinics and are more potent than the single therapies (LONGLEY *et al.* 2003). Unfortunately, inactivation of FPGS is a common resistance mechanism of human cancer cells upon antifolate treatment (RAZ *et al.* 2016). Thus, it would be interesting to investigate whether FPGS-deficient cancer cells induced upon classical antifolate treatment are more sensitive to certain drugs or treatments, which could then be applied in targeted therapies.

5.3 Nucleotide precursor pool imbalances induced by the inactivation of *GLN3* or *URA7* cause dNTP pool imbalances and hypermutator phenotypes.

5.3.1 Exo1, Gln3, Shm2 and Ura7 contribute to lagging-strand DNA replication fidelity.

Similar as reported for Exo1 (HOMBAUER *et al.* 2011a; LIBERTI *et al.* 2013), inactivation of *GLN3*, *SHM2* or *URA7* exclusively increases the mutator phenotypes in the presence of the lagging-strand DNA polymerase alleles *pol1-L868M* and *pol3-L612M*, but not in combination with the leading-strand DNA polymerase allele *pol2-M644G* (Table 4.5). In contrast, inactivation of MMR (*msh2Δ*) causes synergistic increases in mutation rates in both the leading-strand (*pol2-M644G*) and the lagging-strand (*pol3-L612M*) DNA polymerase-compromised background (NICK MCELHINNY *et al.* 2008; HOMBAUER *et al.* 2011a). There are four not mutually exclusive possible explanations for the Pol δ/lagging-strand bias observed in combination with *exo1Δ, glnΔ, shm2Δ* and *ura7Δ* mutations: First, higher replication fidelity of the leading-strand is achieved by the activation of the S-phase checkpoint (NAVAS *et al.* 1995; PURSELL *et al.* 2007; KUMAR *et al.* 2011). This may give more time for DNA proofreading and repair. Second, compared to Pol δ, Pol ε conferred an approximately 10-fold higher nucleotide selectivity (ST CHARLES *et al.* 2015). Third, there are intrinsic differences between the low-fidelity active-site DNA polymerase mutant alleles (PURSELL *et al.* 2007; NICK MCELHINNY *et al.* 2008) and presumable also how they compromise leading- and lagging-strand DNA replication fidelity. Fourth, as proposed by a highly controversial report (JOHNSON *et al.* 2015), Pol δ may be the major lagging- and leading-strand DNA polymerase. Based on the data presented here, none of the possibilities can be ultimately excluded. However, the *CAN1* mutation spectra analysis of strains expressing the WT or low-fidelity active-site DNA polymerase alleles *pol2-M644G* or *pol3-L612M* in the presence or absence of Ura7 supports a role for Pol ε as one of the

two major DNA polymerases and thus the “division of labor” model (LUJAN *et al.* 2016). So, the *pol2-M644G CAN1* spectra in the presence or absence of Ura7 were not significantly different from each other (Table 4.12). Moreover, the same *pol2-M644G*-specific mutation hotspots were detected independent whether Ura7 was present or not (Table 4.13). Thus, the *CAN1* mutation spectra analysis supports the “division of labor” model and argues against Pol δ as major DNA polymerase. Moreover, the *CAN1* mutation spectra analysis rather suggests that the synergistic mutator bias is based on either the different mutational signature of the used DNA polymerase alleles or a more general difference in the leading- and lagging-strand DNA replicases. Mutation spectra of mutational reporters, like *CAN1* or *URA3* mutation spectra, are informative and relatively inexpensive proxies for the general mutational landscape present in specific backgrounds. However, only mutations resulting in a specific event, for example *CAN1* inactivation conferring resistance to the drug canavanine, are detected using this type of analysis. Thus, to examine the global mutational landscape and the effect of a defined dNTP imbalance on DNA replication fidelity in an unbiased way, whole-genome sequencing of these mutants has to be performed. To avoid any editing of MMR, the analysis should be also performed in the absence of MMR. For this, homozygous diploids expressing the WT, *pol2-M644G* or *pol3-L612M* DNA polymerase alleles in the presence or absence of Ura7 and/or Msh2 were generated to investigate in collaboration with the Kunkel lab (NIH, US) the mutational landscape of these strains using whole-genome sequencing.

Interestingly, a previously reported *rnr1* allele (*rnr1-Q288A*) caused increased mutagenesis, activation of DDR, a dNTP pool imbalance characterized by very low dCTP pools and a consequently strongly increased dTTP/dCTP ratio (KUMAR *et al.* 2010). The *CAN1* mutation spectrum analysis in the presence of the *rnr1-Q288A* allele revealed several mutational hotspots (G670A, G788A and G1018A) that were also detected in the *msh6Δ ura7Δ CAN1* mutation spectrum (G788A and G1018A hotspots were as well detected in *msh6Δ gln3Δ*) (Table 4.11). In the previous report the observed mutational hotspots in *rnr1-Q288A* expressing cells were predicted to originate from replication errors occurring during lagging-strand replication. Therefore, the observed common bias for lagging-strand infidelity in the absence of Gln3 or Ura7 or in the presence of *rnr1-Q288A* might be due to the dNTP imbalance with reduced dCTP pools. Upon limiting dNTP pools, the leading-strand DNA polymerase Pol ε activates the S-phase checkpoint (NAVAS *et al.* 1995), which may facilitate replication fidelity preferentially on the leading-strand by increasing the time for DNA proofreading and/or MMR. To comprehensively address the observed lagging-strand bias, common to most of the here identified mutational enhancers, further studies, like the analysis of the mutational landscape on a genome-wide scale, will be required.

5.3.2 Rrm3 and Shm2 suppress the accumulation of mutations.

The helicase Rrm3 facilitates replication fork progression through difficult to replicate genomic regions with natural replication fork barriers (IVESSA *et al.* 2003; MOHANTY *et al.* 2006; AZVOLINSKY *et al.* 2009). Here, Rrm3 was found to preferentially prevent mutations generated by the low-fidelity active-site mutant alleles of the two major DNA polymerases (*pol2-M644G* and *pol3-L612M*) (Table 4.5), which together synthesize approximately 98.5% of the *S. cerevisiae* genome (REIJNS *et al.*

2015). Moreover, compared to Pol α, Pol δ and Pol ε replicate also longer DNA stretches. Therefore, Pol δ and Pol ε are presumably more prone to fork pausing and consequently more dependent on Rrm3 for high-fidelity replication. Alternatively, it is also possible that the increased dNTP pools measured in the absence of Rrm3 (O'ROURKE *et al.* 2005; POLI *et al.* 2012) promote fork progression on the expense of DNA proofreading. In contrast to Pol α, Pol δ and Pol ε confer a DNA proofreading function (LUJAN *et al.* 2016). Thus, the combination of reduced nucleotide selectivity in the presence of the active-site DNA polymerase allele and compromised DNA proofreading due to the increased dNTP pools may cause the observed elevated mutator phenotype. A third possibility is that replication fidelity is increased by a helicase-independent function of Rrm3. This function has been described to restrict DNA replication in situations of replication stress (SYED *et al.* 2016). To clarify, if Rrm3's role facilitating replication fidelity in the context of low-fidelity active-site DNA polymerase alleles is or not dependent on Rrm3's helicase-activity, it would be interesting to investigate the effect on replication fidelity of the reported *rrm3* separation-of-function mutant alleles in combination with the low-fidelity active-site mutant alleles.

The cytoplasmic serine hydroxymethyltransferase Shm2 is part of the folate-one-carbon metabolism (Fig. 1.8) and catalyzes the production of 5,10-methylene-THF (5,10-CH_2-THF), a precursor for the purine and pyrimidine biosynthesis (MCNEIL *et al.* 1994; KASTANOS *et al.* 1997). This study identified that inactivation of *SHM2* in the presence of low-fidelity DNA polymerase alleles (*pol1-L868M*, *pol3-L612M* or *pol2-04*), but not in a WT background or an MMR-deficient background (*msh2Δ*) cause an increase in *CAN1* mutation rate (Table 4.5, 4.7). These findings suggest that mutations induced upon inactivation of *SHM2* are not repaired by MMR and are efficiently counteracted by WT DNA polymerases. Despite the known function in the production of a precursor for purine and pyrimidine biosynthesis (MCNEIL *et al.* 1994; KASTANOS *et al.* 1997), surprisingly, inactivation of *SHM2* caused neither an NTP nor dNTP pool imbalance (Fig. 4.10, Table 4.9) and did also not activate the DDR (Fig. 4.9B-C). One possible explanation is that the absence of Shm2 results in increased oxidative damage. Under these oxidizing conditions, modified pyrimidine bases might be incorporated during DNA replication and eventually undergo deamination events that frequently drive C-T transitions. In agreement with this model, a report in mammalian cells using quantitative metabolic fluctuation analysis identified that approximately 40% of the cellular NADPH production is based on oxidation of 5,10-CH_2-THF (FAN *et al.* 2014). Alternatively, it is possible that the absence of Shm2 may cause dUTP accumulation and increased mutagenesis. Shmt1, the mammalian homolog of budding yeast Shm2, has been reported to prevent genomic uracil accumulation in mice (MACFARLANE *et al.* 2008; MACFARLANE *et al.* 2011) and in human lung cancer cells (PAONE *et al.* 2014). Moreover, mammalian Shmt1 was shown to function as a scaffold protein for DHFR and thymidylate synthase at the nuclear lamina and to support *de novo* dTMP biosynthesis (ANDERSON *et al.* 2012). However, in *S. cerevisiae* inactivation of *SHM2* neither caused altered NTP and dNTP pools nor DDR activation. Furthermore, in contrast to the dUTP-driven mutator phenotype upon *MET7* inactivation, the *pol3-L612M shm2Δ* mutator phenotype was neither suppressed by the overexpression of *DUT1* nor by inactivating *UNG1* (data not shown). Taken together, these findings suggest that if dUTP accumulate in *shm2Δ* cells, the accumulation is much milder than in *met7Δ* cells. Alternatively, the consequence of inactivating the

cytoplasmic serine hydroxymethyltransferase might be different in *S. cerevisiae* and mammalian cells.

5.3.3 Low dCTP pools are an Achilles's heel of DNA replication fidelity.

Within the identified mutants, loss of the transcription factor Gln3 or the CTP synthetase Ura7 resulted in the strongest mutator interactions with low-fidelity polymerase, partial or complete MMR defects (Table 4.4, 4.7). *CAN1* mutation spectra analysis in *msh6Δ gln3Δ* and *msh6Δ ura7Δ* cells revealed that the absence of Gln3 or Ura7 causes primarily base pair substitutions (Table 4.10). Nevertheless, in *exo1Δ* and *msh6Δ* backgrounds, but not in the absence of Msh2 or Msh3, inactivation of *GLN3* or *URA7* resulted in a small increase in frameshift mutations (Table 4.7). However, the increase in frameshift mutations was relatively small about 10% of the increase observed in a completely MMR defective *msh2Δ* strain (Table 4.7). Therefore, the increased frameshift phenotype is most likely not a direct consequence of the altered dNTP pools in *gln3Δ* and *ura7Δ* cells, but rather indirect due to the saturation of MMR.

Ura7 is the major CTP synthetase, which contributes to 70-80% of the total CTP biosynthesis in budding yeast (OZIER-KALOGEROPOULOS *et al.* 1991; OZIER-KALOGEROPOULOS *et al.* 1994)(Table 4.9A). However, the consequences of reduced CTP biosynthesis on dNTP pool homeostasis has not been previously investigated. This study showed for the first time, that inactivation of Ura7 reduced not only the CTP pools, but also caused a severe dNTP imbalance characterized by a 50% reduction in dCTP and increased levels in the other three dNTPs (Fig. 4.10, Table 4.9). Surprisingly, not only the absence of Ura7, but also loss of the transcription factor Gln3 induced an NTP and dNTP pool imbalance characterized by low CTP and dCTP levels (Fig. 4.10, Table 4.9). The GATA-transcription factor Gln3 is negatively regulated by TOR and is activated upon glutamine limitation (COURCHESNE AND MAGASANIK 1988; BECK AND HALL 1999; CRESPO *et al.* 2002). However, a role of Gln3 in dNTP homeostasis has not been previously described. The finding that the severe mutator phenotype in *gln3Δ* double mutants could be suppressed by supplementing media with glutamine (Fig. 4.9E) suggests that the mutator synergies in the absence of Gln3 are largely driven by glutamine deficiency. Glutamine is an important cellular metabolite that is required not only for protein biosynthesis but also as nitrogen source for the *de novo* purine and pyrimidine biosynthesis. Moreover, some cancer cell lines depend on external glutamine for survival ("glutamine addiction") (WISE AND THOMPSON 2010; HENSLEY *et al.* 2013). Consequently, glutamine analogs counteract cancer cell proliferation by inhibiting glutamine-requiring enzymes like CTP synthetase (DENTON *et al.* 1982; WEBER *et al.* 1982). Interestingly, although glutamine is required for purine and pyrimidine *de novo* biosynthesis, glutamine limitation due to *GLN3* inactivation in budding yeast or inhibition of glutamine-requiring enzymes by the glutamine analog *Acivicin* in mammalian cells result in decreased CTP and dCTP pools and increased UTP levels (Fig. 4.10, Table 4.9)(NEIL *et al.* 1979; DENTON *et al.* 1982). Thus, in eukaryotes CTP synthetase and consequently CTP/dCTP pools seem to be most sensitive to glutamine limitations. It would be interesting to examine whether a low glutamine condition, either induced by glutamine analogs or as previously described for the central core of solid tumors (PAN *et al.* 2016), causes increased

mutagenesis in cancer cells and so facilitates tumor evolution and adaptation to cancer drug treatments.

The observation that the inactivation of *DUN1* suppressed the strong mutator phenotypes measured in double mutants carrying *gln3Δ* or *ura7Δ* mutations in DNA replication fidelity-compromised backgrounds suggests that the DDR contributes in part to the observed mutator phenotypes (Fig. 4.9D, Table 4.8). dNTP pool measurement in *dun1Δ gln3Δ* and *dun1Δ ura7Δ* cells revealed that the inactivation of *DUN1* in *gln3Δ* and *ura7Δ* cells suppressed dTTP, dATP and dGTP below WT levels, whereas dCTP levels remained almost unchanged in comparison to dCTP concentrations measured in the absence of Gln3 or Ura7 (Fig. 4.10B, Table 4.9B). Thus, the inactivation of *DUN1* reduces the severity of the dNTP pool imbalance and "normalizes" the ratio between dCTP to the other dNTP by inhibiting RNR induction (Fig. 4.10B, Table 4.9B).

The DNA content profiles of *dun1Δ gln3Δ* and *dun1Δ ura7Δ* strains are in agreement with the different functional requirements for Gln3 and Ura7. Ura7 as major CTP synthetase (OZIER-KALOGEROPOULOS *et al.* 1994) is required primarily during S phase (KOREN *et al.* 2010) where the demand for dCTP is highest (CHABES *et al.* 2003). Consequently, *dun1Δ ura7Δ* cells that not only lack the major CTP synthetase, but also confer overall reduced dNTP biosynthesis due to *DUN1* inactivation (Fig 4.10B, Table 4.9B) (FASULLO *et al.* 2010), progress slower though S phase and therefore show a stronger accumulation of cells in S phase compared to the single mutants (Fig. 4.9C). In contrast, Gln3 activity is primarily required in situations of glutamine limitations (CRESPO *et al.* 2002). In the absence of Dun1 the dNTP production is reduced (FASULLO *et al.* 2010). Therefore, it might be that the cellular demand for glutamine in the absence of Dun1 is lower than in the presence of Dun1. Consequently, *dun1Δ* cells are less prone to generate a situation of glutamine limitation, in which the presence of Gln3 becomes critical. Thus, it could be that *dun1Δ gln3Δ* cells did not strongly accumulate in S phase (Fig. 4.9C) because in the absence of Dun1 glutamine pools are not severely depleted and therefore cells do not require Gln3 activity.

RNR is considered the master regulator of dNTP pool homeostasis (NORDLUND AND REICHARD 2006). RNR possess two allosteric sites, one that controls the overall enzymatic activity (A-site) (Fig. 1.7C) and a second that regulates the substrate specificity (S-site) (Fig. 1.7B). Surprisingly, the absence of either Gln3 or Ura7 causes limitations in the dNTP precursor pool which result in a dNTP imbalance for which neither RNR nor any other mechanism downstream of RNR can compensate. Interestingly, RNR binds at the S-site all dNTPs except dCTP, consequently it can not respond to changes in dCTP concentrations (Fig. 1.7B)(BROWN AND REICHARD 1969). Instead, budding yeast cells compensate high dCTP pools through the activity of Dcd1, which converts dCMP into dUMP (Fig.1.6)(MCINTOSH AND HAYNES 1984; SANCHEZ *et al.* 2012). However, no compensatory mechanism for low CTP/dCTP pools exists in budding yeast cells, suggesting that low dCTP pools are the blind spot of dNTP pool homeostasis regulation (Fig. 1.6). Low dCTP pools due to the absence of Gln3 or Ura7 results in replication stress and activation of the DDR (Fig. 4.9B,C)(KOREN *et al.* 2010). However, as in cells lacking Gln3 or Ura7 the dCTP precursor pool is limiting, the increased activity of RNR due to DDR activation is unable to generate more dCDP. Thus, instead of compensating for the low dCTP pools, the DDR increases the severity of the dNTP pool imbalance (Fig. 4.10B, Table 4.9B).

Presumably additional gene deletions exist that may interfere with the synthesis of substrates required for dNTP biosynthesis. However, they might not be mutagenic as dNTP imbalances may have been buffered by RNR. In these cases, RNR is able to senses the limiting dNTP pools and prevent that the limiting substrate manifests in a dNTP imbalance. Thus, given the sophisticated allosteric regulation of RNR (Fig. 1.7)(BROWN AND REICHARD 1969), gene deletions affecting CTP biosynthesis are most likely the only ones that not only induce a precursor pool alteration but also cause a dNTP imbalance that compromises DNA replication fidelity.

In agreement with the altered dNTP imbalance, *CAN1* mutation spectra analysis revealed that the dNTP pool imbalance largely shapes the mutation spectra. So, the *msh6Δ gln3Δ* and *msh6Δ ura7Δ CAN1* mutation spectra were dominated by G-C to A-T mutations (Table 4.10). These mutations originate most likely from dTTP misinsertions opposite of a template G and were driven by the severe dCTP:dTTP ratio of 1:15 present in *gln3Δ* or *ura7Δ* cells (Table 4.9B). Moreover, the manifestation of replication errors at all mutational hotspots was supported by the next-nucleotide effect (KUNKEL 1992; REHA-KRANTZ 2010) as each mutational hotspot was followed by at least three nucleotides that were more abundant than WT concentrations.

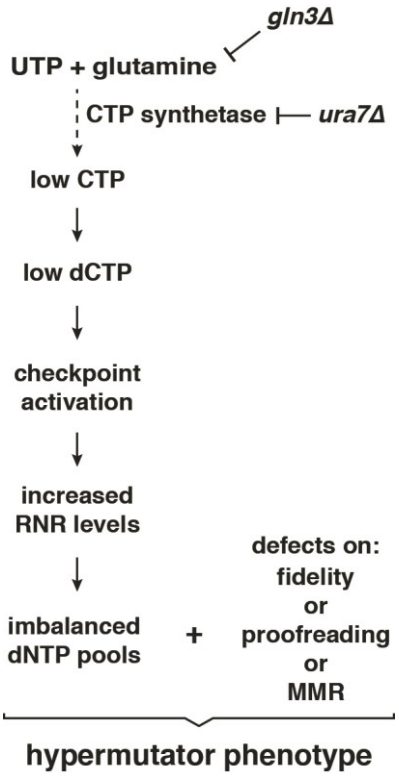

Fig. 5.2 Gln3 or Ura7 promote DNA replication fidelity by counteracting dNTP pool imbalances.
Inactivation of GLN3 or URA7 results in low CTP and dCTP pools, checkpoint activation, increased RNR levels and a severe dNTP pool imbalance. If combined with defects in DNA polymerase fidelity, proofreading or MMR, this dNTP pool imbalances cause a hypermutator phenotype. Figure was adapted from (Schmidt et al. 2017).

Taken together, loss of the transcription factor Gln3 or the CTP synthetase Ura7 results in decreased CTP levels, which leads to reduced dCTP pools and activation of the DDR (Fig. 5-2). Paradoxically, activation of the DDR instead of counteracting the low dCTP pools induces RNR activity creating an even more severe dNTP imbalance. Interestingly, this severe dNTP imbalance does not trigger increased mutagenesis in the presence of WT DNA polymerases and functional MMR, highlighting once more the superb buffer capacity of the eukaryotic DNA replication fidelity

system. However, the combination of this severe dNTP pool imbalance with either compromised DNA polymerase or MMR function results in a hypermutator phenotype.

5.4 A *RNR1* random mutagenesis screen reveals specific residues in *RNR1* with crucial functions in dNTP homeostasis and uncovers a highly mutagenic dNTP imbalance.

5.4.1 A *RNR1* screen identifies novel *rnr1* alleles inducing mutagenic dNTP pool alterations.

Screening a library of mutant *rnr1* alleles for increased mutagenesis in an *exo1Δ* background revealed 24 *rnr1* alleles (Fig. 4.12) that conferred different mutator phenotypes in the *CAN1* inactivation and the two frameshift reversion assays *lys2-10A* and *hom3-10* (Table 4.14). The identified mutations were located either at the A-site, in the surrounding of the S-site (but not restricted to the previously mutagenized loop 2 (KUMAR *et al.* 2010)), at the Rnr1-Rnr1 interface or close to the C-site (Fig. 4.12). dNTP concentration measurements showed that all tested alleles either caused overall increased dNTP pools or imbalanced dNTP pools (Fig. 4.16, Table 4.18), indicating that the measured mutator interactions between the *rnr1* alleles and the absence of Exo1 are driven by dNTP pool alterations. All *rnr1* alleles that resulted in synthetic lethality in the absence of Rnr3, the alternative DNA-damage inducible RNR subunit, or the checkpoint kinase Dun1 (Table 4.16) and presented a constitutive S-phase checkpoint activation (Fig. 4.17B-C) had at least one limiting dNTP concentration. Further analysis of the *rnr1* alleles expressed from the endogenous *RNR1* chromosomal locus revealed that a reduction of up to 20% in the dATP levels cause neither DDR activation (Fig. 4.17C) nor strong accumulation of cells in S phase (Fig. 4.17B). However, a 50% reduction in dATP levels resulted in a constitutive S-phase checkpoint activation (Fig. 4.17B-C). Interestingly, in budding yeast 50% of dATP levels correspond approximately to the dGTP concentration in WT cells, the smallest dNTP pool in budding yeast (CHABES *et al.* 2003) but also in mammalian cells (MATHEWS AND JI 1992; MARTOMO AND MATHEWS 2002). Furthermore, inactivation of *GLN3* or *URA7* caused reduced dCTP concentrations below the WT dGTP concentration (Fig. 4.10B, Table 4.9B) that also triggered DDR activation (Fig. 4.9B-C). Therefore, the results obtained in the presence of *rnr1* alleles or absence of either Gln3 or Ura7 argue for the existence of a dNTP limitation threshold for S-phase checkpoint activation in budding yeast. Thus, it is very likely that reductions in the levels of any of the four dNTPs resulting in concentrations below this threshold (determined by dGTP levels in WT cells) will activate the S-phase checkpoint.

Given the screening strategy, in which mutations were introduced randomly into *RNR1* using mutagenic PCR the here presented approach is unbiased and not restricted to certain domains or regions of Rnr1. Furthermore, screening for mutator phenotypes using three different mutator assays in an *exo1Δ* background allowed the identification of key residues in Rnr1 with important consequences on dNTP pool homeostasis (the limitations of the used mutator assays are discussed below). Moreover, as the used screening strategy depends on cell growth, all identified *rnr1* alleles expressed on a centromeric plasmid had to confer sufficient catalytic activity to complement the *rnr1Δ* background and support cell viability.

Previous studies introduced mutations in the highly conserved loop 2 based on the Rnr1 crystal structure (KUMAR *et al.* 2010; KUMAR *et al.* 2011). Characterization of these alleles in budding yeast revealed that some of the alleles, like *rnr1-Q288A* and *rnr1-R293A,* caused severe dNTP pool imbalances and growth defects, but were only viable in the presence of a suppressed WT-*RNR1* allele (KUMAR *et al.* 2010; KUMAR *et al.* 2011). Thus, the here-described screening strategy overcomes limitations of previous studies characterizing *rnr1* alleles.

A previous mutator screen of NrdA and NrdB, the large and small subunit of *E. coli* RNR, identified NrdA and NdrB alleles that conferred increased mutagenesis and dNTP pool alterations (AHLUWALIA *et al.* 2012). As observed with the here described *rnr1* mutations, NrdA mutations also cluster at the A-site and S-site. Although *S. cerevisiae* Rnr1 and *E. coli* NrdA share 29% protein sequence identity, none of the here identified mutated residues in Rnr1 have been found mutated previously in the NrdA screen. This was unexpected as some of the here identified residues, like Asp226 or Arg256 and others, directly coordinate the specificity effector (Fig. 4.12D-E) and are conserved from *E. coli* up to humans (Fig. 4.12B). The discrepancy between both screens may originate at least in part from the screening strategies using different mutator assays and in case of the *S. cerevisiae RNR1* screen use of the *exo1Δ* as “sensitized mutator background”. Importantly, one advantage of screening in *S. cerevisiae* over screening in *E. coli* is the high protein sequence conservation (67% protein sequence identity) between budding yeast *RNR1* and human *RRM1*. So, in contrast to the *E. coli* NrdA screen in which 6 out of the 15 identified residues were conserved in human (AHLUWALIA *et al.* 2012), 21 out of the 22 identified residues in the *S. cerevisiae RNR1* screen were conserved in humans (Fig. 4.12B). The high degree of protein conservation suggest that mutating these residues in human *RRM1* may have similar consequences for dNTP pool homeostasis as observed in budding yeast.

In the *E. coli* screen not only mutations in *E. coli* NrdA, but also in the small *E. coli* RNR subunit NrdB were found to cause dNTP pool alterations and increased mutagenesis (AHLUWALIA *et al.* 2012). Based on this previous observation, a similar screen as the one described here for *RNR1* was conducted, but in which a *RNR2* randomly mutagenized library was screened for increased mutagenesis in an *exo1Δ rnr2Δ* strain. Surprisingly, no *rnr2* alleles could be identified that resulted in increased mutagenesis (data not shown). This discrepancy may argue for structural differences or different regulatory requirements between *E. coli* and *S. cerevisiae* RNR.

One unpredicted finding of the *RNR1* screen was that all dNTP pool imbalances shared relatively low dATP pools (Fig. 4.16A, Table 4.18). In part, this communality can be rationalized by the frameshift mutator assays, which were used in addition to the *CAN1* forward inactivation assay to identify the *rnr1* alleles. The *lys2-10A* mutator assays scores for a single A:T deletion event in a defined 10 A:T long mononucleotide run (TRAN *et al.* 1997), whereas the *hom3-10* frameshift reversion assay is reverted by a single T:A deletion event in a 7 T:A long mononucleotide run (MARSISCHKY *et al.* 1996). Thus, low dATP pools may facilitate slippage events in A:T or T:A mononucleotide runs and therefore, *rnr1* alleles causing a dNTP imbalance characterized by low dATP are likely to be identified with the used screening approach. However, low dTTP pools should, similar to low dATP pools, support the reversion of both frameshift mutator assays, however, none of the identified *rnr1* alleles caused low dTTP levels (Table 4.18). One possible

explanation for the absence of dNTP imbalances with low dTTP may rely in the activity of Dcd1, which converts dCMP to dUMP and compensates dTTP levels downstream of RNR (MCINTOSH AND HAYNES 1984; SANCHEZ *et al.* 2012). Given that the overall RNR activity is negatively regulated by dATP at the A-site (Fig. 1.7C) (CHABES *et al.* 2003; FAIRMAN *et al.* 2011), it is likely that low dATP pools allow more severe dNTP imbalances independently of DDR activation, like in *rnr1-S242T* or *rnr1-Y285C*. Thus, it would be interesting to perform a *rnr1-F15S* screen, in which not the WT-*RNR1* but the *rnr1-F15S* allele is randomly mutagenized. By screening in a *rnr1-F15S* background that is most likely refractory to dATP inhibition at the A-site (see 5.4.2) and thus showed in average 6.5x increased dNTP pools (Table 4.18, 4.20B), presumably more severe dNTP pool alterations and eventually dNTP imbalances with high dATP pools might be detected. Furthermore, similar to the here presented *RNR1* random mutagenesis screen, additional screens making use of other frameshift reporters scoring for example for single G:C deletion or insertion events (e.g. (TRAN *et al.* 1997)) and/or general forward inactivation assays (e.g. (WHELAN *et al.* 1979; BOEKE *et al.* 1984)) could be performed. It would be interesting to evaluate which type of dNTP pool alteration is facilitating the reversion or inactivation of these reporters. Moreover, this analysis would complement the understanding of how different dNTP pool alterations shape the mutational landscape *in vivo*.

5.4.2 *rnr1-F15S* interferes with A-site regulation.

The *rnr1-F15S* allele was the only allele identified in the *RNR1* screen that did not result in a dNTP pool imbalance, but an overall increase in dNTPs (in average 6.5-fold higher than WT) (Table 4.18). The *F15S* mutation is located at the ATP cone of the A-site in a region that propably affects RNR hexamerzation (Fig. 4.12F). Interestingly, the Phe15 is directly adjacent to the Asp16 residual, which was mutated by the Dealwis group to investigate the eukaryotic RNR's A-site regulation (FAIRMAN *et al.* 2011). In their study, purified human *rrm1-D16R* was unable to form catalytic inactive dATP-dependent hexamers and showed in comparison to the WT increased catalytic activity in the presence of dATP (FAIRMAN *et al.* 2011). Due to the position and analogy, it is therefore likely that the *F15S* mutation also prevents dATP-dependent hexamerization and is refractory to dATP inhibition at the A-site. This may explain the increased, balanced dNTP pools measured in the presence of this mutation (Table 4.18 and 4.20B). These overall increased dNTP pools due to the *rnr1-F15S* allele resulted in no synthetic growth defect or synthetic lethal interaction (Table 4.16) and a 4-fold and 59-fold increase over WT in the *CAN1* inactivation rates in the presence and absence of Exo1, respectively (Table 4.19). Thus, overall increased dNTP pools most likely do not promote the generation of more replication errors by the DNA polymerases, but rather prevent the correction of errors by DNA proofreading due to a strong next-nucleotide effect (KUNKEL 1992; REHA-KRANTZ 2010). However, most replication errors that escape DNA proofreading are then subsequently repaired by MMR (Fig. 5.3).

5.4.3 Two potential mechanisms for *rnr1* mutants that cause low purine dNTP imbalances.

Three identified *rnr1* alleles (*rnr1-A245V*, *rnr1-G271S* and *rnr1-Y285C*) caused a dNTP imbalanced characterized by high pyrimidine and low purine pools (Fig. 4.16 A, Table 4.18). Interestingly, in a *S. cerevisiae* Rnr1 crystal structure two of the identified residues (Gly271 and Tyr285) indirectly

interact with the effector bound to the S-site (XU *et al.* 2006a). Both, the backbone oxide of Gly271 and the side chain of Tyr285 form a hydrogen-bond with a water molecule that interacts with the 2'-hydroxy group of the bound AMP-PNP effector suggesting that similar interactions might be possible with ATP, but not with dNTP effectors. Additionally, a previous study postulated that the Tyr244 in *Salmonella typhimurium*, which is the homolog residue of Tyr285 in *S. cerevisiae*, prevents NTP binding to the S-site because of a steric clash between the 2'-hydroxy group of the ribonucleotides and the tyrosine side-chain (UPPSTEN *et al.* 2003). According to this hypothesis and as NTP concentrations in budding yeast are in average 50-times higher than dNTP concentrations, mutating Tyr285 will favor the binding of the most abundant NTP at the S-site, which correspond to ATP. Under these special conditions, increased ATP binding at the S-site may result primarily in the reduction of pyrimidine nucleotides. The importance of the Tyr285 side chain for dNTP homeostasis is further supported by the observation that not only the here characterized *rnr1-Y285C* allele (Table 4.18 and 4.20B), but also the previously described *rnr1-Y285A* allele and to a lesser extend the *rnr1-Y285F* allele, resulted in low purine and elevated pyrimidine pools (KUMAR *et al.* 2010). Thus, Tyr285 and most likely also the Gly271 are both critical for the discrimination of dNTP over NTP binding at the S-site and mutating those residues results in an ATP-driven increase in pyrimidine pools.

In contrast to Gly271 and Tyr285 that are located at the S-site, Ala245 is located closer to the C-site. Interestingly, replacing the alanine at position 245 with valine resulted in a 60% and 30% reduction in dATP and dGTP pools, respectively and elevated pyrimidine pools (Fig. 4.17A, Table 4.20B). The bulkier side chain of valine in respect to alanine may decrease the space at the C-site, facilitating the binding of smaller pyrimidine NDPs over larger-size purine NDPs, leading to a dNTP imbalance characterized by low purines and elevated pyrimidines. In conclusion, two different mechanisms resulting in the same type of dNTP imbalance characterized by low purines and elevated pyrimidines are proposed: In the first one, low purine and elevated pyrimidine pools are the consequence of missing ATP discrimination at the S-site due to mutations in Gly271 or Tyr285, whereas in the second one, a mutation in Ala245 results in a smaller C-site, which favors pyrimidine NDP over purine NDP reduction at the C-site.

5.4.4 Different dNTP pool alterations rely differentially on DNA proofreading and MMR.

Most of the identified dNTP alterations caused strong mutator phenotype and/or synthetic genetic interactions only in DNA polymerase- or MMR-compromised backgrounds. These findings, similar to the results obtained with *GLN3* or *URA7* deficient strains (Fig. 5-2), highlight the remarkable buffer capacity and robustness of the DNA replication fidelity machinery. Moreover, the collection of *rnr1* mutant alleles and their systematic characterization allows evaluating the *in vivo* requirements for high-fidelity DNA replication in the presence of different dNTP pool alterations.

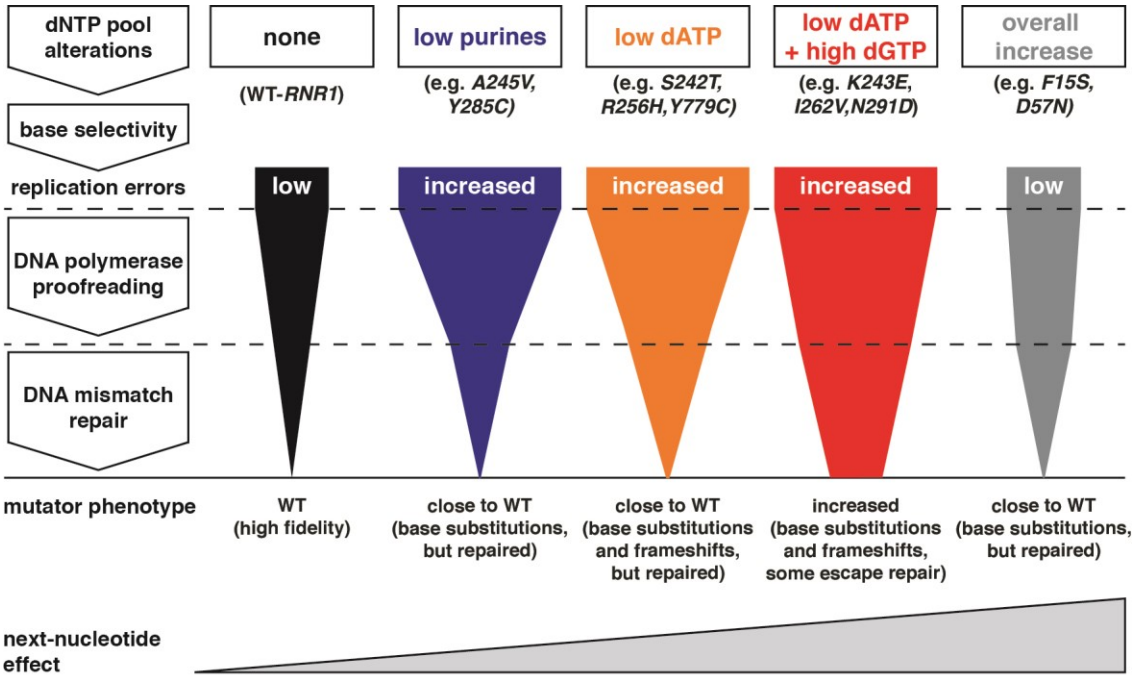

Fig. 5.3 Specific dNTP pool alterations rely differentially on DNA polymerase proofreading and MMR for mutation avoidance.
The funnels below each dNTP pool alteration represent DNA replication errors that are corrected by DNA polymerase proofreading and/or MMR. dNTP pool alterations and funnels are color-coded based on their genetic interactions, dNTP pool alteration and mutator phenotype as in Fig. 4.17. dNTP imbalances characterized by low dATP levels and high dGTP levels cause a mutator phenotype even in the presence of high-fidelity DNA polymerase and functional MMR.

Overall increased dNTP pools with unchanged ratios between the different dNTPs do not increase the amount of replication errors generated by the DNA polymerases. However, overall increased dNTP pools cause a strong next-nucleotide effect that interferes with the proofreading of the generated DNA replication errors. Thus, more DNA replication errors escape DNA proofreading and these replication errors depend on MMR for repair. However, as the amount of generated DNA replication errors in the presence of overall increased dNTP pools is low, MMR can to in large extent correct replication errors that escaped DNA polymerase proofreading. Consistently, overall increased dNTP pools did neither cause a mutator phenotype in a WT background nor synthetic growth defects or synthetic lethality in the absence of DNA proofreading or MMR (Table 4.16). Furthermore, in agreement with the next-nucleotide effect being most detrimental for base substitution replication errors or indels in short mononucleotide runs (KROUTIL *et al.* 1996; KUNKEL 2009), increased mutation rates in the presence of overall increased dNTP pools were primarily observed in the *CAN1* forward inactivation assay and to a lesser degree in the two frameshift-specific reporters (Table 4.19).

In contrast to the overall increased dNTP pools, imbalanced dNTP pools facilitate the generation of DNA replication errors by DNA polymerases as altered ratios between the different dNTPs directly affect DNA polymerases' nucleotide selectivity. Interestingly, different dNTP pool alterations rely differentially on DNA proofreading and MMR. The "low purines" (or "2 out of 4") dNTP imbalances characterized by low purines and elevated pyrimidines showed synthetic growth defects or lethality in the presence of DNA polymerase proofreading-defective alleles, but not in the absence of MMR

(Table 4.16). Moreover, *CAN1* mutation spectrum analysis in *rnr1-Y285C* expressing cells revealed that the mutation spectrum is dominated by base substitutions (Table 4.21). Thus, the “low purines” dNTP imbalance supports primarily the generation of base substitutions and is therefore more dependent on DNA polymerase proofreading than on MMR for survival. This bias for base pair substitutions can be further rationalized by the ratios between the different dNTPs, which strongly affects the nucleotide selectivity of the replicating DNA polymerases. Assuming that the increase in the elevated dNTP pools are similar, a dNTP imbalance with “2 out of 4” elevated dNTP pools, like a “low purines” dNTP imbalance, confers altered ratios in 4 of the 6 dNTP ratios, whereas a dNTP imbalance in which “3 out of 4” dNTPs being elevated, like the “low dATP” dNTP imbalance, has 3 out of the 6 dNTP ratios altered and an overall increase in dNTP pools does not change the dNTP ratios at all. Thus, theoretically a “2 out of 4” dNTP imbalance is most challenging for DNA polymerase nucleotide selectivity and consequently more prone for the generation of base substitutions.

In comparison to a “low purines” dNTP imbalance, the “low dATP” or “low dATP + high dGTP” dNTP imbalances showed increased amount of one-base-pair deletions in the mutation spectra analysis and relied on DNA polymerase proofreading as well as on MMR for survival (Table 4.21 and 4.23). This suggests in line with *in vitro* DNA replication experiments (BEBENEK *et al.* 1992) that limitation in one of the dNTP pools and an increase in the remaining three dNTP pools (“low dATP” or “low dATP + high dGTP”) not only facilitates the generation of base substitutions but also DNA polymerase slippage events, in particular at mononucleotide runs requiring for their replication the limiting dNTP. Moreover, the increase in three out of four dNTPs result in a strong next-nucleotide effect, which favors mismatch extension over polymerase proofreading leading to more replication errors and a strong dependency on MMR for mutation avoidance. Interestingly, the dNTP pool precursor imbalance upon *GLN3* or *URA7* inactivation also results in a “3 out of 4” dNTP imbalance with one limiting dNTP (dCTP) and three elevated dNTP pools (Table 4.9B). Although strong mutator phenotypes were measured in the absence of Gln3 or Ura7 in DNA replication fidelity-compromised backgrounds (Table 4.5,4.7) and a growth defect in the *ura7Δ pol3-01* double mutant was observed (Fig. 4.8 and data not shown), the consequences for DNA replication fidelity of a “low dCTP” dNTP imbalance were less severe as a “low dATP” dNTP imbalance. One possible explanation may be the composition of the budding yeast genome, which consists out of approximately 31% As and Ts, and 19% Gs and Cs (GOFFEAU *et al.* 1996). So, a “3 out of 4” dNTP imbalance that is low in dATP or dTTP may have more severe consequences for DNA replication fidelity, simply because of the higher representation of the former bases in the budding yeast genome.

An exception among the identified *rnr1* alleles were those alleles that caused a dNTP imbalance characterized by low dATP pools, elevated pyrimidine pools and strongly increased dGTP pools (“low dATP + high dGTP”) (Fig. 4.16A, 4.17A, Table 4.18, 4.20B). This type of dNTP imbalance resulted in strong *CAN1* inactivation and frameshift mutator phenotypes even in the presence of DNA proofreading and functional MMR (Fig. 4.13, Table 4.19). For example, strains expressing the *rnr1-K245E* or *rnr1-I262V,N291D* alleles at the endogenous chromosomal *RNR1* locus, presented *CAN1* mutation rates and frameshift reversion rates similar to a strain with a complete MMR

deficiency (*msh2Δ*) (Table 4.19). These findings suggest that in the context of the "low dATP" type of dNTP imbalance strongly elevated dGTP levels confer a high mutagenic potential and are extremely detrimental for DNA replication fidelity. Why are "low dATP + high dGTP" dNTP imbalances so mutagenic? Three not mutually exclusive, potential explanations are: First, strongly elevated dGTP levels in the context of a "low dATP" dNTP imbalance enhance the mutagenic potential of the dNTP imbalance, resulting in increased DNA replication errors and consequently saturation of MMR. As dGTP is the smallest dNTP pool under WT conditions (MATHEWS AND JI 1992; MARTOMO AND MATHEWS 2002; CHABES *et al.* 2003), changes in the dGTP concentration have the strongest impact on the ratios between the different dNTPs, which directly influence DNA polymerase nucleotide selectivity. Second, dGTP as smallest dNTP pool functions as an intrinsic brake during DNA replication. Low dGTP pools may slow down DNA replication, giving so more time for DNA proofreading and potentially also for repair. In contrast, high dGTP concentrations may facilitate DNA polymerization at expenses of DNA proofreading and repair. Third, elevated dGTP concentrations could cause inhibition of DNA polymerase proofreading. During DNA proofreading, dNMPs are excised from the nascent DNA strand. These dNMPs can bind to the exonuclease active site and inhibit DNA proofreading to prevent excessive excision. Earlier studies on DNA replication have shown that dNMPs (as dGMP) cause inhibition of DNA polymerase proofreading *in vitro* (QUE *et al.* 1978; FERSHT AND KNILL-JONES 1983). Despite the fact that *in vivo* dNMPs concentrations are extremely low (ZHANG *et al.* 2011), it is possible that dGMP levels may accumulate when dGTP levels are severely increased. Thus, the accumulation of dGMP may potentially inhibit DNA proofreading and in combination with a dNTP imbalance cause a severe mutator phenotype.

To better understand the molecular mechanism causing this severe mutator phenotype additional experiments are required. So, it would be very interesting to investigate whether DNA replication forks are progressing faster in the presence of the "low dATP + high dGTP" dNTP imbalances in comparison to WT and "low dATP" dNTP pools. Moreover, dGMP concentration measurements in the presence or absence of a "low dATP + high dGTP" dNTP imbalance may support the third previously mentioned scenario.

Interestingly, both chromosomally integrated *rnr1* alleles that induce the "low dATP + high dGTP" dNTP imbalance, showed an altered DNA content profile and an accumulation of cells in G2/M (Fig. 4.17B) suggesting that very high dGTP pools may affect also other cellular processes outside S phase. This idea is supported by the *in vitro* observation that dGTP facilitates tubulin nucleation better than GTP (HAMEL *et al.* 1984). As dGTP pools represent up to 50% of the GTP pools measured in these strains (Table 4.20), dGTP may interfere with microtubule dynamics and chromosome segregation. Furthermore, two studies positively correlate the dGTP concentrations with telomere length (GUPTA *et al.* 2013; MAICHER *et al.* 2017), suggesting that dGTP, as smallest dNTP pool, may not only play an important role for DNA replication fidelity but also in the regulation of other genome maintenance pathways.

5.5 Concluding remarks

The here presented genome-wide screen identified genes that prevent the accumulation of mutations. Among others, the folylpolyglutamate synthetase Met7 as well as the transcription factor Gln3 and the major CTP synthetase Ura7 were identified as novel important factors for genome stability.

In the absence of Met7, cells accumulate and incorporate dUTP during DNA replication given the altered dUTP/dTTP ratio. Increased uracil incorporation in combination with a DSB repair defect seems to trigger increased genome instability (GCRs) (Fig. 5-1).

The absence of the CTP synthetase Ura7 or upon glutamine limitation due to the lack of the transcription factor Gln3, both cause reduced *de novo* CTP biosynthesis resulting in a mutagenic dNTP imbalance (Fig. 5-2). This can neither be compensated by RNR nor by any other mechanism downstream of RNR. Thus, the here presented data emphasizes the importance of the dNTP precursor metabolism for dNTP homeostasis and uncovers CTP/dCTP levels as blind spot in dNTP regulation.

The systematic characterization of different mutagenic dNTP pool alterations induced by *rnr1* alleles revealed differential requirements on DNA proofreading and MMR for cellular survival (Fig. 5-3). In line with *in vitro* data (BEBENEK *et al.* 1992), dNTP imbalances with one limiting dNTP facilitate DNA polymerase slippage events resulting in frameshift mutations *in vivo*. Within the examined dNTP pool alterations, a “low dATP + high dGTP” dNTP imbalance was most detrimental for DNA replication fidelity and caused base substitutions and frameshift mutations even in the presence of WT DNA polymerases and functional MMR. Moreover, the comparison of different dNTP pool alterations and DDR activation argues for a dNTP limitation threshold for S-phase checkpoint activation in budding yeast, which is defined by approximately the dGTP concentration reported in WT cells.

Taken together, this work highlights the pivotal role of the cellular metabolism and dNTP pool homeostasis on DNA replication fidelity. The here identified genes and mutant alleles might act as mini-drivers during human cancer evolution and might represent interesting candidates for future drug target or prognostic markers.

6 REFERENCES

6 REFERENCES

Acharya, S., T. Wilson, S. Gradia, M. F. Kane, S. Guerrette *et al.*, 1996 hMSH2 forms specific mispair-binding complexes with hMSH3 and hMSH6. Proc Natl Acad Sci U S A 93**:** 13629-13634.

Ahluwalia, D., R. J. Bienstock and R. M. Schaaper, 2012 Novel mutator mutants of E. coli nrdAB ribonucleotide reductase: Insight into allosteric regulation and control of mutation rates. DNA Repair 11**:** 480-487.

Ainsworth, W. B., B. T. Hughes, W. C. Au, S. Sakelaris, O. Kerscher *et al.*, 2013 Cytoplasmic localization of Hug1p, a negative regulator of the MEC1 pathway, coincides with the compartmentalization of Rnr2p–Rnr4p. Biochemical and Biophysical Research Communications 439**:** 443-448.

Alani, E., R. Thresher, J. D. Griffith and R. D. Kolodner, 1992 Characterization of DNA-binding and strand-exchange stimulation properties of y-RPA, a yeast single-strand-DNA-binding protein. Journal of Molecular Biology 227**:** 54-71.

Albertson, T. M., M. Ogawa, J. M. Bugni, L. E. Hays, Y. Chen *et al.*, 2009 DNA polymerase ε and δ proofreading suppress discrete mutator and cancer phenotypes in mice. Proceedings of the National Academy of Sciences 106**:** 17101-17104.

Amberg, D. C., D. Burke, J. N. Strathern, D. Burke and Cold Spring Harbor Laboratory., 2005 *Methods in yeast genetics : a Cold Spring Harbor Laboratory course manual*. Cold Spring Harbor Laboratory Press, Cold Spring Harbor, N.Y.

Amin, N. S., M. N. Nguyen, S. Oh and R. D. Kolodner, 2001 exo1-Dependent mutator mutations: model system for studying functional interactions in mismatch repair. Mol Cell Biol 21**:** 5142-5155.

Anderson, D. D., C. F. Woeller, E.-P. Chiang, B. Shane and P. J. Stover, 2012 Serine Hydroxymethyltransferase Anchors de Novo Thymidylate Synthesis Pathway to Nuclear Lamina for DNA Synthesis. Journal of Biological Chemistry 287**:** 7051-7062.

Appling, D. R., 1991 Compartmentation of folate-mediated one-carbon metabolism in eukaryotes. FASEB J 5**:** 2645-2651.

Arana, M. E., and T. A. Kunkel, 2010 Mutator phenotypes due to DNA replication infidelity. Semin Cancer Biol 20**:** 304-311.

Askree, S. H., T. Yehuda, S. Smolikov, R. Gurevich, J. Hawk *et al.*, 2004 A genome-wide screen for Saccharomyces cerevisiae deletion mutants that affect telomere length. Proc Natl Acad Sci U S A 101**:** 8658-8663.

Aye, Y., M. Li, M. J. C. Long and R. S. Weiss, 2014 Ribonucleotide reductase and cancer: biological mechanisms and targeted therapies. Oncogene 34**:** 2011.

Azvolinsky, A., P. G. Giresi, J. D. Lieb and V. A. Zakian, 2009 Highly transcribed RNA polymerase II genes are impediments to replication fork progression in Saccharomyces cerevisiae. Mol Cell 34**:** 722-734.

Bailey, L. B., and R. J. Berry, 2005 Folic acid supplementation and the occurrence of congenital heart defects, orofacial clefts, multiple births, and miscarriage. The American Journal of Clinical Nutrition 81**:** 1213S-1217S.

Bauer, G. A., and P. M. Burgers, 1990 Molecular cloning, structure and expression of the yeast proliferating cell nuclear antigen gene. Nucleic Acids Res 18**:** 261-265.

Beaudin, A. E., and P. J. Stover, 2009 Insights into metabolic mechanisms underlying folate-responsive neural tube defects: A minireview. Birth Defects Research Part A: Clinical and Molecular Teratology 85**:** 274-284.

Bebenek, K., J. D. Roberts and T. A. Kunkel, 1992 The effects of dNTP pool imbalances on frameshift fidelity during DNA replication. Journal of Biological Chemistry 267**:** 3589-3596.

Beck, T., and M. N. Hall, 1999 The TOR signalling pathway controls nuclear localization of nutrient-regulated transcription factors. Nature 402**:** 689-692.

Bell, S. P., and K. Labib, 2016 Chromosome Duplication in *Saccharomyces cerevisiae*. Genetics 203**:** 1027-1067.

Ben-Aroya, S., C. Coombes, T. Kwok, K. A. O'Donnell, J. D. Boeke *et al.*, 2008 Toward a Comprehensive Temperature-Sensitive Mutant Repository of the Essential Genes of Saccharomyces cerevisiae. Molecular Cell 30**:** 248-258.

Bertrand, P., D. X. Tishkoff, N. Filosi, R. Dasgupta and R. D. Kolodner, 1998 Physical interaction between components of DNA mismatch repair and nucleotide excision repair. Proc Natl Acad Sci U S A 95**:** 14278-14283.

Bester, Assaf C., M. Roniger, Yifat S. Oren, Michael M. Im, D. Sarni *et al.*, 2011 Nucleotide Deficiency Promotes Genomic Instability in Early Stages of Cancer Development. Cell 145**:** 435-446.

Bochman, M. L., and A. Schwacha, 2008 The Mcm2-7 Complex Has In Vitro Helicase Activity. Molecular Cell 31**:** 287-293.

Boeke, J. D., F. LaCroute and G. R. Fink, 1984 A positive selection for mutants lacking orotidine-5'-phosphate decarboxylase activity in yeast: 5-fluoro-orotic acid resistance. Mol Gen Genet 197**:** 345-346.

Boiteux, S., and S. Jinks-Robertson, 2013 DNA repair mechanisms and the bypass of DNA damage in Saccharomyces cerevisiae. Genetics 193**:** 1025-1064.

Boland, C. R., and A. Goel, 2010 Microsatellite instability in colorectal cancer. Gastroenterology 138**:** 2073-2087 e2073.

Boland, C. R., and H. T. Lynch, 2013 The history of Lynch syndrome. Fam Cancer 12**:** 145-157.

Bowman, G. D., M. O'Donnell and J. Kuriyan, 2004 Structural analysis of a eukaryotic sliding DNA clamp–clamp loader complex. Nature 429**:** 724.

Breslow, D. K., D. M. Cameron, S. R. Collins, M. Schuldiner, J. Stewart-Ornstein *et al.*, 2008 A comprehensive strategy enabling high-resolution functional analysis of the yeast genome. Nature Methods 5**:** 711.

Briggs, S., and I. Tomlinson, 2013 Germline and somatic polymerase ε and δ mutations define a new class of hypermutated colorectal and endometrial cancers. The Journal of Pathology 230**:** 148-153.

Brill, S. J., and B. Stillman, 1991 Replication factor-A from Saccharomyces cerevisiae is encoded by three essential genes coordinately expressed at S phase. Genes & Development 5**:** 1589-1600.

Brown, N. C., and P. Reichard, 1969 Role of effector binding in allosteric control of ribonucleoside diphosphate reductase. Journal of Molecular Biology 46**:** 39-55.

Brusky, J., Y. Zhu and W. Xiao, 2000 UBC13, a DNA-damage-inducible gene, is a member of the error-free postreplication repair pathway in Saccharomyces cerevisiae. Curr Genet 37**:** 168-174.

Burgers, P. M. J., and T. A. Kunkel, 2017 Eukaryotic DNA Replication Fork. Annual Review of Biochemistry 86**:** 417-438.

Byrnes, J. J., K. M. Downey, V. L. Black and A. G. So, 1976 A new mammalian DNA polymerase with 3' to 5' exonuclease activity: DNA polymerase delta. Biochemistry 15**:** 2817-2823.

Campbell, C. S., H. Hombauer, A. Srivatsan, N. Bowen, K. Gries *et al.*, 2014 Mlh2 is an accessory factor for DNA mismatch repair in Saccharomyces cerevisiae. PLoS Genet 10**:** e1004327.

Chabes, A., V. Domkin and L. Thelander, 1999 Yeast Sml1, a Protein Inhibitor of Ribonucleotide Reductase. Journal of Biological Chemistry 274**:** 36679-36683.

Chabes, A., B. Georgieva, V. Domkin, X. Zhao, R. Rothstein *et al.*, 2003 Survival of DNA damage in yeast directly depends on increased dNTP levels allowed by relaxed feedback inhibition of ribonucleotide reductase. Cell 112**:** 391-401.

Chabes, A., and B. Stillman, 2007 Constitutively high dNTP concentration inhibits cell cycle progression and the DNA damage checkpoint in yeast *Saccharomyces cerevisiae*. Proceedings of the National Academy of Sciences 104**:** 1183-1188.

Chattopadhyay, S., R. G. Moran and I. D. Goldman, 2007 Pemetrexed: biochemical and cellular pharmacology, mechanisms, and clinical applications. Mol Cancer Ther 6**:** 404-417.

Chen, C.-W., N. Tsao, L.-Y. Huang, Y. Yen, X. Liu *et al.*, 2016 The Impact of dUTPase on Ribonucleotide Reductase-Induced Genome Instability in Cancer Cells. Cell Reports 16**:** 1287-1299.

Chen, C., and R. D. Kolodner, 1999 Gross chromosomal rearrangements in Saccharomyces cerevisiae replication and recombination defective mutants. Nat Genet 23**:** 81-85.

Chen, P. C., S. Dudley, W. Hagen, D. Dizon, L. Paxton *et al.*, 2005 Contributions by MutL homologues Mlh3 and Pms2 to DNA mismatch repair and tumor suppression in the mouse. Cancer Res 65**:** 8662-8670.

Cherest, H., D. Thomas and Y. Surdin-Kerjan, 2000 Polyglutamylation of folate coenzymes is necessary for methionine biosynthesis and maintenance of intact mitochondrial genome in Saccharomyces cerevisiae. J Biol Chem 275**:** 14056-14063.

Chilkova, O., B.-H. Jonsson and E. Johansson, 2003 The Quaternary Structure of DNA Polymerase ε from Saccharomyces cerevisiae. Journal of Biological Chemistry 278**:** 14082-14086.

Chilkova, O., P. Stenlund, I. Isoz, C. M. Stith, P. Grabowski *et al.*, 2007 The eukaryotic leading and lagging strand DNA polymerases are loaded onto primer-ends via separate mechanisms but have comparable processivity in the presence of PCNA. Nucleic Acids Research 35**:** 6588-6597.

Church, D. N., S. E. Briggs, C. Palles, E. Domingo, S. J. Kearsey *et al.*, 2013 DNA polymerase epsilon and delta exonuclease domain mutations in endometrial cancer. Hum Mol Genet 22**:** 2820-2828.

Ciccia, A., and S. J. Elledge, 2010 The DNA Damage Response: Making It Safe to Play with Knives. Molecular Cell 40**:** 179-204.

Clark, A. B., F. Valle, K. Drotschmann, R. K. Gary and T. A. Kunkel, 2000 Functional interaction of proliferating cell nuclear antigen with MSH2-MSH6 and MSH2-MSH3 complexes. J Biol Chem 275**:** 36498-36501.

Clausen, A. R., S. A. Lujan, A. B. Burkholder, C. D. Orebaugh, J. S. Williams *et al.*, 2015 Tracking replication enzymology in vivo by genome-wide mapping of ribonucleotide incorporation. Nature Structural &Amp; Molecular Biology 22**:** 185.

Collura, A., P. A. Kemp and S. Boiteux, 2012 Abasic sites linked to dUTP incorporation in DNA are a major cause of spontaneous mutations in absence of base excision repair and Rad17-Mec3-Ddc1 (9-1-1) DNA damage checkpoint clamp in Saccharomyces cerevisiae. DNA Repair (Amst) 11**:** 294-303.

Courchesne, W. E., and B. Magasanik, 1988 Regulation of nitrogen assimilation in Saccharomyces cerevisiae: roles of the URE2 and GLN3 genes. J Bacteriol 170**:** 708-713.

Crespo, J. L., T. Powers, B. Fowler and M. N. Hall, 2002 The TOR-controlled transcription activators GLN3, RTG1, and RTG3 are regulated in response to intracellular levels of glutamine. Proc Natl Acad Sci U S A 99**:** 6784-6789.

Crouse, G. F., 2016 Non-canonical actions of mismatch repair. DNA Repair 38**:** 102-109.

Culligan, K. M., and J. B. Hays, 2000 Arabidopsis MutS Homologs—AtMSH2, AtMSH3, AtMSH6, and a Novel AtMSH7—Form Three Distinct Protein Heterodimers with Different Specificities for Mismatched DNA. The Plant Cell 12**:** 991-1002.

Culotta, V. C., L. W. J. Klomp, J. Strain, R. L. B. Casareno, B. Krems *et al.*, 1997 The Copper Chaperone for Superoxide Dismutase. Journal of Biological Chemistry 272**:** 23469-23472.

Daigaku, Y., A. Keszthelyi, C. A. Müller, I. Miyabe, T. Brooks *et al.*, 2015 A global profile of replicative polymerase usage. Nature Structural &Amp; Molecular Biology 22**:** 192.

Datta, A., J. L. Schmeits, N. S. Amin, P. J. Lau, K. Myung *et al.*, 2000 Checkpoint-dependent activation of mutagenic repair in Saccharomyces cerevisiae pol3-01 mutants. Mol Cell 6**:** 593-603.

Davey, M. J., C. Indiani and M. O'Donnell, 2003 Reconstitution of the Mcm2-7p Heterohexamer, Subunit Arrangement, and ATP Site Architecture. Journal of Biological Chemistry 278**:** 4491-4499.

Denton, J. E., M. S. Lui, T. Aoki, J. Sebolt and G. Weber, 1982 Rapid in vivo inactivation by acivicin of CTP synthetase, carbamoyl-phosphate synthetase II, and amidophosphoribosyltransferase in hepatoma. Life Sciences 30**:** 1073-1080.

DeSouza, L., Y. Shen and A. L. Bognar, 2000 Disruption of cytoplasmic and mitochondrial folylpolyglutamate synthetase activity in Saccharomyces cerevisiae. Arch Biochem Biophys 376**:** 299-312.

Deutschbauer, A. M., R. M. Williams, A. M. Chu and R. W. Davis, 2002 Parallel phenotypic analysis of sporulation and postgermination growth in *Saccharomyces cerevisiae*. Proceedings of the National Academy of Sciences 99**:** 15530-15535.

Dirick, L., W. Bendris, V. Loubiere, T. Gostan, E. Gueydon *et al.*, 2014 Metabolic and Environmental Conditions Determine Nuclear Genomic Instability in Budding Yeast Lacking Mitochondrial DNA. G3: Genes|Genomes|Genetics 4**:** 411-423.

Douglas, M. E., F. A. Ali, A. Costa and J. F. X. Diffley, 2018 The mechanism of eukaryotic CMG helicase activation. Nature 555**:** 265.

Dovrat, D., D. Dahan, S. Sherman, I. Tsirkas, N. Elia *et al.*, 2018 A Live-Cell Imaging Approach for Measuring DNA Replication Rates. Cell Reports 24**:** 252-258.

Drake, J. W., B. Charlesworth, D. Charlesworth and J. F. Crow, 1998 Rates of Spontaneous Mutation. Genetics 148**:** 1667-1686.

Ducker, G. S., and J. D. Rabinowitz, 2017 One-Carbon Metabolism in Health and Disease. Cell Metab 25**:** 27-42.

Echols, H., and M. F. Goodman, 1991 Fidelity Mechanisms in DNA Replication. Annual Review of Biochemistry 60**:** 477-511.

Edelmann, L., and W. Edelmann, 2004 Loss of DNA mismatch repair function and cancer predisposition in the mouse: animal models for human hereditary nonpolyposis colorectal cancer. Am J Med Genet C Semin Med Genet 129C**:** 91-99.

Elledge, S. J., and R. W. Davis, 1990 Two genes differentially regulated in the cell cycle and by DNA-damaging agents encode alternative regulatory subunits of ribonucleotide reductase. Genes & Development 4**:** 740-751.

Elledge, S. J., Z. Zhou, J. B. Allen and T. A. Navas, 1993 DNA damage and cell cycle regulation of ribonucleotide reductase. BioEssays 15**:** 333-339.

Enyenihi, A. H., and W. S. Saunders, 2003 Large-Scale Functional Genomic Analysis of Sporulation and Meiosis in Saccharomyces cerevisiae. Genetics 163**:** 47-54.

Fairman, J. W., S. R. Wijerathna, M. F. Ahmad, H. Xu, R. Nakano *et al.*, 2011 Structural basis for allosteric regulation of human ribonucleotide reductase by nucleotide-induced oligomerization. Nat Struct Mol Biol 18**:** 316-322.

Fan, J., J. Ye, J. J. Kamphorst, T. Shlomi, C. B. Thompson *et al.*, 2014 Quantitative flux analysis reveals folate-dependent NADPH production. Nature 510**:** 298.

Fang, W. H., and P. Modrich, 1993 Human strand-specific mismatch repair occurs by a bidirectional mechanism similar to that of the bacterial reaction. J Biol Chem 268**:** 11838-11844.

Fasullo, M., O. Tsaponina, M. Sun and A. Chabes, 2010 Elevated dNTP levels suppress hyper-recombination in Saccharomyces cerevisiae S-phase checkpoint mutants. Nucleic Acids Research 38**:** 1195-1203.

Fersht, A. R., and J. W. Knill-Jones, 1983 Contribution of 3′ → 5′ exonuclease activity of DNA polymerase III holoenzyme from Escherichia coli to specificity. Journal of Molecular Biology 165**:** 669-682.

Flood, C. L., G. P. Rodriguez, G. Bao, A. H. Shockley, Y. W. Kow *et al.*, 2015 Replicative DNA polymerase delta but not epsilon proofreads errors in Cis and in Trans. PLoS Genet 11**:** e1005049.

Flores-Rozas, H., D. Clark and R. D. Kolodner, 2000 Proliferating cell nuclear antigen and Msh2p-Msh6p interact to form an active mispair recognition complex. Nat Genet 26**:** 375-378.

Flores-Rozas, H., and R. D. Kolodner, 1998 The Saccharomyces cerevisiae MLH3 gene functions in MSH3-dependent suppression of frameshift mutations. Proc Natl Acad Sci U S A 95**:** 12404-12409.

Fortune, J. M., Y. I. Pavlov, C. M. Welch, E. Johansson, P. M. J. Burgers *et al.*, 2005 Saccharomyces cerevisiae DNA Polymerase δ: HIGH FIDELITY FOR BASE SUBSTITUTIONS BUT LOWER FIDELITY FOR SINGLE- AND MULTI-BASE DELETIONS. Journal of Biological Chemistry 280**:** 29980-29987.

Fox, J. T., and P. J. Stover, 2008 Folate-mediated one-carbon metabolism. Vitam Horm 79**:** 1-44.

Franzolin, E., G. Pontarin, C. Rampazzo, C. Miazzi, P. Ferraro *et al.*, 2013 The deoxynucleotide triphosphohydrolase SAMHD1 is a major regulator of DNA precursor pools in mammalian cells. Proceedings of the National Academy of Sciences 110**:** 14272-14277.

Gadsden, M. H., E. M. McIntosh, J. C. Game, P. J. Wilson and R. H. Haynes, 1993 dUTP pyrophosphatase is an essential enzyme in Saccharomyces cerevisiae. EMBO J 12**:** 4425-4431.

Gao, B., R. Mohan and R. S. Gupta, 2009 Phylogenomics and protein signatures elucidating the evolutionary relationships among the Gammaproteobacteria. Int J Syst Evol Microbiol 59**:** 234-247.

Gatbonton, T., M. Imbesi, M. Nelson, J. M. Akey, D. M. Ruderfer *et al.*, 2006 Telomere length as a quantitative trait: genome-wide survey and genetic mapping of telomere length-control genes in yeast. PLoS Genet 2**:** e35.

Gauss, R., M. Trautwein, T. Sommer and A. Spang, 2005 New modules for the repeated internal and N-terminal epitope tagging of genes in Saccharomyces cerevisiae. Yeast 22**:** 1-12.

Georgescu, R. E., L. Langston, N. Y. Yao, O. Yurieva, D. Zhang *et al.*, 2014 Mechanism of asymmetric polymerase assembly at the eukaryotic replication fork. Nat Struct Mol Biol 21**:** 664-670.

Georgescu, R. E., G. D. Schauer, N. Y. Yao, L. D. Langston, O. Yurieva *et al.*, 2015 Reconstitution of a eukaryotic replisome reveals suppression mechanisms that define leading/lagging strand operation. eLife 4**:** e04988.

Gerik, K. J., X. Li, A. Pautz and P. M. J. Burgers, 1998 Characterization of the Two Small Subunits of Saccharomyces cerevisiae DNA Polymerase δ. Journal of Biological Chemistry 273**:** 19747-19755.

Ghodgaonkar, M. M., F. Lazzaro, M. Olivera-Pimentel, M. Artola-Boran, P. Cejka *et al.*, 2013 Ribonucleotides misincorporated into DNA act as strand-discrimination signals in eukaryotic mismatch repair. Mol Cell 50**:** 323-332.

Giaever, G., A. M. Chu, L. Ni, C. Connelly, L. Riles *et al.*, 2002 Functional profiling of the Saccharomyces cerevisiae genome. Nature 418**:** 387.

Goellner, E. M., C. D. Putnam and R. D. Kolodner, 2015 Exonuclease 1-dependent and independent mismatch repair. DNA Repair (Amst).

Goellner, E. M., C. E. Smith, C. S. Campbell, H. Hombauer, A. Desai *et al.*, 2014 PCNA and Msh2-Msh6 Activate an Mlh1-Pms1 Endonuclease Pathway Required for Exo1-Independent Mismatch Repair. Mol Cell.

Goffeau, A., B. G. Barrell, H. Bussey, R. W. Davis, B. Dujon *et al.*, 1996 Life with 6000 Genes. Science 274**:** 546-567.

Goldsby, R. E., L. E. Hays, X. Chen, E. A. Olmsted, W. B. Slayton *et al.*, 2002 High incidence of epithelial cancers in mice deficient for DNA polymerase δ proofreading. Proceedings of the National Academy of Sciences 99**:** 15560-15565.

Goldsby, R. E., N. A. Lawrence, L. E. Hays, E. A. Olmsted, X. Chen *et al.*, 2001 Defective DNA polymerase-δ proofreading causes cancer susceptibility in mice. Nature Medicine 7**:** 638.

Goldstone, D. C., V. Ennis-Adeniran, J. J. Hedden, H. C. T. Groom, G. I. Rice *et al.*, 2011 HIV-1 restriction factor SAMHD1 is a deoxynucleoside triphosphate triphosphohydrolase. Nature 480**:** 379.

Gon, S., R. Napolitano, W. Rocha, S. Coulon and R. P. Fuchs, 2011 Increase in dNTP pool size during the DNA damage response plays a key role in spontaneous and induced-mutagenesis in *Escherichia coli*. Proceedings of the National Academy of Sciences 108**:** 19311-19316.

Gonen, N., and Y. G. Assaraf, 2012 Antifolates in cancer therapy: structure, activity and mechanisms of drug resistance. Drug Resist Updat 15**:** 183-210.

Goodman, M. F., 1997 Hydrogen bonding revisited: Geometric selection as a principal determinant of DNA replication fidelity. Proceedings of the National Academy of Sciences 94**:** 10493-10495.

Greene, C. N., and S. Jinks-Robertson, 2001 Spontaneous frameshift mutations in Saccharomyces cerevisiae: accumulation during DNA replication and removal by proofreading and mismatch repair activities. Genetics 159**:** 65-75.

Guarino, E., I. Salguero and S. E. Kearsey, 2014 Cellular regulation of ribonucleotide reductase in eukaryotes. Seminars in Cell & Developmental Biology 30**:** 97-103.

Gueldener, U., J. Heinisch, G. J. Koehler, D. Voss and J. H. Hegemann, 2002 A second set of loxP marker cassettes for Cre-mediated multiple gene knockouts in budding yeast. Nucleic Acids Res 30**:** e23.

Guillet, M., P. A. Van Der Kemp and S. Boiteux, 2006 dUTPase activity is critical to maintain genetic stability in Saccharomyces cerevisiae. Nucleic Acids Res 34**:** 2056-2066.

Guittet, O., P. Håkansson, N. Voevodskaya, S. Fridd, A. Gräslund *et al.*, 2001 Mammalian p53R2 Protein Forms an Active Ribonucleotide Reductasein Vitro with the R1 Protein, Which Is Expressed Both in Resting Cells in Response to DNA Damage and in Proliferating Cells. Journal of Biological Chemistry 276**:** 40647-40651.

Gupta, A., S. Sharma, P. Reichenbach, L. Marjavaara, A. K. Nilsson *et al.*, 2013 Telomere Length Homeostasis Responds to Changes in Intracellular dNTP Pools. Genetics 193**:** 1095-1105.

Håkansson, P., L. Dahl, O. Chilkova, V. Domkin and L. Thelander, 2006a The Schizosaccharomyces pombe Replication Inhibitor Spd1 Regulates Ribonucleotide Reductase Activity and dNTPs by Binding to the Large Cdc22 Subunit. Journal of Biological Chemistry 281: 1778-1783.

Håkansson, P., A. Hofer and L. Thelander, 2006b Regulation of Mammalian Ribonucleotide Reduction and dNTP Pools after DNA Damage and in Resting Cells. Journal of Biological Chemistry 281: 7834-7841.

Hamatake, R. K., H. Hasegawa, A. B. Clark, K. Bebenek, T. A. Kunkel *et al.*, 1990 Purification and characterization of DNA polymerase II from the yeast Saccharomyces cerevisiae. Identification of the catalytic core and a possible holoenzyme form of the enzyme. Journal of Biological Chemistry 265: 4072-4083.

Hamel, E., J. Lustbader and C. M. Lin, 1984 Deoxyguanosine nucleotide analogues: potent stimulators of microtubule nucleation with reduced affinity for the exchangeable nucleotide site of tubulin. Biochemistry 23: 5314-5325.

Harfe, B. D., B. K. Minesinger and S. Jinks-Robertson, 2000 Discrete in vivo roles for the MutL homologs Mlh2p and Mlh3p in the removal of frameshift intermediates in budding yeast. Curr Biol 10: 145-148.

Harrington, J. M., and R. D. Kolodner, 2007 Saccharomyces cerevisiae Msh2-Msh3 acts in repair of base-base mispairs. Mol Cell Biol 27: 6546-6554.

Hensley, C. T., A. T. Wasti and R. J. DeBerardinis, 2013 Glutamine and cancer: cell biology, physiology, and clinical opportunities. The Journal of Clinical Investigation 123: 3678-3684.

Herr, A. J., S. R. Kennedy, G. M. Knowels, E. M. Schultz and B. D. Preston, 2014 DNA replication error-induced extinction of diploid yeast. Genetics 196: 677-691.

Herr, A. J., M. Ogawa, N. A. Lawrence, L. N. Williams, J. M. Eggington *et al.*, 2011 Mutator suppression and escape from replication error-induced extinction in yeast. PLoS Genet 7: e1002282.

Hoege, C., B. Pfander, G.-L. Moldovan, G. Pyrowolakis and S. Jentsch, 2002 RAD6-dependent DNA repair is linked to modification of PCNA by ubiquitin and SUMO. Nature 419: 135.

Hoffman, C. S., and F. Winston, 1987 A ten-minute DNA preparation from yeast efficiently releases autonomous plasmids for transformaion of Escherichia coli. Gene 57: 267-272.

Hollingsworth, N. M., L. Ponte and C. Halsey, 1995 MSH5, a novel MutS homolog, facilitates meiotic reciprocal recombination between homologs in Saccharomyces cerevisiae but not mismatch repair. Genes & Development 9: 1728-1739.

Holmes, J., Jr., S. Clark and P. Modrich, 1990 Strand-specific mismatch correction in nuclear extracts of human and Drosophila melanogaster cell lines. Proc Natl Acad Sci U S A 87: 5837-5841.

Hombauer, H., C. S. Campbell, C. E. Smith, A. Desai and R. D. Kolodner, 2011a Visualization of eukaryotic DNA mismatch repair reveals distinct recognition and repair intermediates. Cell 147: 1040-1053.

Hombauer, H., A. Srivatsan, C. D. Putnam and R. D. Kolodner, 2011b Mismatch repair, but not heteroduplex rejection, is temporally coupled to DNA replication. Science 334: 1713-1716.

Howlett, N. G., and R. H. Schiestl, 2004 Nucleotide excision repair deficiency causes elevated levels of chromosome gain in Saccharomyces cerevisiae. DNA Repair (Amst) 3: 127-134.

Hu, C.-M., M.-T. Yeh, N. Tsao, C.-W. Chen, Q.-Z. Gao *et al.*, 2012 Tumor Cells Require Thymidylate Kinase to Prevent dUTP Incorporation during DNA Repair. Cancer Cell 22: 36-50.

Huang, M., Z. Zhou and S. J. Elledge, 1998 The DNA Replication and Damage Checkpoint Pathways Induce Transcription by Inhibition of the Crt1 Repressor. Cell 94: 595-605.

Huang, M. E., A. G. Rio, A. Nicolas and R. D. Kolodner, 2003 A genomewide screen in Saccharomyces cerevisiae for genes that suppress the accumulation of mutations. Proc Natl Acad Sci U S A 100: 11529-11534.

International Human Genome Sequencing, C., E. S. Lander, L. M. Linton, B. Birren, C. Nusbaum *et al.*, 2001 Initial sequencing and analysis of the human genome. Nature 409: 860.

Ivessa, A. S., B. A. Lenzmeier, J. B. Bessler, L. K. Goudsouzian, S. L. Schnakenberg *et al.*, 2003 The Saccharomyces cerevisiae helicase Rrm3p facilitates replication past nonhistone protein-DNA complexes. Mol Cell 12: 1525-1536.

Ivessa, A. S., J. Q. Zhou and V. A. Zakian, 2000 The Saccharomyces Pif1p DNA helicase and the highly related Rrm3p have opposite effects on replication fork progression in ribosomal DNA. Cell 100: 479-489.

Iyer, R. R., A. Pluciennik, V. Burdett and P. L. Modrich, 2006 DNA mismatch repair: functions and mechanisms. Chem Rev 106: 302-323.

Janke, C., M. M. Magiera, N. Rathfelder, C. Taxis, S. Reber *et al.*, 2004 A versatile toolbox for PCR-based tagging of yeast genes: new fluorescent proteins, more markers and promoter substitution cassettes. Yeast 21: 947-962.

Jasencakova, Z., and A. Groth, 2010 Replication stress, a source of epigenetic aberrations in cancer? BioEssays 32: 847-855.

Johansson, E., and N. Dixon, 2013 Replicative DNA Polymerases. Cold Spring Harbor Perspectives in Biology 5.

Johnson, R. E., R. Klassen, L. Prakash and S. Prakash, 2015 A Major Role of DNA Polymerase delta in Replication of Both the Leading and Lagging DNA Strands. Mol Cell 59: 163-175.

Jong, A. Y., C. L. Kuo and J. L. Campbell, 1984 The CDC8 gene of yeast encodes thymidylate kinase. Journal of Biological Chemistry 259: 11052-11059.

Jong, A. Y., and J. J. Ma, 1991 Saccharomyces cerevisiae nucleoside-diphosphate kinase: Purification, characterization, and substrate specificity. Archives of Biochemistry and Biophysics 291: 241-246.

Kadyrov, F. A., L. Dzantiev, N. Constantin and P. Modrich, 2006 Endonucleolytic function of MutLalpha in human mismatch repair. Cell 126: 297-308.

Kastanos, E. K., Y. Y. Woldman and D. R. Appling, 1997 Role of mitochondrial and cytoplasmic serine hydroxymethyltransferase isozymes in de novo purine synthesis in Saccharomyces cerevisiae. Biochemistry 36: 14956-14964.

Kaufer, N. F., H. M. Fried, W. F. Schwindinger, M. Jasin and J. R. Warner, 1983 Cycloheximide resistance in yeast: the gene and its protein. Nucleic Acids Res 11: 3123-3135.

Kim, N., S.-y. N. Huang, J. S. Williams, Y. C. Li, A. B. Clark *et al.*, 2011 Mutagenic Processing of Ribonucleotides in DNA by Yeast Topoisomerase I. Science 332: 1561-1564.

Kim, N., and S. Jinks-Robertson, 2009 dUTP incorporation into genomic DNA is linked to transcription in yeast. Nature 459: 1150.

Kleczkowska, H. E., G. Marra, T. Lettieri and J. Jiricny, 2001 hMSH3 and hMSH6 interact with PCNA and colocalize with it to replication foci. Genes Dev 15: 724-736.

Koh, K. D., S. Balachander, J. R. Hesselberth and F. Storici, 2015 Ribose-seq: global mapping of ribonucleotides embedded in genomic DNA. Nature Methods 12: 251.

Kohalmi, S. E., M. Glattke, E. M. McIntosh and B. A. Kunz, 1991 Mutational specificity of DNA precursor pool imbalances in yeast arising from deoxycytidylate deaminase deficiency or treatment with thymidylate. Journal of Molecular Biology 220: 933-946.

Kohnken, R., K. M. Kodigepalli and L. Wu, 2015 Regulation of deoxynucleotide metabolism in cancer: novel mechanisms and therapeutic implications. Molecular Cancer 14: 176.

Kolas, N. K., A. Svetlanov, M. L. Lenzi, F. P. Macaluso, S. M. Lipkin *et al.*, 2005 Localization of MMR proteins on meiotic chromosomes in mice indicates distinct functions during prophase I. J Cell Biol 171: 447-458.

Kolodner, R. D., 2016 A personal historical view of DNA mismatch repair with an emphasis on eukaryotic DNA mismatch repair. DNA Repair (Amst) 38: 3-13.

Kool, E. T., 2002 Active Site Tightness and Substrate Fit in DNA Replication. Annual Review of Biochemistry 71: 191-219.

Koren, A., I. Soifer and N. Barkai, 2010 MRC1-dependent scaling of the budding yeast DNA replication timing program. Genome Res 20: 781-790.

Krishna, T. S. R., X.-P. Kong, S. Gary, P. M. Burgers and J. Kuriyan, 1994 Crystal structure of the eukaryotic DNA polymerase processivity factor PCNA. Cell 79: 1233-1243.

Kroutil, L. C., K. Register, K. Bebenek and T. A. Kunkel, 1996 Exonucleolytic Proofreading during Replication of Repetitive DNA. Biochemistry 35: 1046-1053.

Kubota, T., K. Nishimura, M. T. Kanemaki and A. D. Donaldson, 2013 The Elg1 replication factor C-like complex functions in PCNA unloading during DNA replication. Mol Cell 50: 273-280.

Kumar, D., A. L. Abdulovic, J. Viberg, A. K. Nilsson, T. A. Kunkel *et al.*, 2011 Mechanisms of mutagenesis in vivo due to imbalanced dNTP pools. Nucleic Acids Res 39: 1360-1371.

Kumar, D., J. Viberg, A. K. Nilsson and A. Chabes, 2010 Highly mutagenic and severely imbalanced dNTP pools can escape detection by the S-phase checkpoint. Nucleic Acids Res 38: 3975-3983.

Kunkel, T. A., 1992 Biological asymmetries and the fidelity of eukaryotic DNA replication. BioEssays 14: 303-308.

Kunkel, T. A., 2009 Evolving views of DNA replication (in)fidelity. Cold Spring Harb Symp Quant Biol 74: 91-101.

Kunkel, T. A., and D. A. Erie, 2015 Eukaryotic Mismatch Repair in Relation to DNA Replication. Annu Rev Genet 49: 291-313.

Kunkel, T. A., R. K. Hamatake, J. Motto-Fox, M. P. Fitzgerald and A. Sugino, 1989 Fidelity of DNA polymerase I and the DNA polymerase I-DNA primase complex from Saccharomyces cerevisiae. Molecular and Cellular Biology 9: 4447-4458.

Kunz, B. A., S. E. Kohalmi, T. A. Kunkel, C. K. Mathews, E. M. McIntosh *et al.*, 1994 International Commission for Protection Against Environmental Mutagens and Carcinogens. Deoxyribonucleoside triphosphate levels: a critical factor in the maintenance of genetic stability. Mutat Res 318: 1-64.

Kuo, C. L., and J. L. Campbell, 1983 Cloning of Saccharomyces cerevisiae DNA replication genes: isolation of the CDC8 gene and two genes that compensate for the cdc8-1 mutation. Molecular and Cellular Biology 3: 1730-1737.

Laguette, N., B. Sobhian, N. Casartelli, M. Ringeard, C. Chable-Bessia *et al.*, 2011 SAMHD1 is the dendritic- and myeloid-cell-specific HIV-1 restriction factor counteracted by Vpx. Nature 474: 654.

Lamb, A. L., A. S. Torres, T. V. O'Halloran and A. C. Rosenzweig, 2000 Heterodimer Formation between Superoxide Dismutase and Its Copper Chaperone. Biochemistry 39: 14720-14727.

Lang, G. I., and A. W. Murray, 2008 Estimating the per-base-pair mutation rate in the yeast Saccharomyces cerevisiae. Genetics 178: 67-82.

Lang, G. I., L. Parsons and A. E. Gammie, 2013 Mutation rates, spectra, and genome-wide distribution of spontaneous mutations in mismatch repair deficient yeast. G3 (Bethesda) 3: 1453-1465.

Lange, S. S., K. Takata and R. D. Wood, 2011 DNA polymerases and cancer. Nat Rev Cancer 11: 96-110.

Langle-Rouault, F., G. Maenhaut-Michel and M. Radman, 1987 GATC sequences, DNA nicks and the MutH function in Escherichia coli mismatch repair. EMBO J 6: 1121-1127.

Lee, Y. D., and S. J. Elledge, 2006 Control of ribonucleotide reductase localization through an anchoring mechanism involving Wtm1. Genes & Development 20: 334-344.

Lee, Y. D., J. Wang, J. Stubbe and S. J. Elledge, 2008 Dif1 Is a DNA-Damage-Regulated Facilitator of Nuclear Import for Ribonucleotide Reductase. Molecular Cell 32: 70-80.

Li, L., K. M. Murphy, U. Kanevets and L. J. Reha-Krantz, 2005 Sensitivity to phosphonoacetic acid: a new phenotype to probe DNA polymerase delta in Saccharomyces cerevisiae. Genetics 170: 569-580.

Li, Z., A. H. Pearlman and P. Hsieh, 2016 DNA mismatch repair and the DNA damage response. DNA Repair 38: 94-101.

Liberti, S. E., A. A. Larrea and T. A. Kunkel, 2013 Exonuclease 1 preferentially repairs mismatches generated by DNA polymerase alpha. DNA Repair (Amst) 12: 92-96.

Lill, R., and U. Mühlenhoff, 2008 Maturation of Iron-Sulfur Proteins in Eukaryotes: Mechanisms, Connected Processes, and Diseases. Annual Review of Biochemistry 77: 669-700.

Loeb, L. A., 2001 A Mutator Phenotype in Cancer. Cancer Research 61: 3230-3239.

Longhese, M. P., P. Plevani and G. Lucchini, 1994 Replication factor A is required in vivo for DNA replication, repair, and recombination. Molecular and Cellular Biology 14: 7884-7890.

Longley, D. B., D. P. Harkin and P. G. Johnston, 2003 5-fluorouracil: mechanisms of action and clinical strategies. Nat Rev Cancer 3: 330-338.

Lu, Q., X. Zhang, N. Almaula, C. K. Mathews and M. Inouye, 1995 The Gene for Nucleoside Diphosphate Kinase Functions as a Mutator Gene inEscherichia coli. Journal of Molecular Biology 254: 337-341.

Lujan, S. A., A. R. Clausen, A. B. Clark, H. K. MacAlpine, D. M. MacAlpine *et al.*, 2014 Heterogeneous polymerase fidelity and mismatch repair bias genome variation and composition. Genome Res 24: 1751-1764.

Lujan, S. A., J. S. Williams, A. R. Clausen, A. B. Clark and T. A. Kunkel, 2013 Ribonucleotides are signals for mismatch repair of leading-strand replication errors. Mol Cell 50: 437-443.

Lujan, S. A., J. S. Williams and T. A. Kunkel, 2016 DNA Polymerases Divide the Labor of Genome Replication. Trends Cell Biol 26: 640-654.

Lynch, M., W. Sung, K. Morris, N. Coffey, C. R. Landry *et al.*, 2008 A genome-wide view of the spectrum of spontaneous mutations in yeast. Proceedings of the National Academy of Sciences 105: 9272-9277.

MacFarlane, A. J., D. D. Anderson, P. Flodby, C. A. Perry, R. H. Allen *et al.*, 2011 Nuclear Localization of de Novo Thymidylate Biosynthesis Pathway Is Required to Prevent Uracil Accumulation in DNA. Journal of Biological Chemistry 286: 44015-44022.

MacFarlane, A. J., X. Liu, C. A. Perry, P. Flodby, R. H. Allen *et al.*, 2008 Cytoplasmic Serine Hydroxymethyltransferase Regulates the Metabolic Partitioning of Methylenetetrahydrofolate but Is Not Essential in Mice. Journal of Biological Chemistry 283: 25846-25853.

Magdalou, I., B. S. Lopez, P. Pasero and S. A. E. Lambert, 2014 The causes of replication stress and their consequences on genome stability and cell fate. Seminars in Cell & Developmental Biology 30: 154-164.
Maicher, A., I. Gazy, S. Sharma, L. Marjavaara, G. Grinberg *et al.*, 2017 Rnr1, but not Rnr3, facilitates the sustained telomerase-dependent elongation of telomeres. PLoS Genet 13: e1007082.
Mailand, N., I. Gibbs-Seymour and S. Bekker-Jensen, 2013 Regulation of PCNA–protein interactions for genome stability. Nature Reviews Molecular Cell Biology 14: 269.
Makarova, K. S., E. V. Koonin and Z. Kelman, 2012 The CMG (CDC45/RecJ, MCM, GINS) complex is a conserved component of the DNA replication system in all archaea and eukaryotes. Biology Direct 7: 7.
Manhart, C. M., and E. Alani, 2016 Roles for mismatch repair family proteins in promoting meiotic crossing over. DNA Repair 38: 84-93.
Marsischky, G. T., N. Filosi, M. F. Kane and R. Kolodner, 1996 Redundancy of Saccharomyces cerevisiae MSH3 and MSH6 in MSH2-dependent mismatch repair. Genes Dev 10: 407-420.
Martomo, S. A., and C. K. Mathews, 2002 Effects of biological DNA precursor pool asymmetry upon accuracy of DNA replication in vitro. Mutation Research/Fundamental and Molecular Mechanisms of Mutagenesis 499: 197-211.
Masselot, M., and H. De Robichon-Szulmajster, 1975 Methionine biosynthesis in Saccharomyces cerevisiae. I. Genetical analysis of auxotrophic mutants. Mol Gen Genet 139: 121-132.
Mathews, C. K., 2006 DNA precursor metabolism and genomic stability. The FASEB Journal 20: 1300-1314.
Mathews, C. K., 2015 Deoxyribonucleotide metabolism, mutagenesis and cancer. Nature Reviews Cancer 15: 528.
Mathews, C. K., and J. Ji, 1992 DNA precursor asymmetries, replication fidelity, and variable genome evolution. BioEssays 14: 295-301.
Mattano, S. S., T. D. Palella and B. S. Mitchell, 1990 Mutations Induced at the Hypoxanthine-Guanine Phosphoribosyltransferase Locus of Human T-Lymphoblasts by Perturbations of Purine Deoxyribonucleoside Triphosphate Pools. Cancer Research 50: 4566-4571.
McBurney, M. W., and G. F. Whitmore, 1974 Isolation and biochemical characterization of folate deficient mutants of chinese hamster cells. Cell 2: 173-182.
McCulloch, S. D., and T. A. Kunkel, 2008 The fidelity of DNA synthesis by eukaryotic replicative and translesion synthesis polymerases. Cell Res 18: 148-161.
McIntosh, E. M., and R. H. Haynes, 1984 Isolation of a Saccharomyces cerevisiae mutant strain deficient in deoxycytidylate deaminase activity and partial characterization of the enzyme. Journal of Bacteriology 158: 644-649.
McNeil, J. B., E. M. McIntosh, B. V. Taylor, F. R. Zhang, S. Tang *et al.*, 1994 Cloning and molecular characterization of three genes, including two genes encoding serine hydroxymethyltransferases, whose inactivation is required to render yeast auxotrophic for glycine. J Biol Chem 269: 9155-9165.
Mertz, T. M., S. Sharma, A. Chabes and P. V. Shcherbakova, 2015 Colon cancer-associated mutator DNA polymerase δ variant causes expansion of dNTP pools increasing its own infidelity. Proceedings of the National Academy of Sciences 112: E2467-E2476.
Merz, S., and B. Westermann, 2009 Genome-wide deletion mutant analysis reveals genes required for respiratory growth, mitochondrial genome maintenance and mitochondrial protein synthesis in Saccharomyces cerevisiae. Genome Biology 10: R95.
Meurisse, J., A. Bacquin, N. Richet, J.-B. Charbonnier, F. Ochsenbein *et al.*, 2014 Hug1 is an intrinsically disordered protein that inhibits ribonucleotide reductase activity by directly binding Rnr2 subunit. Nucleic Acids Research 42: 13174-13185.
Miller, J. H., P. Funchain, W. Clendenin, T. Huang, A. Nguyen *et al.*, 2002 *Escherichia coli* Strains (*ndk)* Lacking Nucleoside Diphosphate Kinase Are Powerful Mutators for Base Substitutions and Frameshifts in Mismatch-Repair-Deficient Strains. Genetics 162: 5-13.
Miyabe, I., T. A. Kunkel and A. M. Carr, 2011 The Major Roles of DNA Polymerases Epsilon and Delta at the Eukaryotic Replication Fork Are Evolutionarily Conserved. PLOS Genetics 7: e1002407.
Mnaimneh, S., A. P. Davierwala, J. Haynes, J. Moffat, W.-T. Peng *et al.*, 2004 Exploration of Essential Gene Functions via Titratable Promoter Alleles. Cell 118: 31-44.
Mohanty, B. K., N. K. Bairwa and D. Bastia, 2006 The Tof1p-Csm3p protein complex counteracts the Rrm3p helicase to control replication termination of Saccharomyces cerevisiae. Proc Natl Acad Sci U S A 103: 897-902.
Morrison, A., H. Araki, A. B. Clark, R. K. Hamatake and A. Sugino, 1990 A third essential DNA polymerase in S. cerevisiae. Cell 62: 1143-1151.
Morrison, A., J. B. Bell, T. A. Kunkel and A. Sugino, 1991 Eukaryotic DNA polymerase amino acid sequence required for 3'----5' exonuclease activity. Proc Natl Acad Sci U S A 88: 9473-9477.
Morrison, A., A. L. Johnson, L. H. Johnston and A. Sugino, 1993 Pathway correcting DNA replication errors in Saccharomyces cerevisiae. EMBO J 12: 1467-1473.
Morrison, A., and A. Sugino, 1994 The 3'-->5' exonucleases of both DNA polymerases delta and epsilon participate in correcting errors of DNA replication in Saccharomyces cerevisiae. Mol Gen Genet 242: 289-296.
Muramatsu, S., K. Hirai, Y.-S. Tak, Y. Kamimura and H. Araki, 2010 CDK-dependent complex formation between replication proteins Dpb11, Sld2, Pol ε, and GINS in budding yeast. Genes & Development 24: 602-612.
Murima, P., J. D. McKinney and K. Pethe, 2014 Targeting bacterial central metabolism for drug development. Chem Biol 21: 1423-1432.
Navas, T. A., Z. Zhou and S. J. Elledge, 1995 DNA polymerase epsilon links the DNA replication machinery to the S phase checkpoint. Cell 80: 29-39.
Neil, G. L., A. E. Berger, R. P. McPartland, G. B. Grindey, A. Bloch *et al.*, 1979 Biochemical and Pharmacological Effects of the Fermentation-derived Antitumor Agent, (α*S*,5*S*)-α-Amino-3-chloro-4,5-dihydro-5-isoxazoleacetic Acid (AT-125). Cancer Research 39: 852-856.
Nick McElhinny, S. A., D. A. Gordenin, C. M. Stith, P. M. Burgers and T. A. Kunkel, 2008 Division of labor at the eukaryotic replication fork. Mol Cell 30: 137-144.
Nick McElhinny, S. A., D. Kumar, A. B. Clark, D. L. Watt, B. E. Watts *et al.*, 2010a Genome instability due to ribonucleotide incorporation into DNA. Nat Chem Biol 6: 774-781.
Nick McElhinny, S. A., C. M. Stith, P. M. Burgers and T. A. Kunkel, 2007 Inefficient proofreading and biased error rates during inaccurate DNA synthesis by a mutant derivative of Saccharomyces cerevisiae DNA polymerase delta. J Biol Chem 282: 2324-2332.
Nick McElhinny, S. A., B. E. Watts, D. Kumar, D. L. Watt, E.-B. Lundström *et al.*, 2010b Abundant ribonucleotide incorporation into DNA by yeast replicative polymerases. Proceedings of the National Academy of Sciences 107: 4949-4954.

Niimi, A., S. Limsirichaikul, S. Yoshida, S. Iwai, C. Masutani *et al.*, 2004 Palm Mutants in DNA Polymerases α and η Alter DNA Replication Fidelity and Translesion Activity. Molecular and Cellular Biology 24**:** 2734-2746.
Nikkanen, J., S. Forsström, L. Euro, I. Paetau, Rebecca A. Kohnz *et al.*, 2016 Mitochondrial DNA Replication Defects Disturb Cellular dNTP Pools and Remodel One-Carbon Metabolism. Cell Metabolism 23**:** 635-648.
Nishant, K. T., A. J. Plys and E. Alani, 2008 A mutation in the putative MLH3 endonuclease domain confers a defect in both mismatch repair and meiosis in Saccharomyces cerevisiae. Genetics 179**:** 747-755.
Nordlund, P., and P. Reichard, 2006 Ribonucleotide reductases. Annu Rev Biochem 75**:** 681-706.
Nzila, A., 2006 The past, present and future of antifolates in the treatment of Plasmodium falciparum infection. J Antimicrob Chemother 57**:** 1043-1054.
O'Rourke, T. W., N. A. Doudican, H. Zhang, J. S. Eaton, P. W. Doetsch *et al.*, 2005 Differential involvement of the related DNA helicases Pif1p and Rrm3p in mtDNA point mutagenesis and stability. Gene 354**:** 86-92.
Okazaki, R., T. Okazaki, K. Sakabe, K. Sugimoto and A. Sugino, 1968 Mechanism of DNA chain growth. I. Possible discontinuity and unusual secondary structure of newly synthesized chains. Proc Natl Acad Sci U S A 59**:** 598-605.
Ozier-Kalogeropoulos, O., M. T. Adeline, W. L. Yang, G. M. Carman and F. Lacroute, 1994 Use of synthetic lethal mutants to clone and characterize a novel CTP synthetase gene in Saccharomyces cerevisiae. Mol Gen Genet 242**:** 431-439.
Ozier-Kalogeropoulos, O., F. Fasiolo, M. T. Adeline, J. Collin and F. Lacroute, 1991 Cloning, sequencing and characterization of the Saccharomyces cerevisiae URA7 gene encoding CTP synthetase. Mol Gen Genet 231**:** 7-16.
Pai, C. C., and S. Kearsey, 2017 A Critical Balance: dNTPs and the Maintenance of Genome Stability. Genes 8**:** 57.
Palles, C., J. B. Cazier, K. M. Howarth, E. Domingo, A. M. Jones *et al.*, 2013 Germline mutations affecting the proofreading domains of POLE and POLD1 predispose to colorectal adenomas and carcinomas. Nat Genet 45**:** 136-144.
Pan, M., M. A. Reid, X. H. Lowman, R. P. Kulkarni, T. Q. Tran *et al.*, 2016 Regional glutamine deficiency in tumours promotes dedifferentiation through inhibition of histone demethylation. Nature Cell Biology 18**:** 1090.
Paone, A., M. Marani, A. Fiascarelli, S. Rinaldo, G. Giardina *et al.*, 2014 SHMT1 knockdown induces apoptosis in lung cancer cells by causing uracil misincorporation. Cell Death Dis 5**:** e1525.
Papadopoulou, C., G. Guilbaud, D. Schiavone and Julian E. Sale, 2015 Nucleotide Pool Depletion Induces G-Quadruplex-Dependent Perturbation of Gene Expression. Cell Reports 13**:** 2491-2503.
Pardo, B., L. Crabbé and P. Pasero, 2017 Signaling pathways of replication stress in yeast. FEMS Yeast Research 17**:** fow101-fow101.
Pavlov, Y. I., C. Frahm, S. A. Nick McElhinny, A. Niimi, M. Suzuki *et al.*, 2006 Evidence that errors made by DNA polymerase alpha are corrected by DNA polymerase delta. Curr Biol 16**:** 202-207.
Peltomaki, P., 2003 Role of DNA mismatch repair defects in the pathogenesis of human cancer. J Clin Oncol 21**:** 1174-1179.
Petruska, J., and M. F. Goodman, 1995 Enthalpy-Entropy Compensation in DNA Melting Thermodynamics. Journal of Biological Chemistry 270**:** 746-750.
Pluciennik, A., L. Dzantiev, R. R. Iyer, N. Constantin, F. A. Kadyrov *et al.*, 2010 PCNA function in the activation and strand direction of MutLalpha endonuclease in mismatch repair. Proc Natl Acad Sci U S A 107**:** 16066-16071.
Poli, J., O. Tsaponina, L. Crabbé, A. Keszthelyi, V. Pantesco *et al.*, 2012 dNTP pools determine fork progression and origin usage under replication stress. The EMBO Journal 31**:** 883-894.
Poloumienko, A., A. Dershowitz, J. De, C. S. Newlon and T. Stearns, 2001 Completion of Replication Map of Saccharomyces cerevisiae Chromosome III. Molecular Biology of the Cell 12**:** 3317-3327.
Powell, R. D., P. J. Holland, T. Hollis and F. W. Perrino, 2011 Aicardi-Goutières Syndrome Gene and HIV-1 Restriction Factor SAMHD1 Is a dGTP-regulated Deoxynucleotide Triphosphohydrolase. Journal of Biological Chemistry 286**:** 43596-43600.
Prakash, S., and L. Prakash, 2002 Translesion DNA synthesis in eukaryotes: A one- or two-polymerase affair. Genes & Development 16**:** 1872-1883.
Prindle, M. J., and L. A. Loeb, 2012 DNA polymerase delta in DNA replication and genome maintenance. Environ Mol Mutagen 53**:** 666-682.
Prolla, T. A., S. M. Baker, A. C. Harris, J. L. Tsao, X. Yao *et al.*, 1998 Tumour susceptibility and spontaneous mutation in mice deficient in Mlh1, Pms1 and Pms2 DNA mismatch repair. Nat Genet 18**:** 276-279.
Pursell, Z. F., I. Isoz, E. B. Lundstrom, E. Johansson and T. A. Kunkel, 2007 Yeast DNA polymerase epsilon participates in leading-strand DNA replication. Science 317**:** 127-130.
Putnam, C. D., 2016 Evolution of the methyl directed mismatch repair system in Escherichia coli. DNA Repair 38**:** 32-41.
Putnam, C. D., T. K. Hayes and R. D. Kolodner, 2009 Specific pathways prevent duplication-mediated genome rearrangements. Nature 460**:** 984-989.
Putnam, C. D., and R. D. Kolodner, 2010 Determination of gross chromosomal rearrangement rates. Cold Spring Harb Protoc 2010**:** pdb prot5492.
Putnam, C. D., and R. D. Kolodner, 2017 Pathways and Mechanisms that Prevent Genome Instability in *Saccharomyces cerevisiae*. Genetics 206**:** 1187-1225.
Que, B. G., K. M. Downey and A. G. So, 1978 Mechanisms of selective inhibition of 3' to 5' exonuclease activity of Escherichia coli DNA polymerase I by nucleoside 5'-monophosphates. Biochemistry 17**:** 1603-1606.
Raghuraman, M. K., E. A. Winzeler, D. Collingwood, S. Hunt, L. Wodicka *et al.*, 2001 Replication dynamics of the yeast genome. Science 294**:** 115-121.
Raz, S., M. Stark and Y. G. Assaraf, 2016 Folylpoly-γ-glutamate synthetase: A key determinant of folate homeostasis and antifolate resistance in cancer. Drug Resistance Updates 28**:** 43-64.
Reenan, R. A., and R. D. Kolodner, 1992 Characterization of insertion mutations in the Saccharomyces cerevisiae MSH1 and MSH2 genes: evidence for separate mitochondrial and nuclear functions. Genetics 132**:** 975-985.
Reha-Krantz, L. J., 2010 DNA polymerase proofreading: Multiple roles maintain genome stability. Biochim Biophys Acta 1804**:** 1049-1063.
Reha-Krantz, L. J., and R. L. Nonay, 1994 Motif A of bacteriophage T4 DNA polymerase: role in primer extension and DNA replication fidelity. Isolation of new antimutator and mutator DNA polymerases. Journal of Biological Chemistry 269**:** 5635-5643.
Reichard, P., 1988 Interactions Between Deoxyribonucleotide and DNA Synthesis. Annual Review of Biochemistry 57**:** 349-374.

Reijns, M. A., H. Kemp, J. Ding, S. M. de Proce, A. P. Jackson *et al.*, 2015 Lagging-strand replication shapes the mutational landscape of the genome. Nature 518**:** 502-506.
Reijns, Martin A. M., B. Rabe, Rachel E. Rigby, P. Mill, Katy R. Astell *et al.*, 2012 Enzymatic Removal of Ribonucleotides from DNA Is Essential for Mammalian Genome Integrity and Development. Cell 149**:** 1008-1022.
Rentoft, M., K. Lindell, P. Tran, A. L. Chabes, R. J. Buckland *et al.*, 2016 Heterozygous colon cancer-associated mutations of *SAMHD1* have functional significance. Proceedings of the National Academy of Sciences 113**:** 4723-4728.
Reyes, G. X., T. T. Schmidt, R. D. Kolodner and H. Hombauer, 2015 New insights into the mechanism of DNA mismatch repair. Chromosoma.
Ritter, E. J., W. J. Scott, J. G. Wilson, B. C. Lampkin and J. E. Neely, 1980 Effect of 5-fluoro-2'-deoxyuridine on deoxyribonucleotide pools in vivo. J Natl Cancer Inst 65**:** 603-605.
Roberts, J. D., and T. A. Kunkel, 1988 Fidelity of a human cell DNA replication complex. Proceedings of the National Academy of Sciences 85**:** 7064-7068.
Roberts, J. D., D. Nguyen and T. A. Kunkel, 1993 Frameshift fidelity during replication of double-stranded DNA in HeLa cell extracts. Biochemistry 32**:** 4083-4089.
Roberts, J. D., D. C. Thomas and T. A. Kunkel, 1991 Exonucleolytic proofreading of leading and lagging strand DNA replication errors. Proceedings of the National Academy of Sciences 88**:** 3465-3469.
Ross-Macdonald, P., and G. S. Roeder, 1994 Mutation of a meiosis-specific MutS homolog decreases crossing over but not mismatch correction. Cell 79**:** 1069-1080.
Rouse, J., and S. P. Jackson, 2002 Interfaces Between the Detection, Signaling, and Repair of DNA Damage. Science 297**:** 547-551.
Rubinstein, L., L. Ungar, Y. Harari, V. Babin, S. Ben-Aroya *et al.*, 2014 Telomere length kinetics assay (TELKA) sorts the telomere length maintenance (tlm) mutants into functional groups. Nucleic Acids Res 42**:** 6314-6325.
Sanchez-Pulido, L., and C. P. Ponting, 2011 Cdc45: the missing RecJ ortholog in eukaryotes? Bioinformatics 27**:** 1885-1888.
Sanchez, A., S. Sharma, S. Rozenzhak, A. Roguev, N. J. Krogan *et al.*, 2012 Replication fork collapse and genome instability in a deoxycytidylate deaminase mutant. Mol Cell Biol 32**:** 4445-4454.
Santucci-Darmanin, S., S. Neyton, F. Lespinasse, A. Saunieres, P. Gaudray *et al.*, 2002 The DNA mismatch-repair MLH3 protein interacts with MSH4 in meiotic cells, supporting a role for this MutL homolog in mammalian meiotic recombination. Hum Mol Genet 11**:** 1697-1706.
Schirch, V., and W. B. Strong, 1989 Interaction of folylpolyglutamates with enzymes in one-carbon metabolism. Arch Biochem Biophys 269**:** 371-380.
Schmidt, T. T., G. Reyes, K. Gries, C. U. Ceylan, S. Sharma *et al.*, 2017 Alterations in cellular metabolism triggered by URA7 or GLN3 inactivation cause imbalanced dNTP pools and increased mutagenesis. Proc Natl Acad Sci U S A 114**:** E4442-E4451.
Scott, A. D., M. Neishabury, D. H. Jones, S. H. Reed, S. Boiteux *et al.*, 1999 Spontaneous mutation, oxidative DNA damage, and the roles of base and nucleotide excision repair in the yeast Saccharomyces cerevisiae. Yeast 15**:** 205-218.
Seiple, L., P. Jaruga, M. Dizdaroglu and J. T. Stivers, 2006 Linking uracil base excision repair and 5-fluorouracil toxicity in yeast. Nucleic Acids Res 34**:** 140-151.
Shcherbakova, P. V., Y. I. Pavlov, O. Chilkova, I. B. Rogozin, E. Johansson *et al.*, 2003 Unique Error Signature of the Four-subunit Yeast DNA Polymerase ϵ. Journal of Biological Chemistry 278**:** 43770-43780.
Shlien, A., B. B. Campbell, R. de Borja, L. B. Alexandrov, D. Merico *et al.*, 2015 Combined hereditary and somatic mutations of replication error repair genes result in rapid onset of ultra-hypermutated cancers. Nat Genet 47**:** 257-262.
Shlomai, J., and A. Kornberg, 1978 Deoxyuridine triphosphatase of Escherichia coli. Purification, properties, and use as a reagent to reduce uracil incorporation into DNA. Journal of Biological Chemistry 253**:** 3305-3312.
Sia, E. A., R. J. Kokoska, M. Dominska, P. Greenwell and T. D. Petes, 1997 Microsatellite instability in yeast: dependence on repeat unit size and DNA mismatch repair genes. Mol Cell Biol 17**:** 2851-2858.
Sikorski, R. S., and P. Hieter, 1989 A system of shuttle vectors and yeast host strains designed for efficient manipulation of DNA in Saccharomyces cerevisiae. Genetics 122**:** 19-27.
Smith, D. J., and I. Whitehouse, 2012 Intrinsic coupling of lagging-strand synthesis to chromatin assembly. Nature 483**:** 434.
Smith, S., J. Y. Hwang, S. Banerjee, A. Majeed, A. Gupta *et al.*, 2004 Mutator genes for suppression of gross chromosomal rearrangements identified by a genome-wide screening in Saccharomyces cerevisiae. Proc Natl Acad Sci U S A 101**:** 9039-9044.
Snowden, T., S. Acharya, C. Butz, M. Berardini and R. Fishel, 2004 hMSH4-hMSH5 recognizes Holliday Junctions and forms a meiosis-specific sliding clamp that embraces homologous chromosomes. Mol Cell 15**:** 437-451.
Song, S., Z. F. Pursell, W. C. Copeland, M. J. Longley, T. A. Kunkel *et al.*, 2005 DNA precursor asymmetries in mammalian tissue mitochondria and possible contribution to mutagenesis through reduced replication fidelity. Proceedings of the National Academy of Sciences of the United States of America 102**:** 4990-4995.
Srivatsan, A., N. Bowen and R. D. Kolodner, 2014 Mispair-specific recruitment of the Mlh1-Pms1 complex identifies repair substrates of the Saccharomyces cerevisiae Msh2-Msh3 complex. J Biol Chem 289**:** 9352-9364.
St Charles, J. A., S. E. Liberti, J. S. Williams, S. A. Lujan and T. A. Kunkel, 2015 Quantifying the contributions of base selectivity, proofreading and mismatch repair to nuclear DNA replication in Saccharomyces cerevisiae. DNA Repair (Amst) 31**:** 41-51.
Stinchcomb, D. T., K. Struhl and R. W. Davis, 1979 Isolation and characterisation of a yeast chromosomal replicator. Nature 282**:** 39-43.
Stirling, P. C., Y. Shen, R. Corbett, S. J. M. Jones and P. Hieter, 2014 Genome Destabilizing Mutator Alleles Drive Specific Mutational Trajectories in *Saccharomyces cerevisiae*. Genetics 196**:** 403-412.
Stocki, S. A., R. L. Nonay and L. J. Reha-Krantz, 1995 Dynamics of Bacteriophage T4 DNA Polymerase Function: Identification of Amino Acid Residues that Affect Switching between Polymerase and 3′ → 5′ Exonuclease Activities. Journal of Molecular Biology 254**:** 15-28.
Stover, P. J., and M. S. Field, 2011 Trafficking of intracellular folates. Adv Nutr 2**:** 325-331.
Syed, S., C. Desler, L. J. Rasmussen and K. H. Schmidt, 2016 A Novel Rrm3 Function in Restricting DNA Replication via an Orc5-Binding Domain Is Genetically Separable from Rrm3 Function as an ATPase/Helicase in Facilitating Fork Progression. PLOS Genetics 12**:** e1006451.
Takayama, Y., Y. Kamimura, M. Okawa, S. Muramatsu, A. Sugino *et al.*, 2003 GINS, a novel multiprotein complex required for chromosomal DNA replication in budding yeast. Genes & Development 17**:** 1153-1165.

Tanaka, H., H. Arakawa, T. Yamaguchi, K. Shiraishi, S. Fukuda *et al.*, 2000 A ribonucleotide reductase gene involved in a p53-dependent cell-cycle checkpoint for DNA damage. Nature 404**:** 42.
Tattersall, M. H., and K. R. Harrap, 1973 Changes in the deoxyribonucleoside triphosphate pools of mouse 5178Y lymphoma cells following exposure to methotrexate or 5-fluorouracil. Cancer Res 33**:** 3086-3090.
Taylor, G. R., B. J. Barclay, R. K. Storms, J. D. Friesen and R. H. Haynes, 1982 Isolation of the thymidylate synthetase gene (TMP1) by complementation in Saccharomyces cerevisiae. Molecular and Cellular Biology 2**:** 437-442.
Tham, K.-C., R. Kanaar and J. H. G. Lebbink, 2016 Mismatch repair and homeologous recombination. DNA Repair 38**:** 75-83.
Thomas, D. C., J. D. Roberts and T. A. Kunkel, 1991 Heteroduplex repair in extracts of human HeLa cells. J Biol Chem 266**:** 3744-3751.
Tinkelenberg, B. A., M. J. Hansbury and R. D. Ladner, 2002 dUTPase and Uracil-DNA Glycosylase Are Central Modulators of Antifolate Toxicity in *Saccharomyces cerevisiae*. Cancer Research 62**:** 4909-4915.
Tishkoff, D. X., N. S. Amin, C. S. Viars, K. C. Arden and R. D. Kolodner, 1998 Identification of a human gene encoding a homologue of Saccharomyces cerevisiae EXO1, an exonuclease implicated in mismatch repair and recombination. Cancer Res 58**:** 5027-5031.
Tishkoff, D. X., A. L. Boerger, P. Bertrand, N. Filosi, G. M. Gaida *et al.*, 1997 Identification and characterization of Saccharomyces cerevisiae EXO1, a gene encoding an exonuclease that interacts with MSH2. Proc Natl Acad Sci U S A 94**:** 7487-7492.
Tomasetti, C., L. Li and B. Vogelstein, 2017 Stem cell divisions, somatic mutations, cancer etiology, and cancer prevention. Science 355**:** 1330-1334.
Tong, A. H., and C. Boone, 2006 Synthetic genetic array analysis in Saccharomyces cerevisiae. Methods Mol Biol 313**:** 171-192.
Tran, H. T., D. A. Gordenin and M. A. Resnick, 1999 The 3'-->5' exonucleases of DNA polymerases delta and epsilon and the 5'-->3' exonuclease Exo1 have major roles in postreplication mutation avoidance in Saccharomyces cerevisiae. Mol Cell Biol 19**:** 2000-2007.
Tran, H. T., J. D. Keen, M. Kricker, M. A. Resnick and D. A. Gordenin, 1997 Hypermutability of homonucleotide runs in mismatch repair and DNA polymerase proofreading yeast mutants. Mol Cell Biol 17**:** 2859-2865.
Trudel, M., T. Van Genechten and M. Meuth, 1984 Biochemical characterization of the hamster thy mutator gene and its revertants. J Biol Chem 259**:** 2355-2359.
Tsaponina, O., E. Barsoum, S. U. Åström and A. Chabes, 2011 Ixr1 Is Required for the Expression of the Ribonucleotide Reductase Rnr1 and Maintenance of dNTP Pools. PLoS Genet 7**:** e1002061.
Tse, L., T. M. Kang, J. Yuan, D. Mihora, E. Becket *et al.*, 2016 Extreme dNTP pool changes and hypermutability in dcd ndk strains. Mutation Research/Fundamental and Molecular Mechanisms of Mutagenesis 784-785**:** 16-24.
Tsunehiro, F., N. Junichi, K. Narimichi and W. Kazutada, 1993 Isolation, overexpression and disruption of a Saccharomyces cerevisiae YNK gene encoding nucleoside diphosphate kinase. Gene 129**:** 141-146.
Uppsten, M., M. Färnegårdh, A. Jordan, R. Eliasson, H. Eklund *et al.*, 2003 Structure of the Large Subunit of Class Ib Ribonucleotide Reductase from Salmonella typhimurium and its Complexes with Allosteric Effectors. Journal of Molecular Biology 330**:** 87-97.
Van Triest, B., H. M. Pinedo, G. Giaccone and G. J. Peters, 2000 Downstream molecular determinants of response to 5-fluorouracil and antifolate thymidylate synthase inhibitors. Ann Oncol 11**:** 385-391.
Veatch, J. R., M. A. McMurray, Z. W. Nelson and D. E. Gottschling, 2009 Mitochondrial Dysfunction Leads to Nuclear Genome Instability via an Iron-Sulfur Cluster Defect. Cell 137**:** 1247-1258.
Venkatesan, R. N., J. J. Hsu, N. A. Lawrence, B. D. Preston and L. A. Loeb, 2006 Mutator phenotypes caused by substitution at a conserved motif A residue in eukaryotic DNA polymerase delta. J Biol Chem 281**:** 4486-4494.
Venkatesan, R. N., P. M. Treuting, E. D. Fuller, R. E. Goldsby, T. H. Norwood *et al.*, 2007 Mutation at the Polymerase Active Site of Mouse DNA Polymerase δ Increases Genomic Instability and Accelerates Tumorigenesis. Molecular and Cellular Biology 27**:** 7669-7682.
Venter, J. C., M. D. Adams, E. W. Myers, P. W. Li, R. J. Mural *et al.*, 2001 The Sequence of the Human Genome. Science 291**:** 1304-1351.
Visentin, M., R. Zhao and I. D. Goldman, 2012 The antifolates. Hematol Oncol Clin North Am 26**:** 629-648, ix.
Wach, A., A. Brachat, R. Pohlmann and P. Philippsen, 1994 New heterologous modules for classical or PCR-based gene disruptions in Saccharomyces cerevisiae. Yeast 10**:** 1793-1808.
Wang, J., G. J. S. Lohman and J. Stubbe, 2007 Enhanced subunit interactions with gemcitabine-5′-diphosphate inhibit ribonucleotide reductases. Proceedings of the National Academy of Sciences 104**:** 14324-14329.
Wang, J., G. J. S. Lohman and J. Stubbe, 2009 Mechanism of Inactivation of Human Ribonucleotide Reductase with p53R2 by Gemcitabine 5′-Diphosphate. Biochemistry 48**:** 11612-11621.
Wanrooij, P. H., M. K. M. Engqvist, J. M. E. Forslund, C. Navarrete, A. K. Nilsson *et al.*, 2017 Ribonucleotides incorporated by the yeast mitochondrial DNA polymerase are not repaired. Proceedings of the National Academy of Sciences 114**:** 12466-12471.
Warner, H. R., B. K. Duncan, C. Garrett and J. Neuhard, 1981 Synthesis and metabolism of uracil-containing deoxyribonucleic acid in Escherichia coli. Journal of Bacteriology 145**:** 687-695.
Watson, J. D., and F. H. Crick, 1953 Genetical implications of the structure of deoxyribonucleic acid. Nature 171**:** 964-967.
Watt, D. L., R. J. Buckland, S. A. Lujan, T. A. Kunkel and A. Chabes, 2016 Genome-wide analysis of the specificity and mechanisms of replication infidelity driven by imbalanced dNTP pools. Nucleic Acids Research 44**:** 1669-1680.
Weber, G., N. Prajda, M. S. Lui, J. E. Denton, T. Aoki *et al.*, 1982 Multi-enzyme-targeted chemotherapy by acivicin and actinomycin. Adv Enzyme Regul 20**:** 75-96.
Wei, K., A. B. Clark, E. Wong, M. F. Kane, D. J. Mazur *et al.*, 2003 Inactivation of Exonuclease 1 in mice results in DNA mismatch repair defects, increased cancer susceptibility, and male and female sterility. Genes Dev 17**:** 603-614.
Weinberg, G., B. Ullman and D. W. Martin, Jr., 1981 Mutator phenotypes in mammalian cell mutants with distinct biochemical defects and abnormal deoxyribonucleoside triphosphate pools. Proc Natl Acad Sci U S A 78**:** 2447-2451.
Weinberg, G. L., B. Ullman, C. M. Wright and D. W. Martin, Jr., 1985 The effects of exogenous thymidine on endogenous deoxynucleotides and mutagenesis in mammalian cells. Somat Cell Mol Genet 11**:** 413-419.
Wellinger, R. J., and V. A. Zakian, 2012 Everything You Ever Wanted to Know About *Saccharomyces cerevisiae* Telomeres: Beginning to End. Genetics 191**:** 1073-1105.
Welsh, K. M., A. L. Lu, S. Clark and P. Modrich, 1987 Isolation and characterization of the Escherichia coli mutH gene product. J Biol Chem 262**:** 15624-15629.

Whelan, W. L., E. Gocke and T. R. Manney, 1979 THE *CAN1* LOCUS OF *SACCHAROMYCES CEREVISIAE*: FINE-STRUCTURE ANALYSIS AND FORWARD MUTATION RATES. Genetics 91**:** 35-51.
Williams, J. S., S. A. Lujan and T. A. Kunkel, 2016 Processing ribonucleotides incorporated during eukaryotic DNA replication. Nat Rev Mol Cell Biol 17**:** 350-363.
Williams, L. N., A. J. Herr and B. D. Preston, 2013 Emergence of DNA polymerase epsilon antimutators that escape error-induced extinction in yeast. Genetics 193**:** 751-770.
Williams, L. N., L. Marjavaara, G. M. Knowels, E. M. Schultz, E. J. Fox *et al.*, 2015 dNTP pool levels modulate mutator phenotypes of error-prone DNA polymerase epsilon variants. Proc Natl Acad Sci U S A 112**:** E2457-2466.
Wise, D. R., and C. B. Thompson, 2010 Glutamine addiction: a new therapeutic target in cancer. Trends in Biochemical Sciences 35**:** 427-433.
Wyrick, J. J., J. G. Aparicio, T. Chen, J. D. Barnett, E. G. Jennings *et al.*, 2001 Genome-wide distribution of ORC and MCM proteins in S. cerevisiae: high-resolution mapping of replication origins. Science 294**:** 2357-2360.
Xu, H., C. Faber, T. Uchiki, J. W. Fairman, J. Racca *et al.*, 2006a Structures of eukaryotic ribonucleotide reductase I provide insights into dNTP regulation. Proceedings of the National Academy of Sciences of the United States of America 103**:** 4022-4027.
Xu, H., C. Faber, T. Uchiki, J. Racca and C. Dealwis, 2006b Structures of eukaryotic ribonucleotide reductase I define gemcitabine diphosphate binding and subunit assembly. Proceedings of the National Academy of Sciences of the United States of America 103**:** 4028-4033.
Yoshioka, A., S. Tanaka, O. Hiraoka, Y. Koyama, Y. Hirota *et al.*, 1987 Deoxyribonucleoside triphosphate imbalance. 5-Fluorodeoxyuridine-induced DNA double strand breaks in mouse FM3A cells and the mechanism of cell death. J Biol Chem 262**:** 8235-8241.
Yu, C., H. Gan, J. Han, Z. X. Zhou, S. Jia *et al.*, 2014 Strand-specific analysis shows protein binding at replication forks and PCNA unloading from lagging strands when forks stall. Mol Cell 56**:** 551-563.
Zanotti, K. J., and P. J. Gearhart, 2016 Antibody diversification caused by disrupted mismatch repair and promiscuous DNA polymerases. DNA Repair 38**:** 110-116.
Zhang, D., and M. O'Donnell, 2016 The Eukaryotic Replication Machine. Enzymes 39**:** 191-229.
Zhang, W., S. Tan, E. Paintsil, G. E. Dutschman, E. A. Gullen *et al.*, 2011 Analysis of deoxyribonucleotide pools in human cancer cell lines using a liquid chromatography coupled with tandem mass spectrometry technique. Biochemical Pharmacology 82**:** 411-417.
Zhang, Z., X. An, K. Yang, D. L. Perlstein, L. Hicks *et al.*, 2006 Nuclear localization of the *Saccharomyces cerevisiae* ribonucleotide reductase small subunit requires a karyopherin and a WD40 repeat protein. Proceedings of the National Academy of Sciences 103**:** 1422-1427.
Zhao, X., B. Georgieva, A. Chabes, V. Domkin, J. H. Ippel *et al.*, 2000 Mutational and Structural Analyses of the Ribonucleotide Reductase Inhibitor Sml1 Define Its Rnr1 Interaction Domain Whose Inactivation Allows Suppression of *mec1* and *rad53* Lethality. Molecular and Cellular Biology 20**:** 9076-9083.
Zhou, Z., and S. J. Elledge, 1993 DUN1 encodes a protein kinase that controls the DNA damage response in yeast. Cell 75**:** 1119-1127.

7 SUPPLEMENT

7 SUPPLEMENT

7.1 Supplementary data

Fig. S 7.1 *CAN1* mutation spectrum of the WT.
Genomic DNA of individual Can^R clones was purified, the *CAN1* gene amplified and sequenced. Individual mutations are shown.

Fig. S 7.2 *CAN1* mutation spectrum of *met7Δ*.
Genomic DNA of individual Can^R clones was purified, the *CAN1* gene amplified and sequenced. Individual mutations are shown.

Fig. S 7.3 *CAN1* mutation spectrum of *msh6Δ*.
Genomic DNA of individual Can^R clones was purified, the *CAN1* gene amplified and sequenced. Individual mutations are shown. Mutational hotspots are indicated in blue.

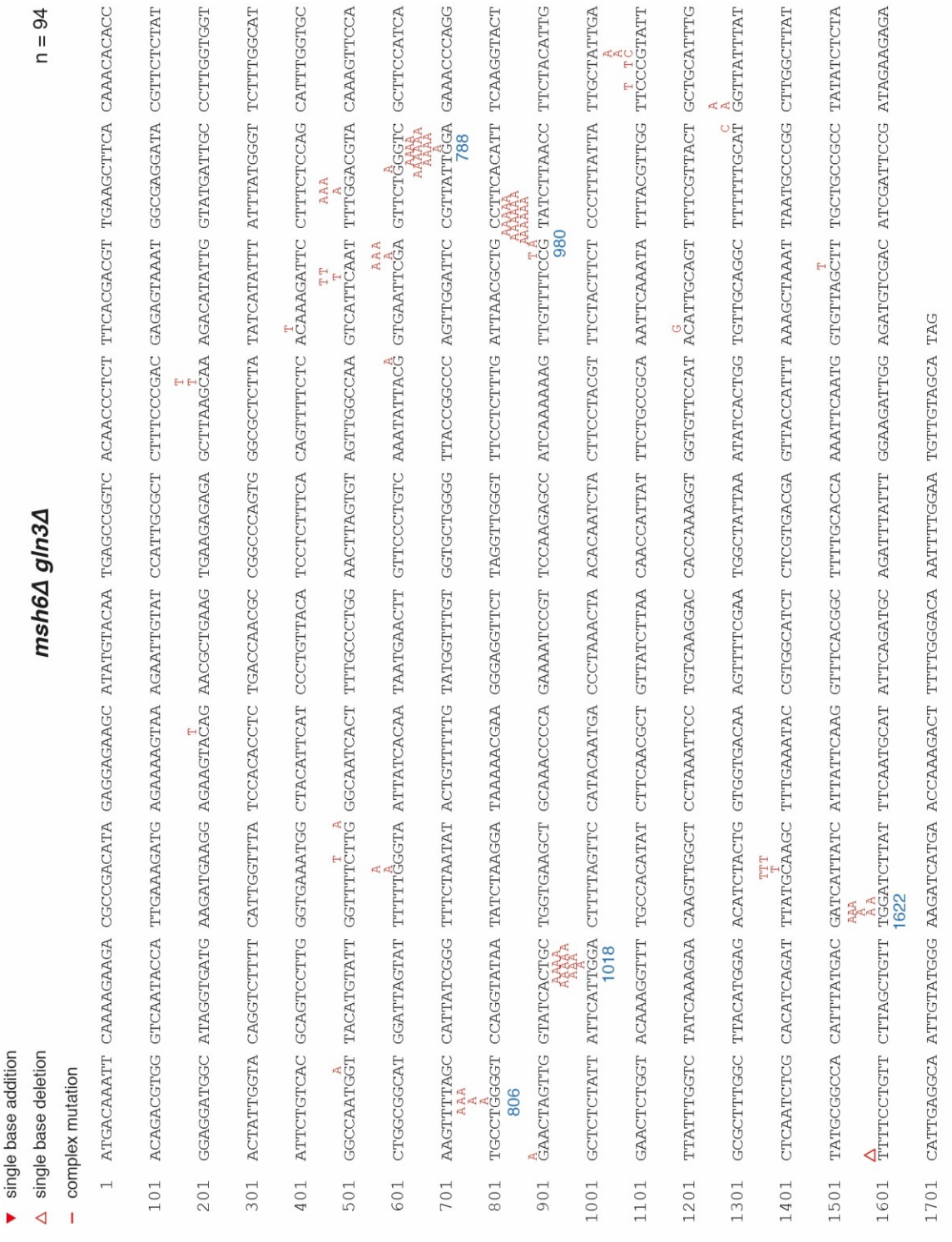

Fig. S 7.4 *CAN1* mutation spectrum of *msh6Δ gln3Δ*.
Genomic DNA of individual Can^R clones was purified, the *CAN1* gene amplified and sequenced. Individual mutations are shown. Mutational hotspots are indicated in blue.

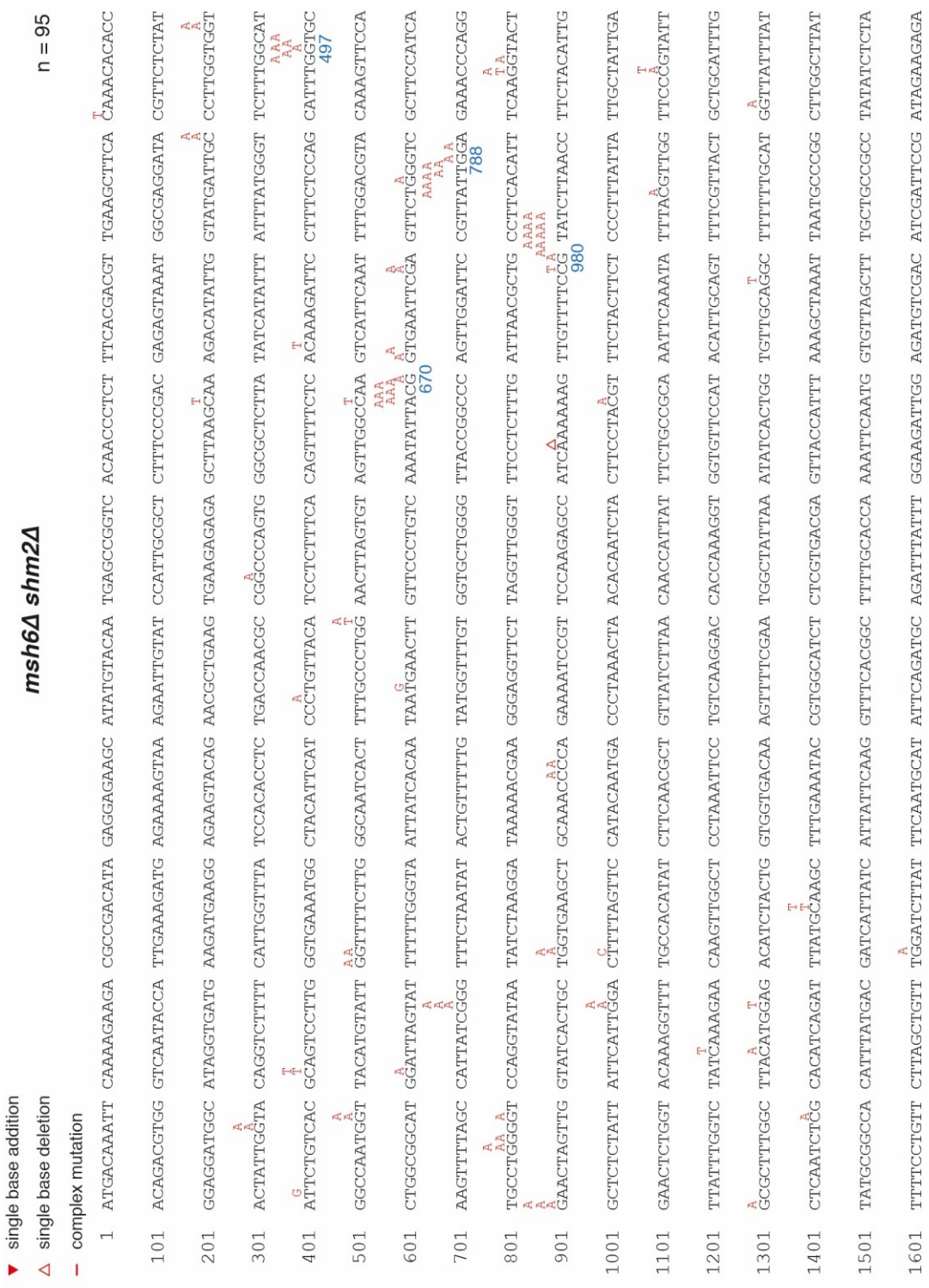

Fig. S 7.5 *CAN1* mutation spectrum of *msh6Δ shm2Δ*.
Genomic DNA of individual Can^R clones was purified, the *CAN1* gene amplified and sequenced. Individual mutations are shown. Mutational hotspots are indicated in blue.

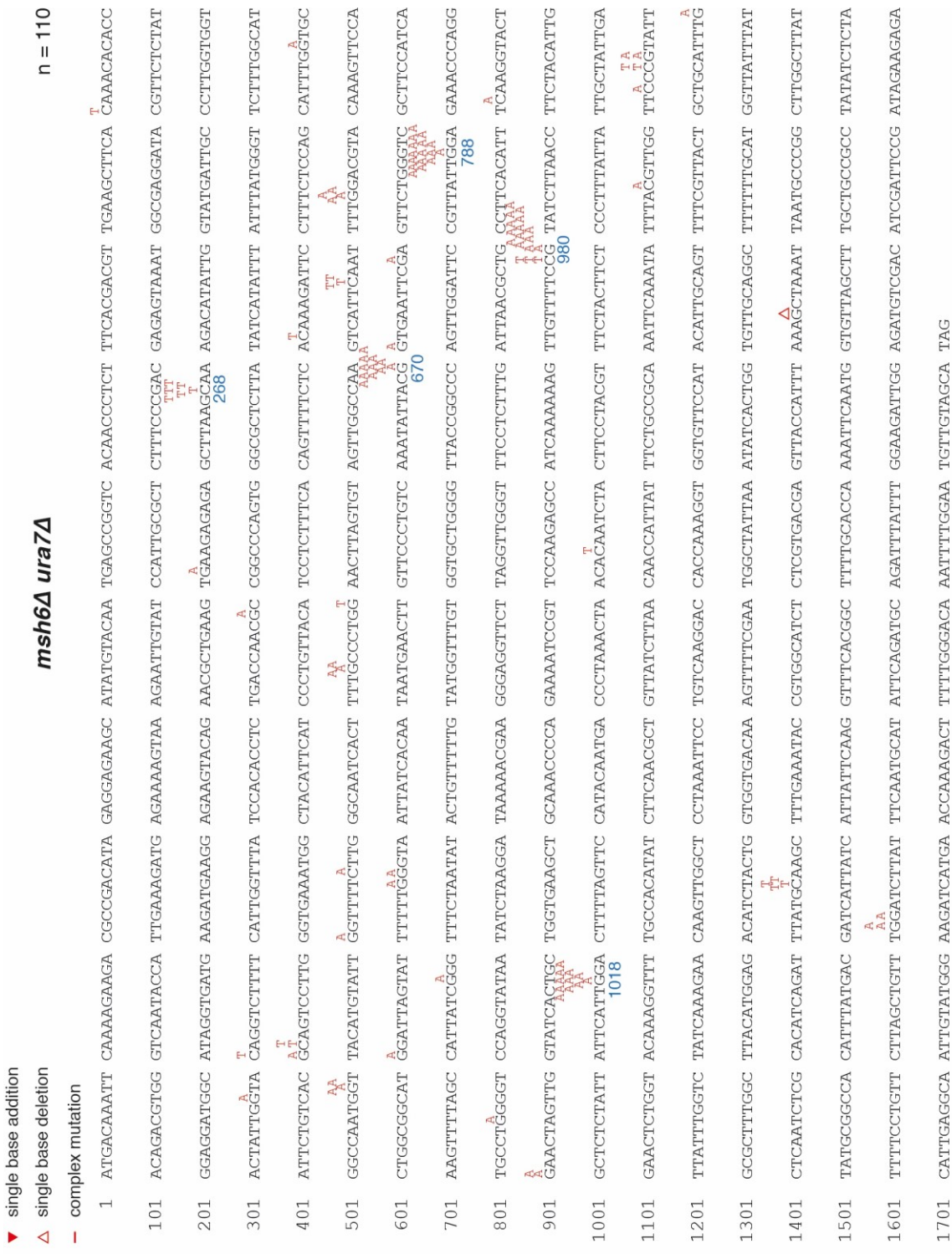

Fig. S 7.6 *CAN1* mutation spectrum of *msh6Δ ura7Δ*.
Genomic DNA of individual Can^R clones was purified, the *CAN1* gene amplified and sequenced. Individual mutations are shown. Mutational hotspots are indicated in blue.

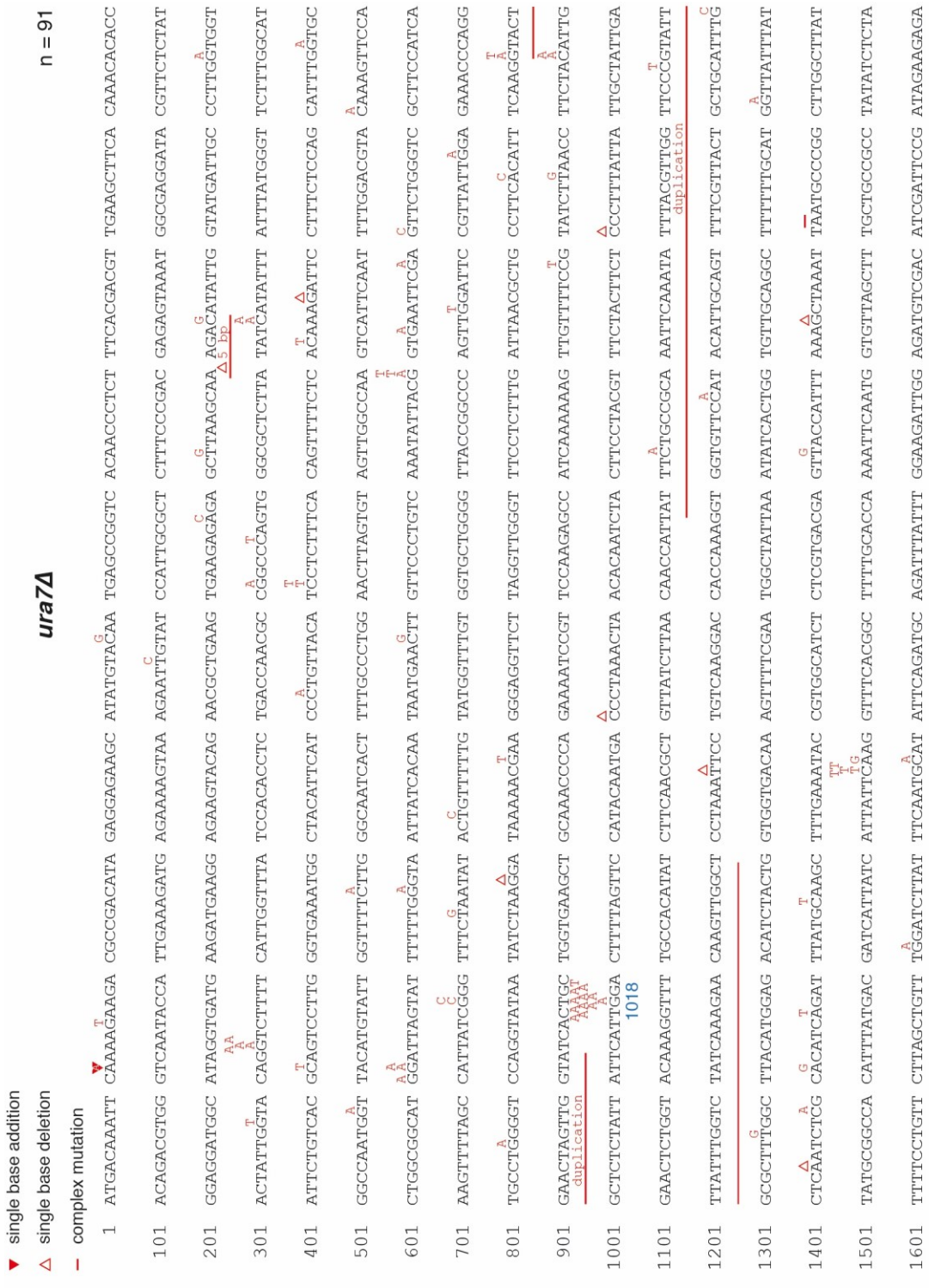

Fig. S 7.7 *CAN1* mutation spectrum of *ura7Δ*.
Genomic DNA of individual Can^R clones was purified, the *CAN1* gene amplified and sequenced. Individual mutations are shown. Mutational hotspots are indicated in blue.

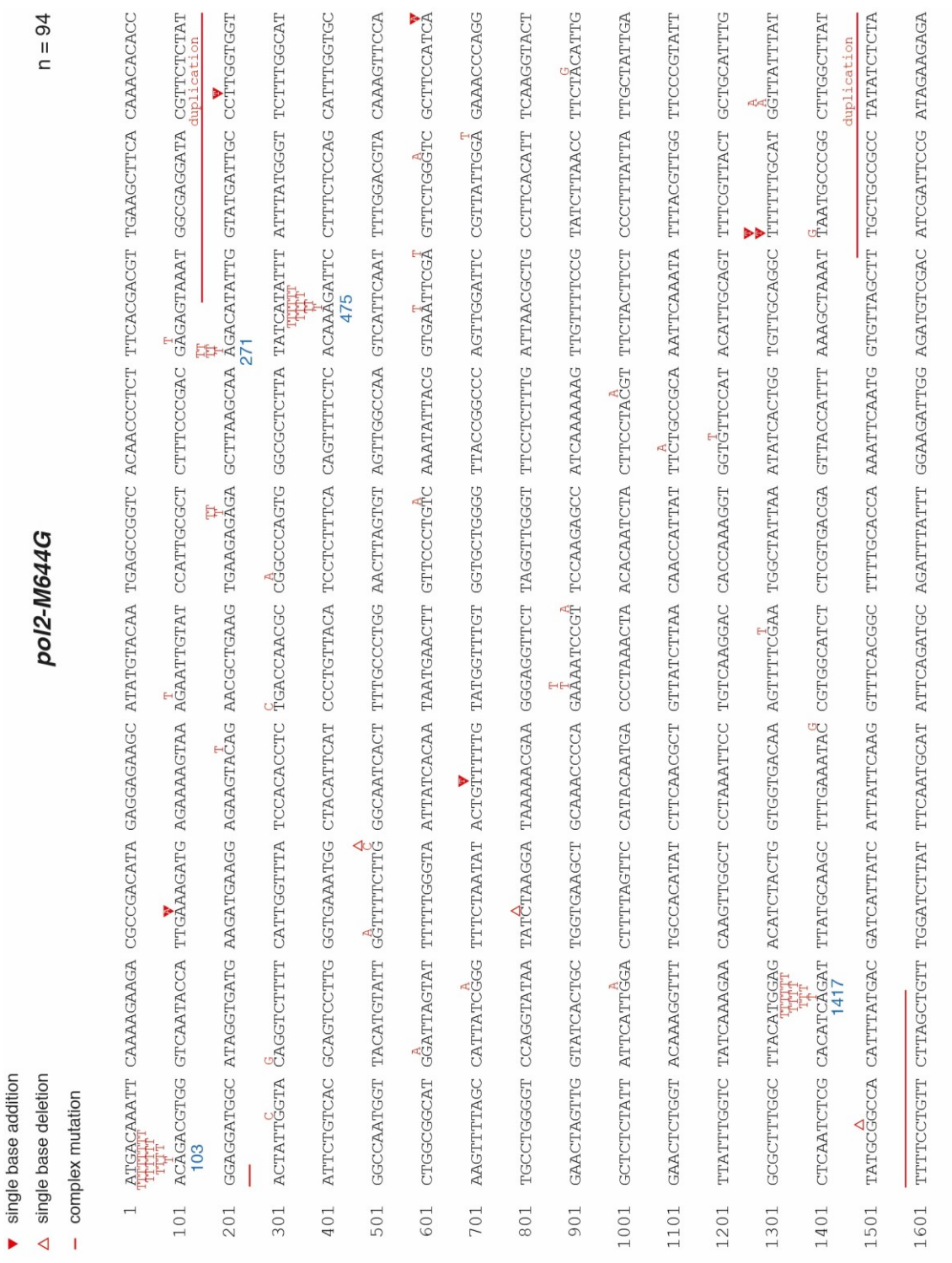

Fig. S 7.8 *CAN1* mutation spectrum of the *pol2-M644G*.
Genomic DNA of individual Can^R clones was purified, the *CAN1* gene amplified and sequenced. Individual mutations are shown. Mutational hotspots are indicated in blue.

Fig. S 7.9 *CAN1* mutation spectrum of *pol2-M644G ura7Δ*.
Genomic DNA of individual Can^R clones was purified, the *CAN1* gene amplified and sequenced. Individual mutations are shown. Mutational hotspots are indicated in blue.

Fig. S 7.10 *CAN1* mutation spectrum of *pol3-L612M*.
Genomic DNA of individual Can^R clones was purified, the *CAN1* gene amplified and sequenced. Individual mutations are shown. Mutational hotspots are indicated in blue.

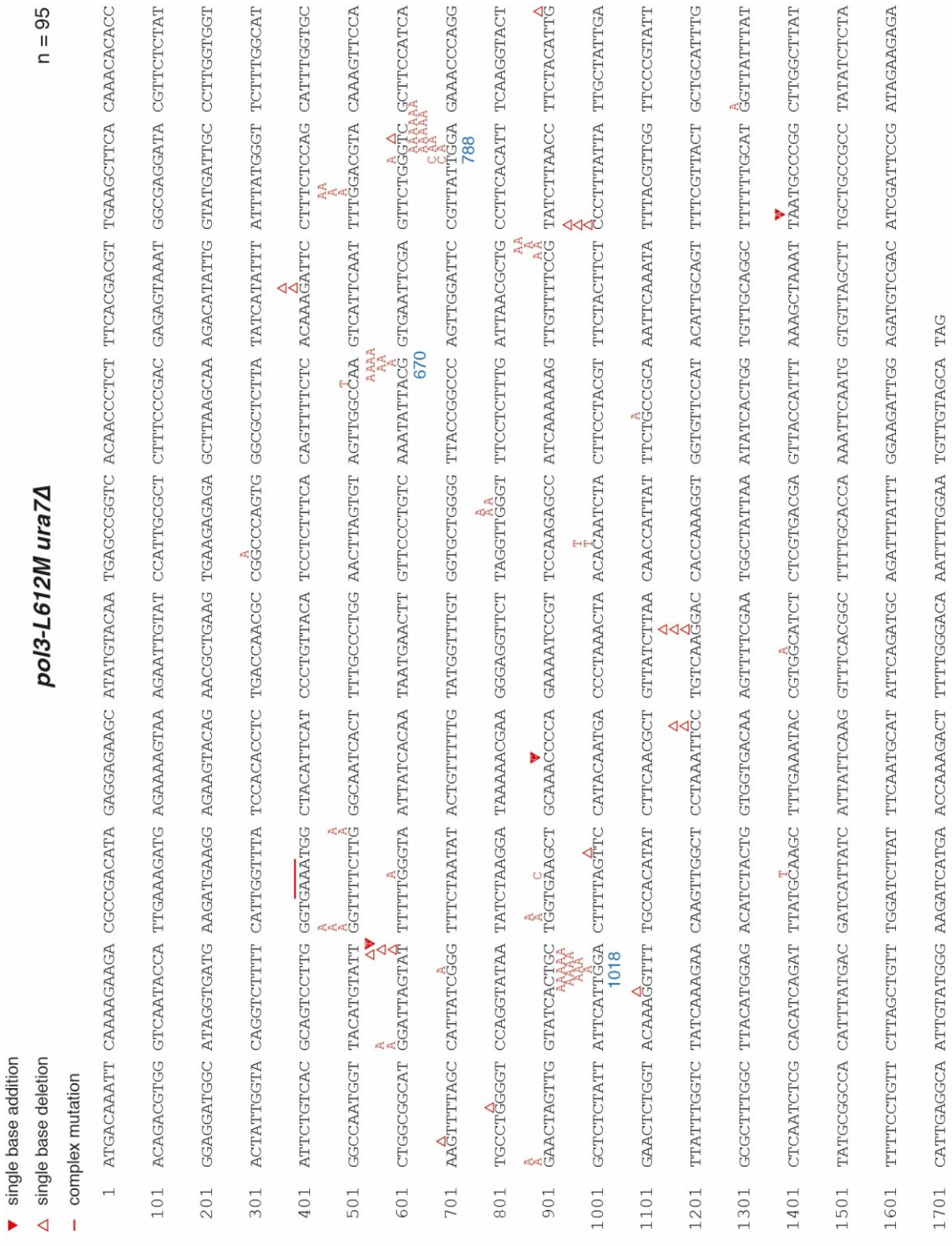

Fig. S 7.11 *CAN1* mutation spectrum of *pol3-L612M ura7*
Genomic DNA of individual Can^R clones was purified, the *CAN1* gene amplified and sequenced. Individual mutations are shown. Mutational hotspots are indicated in blue.

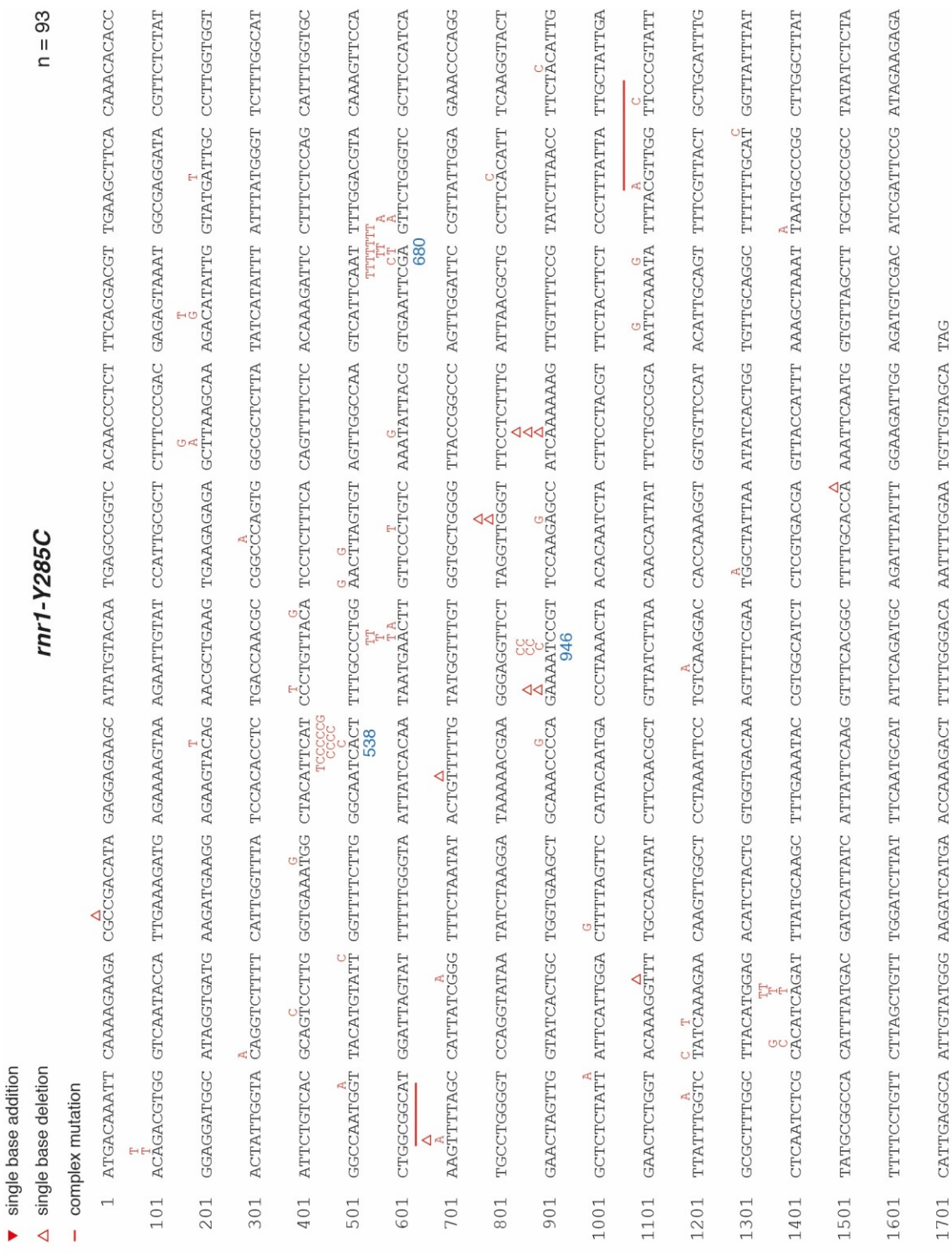

Fig. S 7.12 *CAN1* mutation spectrum of *rnr1-Y285C*.
Genomic DNA of individual Can^R clones was purified, the *CAN1* gene amplified and sequenced. Individual mutations are shown. Mutational hotspots are indicated in blue.

Fig. S 7.13 *CAN1* mutation spectrum of *rnr1-R256H,Y779C*.
Genomic DNA of individual Can^R clones was purified, the *CAN1* gene amplified and sequenced. Individual mutations are shown. Mutational hotspots are indicated in blue.

Fig. S 7.14 *CAN1* mutation spectrum of *rnr1-I262V,N291D*.
Genomic DNA of individual Can^R clones was purified, the *CAN1* gene amplified and sequenced. Individual mutations are shown. Mutational hotspots are indicated in blue.

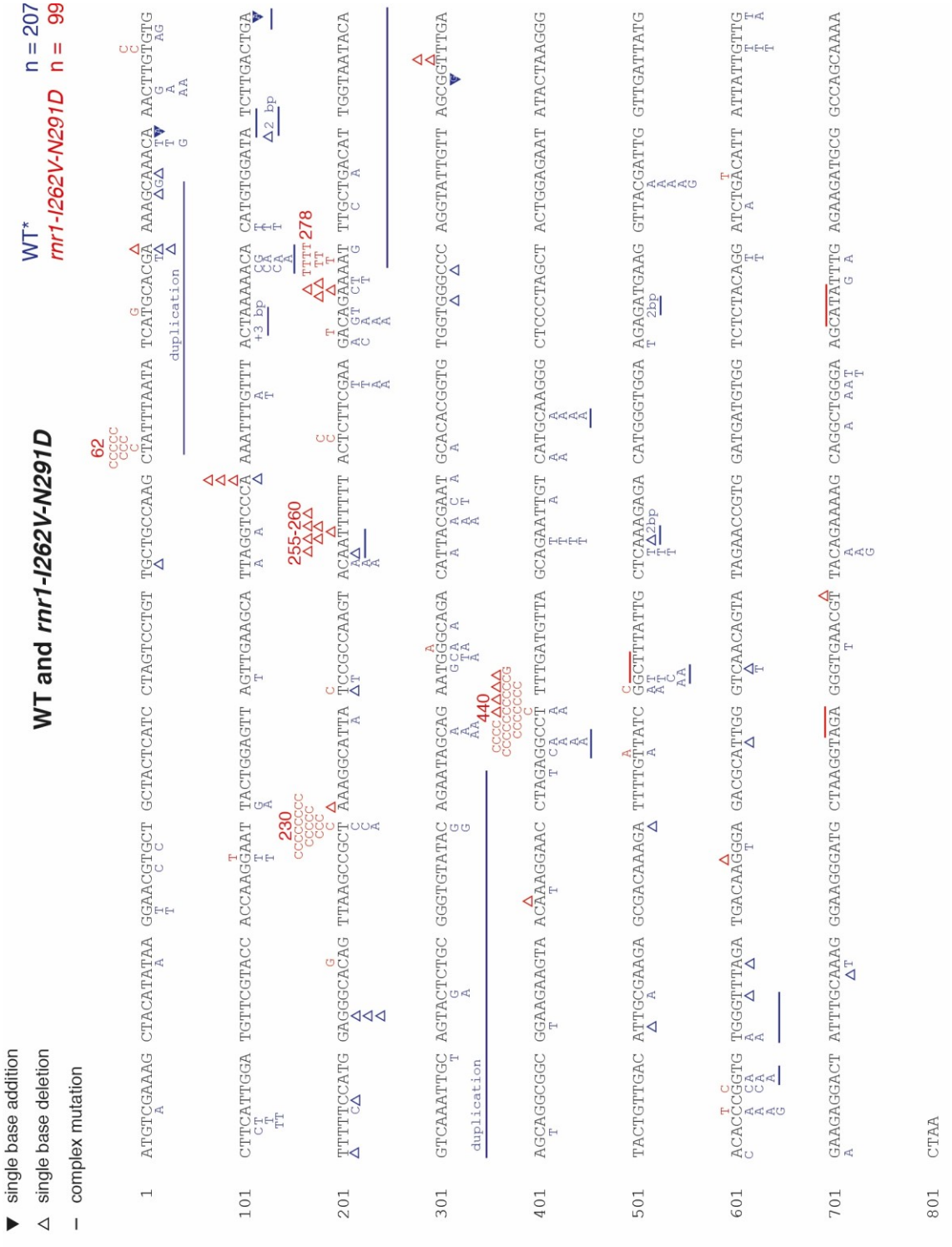

Fig. S 7.15 *URA3* mutation spectrum of the WT and *rnr1-I262V,N291D*.
Genomic DNA of individual 5-FOA^R clones was purified, the *URA3* gene amplified and sequenced. Individual mutations are shown. Mutational hotspots are indicated in red. The WT spectrum was taken from (LANG AND MURRAY 2008).

7.2 Acknowledgements

After all these words, numbers and yeast strains it is time to say thank you to all the people who contributed to this work and supported me during my PhD. First of all, I like to thank Dr. Hans Hombauer for giving me the opportunity to do my PhD studies in his lab. You have been a true source of motivation and a great teacher of yeast genetics and science in general. I appreciate the scientific discussions and your mentoring. I hope that we will stay in touch. Moreover, I like to thank Prof. Dr. Michael Knop and Prof. Dr. Sylvia Erhardt for complementing my thesis advisory committee and their helpful input during the meetings. A special thanks goes to Prof. Dr. Sylvia Erhardt for being willing to take over the first examination. I was truly relieved after you wrote me that you would be my “new” PhD first examiner. Furthermore, I like to thank Prof. Dr. Sylvia Erhardt, Dr. Hans Hombauer, Prof. Dr. Karsten Rippe and Dr. Michael Milsom for being part of my PhD committee.

My PhD work would have not been possible without collaborations. I would like to thank Prof. Dr. Michael Knop and Matthias Meurer for sharing reagents and supporting us with the robot for the genome-wide screen. I would like to thank Tina Wagner for performing the telomere-specific Southern blot and Prof. Dr. Brian Luke for scientific mentoring and support since I had been a rotation student in his lab during my master studies. A big thanks to Prof. Dr. Andrei Chabes and Dr. Sushma Sharma who made a tremendous effort to measure all the NTP and dNTP concentrations in the different yeast strains. Without both of you this analysis would have not been possible and it was a pleasure to work together with you.

I like to acknowledge the DKFZ core facilities: Dr. Steffen Schmitt and the flow cytometry core facility for advice and technical support with the FACS machines, Claudia Tessmer from the monoclonal antibody core facility for immunizing the guinea pigs and taking care of the animals, and Prof. Dr. Annette Kopp-Schneider and Dr. Manuel Wiesnfarth from the DKFZ biostatistics group for help with the statistical analysis of mutation spectra and mutational hotspots. Moreover, I like to acknowledge Prof. Dr. Tobias Dick, Prof. Dr. Richard Kolodner and Prof. Dr. Gislene Pereira for reagents, strains and plasmids. I also like to thank the Liu lab for sharing machines and reagents as well as for the floor events.

I like to thank Anna, Hannah, Hassan, Kerstin, Umran and Ximena from the Hombauer lab for the nice working atmosphere and the coffee breaks. You were always there with a helping hand and had time for discussions. Special thanks go to Kerstin, Ximena, Umran and Maike for your contributions to the projects. I appreciated a lot working together with you. I also would like to thank the rotation students Irmela, Robert and Bakar for their help. I also like to acknowledge Sofie and Frank for technical assistance.

I thank my friends for their unlimited understanding and patience. I am glad to know you! In particular, I like to thank Anna, Daniel, Dirk, Henning, Janina, Julia, Matthias, Max, Sarah, Tim and Tina who I met in the initial course of my bachelor studies almost 10 years ago. You made my studies a wonderful, unforgettable experience. I hope to see you all in California.

I like to thank my parents and my siblings Christine, Florian and Jonas for their trust in me and their infinite support. For me, you have always been the fundament. Finally, I like to thank Tanja for your

encouragements, your laugh and patience with me. I am looking forward on the next things to come.